MARTIN MARIETTA ENERGY SYSTEMS LIBRARIES
3 4456 0349889 1

[redacted]

CENTRAL RESEARCH LIBRARY
DOCUMENT COLLECTION

[redacted]

ORNL-2004
Progress

DECLASSIFIED

CLASSIFICATION CHANGED TO
BY AUTHORITY OF: TID-1219
BY: M. Tallent 3/29/60

[redacted]

HOMOGENEOUS REACTOR PROJECT

QUARTERLY PROGRESS REPORT

FOR PERIOD ENDING OCTOBER 31, 1955

CENTRAL RESEARCH LIBRARY
DOCUMENT COLLECTION
LIBRARY LOAN COPY
DO NOT TRANSFER TO ANOTHER PERSON
If you wish someone else to see this document, send in name with document and the library will arrange a loan.

OAK RIDGE NATIONAL LABORATORY
OPERATED BY
UNION CARBIDE NUCLEAR COMPANY
A Division of Union Carbide and Carbon Corporation
UCC
POST OFFICE BOX P · OAK RIDGE, TENNESSEE

[redacted]

[redacted]

ORNL-2004

COPY NO. 7

Contract No. W-7405-eng-26

HOMOGENEOUS REACTOR PROJECT

QUARTERLY PROGRESS REPORT

For Period Ending October 31, 1955

Project Director – J. A. Swartout
Associate Director – C. E. Winters

Homogeneous Reactor Test – S. E. Beall
Reactor Design and Analysis – J. A. Lane and R. B. Briggs
Engineering Development – J. A. Lane
Corrosion and Materials – E. G. Bohlmann
Chemical Engineering Development – F. R. Bruce
Supporting Chemical Research – E. H. Taylor

Compiled by

H. F. McDuffie
V. K. Hill

DATE RECEIVED BY INFORMATION AND REPORTS DIVISION

(NOVEMBER 10, 1955)

DATE ISSUED

JAN 5 1956

OAK RIDGE NATIONAL LABORATORY
Operated by
UNION CARBIDE NUCLEAR COMPANY
A Division of Union Carbide and Carbon Corporation
Post Office Box P
Oak Ridge, Tennessee

[redacted]

MARTIN MARIETTA ENERGY SYSTEMS LIBRARIES

3 4456 0349889 1

[redacted]

[redacted]

[redacted]

INTERNAL DISTRIBUTION

1. C. E. Center
2. [redacted]iology Library
3. [redacted]th Physics Library
4. Met[redacted]rgy Library
5-6. Reac[redacted]xperimental Engine[redacted]g Library
7-9. Central Re[redacted]rch Library
10-18. Laboratory [redacted]rds Dept.
19. Laboratory Re[redacted]s, ORNL R.C.
20. G. M. Adamson
21. R. E. Aven
22. S. E. Beall
23. D. S. Billington
24. E. P. Blizard
25. E. G. Bohlmann
26. C. J. Borkowski
27. G. E. Boyd
28. R. B. Briggs
29. F. R. Bruce
30. A. D. Callihan
31. D. W. Cardwell
32. W. L. Carter
33. G. H. Cartledge
34. R. A. Charpie
35. W. E. Clark
36. G. H. Clewett
37. T. E. Cole
38. E. L. Compere
39. D. D. Cowen
40. S. Cromer
41. F. L. Culler
42. J. S. Culver
43. J. S. Drury
44. W. K. Eister
45. L. B. Emlet (K-25[redacted]
46. D. E. Ferguson
47. W. J. Fretague[redacted]
48. J. H. Frye, J[redacted]
49. J. L. Gabba[redacted]
50. W. R. Gall[redacted]
51. H. E. Goe[redacted]
52. C. B. Gra[redacted]m
53. J. C. Grie[redacted]s
54. P. N. Haubenreich
55. J. W. Hill
56. C. J. Hochanadel
57. A. Hollaender[redacted]
58. A. S. Househ[redacted]r
59. H. K. Jackso[redacted]
60. G. H. Jenks[redacted]
61. W. H. Jord[redacted]
62. P. R. Ka[redacted]
63. C. P. K[redacted]
64. M. T. [redacted]ley
65. R. B. [redacted]rsmeyer
66. A. S[redacted]itzes
67. K[redacted] Kraus
68. [redacted]. Lane
69. [redacted]. E. Leuze
7[redacted]S. C. Lind
[redacted] R. B. Lindauer
[redacted]2. R. S. Livingston
73. M. I. Lundin
74. R. N. Lyon
75. J. L. Marsh (C&CCC, South Charleston)
76. W. L. Marshall
77. H. F. McDuffie
78. J. P. McBride
79. R. A. McNees
80. J. R. McWherter
[redacted]1. O. Menis
[redacted] E. C. Miller
8[redacted]K. Z. Morgan
84. [redacted] J. Murphy
85. [redacted]. Nurmi
86. J. [redacted]Murray (Y-12)
87. L. F[redacted]arsly
88. H. F. [redacted]pendiek
89. L. R. Q[redacted]es
90. P. M. Rey[redacted]
91. A. M. Rom[redacted]
92. W. L. Ross
93. H. C. Savage
94. C. H. Secoy
95. C. L. Segaser
96. E. D. Shipley
97. M. J. Skinner
98. R. W. Stoughton
99. A. H. Snell
100. I. Spiewak
101. C. D. Susano
102. J. A. Swartout

[redacted]

[redacted]

103. E. H. Taylor
104. G. Thomas
105. P. Thomason
106. M. Tobias
107. D. S. Tomb
108. W. E. Unger
109. R. Van Winkle
110. B. Weaver
111. A. M. Weinberg
112. T. A. Welton
113. E. P. Wigner (consultant)
114. G. C. Williams
115. J. C. Wilson
116. C. E. Winters
117. F. C. VonderLage
118. F. C. Zapp
119. ORNL Document Reference Library, Y-12 Branch
120. HRD Director's Office, Y-12

EXTERNAL DISTRIBUTION

121. AF Plant Representative, Burbank
122. AF Plant Representative, Marietta
123-124. AF Plant Representative, Seattle
125. AF Plant Representative, Wood Ridge
126. Aircraft Laboratory Design Branch (WADC)
127. ANP Project Office, Fort Worth
128. Alco Products, Inc.
129-140. Argonne National Laboratory
141. Armed Forces Special Weapons Project, Sandia
142. Armed Forces Special Weapons Project, Washington
143. Army Chemical Center
144-147. Atomic Energy Commission, Washington
148. Battelle Memorial Institute
149-154. Bettis Plant (WAPD)
155-157. Brookhaven National Laboratory
158. Bureau of Ships
159. Chicago Operations Office
160. Chicago Patent Group
161. Chief of Naval Research
162. Combustion Engineering, Inc. (CERD)
163. Department of the Navy – Op-32
164-167. duPont Company, Aiken
168. duPont Company, Wilmington
169. Duquesne Light Company
170. Engineer Research and Development Laboratories
171-172. General Electric Company (ANPD)
173-180. General Electric Company, Richland
181. Hanford Operations Office
182. Headquarters, Air Force Special Weapons Center
183. Iowa State College
184-187. Knolls Atomic Power Laboratory
188-191. Los Alamos Scientific Laboratory
192. Massachusetts Institute of Technology (Benedict)
193. Materials Laboratory (WADC)
194. Materials Laboratory Plans Office (WADC)
195. Mound Laboratory
196. National Advisory Committee for Aeronautics, Cleveland

[redacted]

[redacted]

197. National Advisory Committee for Aeronautics, Washington
198-199. Naval Research Laboratory
200-201. New York Operations Office
202. North American Aviation, Inc.
203. Nuclear Development Corporation
204. Nuclear Materials, Inc.
205. Office of the Quartermaster General
206. Patent Branch, Washington
207-213. Phillips Petroleum Company (NRTS)
214. Powerplant Laboratory (WADC)
215. San Francisco Operations Office
216. Sylvania Electric Products, Inc.
217. USAF Project RAND
218. U. S. Naval Postgraduate School
219. University of California Radiation Laboratory, Berkeley
220. University of California Radiation Laboratory, Livermore
221. Vitro Engineering Division
222. Vitro Laboratories
223. Division of Research and Development, AEC, ORO
224-338. Technical Information Service, Oak Ridge

[redacted]

[redacted]

Reports previously issued in this series are as follows:

ORNL-527	Date issued, December 28, 194[illegible]
ORNL-630	Period Ending February 28, 1950
ORNL-730	Feasibility Report – Date Issued, July 6, 1950
ORNL-826	Period Ending August 31, 1950
ORNL-925	Period Ending November 30, 1950
ORNL-990	Period Ending February 28, 1951
ORNL-1057	Period Ending May 15, 1951
ORNL-1121	Period Ending August 15, 1951
ORNL-1221	Period Ending November 15, 1951
ORNL-1280	Period Ending March 15, 1952
ORNL-1318	Period Ending May 1, 1952
ORNL-1424	Period Ending October 1, 1952
ORNL-1478	Period Ending January 1, 1953
ORNL-1554	Period Ending March 31, 1953
ORNL-1605	Period Ending July 31, 1953
ORNL-1658	Period Ending October 31, 1953
ORNL-1678	Period Ending January 31, 1954
ORNL-1753	Period Ending April 30, 1954
ORNL-1772	Period Ending July 31, 1954
ORNL-1813	Period Ending October 31, 1954
ORNL-1853	Period Ending January 31, 1955
ORNL-1895	Period Ending April 30, 1955
ORNL-1943	Period Ending July 31, 1955

[redacted]

[redacted]

HRP QUARTERLY PROGRESS REPORT

SUMMARY

PART I. HOMOGENEOUS REACTOR TEST

1. Operations

The reactor-tank roof structure was assembled during the quarter in order that a pressure test of the entire tank might be made. After a successful test, the details of which are reported below, the roof structure of the tank was disassembled in preparation for installation of the reactor components and associated piping. Several of the components were installed, and the sections of prefabricated piping were connected. Performance testing of other components was carried out and is being extended past scheduled installation dates in order to correct difficulties which have been found.

Construction work in the control-room area is ahead of schedule although installation of control and interlock wiring has not been begun.

The work of the steam system contractor is 90% complete and this construction crew is expected to leave the area by December 1, 1955.

A training program was started for the personnel, including industrial loanees, who comprise the reactor and chemical-plant operating group. Twelve technical people are participating at the present time.

2. Design

During this quarter HRT drawings have been approved for construction of the following:

leak-detector system,
heat exchanger blast shield,
refrigeration piping and equipment installation,
reactor thermal shield.

The drawings for construction of the HRT are now approximately 90% complete.

Calculations have been completed on cooling requirements of the thermal shield, gas production in the storage tanks, and space-cooler heat loads.

Hydrostatic and air-pressure tests of the cell tank have been completed which show that the tank can withstand 30-psi internal gas pressure without exceeding the yield strength of its members.

3. Component Development

Operation of the 300- and 400-gpm pumps and loops has been relatively free from trouble. Corrosion rates in the systems were satisfactory.

Delivery of one of the two stainless steel pumps for the HRT startup is expected in October; delivery of the other pump is expected in early November.

Fabrication of the two HRT heat exchangers, excluding installation of blast shields, was completed. Small leaks, which developed around the tube joints during thermal-cycle testing, were repaired, and the exchangers are ready for a final leak test. Excessive leakage of the head gasket occurred during initial thermal-cycle tests; this was remedied by the use of longer bolts and by preheating the steam drum before cycling. The flanged joints are being seal-welded before installation as further insurance against leaks.

Experimental results of the first phase of the HRT dump test program agreed well with those given by calculations. The apparatus is being modified to permit study of the simultaneous dumping of two vessels.

The test model of the HRT purge pump has run 1600 hr without trouble.

In the past quarter, the mockup loop ran for 633 hr, of which 110 hr represented a continuous UO_2SO_4 run at 300°C and 2000 psi. Solids were found in the pressurizer, and the corrosion rates were high. The next mockup run will be gas-pressurized, with all other variables held at about the same level as in the previous run.

In the course of further tests on the isolation chamber of the HRT sampler, two holes were drilled in the sleeve to improve venting action.

Models have been constructed of the proposed freezing unit to be used on HRT piping, and the necessary refrigeration equipment has been procured.

4. Controls and Instruments

Design drawings of the layout and piping for the remote-instrument cubicles have been completed. An estimated 75% of the main control-panel instruments have been checked prior to installation. The tank-weighing cells for the low-pressure systems have been installed, and calibration of the cells is in progress. Assembly of both the pneumatic and electrical high-pressure transmitters has been

[redacted]

started by the vendor. Two prototype pressurizer liquid-level transmitters, incorporating different damping mechanisms, are being developed. The low-pressure valves are being fabricated; the auxiliary-system valves were checked and sent to the field for installation. A systematic valve-trim-material testing program is under way, with the performance of type 347 stainless steel serving as the basis for comparison.

5. Fuel Processing Plant

The HRT fuel-processing-plant flowsheet has been revised to show the carrier designed to carry out the evaporation step. The underflow pot will now be discharged directly to either of the duplicate carriers for evaporation of the heavy water to avoid the problem of transferring heavy slurry concentrates. Also, provision will be made for either of the two carrier evaporators to be replaced with a small heavily shielded carrier of sufficient capacity to accommodate single underflow-pot discharge batches. The increased shielding will permit the removal of single batches, within a relatively short time after discharge, to a shielded chemical facility for complete dissolution of the small-carrier contents and for accurate sampling of the solution.

In hydroclone performance tests $Nd_2(SO_4)_3$, precipitated in a loop at 300°C, was concentrated by a factor of 65 from simulated reactor fuel. The hydroclone plugged when there was no filter in the system. A hydroclone has operated satisfactorily for 1366 hr. Studies of heat transfer on a hydroclone underflow pot indicated that convective heat transfer is effective in maintaining satisfactory temperature distribution in a simple cylindrical tank with a cooling jacket. It was found to be unfeasible to transfer uranyl sulfate solution, containing the quantity of fission and corrosion products expected in the underflow pot, after more than a fourfold concentration by evaporation.

PART II. REACTOR DESIGN AND ANALYSIS

6. Thorium Breeder Reactor

The TBR conceptual design has been extended to cover preliminary studies of reactor station operation under reduced steam-generator capacity. Assuming that the total core-heat-exchanger requirements are distributed among four steam generators, each the size of the blanket exchanger, the maximum power obtainable by reducing the steam pressure on removal of one or more generators from service has been calculated. For example, a loss of one core generator need reduce the plant electrical putput only about 13%, although 20% of the heat-exchanger surface is taken out of service.

The Oracle coding for the three-plane piping stress analysis has been extended to include deflections and rotations at any point, rotation of anchor points from external causes, and transverse bending and torsion.

A preliminary study of the physical, geometrical, and process design parameters for pilot-plant-size thorium breeder reactors was completed, and the results are presented.

The feasibility is being investigated of designing, for 5-Mw and higher powered reactors, a gas letdown system wherein the pressure drop is taken across a fairly long tube (and orifice, if necessary) rather than across a throttling valve. A pressure profile is shown for the letdown stream of the HRT as it passes through twelve $^3/_{16}$-in. lines and finally discharges into a container at atmospheric pressure.

7. Reactor Analysis

An investigation has been made of the behavior of the TBR under conditions which involve interruption of normal operation. If energy removal from the core circuit should suddenly stop, the fluid temperature would rise about 30°C in the first minute and then continue to rise at a much lower rate. If fluid circulation were suddenly stopped in the core circuit, the fluid temperature would rise about 45°C in the first minute and then continue to rise at a much lower rate. If the circulating pump should fail, the core temperature would rise about 10°C but would return to normal operating temperature in less than a minute. After the short transient period, the core would remain critical at a power level of about 60 Mw, with fluid circulating by natural convection. If the steam pressure on the shell side of the core heat exchanger should decrease rapidly, the temperature of the fluid entering the reactor core would be lowered abnormally, leading to an increase in reactivity. The relation between rate of decrease in shell-side temperature, initial reactor power level, and the accompanying pressure rise in the core is presented in graphical form.

An investigation was made of the safety of particular one- and two-region reactors for the

[redacted]

case of reactivity addition resulting from the injection of cool fluid into the reactor core. For the same cooling incident, the one-region reactor should have the higher degree of safety; this was indicated by a lower calculated core-pressure rise. The results indicated that, for a given power level, increasing the size of a reactor (and thereby lowering the absolute value of the temperature coefficient of reactivity) is desirable from the standpoint of reactor safety *if* the most dangerous situation corresponds to reactivity addition by means of the temperature coefficient itself.

The economic effect of adding Li_2SO_4 to a UO_2SO_4-D_2O plutonium-producing power reactor system has been studied. The results are presented in terms of electrical-power generation costs as a function of U^{238} concentration and Li_2SO_4 concentration. On the basis of these calculations, the addition of Li_2SO_4 to the fuel solution, in the same molar concentration as the uranium, adds about 0.8 mill/kwhr to the fuel cost near the optimum uranium concentration of 500 g/liter (reactor temperature, 280°C), when a credit of $40 per gram for the plutonium produced is assumed. Assigning a plutonium credit of $20 per gram lowers the cost differential to about 0.4 mill/kwhr.

A preliminary study has been made of the effect of the fuel-removal method upon the breeding ratio. The results obtained for batch removal of the fuel are compared with those for continuous removal, the same average removal time being used for each case (for the purpose of this calculation). For the two specific reactors considered, the breeding ratio appeared to be approximately 0.01 to 0.03 higher if the fuel fluid was removed from the reactor on a batch basis.

The two-group, two-region Oracle code for spherical reactors has been improved and modified to comply with changes in Oracle operations. The revised code permits the calculation of reactivity coefficients and reactivity changes associated with changes in parameter values. A similar code will be available for cylindrical reactors as soon as several Bessel function subroutines are completed.

PART III. ENGINEERING DEVELOPMENT

8. Development of Fuel-System Components

Severe stress-corrosion cracking was observed in portions of the high-pressure recombiner loop in contact with superheated vapors. It is believed that chloride present in the loop was responsible.

A low-pressure natural-circulation recombiner was designed and fabricated. Tests have indicated the feasibility of the design.

Allis-Chalmers Mfg. Co. is completing details and procuring materials to fabricate the 20-cfm gas circulator.

Several 5-gpm pumps have operated for periods up to 9400 hr.

The 4000-gpm loop was operated on oxygenated water at 1000 psi and 250°C for approximately 150 hr before UO_2SO_4 was added.

A contract has been made with the Crane Co. to produce test lengths of 20- and 3½-in. steel pipe lined with titanium. A contract has been made with The Pfaudler Co. for design and fabrication of a small titanium-lined heat exchanger, which should be completed and ready for testing early in 1956. A third contract is to be awarded to the Armour Research Foundation for developing a method of metallurgically cladding titanium.

9. Development of Blanket-System Components

A total of 787 hr of slurry operation has been logged by the Westinghouse 200A slurry pump, in addition to several hundred hours of operation with water. During this period so much difficulty was experienced in sealing the pump casing with a gasket that a seal-weld cutter has been ordered which will allow welding of the pump casing without greatly decreasing the ease of pump disassembly. Some bearing difficulties have also been experienced, but these in general are attributed to correctable causes. In the most recent run very serious caking has been found in the loop. No satisfactory explanation has been found for the caking, which was completely unexpected.

Four slurry dump-tank systems which show promise are now being studied.

Equipment for studying the rheological and heat-transfer properties of slurries is now being calibrated.

The mean slurry velocity required to move sedimented thorium oxide was measured in a ¾-in. glass pipe as a function of slurry concentration. For the slurry used in the test, the required velocity reached a maximum of 2.4 fps at about 700 g of thorium per kilogram of H_2O. The velocity required for resuspension (pickup) of the solid increased steadily with concentration and reached a value of 7.4 fps at 1645 g per kilogram of H_2O.

The blanket-mockup piping is 95% complete. Instrumentation remains to be completed.

[redacted]

[redacted]

PART IV. CORROSION AND MATERIALS

10. Solution Corrosion Tests

10.1 Pump Loops. – Operation of 11 dynamic-corrosion test loops is continuing.

The 4000-gpm loop is in operation to obtain corrosion and solution stability data under the proposed HRT uranyl sulfate startup conditions.

A survey of the operating life of Graphitar No. 14 bearings in the Westinghouse model 100A pumps was made. This survey involved 37 bearing replacements in a number of pumps having more than 80,000 hr of cumulative operating time. A wide range of bearing life was found, although approximately 73% of the failures occurred in less than 4000 hr.

One of the major problems investigated in the dynamic test program during the past quarter was the effect of acid on the stability of 0.04 *m* uranyl sulfate and on the corrosiveness of such solutions. It was found that at least 0.01 *m* sulfuric acid was necessary to prevent hydrolytic precipitation of uranium and copper at 300°C; it may be safer to use 0.015 *m* sulfuric acid. As was expected, an increase in acid concentration increased corrosion generally and substantially decreased the critical velocity. In a solution containing 0.04 *m* uranyl sulfate, 0.005 *m* copper sulfate, and 0.015 *m* sulfuric acid, the critical velocity was 50 to 60 fps at 300°C and 25 to 35 fps at 250°C.

The addition of equimolal amounts of lithium sulfate to 1.5 to 4.4 *m* uranyl sulfate solutions substantially reduced the corrosion by the solutions. In addition, when lithium sulfate is present, the solutions are phase stable to at least 350°C (and possibly higher) and have substantially lower vapor pressures than those of water. For example, with a solution 4.4 *m* in uranyl sulfate and lithium sulfate, the vapor pressure is only 1200 psi at 360°C, compared with 2710 psi for water at the same temperature.

One incidence of very damaging corrosion to titanium has been observed. A titanium impeller hub rubbed against the seal rings, apparently causing a removal of the protective oxide film and producing sufficient heat to cause a rapid reaction between the titanium and its oxygen-saturated aqueous environment. Metallographic examination showed that the temperature of the metal in the hub had reached the melting point of titanium, about 2000°C.

10.2 Laboratory Studies. – Valve bodies, fabricated from type 303 stainless steel, and valve stems of hardened type 420 stainless steel were found to be corrosion resistant to a solution of the following composition at room temperature: 0.17 *m* uranyl sulfate, 0.03 *m* copper sulfate, 0.8 *m* sulfuric acid, and 0.004 *m* chromic acid. Without chromic acid or with more than 0.8 *m* sulfuric acid, the attack was severe.

A series of cast zirconium alloys was corrosion-tested in dilute uranyl sulfate solutions at 300°C. The alloying elements consisted of aluminum, chromium, columbium, cesium, cerium, silver, tin, and yttrium. Except for the tin alloy (Zircaloy-2), only the chromium and the cerium alloy exhibited promising corrosion behavior under the conditions of test.

11. Slurry Corrosion Tests

11.1 Pump Loops. – Additional dynamic-corrosion tests were made with thorium oxide slurries. The tests were performed primarily to determine loop operating conditions necessary for maintaining equilibrium and theoretical thorium concentrations necessary for long-term dynamic corrosion data.

Slurries were circulated with concentrations ranging from 280 to 1030 g of thorium per kilogram of water, at 300°C, and at velocities of from 8 to 75 fps. A strong dependence of corrosion rate on velocity was noted. Zircaloy-2, titanium and its alloys, gold, and platinum showed the best behavior, the various stainless steels were the next best, various Stellites showed high attack rates, and pins of thoria containing 0.5% CaO disintegrated.

11.2 Toroids. – In order to compare thorium oxide produced at the Feed Materials Processing Center at Fernald, Ohio, with a standard ORNL production batch, aqueous slurries were circulated in toroids. At slurry concentrations of 1000 g of thorium per kilogram of water, a relative velocity of 26 fps, and in the presence of excess oxygen, little difference was observed between the two oxides in their attack rates on type 347 stainless steel, titanium 75A, or Zircaloy-2 at approximately 250°C.

Thorium oxide slurries at 1000 g of thorium per kilogram of water, 26 fps relative velocity (in toroids), approximately 200°C, and with excess oxygen severely attacked 54S aluminum. Circulating distilled water at 26 fps relative velocity and 200°C with oxygen also caused severe attack of 54S aluminum, but the alloy showed relatively

[redacted]

[redacted]

good resistance to oxygenated, 200°C distilled water in static autoclave tests. The use of 10 ppm Ni(II) in solution decreased the attack by circulating water, but even 400 ppm Ni(II) did not alter the severe attack by circulating thorium oxide slurries.

12. Radiation-Corrosion Tests

12.1 In-Pile Loops. – A loop package containing specimens of 41 different materials for use in the LITR HB-4 beam hole facility was completed. A loop package designed for operation at 300°C and 2000 psi in the new LITR HB-2 beam hole facility now under construction is under test.

A loop package was operated for approximately 1700 hr in the LITR HB-4 beam hole facility. The run was terminated by pump failure apparently due to movement of the rear bearing assembly which locked the rotor.

Test results from the fourth in-pile loop, designated EE, have been obtained. The generalized corrosion attack, based on oxygen consumption and nickel concentration increase, showed the same decrease with time as had been observed in previous experiments, although the initial rate was not so high. A lithium tracer technique for estimating solution sample dilution showed that uranium and copper concentrations were in fair agreement with calculated values. The coupon data for Zircaloy-2 were in agreement with those obtained in previous tests. The corrosion rate increased with power density as determined by induced activity measurement, with some indications of less than linear dependence at the higher power densities (~4 to 5 w/ml). No similar dependence on power density was observed for the titanium 55AX coupons (also exposed in this loop), although there is some suggestion of a velocity effect. The data for the type 347 stainless steel coupons did not correlate well with those obtained previously in experiment DD. In this instance (EE) an abrupt transition from less than 2 mpy to a rate of 50 to 60 mpy was indicated rather than a gradual increase, over the same range, such as had been observed previously.

Couple and stress specimens included in this test showed no effects ascribable to these factors. The stress specimens must still be examined metallographically.

12.2 LITR Bomb Tests. – The bomb-dismantling facility has been put into operation; weight loss data, activation analyses of pin specimens, and solution analyses are now being obtained. As a result, some changes in previously reported and recent data will be necessary; consequently, only a brief summary is presented this quarter.

12.3 MTR Bomb Tests. – A second MTR bomb test (ORNL 15-2), for testing the corrosion resistance of Zircaloy-2, has been completed. A corrosion rate of about 49 mpy was observed at a power density of 35 w/ml and wall temperature of 275 to 280°C.

13. Metallurgy

Specimens of the Zircaloy-2 plate used in the HRT core tank have been heat-treated to provide metallographic standards for interpretation of matrix and weld structures. The beta-to-(alpha-plus-beta) temperature has been established as 985 ± 2°C and the alpha-to-(alpha-plus-beta) temperature to be between 825 and 830°C. Full annealing of the hot-worked alpha structure and partial solution of stringers have been found to occur at 800°C.

The linear coefficient of thermal expansion of the Zircaloy-2 HRT core-tank material has been determined as a function of the rolling direction. The data indicate that there was considerable preferred orientation in the plate.

No harmful effects were found when nitrogen was substituted for the more expensive argon as the backup gas in inert arc butt-welding of type 347 stainless steel pipes.

Stress corrosion studies on stainless steels in boiling 42% magnesium chloride have continued. If it exists, the threshold stress value for type 304L stainless steel is below 10,000 psi and possibly below 5,000 psi. Inconel-X specimens, heat-treated to spring temper, have been installed in the equipment at 70,000-psi stress. Potential measurements on cold-worked and annealed type 304L specimens have been made in an etching solution of HCl, picric acid, and alcohol, versus a calomel electrode. The cold-worked material was negative with respect to the annealed specimen.

Efforts are being made to develop on zirconium an oxide film which has a cubic structure. It is thought that such a film may be more corrosion-resistant than the monoclinic film usually obtained. Alloys containing columbium produce films with a very high cubic content and are easy to fabricate.

Impact tests on Zircaloy-2 specimens, irradiated

[redacted]

[redacted]

in air at the MTR, indicate that they were not damaged to the same extent as were the specimens exposed to a fissioning uranyl sulfate solution in in-pile corrosion loop run GG.

The procedure is outlined by which a satisfactory closure weld was made in the HRT pressure shell. This shell is a duplex stainless steel–carbon steel vessel. An Armco iron deposit was used to make the transition from austenitic to ferritic material.

PART V. CHEMICAL ENGINEERING DEVELOPMENT

14. Thorium Oxide Slurry Development

Slurries of thorium oxide, prepared by the thermal decomposition of the oxalate at 650 and 900°C, were irradiated at 300°C in the LITR for 66 and 175 hr, respectively, without apparent change. A 650°C preparation irradiated for one month at 300°C in the ORNL Graphite Reactor also showed no apparent change. Slurries containing 1000 g of thorium per kilogram of H_2O were stirred without difficulty at 300°C in the dash-pot irradiation bomb both in- and out-of-pile.

The addition of 0.02 *m* silver to a slurry containing 660 g of thorium per kilogram of H_2O, prepared from 900°C recalcined oxide, resulted in a hydrogen and oxygen combination rate, at 280°C and at a hydrogen pressure of 500 psi, of 13 moles of hydrogen per hour per liter of slurry. Nickel and copper, as metal and oxide powders, were much less effective even at 0.1 *m* concentration, combining 2 or less moles of hydrogen per hour per liter under the same conditions. Palladium, 1030 parts per million parts of thorium, in a thorium oxide slurry containing uranium oxide, 0.5% uranium by weight of thorium, gave a combination rate of 19 moles of hydrogen per hour per liter at 115°C and at a hydrogen pressure of 500 psi.

In laboratory studies, pyrohydrolysis of thorium oxalate yielded more finely divided oxide than did thermal decomposition. Unlike the latter preparation, the oxide particles from pyrohydrolysis appeared to have the same dimensions as the x-ray crystallites; their size was independent of the oxalate precipitation temperature, and they showed no tendency to grow on recalcination up to 900°C. The settling rates of thorium oxide slurries increased with increasing calcination temperature of the oxide and decreasing slurry concentration. In the absence of a dispersing agent, the settling rates were higher and the bulk densities lower at pH's above 7. Slow settling rates, pronounced dispersion effects, and higher bulk densities were obtained at lower pH's with sulfuric acid, phosphoric acid, and thorium phosphate additives. The average sedimentation particle size of thorium oxide slurry solids was considerably decreased by pumping at elevated temperatures, approaching an equilibrium value of about 0.5 μ in a relatively short time.

A high-temperature capillary viscometer is under laboratory test with slurries. An apparatus to study the settling properties of thorium oxide suspensions at elevated temperatures with the use of x-ray absorption techniques has been designed and is under construction.

15. Fuel Processing

X-ray diffraction studies showed that the structure of the solids precipitated at elevated temperatures from simulated fuel solutions containing rare-earth sulfates varied not only with the concentration of the rare-earth sulfate but also with the acidity. Apparently simpler solids were obtained when the amount of sulfuric acid present was larger than 25 mole % excess. However, the final concentration of rare-earth sulfates remaining in solution was not significantly affected by varying the excess acid from 25 to 100 mole %. The behavior of cerium sulfate in the presence of oxygenated fuel solution that was in contact with a Zircaloy-2 surface hotter than the solution was not consistent. In some instances crystalline solids were deposited on the hot surface, and in other cases these were absent. Synthetic solids, partially simulating those expected from reactor operations, dissolved slowly in boiling 63% nitric acid.

16. Plutonium Producer Blanket Processing

The adsorption of plutonium on Zircaloy-2 and on titanium from 1.26 *m* UO_2SO_4 under simulated reactor conditions is essentially nonreversible. In continuous-flow experiments as much as 0.5 mg/cm^2 was adsorbed on both titanium and Zircaloy-2 with no indication of an approach to equilibrium. The rate of adsorption was markedly dependent on the concentration of plutonium in solution. When about 1 liter of 1.26 *m* UO_2SO_4, containing 100 mg of plutonium per kilogram of H_2O, was passed over Zircaloy-2 at 250°C, about 30 μg of plutonium per square centimeter was adsorbed. When the uranyl

[redacted]

[redacted]

sulfate contained 3 mg of plutonium per kilogram of H_2O, only 0.1 μg of plutonium per square centimeter was adsorbed. This latter value is of most interest, since the soluble plutonium in the blanket solution will be about 3 mg per kilogram of H_2O. Essentially all the plutonium on the metal walls is present as crystalline PuO_2.

Factors for PuO_2 concentration by a ¼-in.-dia hydroclone from a water slurry at room temperature varied from 3.0 to 4.6. Much greater concentration can be expected at 250°C.

Measurements of plutonium solubility and adsorption, determined by experiments in which 1.26 *m* UO_2SO_4 (0.03% U^{235}) was irradiated in the LITR at 250°C, were not reproducible. Plutonium in solution was calculated as 6 to 28 mg per kilogram of H_2O. Adsorption of plutonium was only 1 to 3 $\mu g/cm^2$; however, this represented 20 to 50% of the total plutonium present. At least 80% of the neptunium was in solution.

17. Thermal Breeder Blanket Processing

The low protactinium recoveries obtained when large amounts of ThO_2 were leached with 6 to 8 *M* H_2SO_4 for 3 hr were apparently a result of poor contacting, which resulted in slower leaching rates. Higher recoveries from 3- to 11-g batches of ThO_2 were obtained by diluting to dissolve the $Th(SO_4)_2$ and recrystallizing the $Th(SO_4)_2$ by evaporation at 80°C. In these tests, 60 to 70% of the protactinium was leached, with thorium losses of less than 0.5%. In order to remove 95% of the protactinium, it was necessary to dissolve 6 to 11% of the thorium. This procedure involves large volumes and is not attractive for full-scale processing.

The $Th(SO_4)_2$, obtained by refluxing ThO_2 in sulfuric acid, was converted to ThO_2 by calcination in air at 900°C for 24 hr. Washing in water for 2 hr reduced the sulfate content from 0.11% to only 100 ppm.

18. Equipment Decontamination

Since fission products are bound in the corrosion film, deposited on stainless steel by uranyl sulfate reactor fuels at 250 to 300°C, removal of this film is necessary for adequate decontamination. The use of strong reducing agents is the most promising method for effectively removing this oxide film. Of the reducing agents tested, $TiCl_3$ gave the most rapid reduction and dissolution of the scale. At room temperature, solution containing 20, 10, 2, and 1% $TiCl_3$ removed such a scale in 1, 4, 20, and 25 hr, respectively. Although these results are encouraging, the use of $TiCl_3$ is probably not practical, since it oxidizes and hydrolyzes to produce a TiO_2 precipitate and HCl, and it would be difficult to remove these materials from the reactor system.

19. Summary of Vitro Work

The equilibrium distribution of elemental iodine between the vapor and liquid phases in a simulated reactor fuel was studied, with particular emphasis given to the effect of temperature and iodine concentration on the equilibrium constant, that is, on the ratio of mole fraction of iodine in the vapor phase to mole fraction of elemental iodine in the liquid phase. The results obtained from experimental studies in a large pressure vessel indicate an equilibrium constant of 7. When the simulated fuel solution was replaced by water, an equilibrium constant of 0.25 was obtained, with pH having little effect in the range 3.8 to 9.9.

PART VI. SUPPORTING CHEMICAL RESEARCH

20. Aqueous Systems at Elevated Temperatures

20.1 Alkaline Carbonate–Uranium Trioxide Systems at 250°C. – Continued work has defined more precisely the scope of the unsaturated liquid range in the system Li_2O-UO_3-CO_2-H_2O at 250°C and at a pressure of 1500 psi. Compositions which contain as much as 8 g of uranium per kilogram of water and which will remain homogeneous at 250°C can now be specified. A single trial in the ammonium carbonate system indicated a very small uranium solubility.

20.2 Oxidation of Chromic(III) Hydroxide by Oxygen at 250°C. – Above a pH of approximately 2.0, Cr(III) is oxidized rapidly to Cr(VI) when treated with 300-psi oxygen at 250°C. The Cr(VI) dissolves in aqueous solutions. Below a pH of 2.0 the reaction is reversed, and Cr(III) is precipitated from solution under the same conditions. The equilibrium does not appear to be sensitive to the oxygen pressure in the range 200 to 1500 psi.

20.3 The Quaternary Systems NiO-UO_3-SO_3-H_2O and CuO-UO_3-SO_3-H_2O. – Because of indications of attack on pyrex vessels at 100°C, particularly in the nickel system, the use of fluorothene tubes is being developed. Three solid phases, which have previously been encountered and reported, have been proved to be identical with naturally occurring minerals. It has been shown that the

[redacted]

[redacted]

composition $3CuO \cdot SO_3 \cdot 2H_2O$ is identical with the mineral antlerite and that the composition $CuO \cdot 2UO_3 \cdot 2SO_3 \cdot 7H_2O$ is identical with the mineral johannite. The material heretofore called K-salt and assigned the composition $8UO_3 \cdot 3SO_3 \cdot 16-18H_2O$ has been shown to be identical with the mineral uranopilite (composition $6UO_3 \cdot SO_3 \cdot 17H_2O$).

21. Adsorption on Inorganic Materials

Study of the adsorption of ions by inorganic materials continued, with principal emphasis on zirconium phosphate, zirconium tungstate, and zirconium hydroxide. Details are given concerning the effect of firing temperature on the adsorptive properties of these materials. As expected, capacities of the materials decrease with increases of the firing temperature, though this effect is relatively minor up to about 200 to 300°C. Most of the work on selectivities of the materials centered around the alkali metals (lithium to cesium). Excellent separations may be achieved with both zirconium tungstate and zirconium phosphate. Strong adsorption of protactinium by zirconium phosphate from a number of concentrated electrolyte solutions was demonstrated.

22. HRP Analytical Chemistry

During the past quarter, methods for analyzing solutions of uranyl sulfate for mercury, tin, and chloride have been developed.

Methods have been developed for the determination of carbonate, silicon, and titanium in thorium oxide. The use of the Andreasen pipet method to determine the particle-size distribution of thorium oxide in different media has been investigated.

A semiquantitative method has been devised for the determination of carbon dioxide in the oxygen off-gases from dynamic test loops.

[redacted]

[redacted]

CONTENTS

SUMMARY vii

PART I. HOMOGENEOUS REACTOR TEST

1. OPERATIONS 3
   - 1.1 Construction 3
     - 1.1.1 Reactor Shield Tank 3
     - 1.1.2 Reactor Assembly 3
     - 1.1.3 Control-Room Area 3
     - 1.1.4 Steam System 3
   - 1.2 Operations Training 7

2. DESIGN 8
   - 2.1 General Status of Design 8
   - 2.2 Thermal Shield 8
   - 2.3 Heat Exchanger Blast Shield 11
   - 2.4 Freeze Units 11
   - 2.5 Refrigeration System 11
   - 2.6 Dissociation of D_2O in Storage Tanks 13
   - 2.7 Space-Cooler Heat Loads 13
   - 2.8 Leak-Detection System 14
   - 2.9 Pressure Test of Shield Tank 16

3. REACTOR COMPONENT DEVELOPMENT 17
   - 3.1 Pump Development 17
     - 3.1.1 400A Pump and Loop 17
     - 3.1.2 Pump and Loop 17
     - 3.1.3 400B Pump and Loop 19
   - 3.2 Fuel and Blanket Reactor Pumps 20
   - 3.3 HRT Heat Exchangers 21
   - 3.4 HRT Dump Test 21
   - 3.5 HRT Diaphragm Pump Testing 21
   - 3.6 HRT Mockup Loop 22
   - 3.7 HRT Sampler 25
   - 3.8 HRT Thermal Insulation 26
   - 3.9 Reflux Condenser-Recombiner 26
   - 3.10 HRT Freeze Plug Test 26
   - 3.11 Pressure-Balancing Valve 26

4. REACTOR CONTROLS AND INSTRUMENTATION 27
   - 4.1 General Status 27
   - 4.2 Differential-Pressure Transmitters 27
   - 4.3 Liquid-Level Transmitter 28
   - 4.4 Valves and Operators 28
     - 4.4.1 HRT Low-Pressure Valves 28
     - 4.4.2 HRT High-Pressure Valves 29
     - 4.4.3 HRT Auxiliary-System Valves 31
     - 4.4.4 Valve-Trim Testing Program 31

[redacted]

[redacted]

5. HRT FUEL PROCESSING PLANT 33

5.1 Design 33
5.2 Construction 34
5.3 Component Development 34
5.3.1 Hydroclone Development 34
5.3.2 Evaporator 39
5.3.3 Pumps 39
5.3.4 Freeze Plugs 39

PART II. REACTOR DESIGN AND ANALYSIS

6. THORIUM BREEDER REACTOR 43

6.1 TBR Design 43
6.1.1 Reduced-Power Study 43
6.1.2 Piping-Flexibility Analysis 44
6.2 TBR Pilot Plant 44
6.2.1 Preliminary Considerations 44
6.2.2 Letdown System 45

7. REACTOR ANALYSIS 48

7.1 Thorium Breeder Reactor Safety 48
7.1.1 Case 1 – Cessation of Heat Removal 48
7.1.2 Case 2 – Interruption of Flow 49
7.1.3 Case 3 – Circulating-Pump Failure 49
7.1.4 Case 4 – Steam Pressure Decrease 49
7.2 Temperature Coefficient and Reactor Safety 51
7.3 Effect of Li_2SO_4 on the Fuel Cost of a Plutonium-Producing Power Reactor 53
7.4 Breeding Ratio and Fuel-Removal Method 56
7.4.1 One-Region Reactor 60
7.4.2 Two-Region Reactor 60
7.5 Mathematics and Computations 61

PART III. ENGINEERING DEVELOPMENT

8. DEVELOPMENT OF FUEL-SYSTEM COMPONENTS 65

8.1 Recombiner Development 65
8.1.1 High-Pressure Recombiner Loop 65
8.1.2 Natural-Circulation Catalytic Recombiner 65
8.1.3 Battelle and Syracuse Subcontracts 66
8.2 Small Reactor Components 66
8.2.1 20-cfm Canned-Rotor Gas Circulator 66
8.2.2 ORNL Gas Circulator 66
8.2.3 Small Circulating Pumps 66
8.3 4000-gpm Loop 67
8.4 Titanium-Lined Equipment 67

9. DEVELOPMENT OF BLANKET-SYSTEM COMPONENTS 68

9.1 Westinghouse 200A Slurry Pump 68
9.2 Dump Tank–Evaporator Tests 68
9.3 Rheological Properties of Slurry Systems 69
9.4 Heat-Transfer Studies 70

[redacted]

[redacted]

9.5 Slurry-Transport Velocities 71
9.6 Slurry Blanket Mockup 71

PART IV. CORROSION AND MATERIALS

10. SOLUTION CORROSION TESTS 79
10.1 Pump Loops 79
10.1.1 Operation and Maintenance 79
10.1.2 Data and Discussion 81
10.2 Laboratory Studies 103
10.2.1 Corrosion of Type 303 Stainless Steel High-Pressure Valves by Sulfuric Acid and Uranyl Sulfate Solutions at Room Temperature 103
10.2.2 Corrosion of Cast Zirconium Alloys 103

11. SLURRY CORROSION TESTS 106
11.1 Pump Loops 106
11.1.1 Operation and Maintenance 106
11.1.2 Data and Discussion 109
11.2 Toroids 115
11.2.1 Operation and Maintenance 115
11.2.2 Data and Discussion 116

12. RADIATION CORROSION 121
12.1 In-Pile Loop 121
12.1.1 Development and Construction 121
12.1.2 LITR Operation – In-Pile Loop EE Corrosion Test 123
12.1.3 Remote Dismantling and Inspection of Loop EE 131
12.1.4 Discussion of Results of Experiment EE 146
12.2 LITR Bomb Tests 150
12.2.1 Introduction 150
12.2.2 Experimental Conditions and Results 151
12.3 MTR Bomb Tests 152
12.3.1 Experiment ORNL-15-1 152
12.3.2 Experiment ORNL-15-2 152

13. METALLURGY 156
13.1 Physical Metallurgy of Zirconium and Its Alloys 156
13.1.1 Properties of Zircaloy-2 Core-Tank Material 156
13.2 Welding Development 156
13.2.1 Substitution of Nitrogen for Argon as a Backup Gas in Inert Gas Arc Welding of Type 347 Stainless Steel 156
13.2.2 Development of a Procedure for the Welding of Titanium–Carbon Steel Composites 157
13.3 Metallurgy of Corrosion 159
13.3.1 Stress Corrosion Cracking of Austenitic Stainless Steels 159
13.3.2 Stress Corrosion Cracking of Inconel-X 159
13.3.3 Effect of Hydrogen Content on the Corrosion Resistance of Zirconium Alloys 159
13.3.4 Nature of Zirconium Oxide Films 159
13.4 Mechanical Metallurgy of Zirconium Alloys 161
13.5 Effects of Radiation on Structural Metals and Alloys 161
13.6 Metallurgical Engineering Services 162
13.6.1 Closure Joint in the HRT Pressure Vessel 162

[redacted]

[redacted]

PART V. CHEMICAL ENGINEERING DEVELOPMENT

14. THORIUM OXIDE SLURRY DEVELOPMENT 167

14.1 Thorium Oxide Slurry Irradiation Studies 167
14.1.1 Slurry Irradiations in the LITR 167
14.1.2 Slurry Irradiations in the Graphite Reactor 168
14.1.3 Slurry Irradiations in the Co^{60} Source 168
14.1.4 Postirradiation Examination of Slurries 168
14.1.5 Development of Facilities for Irradiation Studies 169
14.2 Gas Recombination 169
14.3 Laboratory Studies 172
14.3.1 The Preparation of Thorium Oxide by the Pyrohydrolysis of Thorium Oxalate 172
14.3.2 Hindered Settling Properties of Thorium Oxide Slurries 172
14.3.3 Characterization of Pumped Slurries 179
14.3.4 Slurry Viscosity Measurements at Elevated Temperature 179
14.3.5 Hindered Settling of ThO_2 Suspensions at Elevated Temperatures 184

15. FUEL PROCESSING 186

15.1 Fission-Product Chemistry 186
15.1.1 Rare-Earth Sulfate Precipitation from Fuel Solution 186
15.1.2 Effects of Various Solutes on Neodymium Sulfate Solubility 186
15.1.3 Reactor Solids Dissolution 187
15.1.4 In-Pile Solids Precipitation 188
15.1.5 Iodine 188

16. PLUTONIUM-PRODUCER BLANKET PROCESSING 189

16.1 Adsorption of Plutonium on Metals 189
16.2 Separation of PuO_2 by a Hydroclone 191
16.3 In-Pile Chemistry of Plutonium and Neptunium 192
16.4 Test Loops 192

17. THERMAL-BREEDER BLANKET PROCESSING 193

17.1 Leaching of Irradiated Thorium Oxide 193
17.2 Conversion of $Th(SO_4)_2$ to ThO_2 194

18. EQUIPMENT DECONTAMINATION 195

18.1 Scale Removal from Stainless Steel 195

19. SUMMARY OF WORK OF VITRO LABORATORIES 196

PART VI. SUPPORTING CHEMICAL RESEARCH

20. AQUEOUS SYSTEMS AT ELEVATED TEMPERATURES 201

20.1 Alkaline Carbonate–Uranium Trioxide Systems at 250°C 201
20.2 Oxidation of Chromic(III) Hydroxide by Oxygen at 250°C 204
20.2.1 Experiment and Discussion 204
20.2.2 Preparation and Characteristics of the Solid Phases 206
20.2.3 Summary 206
20.3 The Quaternary Systems $NiO-UO_3-SO_3-H_2O$ and $CuO-UO_3-SO_3-H_2O$ 206

[redacted]

[redacted]

21. ADSORPTION ON INORGANIC MATERIALS 208
21.1 Zirconium Hydroxide 208
21.2 Zirconium Tungstate 208
21.3 Zirconium Phosphate 209
21.4 Adsorption of Protactinium on Zirconium Phosphate 211

22. HRP ANALYTICAL CHEMISTRY 213
22.1 Analysis of Uranyl Sulfate Solutions 213
22.2 Analysis of Thorium Oxide 213
22.3 Analysis of Off-Gases from Dynamic Loop Tests 214

[redacted]

Part I

HOMOGENEOUS REACTOR TEST

S. E. Beall

1. OPERATIONS

S. E. Beall

R. E. Brooksbank
W. D. Burch
N. W. Curtis[1]
J. R. Engel
J. L. Gory
J. J. Hairston
B. H. Hamling
P. N. Haubenreich
J. W. Hill, Jr.
R. W. Jurgensen[2]
S. I. Kaplan
J. O. Kolb
W. L. Morgan
J. D. Perret
H. K. Search[1]
R. VanWinkle
H. E. Williamson

1.1 CONSTRUCTION

J. J. Hairston
P. N. Haubenreich
S. I. Kaplan
J. O. Kolb
W. L. Morgan
R. VanWinkle

1.1.1 Reactor Shield Tank

The roof structure of the shield tank was completed in August. The roof was assembled at this stage of reactor construction, with the same procedures being used which will be used when the reactor is ready for startup, so that the tank could be given pressure tests. The details of the successful pressure tests are reported in Sec. 2.9 of this report. Figure 1.1 is a photograph of the reactor tank with all the shielding plugs in position. The north wall, between the reactor tank and control area, is shown uncovered.

After the pressure tests, the roof structure was disassembled and the tank cleaned in preparation for the mounting of equipment.

No unexpected problems arose during the handling of the roof members. Welding of the $\frac{1}{8}$-in. steel seal sheets located between the two layers of concrete plugs was difficult, but a gas-tight seal (<100 cc/min) appears attainable.

1.1.2 Reactor Assembly

After completion of the pressure tests, installation of prefabricated reactor piping and components commenced. The blanket low-pressure assembly (dump tanks, recombiner, condenser, etc.), outer storage tanks for fuel and blanket, feed pumps, and other smaller vessels are in place and pipelines are being attached. Figure 1.2 shows a portion of the installed equipment.

The fuel low-pressure assembly will not be moved from its test stand until several studies now in progress are completed. These studies include performance of the equipment during a simulated full-scale dump, recombination tests, and entrainment measurements. Sufficient data have been collected to show that several revisions must be made if performance is to be completely satisfactory. The discharge point of the dump line is being relocated in the top of the dump tanks to prevent flooding of the entrainment separator. The recombiner did not perform at 100% efficiency when fed with wet steam mixed with a small flow (<2 cfm) of $H_2 + O_2$. This problem might be solved by adding a superheater to the vapor line entering the recombiner. A second vent line must be installed in the recombiner condenser to prevent the transfer of liquid through the present vent during a dump. Four additional weeks of testing will be required to check out these revisions.

1.1.3 Control-Room Area

All recorders and indicators have been mounted in the main control panels and are being connected. Except for the wiring of these panels and associated interlocks, the electrical work in this area is complete.

The leak-detection system is partially complete. Two hundred and eighty Boder high-pressure needle valves have been installed on the control-room side, but more work on this system remains to be done on the reactor side of the shield wall.

1.1.4 Steam System

The reactor steam-system equipment and piping is being installed by the V. L. Nicholson Company, the subcontractor who was responsible for the installation of the reactor tank. The air-cooled steam condenser, the deaerator, and the steam drums are complete. The valve-control station is 30% finished and will require one additional month for completion. Figure 1.3 is a photograph of much of the outside steam system.

[1]On loan from Pennsylvania Power and Light Company.

[2]On loan from American Gas and Electric Company.

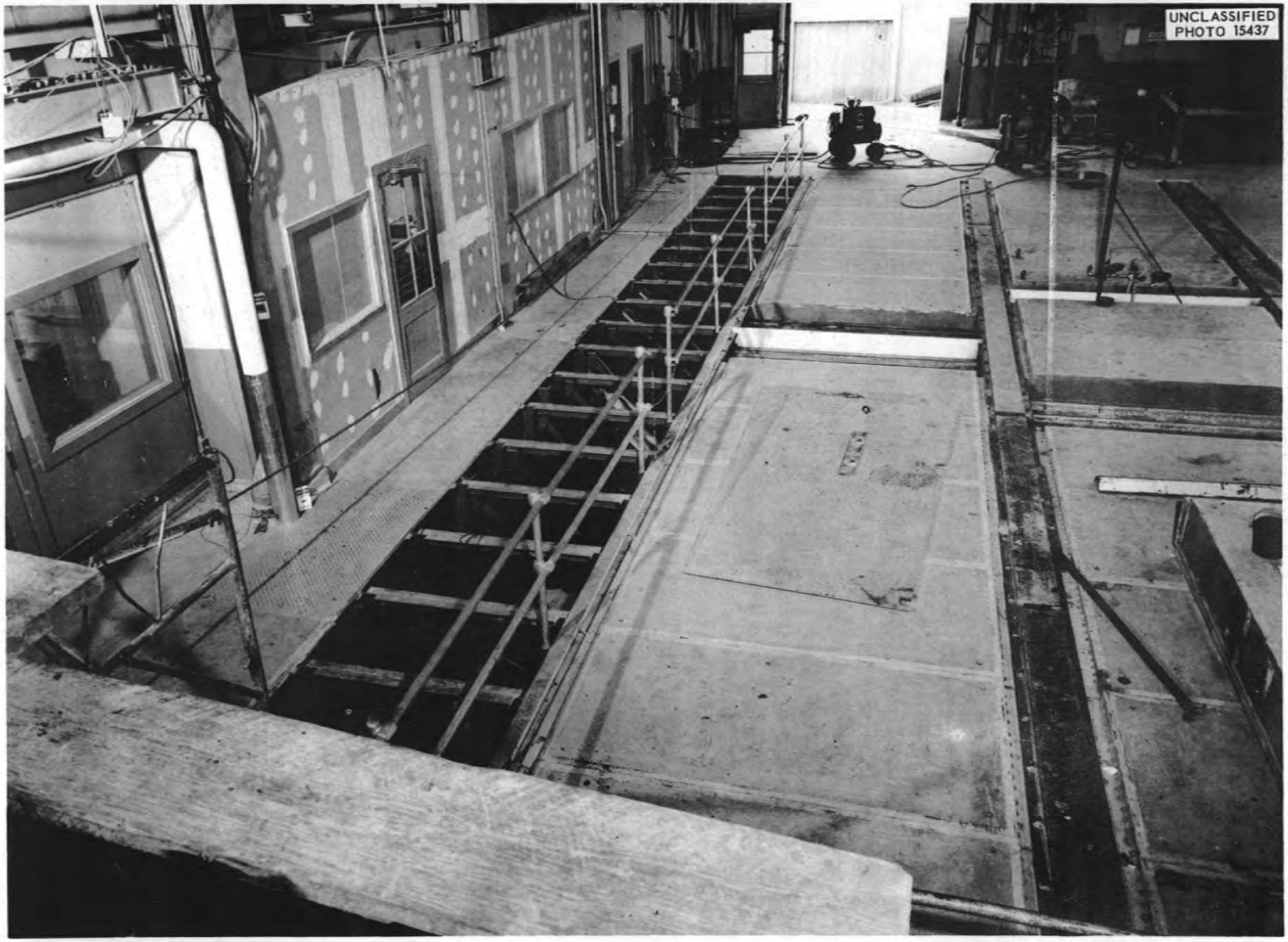

Fig. 1.1. Photo of the Reactor Tank with All the Shielding Plugs in Position.

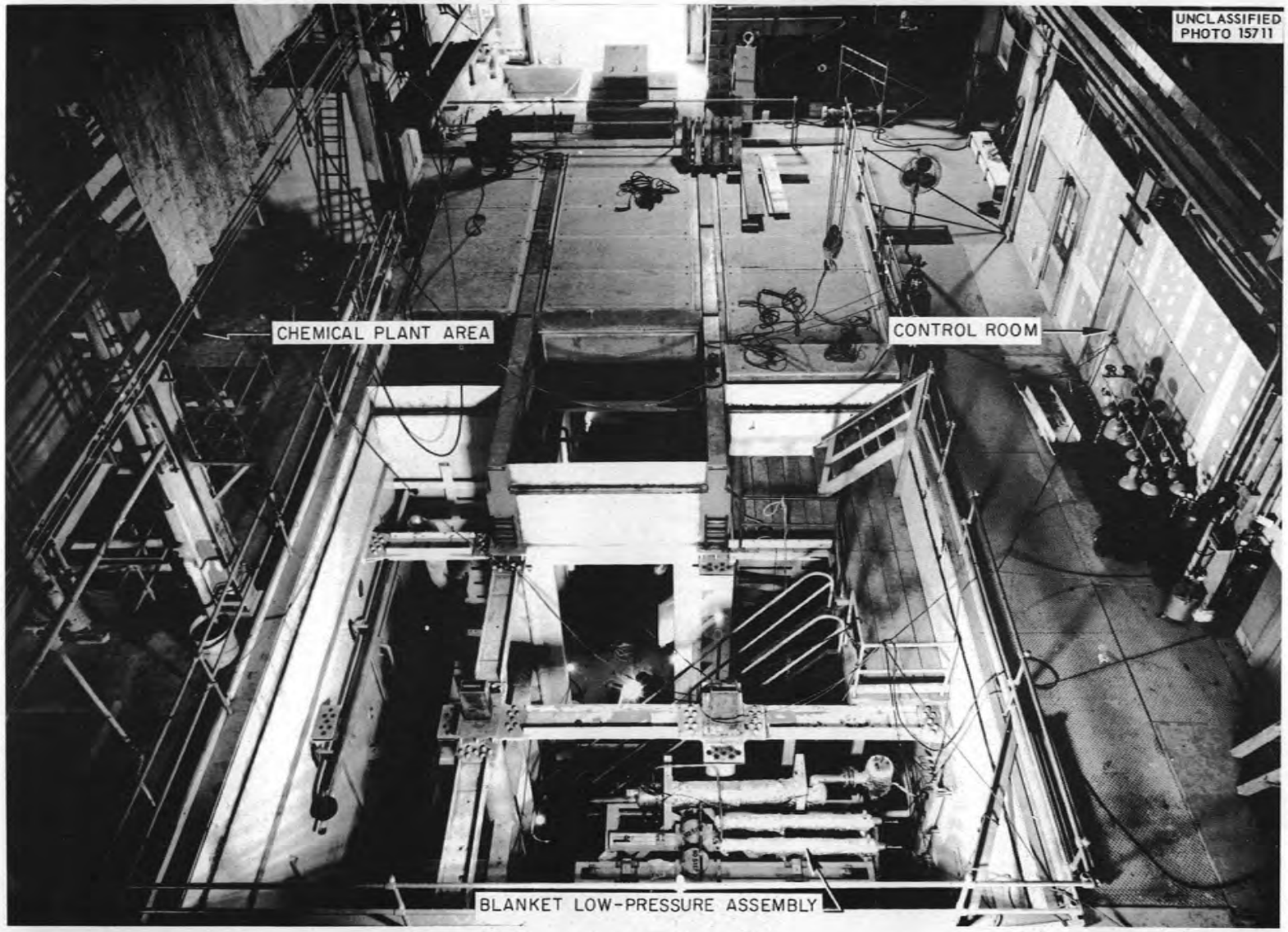

Fig. 1.2. Photo of Reactor Cell Showing Reactor Parts in Position.

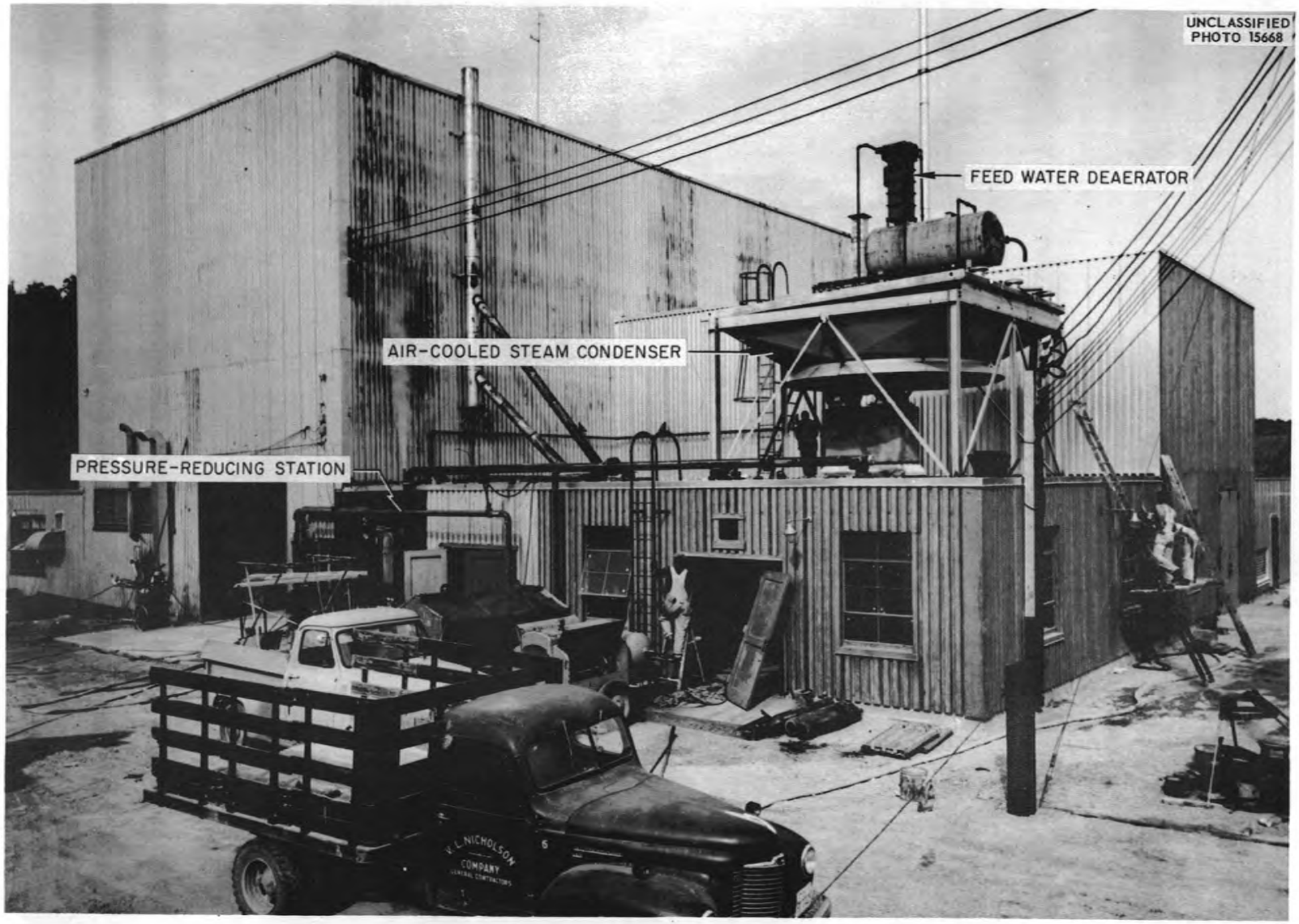

Fig. 1.3. Outside Steam System, Viewed from Southwest Corner of Area.

1.2 OPERATIONS TRAINING

J. W. Hill, Jr.

R. E. Brooksbank	B. H. Hamling
W. D. Burch	R. W. Jurgensen
N. W. Curtis	J. O. Kolb
J. R. Engel	J. D. Perret
J. L. Gory	H. K. Search

H. E. Williamson

A training program for HRT operating personnel was begun on October 17, 1955. The first three weeks of this program were devoted to study of all phases of reactor operations with lectures by members from various groups in the HRP. During the next three months small groups of trainees will gain experience at the following locations: HRT equipment mockup, out-of-pile corrosion test loops, in-pile corrosion loops, chemical processing equipment for reactor fuel, HRT site, Low-Intensity Test Reactor, and Bulk Shielding Facility. After February 1, 1956, the trainees will perform test work at the HRT site, assist in training technicians for the operating staff, and prepare portions of an operating manual.

2. DESIGN

W. R. Gall

R. H. Chapman
C. J. Claffey
H. N. Culver[1]
R. W. Jurgensen[2]
J. E. Kuster[3]
M. C. Lawrence[4]
M. I. Lundin
T. H. Mauney
R. G. McGrath[5]
C. Michelson[1]
R. C. Robertson
J. N. Robinson
C. L. Segaser
W. F. Taylor[6]
W. Terry
T. H. Thomas

2.1 GENERAL STATUS OF DESIGN

During this quarter HRT drawings were approved for construction of the following: leak-detector system, heat exchanger blast shield, refrigeration piping and equipment installation, and reactor thermal shield.

Calculations were completed on cooling requirements of the thermal shield, gas production in the storage tanks, and space-cooler heat loads.

The design work required for construction of the HRT is approximately 90% complete.

Hydrostatic and air-pressure tests of the cell tank were completed; the tests showed that the tank can withstand 30 psi internal gas pressure without exceeding the yield strength of its members.

2.2 THERMAL SHIELD

The reactor core and pressure-vessel assembly is surrounded by a 2-ft-thick cylindrical shield, in order to reduce the thermal-neutron flux in other sections of the cell.

A closed cooling-water circuit, shown schematically in Fig. 2.1, was designed for this thermal shield to maintain the temperature of the shielding material (barytes-aggregate–water mixture) below 180°F, the saturation temperature of water at the 7.5-psia cell pressure. At this temperature, there is no excessive loss of water from the shield. The closed cooling-water circuit is required to prevent leaching of soluble boron, which is added to the mixture as a colemanite ore.

[1]On loan from TVA.

[2]On loan from American Gas and Electric Company.

[3]On loan from Maxon Construction Co.

[4]On loan from General Dynamics Corp.

[5]On loan from Westinghouse Electric Corporation.

[6]On loan from Pioneer Service & Engineering Co.

At 10-Mw reactor core power, heat will be generated in the thermal shield in the following amounts:

	D_2O Reflector Heat (kw)	UO_2SO_4 Blanket Heat (kw)
Top shield	3.1	8.8
Side shield	8.2	18.0
Bottom shield	1.5	3.2
Total	12.8	30.0

Volumetric heat generation rates were calculated to range between 100 and 1000 Btu/ft^3/hr.

The cylindrical approximation method[7] was used in making the temperature-difference calculations required to specify the diameter and spacing of the cooling-water passages. As determined by this method, the maximum temperature difference between the surface of the coolant passage and the shield constituents is

$$(T - T_0)_{max} = \frac{Q}{4K}\left[\beta^2 \ln\left(\frac{\beta}{a}\right) + a^2 - \beta^2\right] ,$$

where

T = temperature of shield, °F,

T_0 = temperature at coolant-passage wall, °F,

Q = rate of heat generation per unit solid volume, Btu/ft^3,

K = thermal conductivity of shield constituents, Btu/hr·ft^2·°F,

β = radius of adiabatic cylinder equal to one-half the coolant pipe spacing, ft,

a = radius of coolant passage, ft.

[7]F. A. Fend, E. M. Baroody, and J. C. Bell, *An Approximate Calculation of the Temperature Distribution Surrounding Coolant Holes in a Heat-Generating Solid*, BMI-T-42 (Oct. 25, 1950).

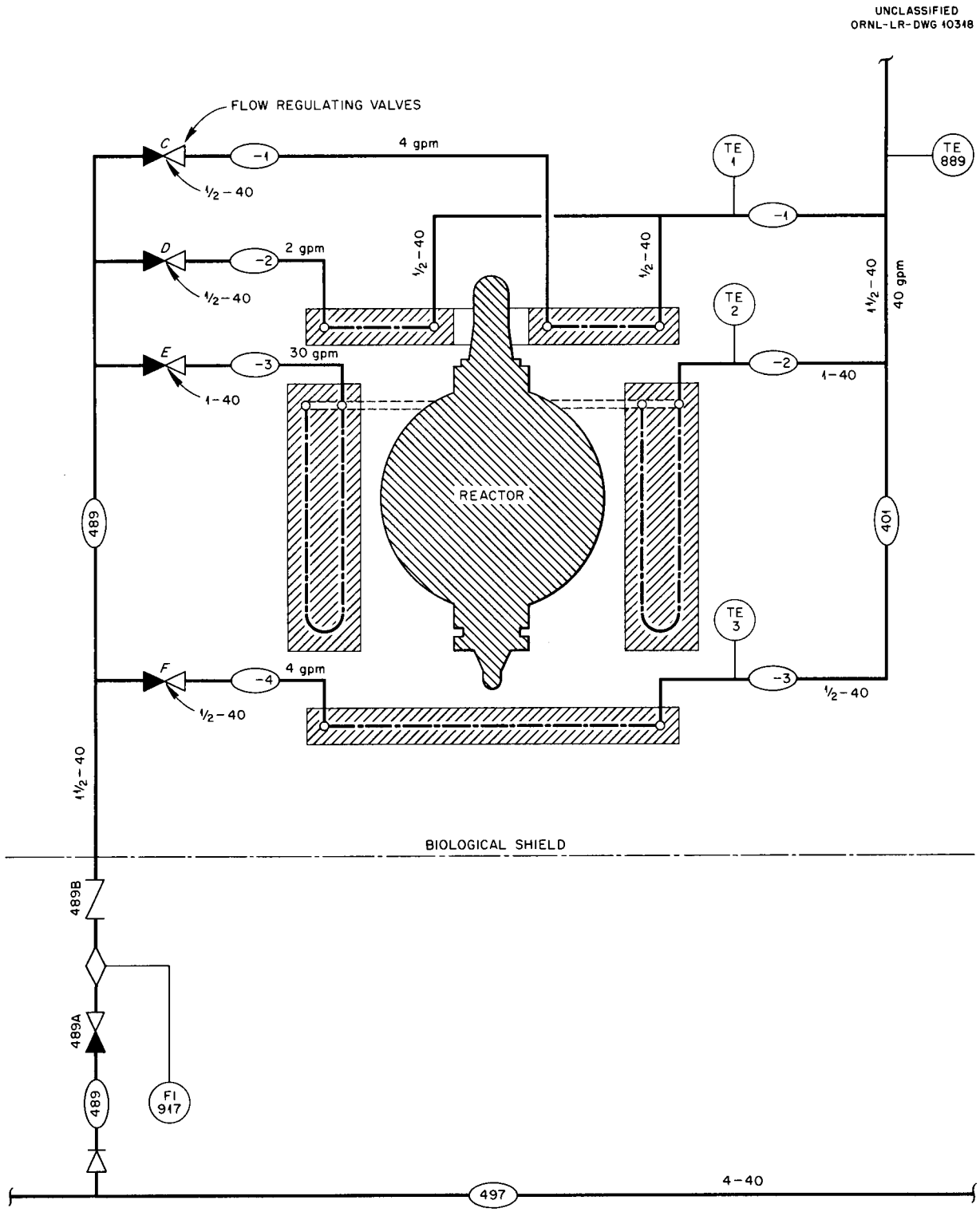

Fig. 2.1. Thermal-Shield Coolant Distribution and Control.

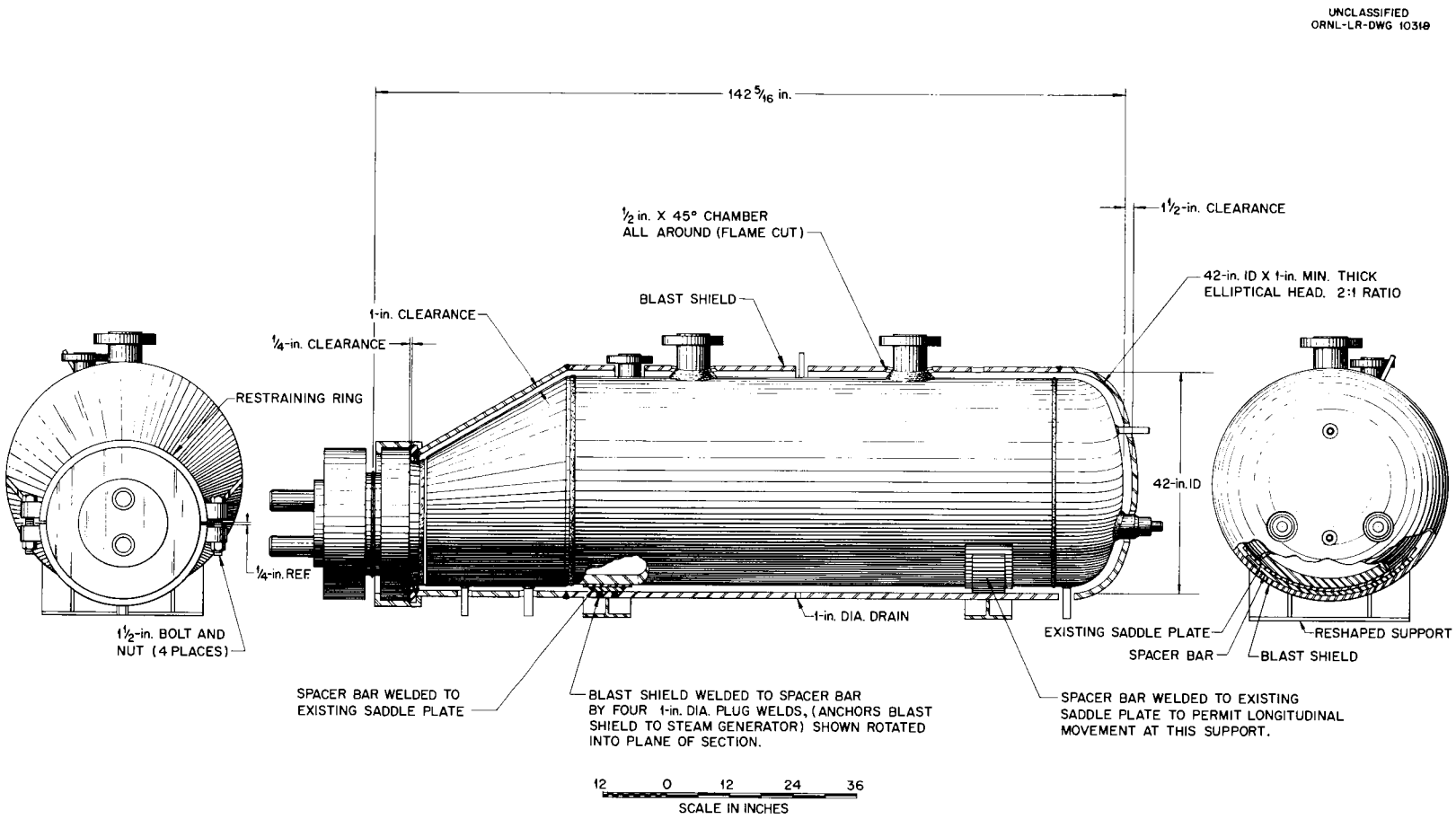

Fig. 2.2. Blast Shield for HRT Steam Generator.

The thermal conductivities of the barytes-aggregate–water mixture, specified for the side and bottom shields, and of the steel-shot–water mixture, specified for the top shield, were calculated from empirical relationships[8] to be 0.7 and 2 Btu/hr·ft^2(°F/ft), respectively. Pipe sizes and spacing specified for the shields were the following:

Side shield	$\frac{3}{8}$-in. pipes at ~12-in. intervals
Bottom shield	$\frac{1}{4}$-in. pipes at 13- to 17-in. intervals
Top shield	$\frac{1}{4}$-in. pipes at 8- to 15-in. intervals

Although this system should keep the shield mixture below 180°F, a fill-and-vent system has been designed to replace water lost from the shield by evaporation and radiolytic decomposition.

2.3 HEAT EXCHANGER BLAST SHIELD

Blast shields are being installed around the heat exchangers as protection in the event of a fracture of the vessel wall, which is a very remote possibility. Such a failure could damage the seal on the reactor cell. A report[9] was prepared describing the design basis and calculations for these shields. The final design, Fig. 2.2, consists of a 1-in.-thick carbon steel shell surrounding the heat exchanger vessel with an average 1-in. annulus between the blast shield and heat exchanger. The blast shield was calculated to be capable of absorbing approximately 30 × 10^6 ft-lb of energy at rupture. The energy released by the heat exchanger shell was estimated to be about 3 × 10^6 ft-lb, assuming an efficiency of energy transfer from fluid to the shell of 1.5%.

2.4 FREEZE UNITS

Freeze units are to be used in the Homogeneous Reactor Test to isolate parts of the system by freezing plugs of ice in the process lines.

The mechanical and thermodynamic designs of prototype units for both permanent and temporary use on the process piping were prepared. Detail drawings for the three sizes to be tested were completed. Results of the calculations are summarized in Table 2.1, and drawings of the temporary and permanent freeze units are shown in Figs. 2.3 and 2.4.

2.5 REFRIGERATION SYSTEM

Refrigeration is required in the cold traps, which remove D_2O vapor from the off-gas stream, and in freeze units, which seal off process lines with ice plugs.

[8] W. H. McAdams, *Heat Transmission*, 3d ed., p 290, McGraw-Hill, New York, 1954.

[9] C. L. Segaser, *A Study of Design Criteria for a Proposed HRT Heat Exchanger Blast Shield*, ORNL CF-55-7-84 (July 25, 1955).

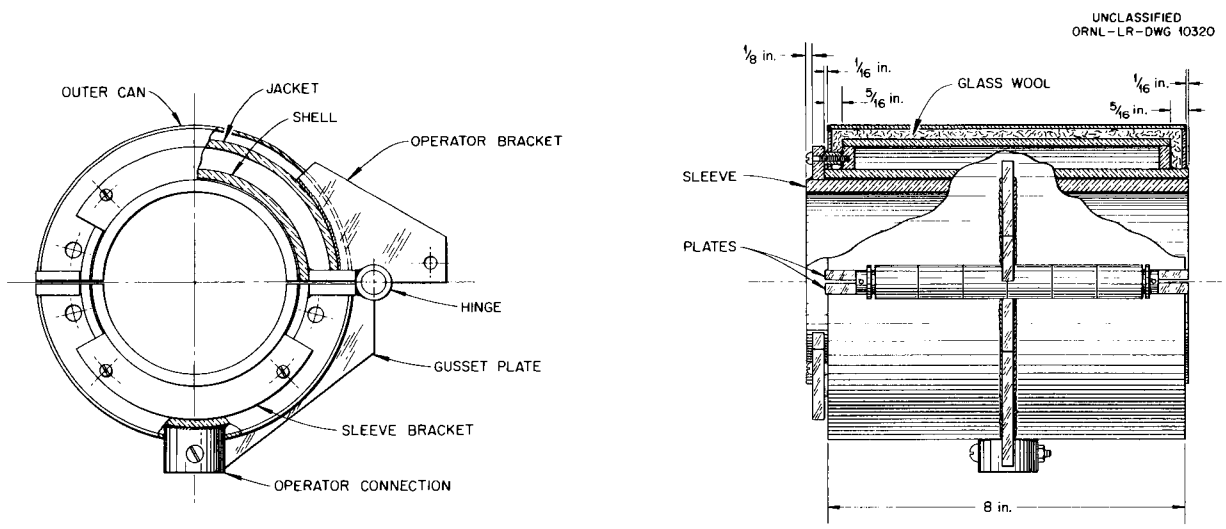

Fig. 2.3. Temporary Freeze Unit.

TABLE 2.1. SUMMARY OF REFRIGERATION LOADS AND TIME REQUIRED TO FREEZE TO CLOSURE

Line Size (in.)	Wall Thickness		Heat Removed in Freezing (Btu)	Average Freezing Heat Load (Btu/hr)	Heat Gain Along Pipe, Both Ends (Btu/hr)	Heat Gain Through Insulation (Btu/hr)	Maximum Heat Flux (Btu/hr)	Time Required to Freeze (min)
	Schedule No.	Inch						
Temporary-Type Freeze Units, Freon-22 Refrigerant								
4	40		1048	533	293	151	977	118
4		0.5	792	523	396	151	1070	91
3½		0.469	603	518	356	151	1025	70
3	40		609	522	219	107	848	70
2		0.312	141	172	175	52	399	49
1½	80		103	347	118	52	517	18
1	40		30	189	64	28	281	10
1	80		25	192	75	28	295	7.8
¾	40		18	178	46	28	252	6.1
½	40		10	167	36	28	231	3.6
½	80		8	170	42	28	240	2.8
¼	80		2.5	167	24	28	219	0.9
⅛	80		1.3	163	15	28	206	0.5
Permanent-Type Freeze Units, Freon-11 Refrigerant								
½	40		12	214	38	10	262	3.4
½	80		9.5	216	44	10	270	2.6
¼	80		2.9	181	23	8	212	0.9

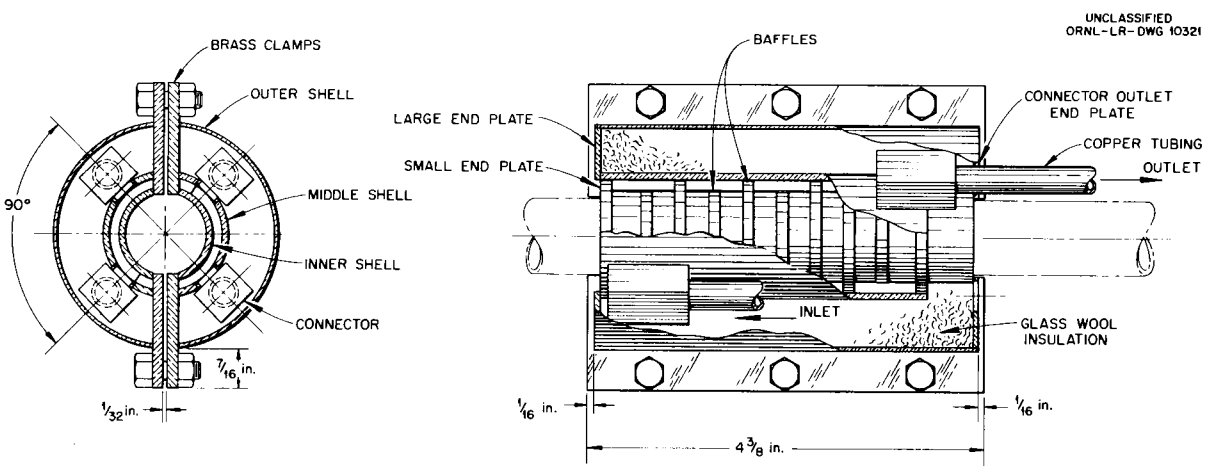

Fig. 2.4. Permanent Freeze Unit.

The primary compression refrigeration system uses Freon-12 as the refrigerant. This system cools a secondary liquid coolant which is circulated by pumps through the units to be cooled. Defrosting is accomplished by circulating warming liquid through a heating tank and then through the cooling units. The chilling and defrosting phases are alternated by an arrangement of solenoid valves and a programming clock. This system was selected because the liquid-coolant system offers a greater choice of coolants, affords greater reliability of equipment located inside the reactor cell, and simplifies the control of defrosting.

In the primary refrigeration system is a two-stage 5-hp Brunner compressor with a water-cooled shell-and-tube condenser. Downstream from the condenser is a flash tank operated at the interstage pressure to subcool the liquid F-12. The F-12 evaporator is a 1-in. pipe coil located in a 100-gal chiller and storage tank for the secondary coolant, which has been tentatively specified as Freon-11. Two 10-gpm pumps, equipped with mechanical seals and designed for service at −25°F are provided for circulating the F-11. The tank for storage and warming of the F-11 for defrosting is a conventional 55-gal electric hot water heater.

The refrigeration equipment, with valves and controls, is located in the control area and arranged to supply the blanket and fuel systems separately. The refrigerant lines in this area are insulated with block cork in the standard manner. However, the shield penetrations and lines inside the cell are "canned," either 2, 4, or 6 lines to a can, in $6\frac{5}{8}$-in.-OD 16-gage galvanized sheet metal cans with solder joints, packed with granulated cork and tested to 15 psi air pressure, Fig. 2.5. The cans are designed to permit operation of the refrigeration system, when the cell is flooded, without ice formation on the lines or water damage to the insulation.

There is evidence of radiation damage to Freons; this may release corrosive products.[10] Experimental work has been initiated to determine the extent and type of damage in conditions simulating those in the cold traps. Depending on the outcome of these experiments, it may be necessary to specify another liquid instead of F-11 for use in the secondary refrigerant system.

[10] C. Michelson, *Radiation Damage to Freon*, ORNL CF-55-9-163 (Sept. 30, 1955).

2.6 DISSOCIATION OF D_2O IN STORAGE TANKS

The fuel and blanket storage tanks are to be used to isolate solutions after the reactor has been shut down for a period of 1 hr. Energy released in the solutions will be in the form of gamma- and beta-decay energy for which $G = 0.4$ molecule produced per 100 ev of energy absorbed. For a fuel solution operated at a reactor power of 5 Mw, the pounds of D_2O dissociated, W, is given by

$$W = 0.021(t^{0.8} - 26.5) ,$$

where t = time after shutdown in minutes (less 60 min).

Using this formula, the value of the D_2O that would be dissociated the first day of storage would be approximately $200, assuming a cost of $28 per pound. Even at this maximum rate of loss, the recombination and recovery of the gas is not economical at the present time. Although efforts will be continued to find a simple, low-cost system for recovering this gas in future installations, the gas from the HRT will be diluted and then be discharged by the stack fan.

2.7 SPACE-COOLER HEAT LOADS

Air within the reactor shield will be cooled by four coolers, each consisting of finned water tubes and a blower for circulating air across the tubes. Water from the process-water supply system will flow through the tubes and will be discharged into the return line to the cooling tower. Each cooler is capable of removing 170,000 Btu/hr with inlet air at 150°F and inlet water at 75°F.

A summary from another report[11] of the estimated heat load for the four cooler units at a reactor power of 10 Mw is given below. These estimates are based on the use of aluminum-foil insulation[12] with an insulating efficiency of 90%, as compared to bare-metal heat losses.

[11] F. C. Zapp, *HRT Space Cooler Heat Load*, ORNL CF-55-10-17 (Oct. 5, 1955).

[12] F. C. Zapp, *HRT Aluminum Insulation (Within Cell)*, ORNL CF-55-9-36 (Sept. 7, 1955).

Structures Producing Heat	Heat Removed (Btu/hr)
High-pressure equipment and piping	116,000
Low-pressure equipment and piping	12,000
Cell walls and structure	260,000
Blast shield	10,000
Thermal shield	12,000
Pipe flanges (bare)	268,000
Total	678,000

Capacity of 4 coolers at 170,000 Btu/hr each = 680,000 Btu/hr

Normally, the reactor power will be only 5 Mw, which requires approximately 130,000 Btu/hr less heat removal. However, in view of the possibility of operation at 10 Mw for more than a few hours at a time and the narrow margin of safety at this power level, a study is being made of the possibility of insulating the flanges; if insulation is feasible, the load will be reduced approximately 200,000 Btu/hr.

2.8 LEAK-DETECTION SYSTEM

The HRT leak-detection system is designed to detect leakage in flanged joints and in valve bellows

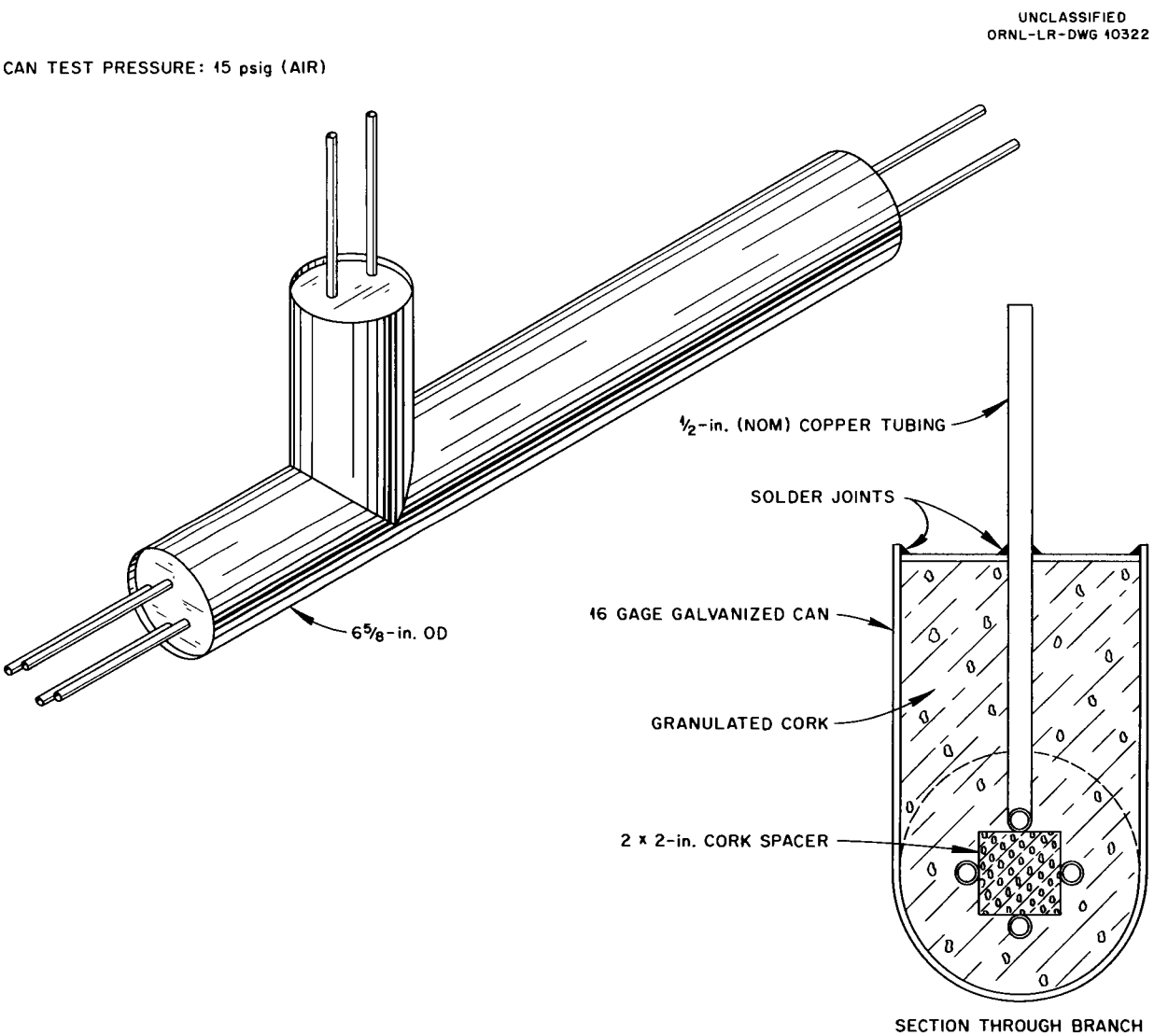

Fig. 2.5. Typical Canned Refrigeration Lines Inside Cell.

and to prevent escape of the leakage from the system. It also serves, when joints are being tightened remotely, as a means of determining when a seal is obtained. The system, as shown in Figs. 2.6 and 2.7, is essentially the same as that used in the HRE.[13]

Under a pressure approximately 500 psi greater than that in the reactor system, D_2O is supplied to the sealed annuli which are formed in the gasket grooves by the stainless steel oval section ring gasket when it is properly seated. Four separate systems of this type are provided, two at 2500 psi for fuel and blanket high pressure and two at 500 psi for the low-pressure joints.

A hole ($\frac{1}{8}$-in. dia) is drilled through one flange at each pipe joint to the annulus of the V-joint. The oval ring gasket is also drilled ($\frac{1}{8}$-in. dia) to interconnect the annuli of the two flanges, as shown in Fig. 2.7. Thick-walled $\frac{1}{4}$-in.-OD stainless steel tubing connects each flange pair with a header in the control area.

The individual systems are divided into sections to expedite the search for a flange leak. Each system has a pressure gage and a low-pressure alarm.

A common pressurizing vessel, supplied with oxygen at 3000 psig, is connected to the four leak-detection systems.

[13] C. E. Winters *et al.*, *HRP Quar. Prog. Rep. May 15, 1951*, ORNL-1057, pp 16, 20, 21.

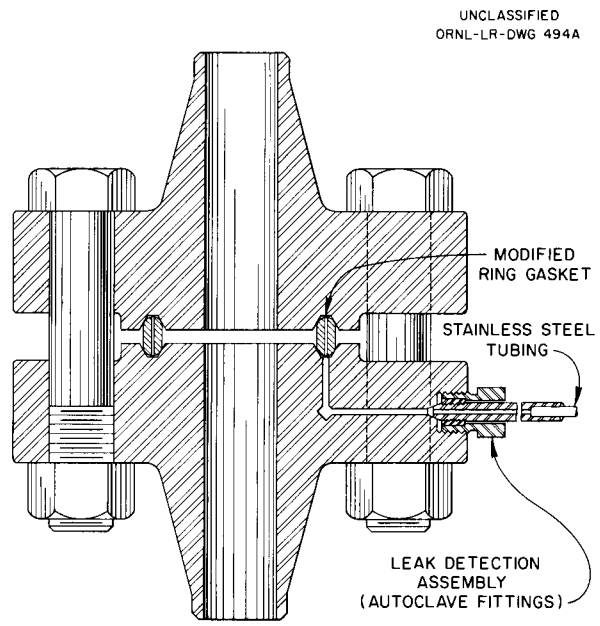

Fig. 2.7. Ring-Joint-Flange Leak Detector.

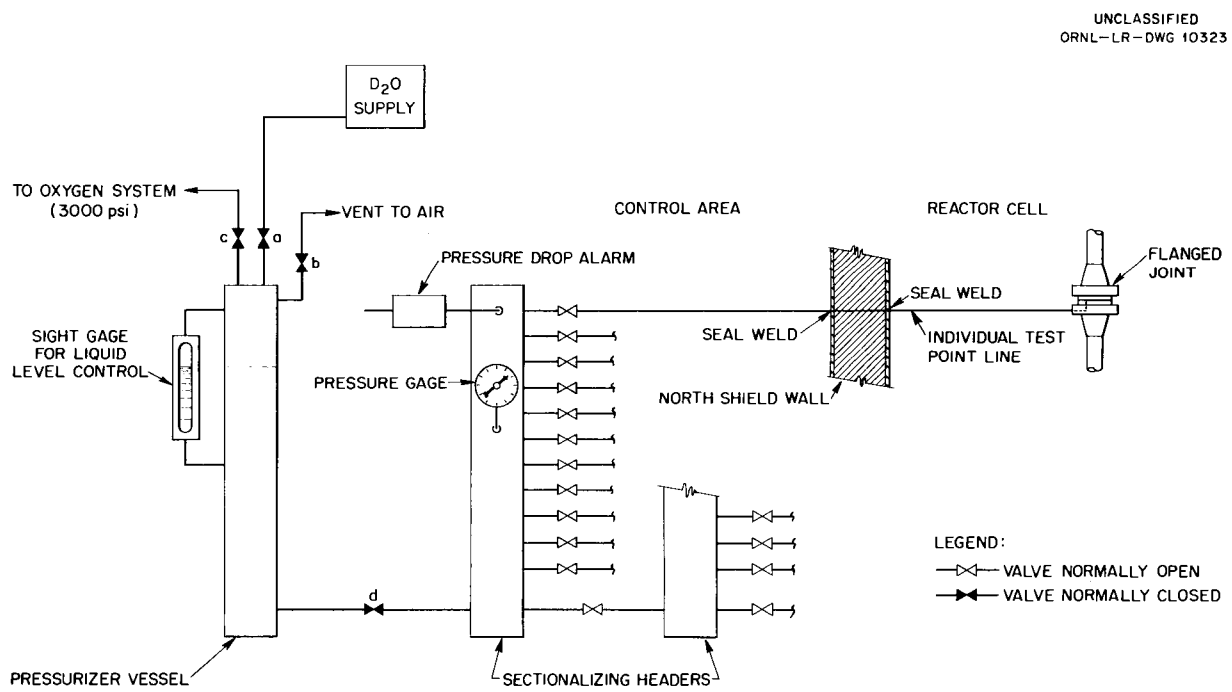

Fig. 2.6. Schematic Diagram of Leak-Detector System.

All the valves are 6000-psi bar-stock stainless steel needle valves, connected with compression-type fittings. Valves are mounted to provide easy access for maintenance and operation.

2.9 PRESSURE TEST OF SHIELD TANK

In the event of a reactor accident in which all the hot high-pressure liquid in the reactor circulating systems and steam systems is emptied into the shield tank, a pressure of 30 psig might result. A pressure test of the HRT shield tank was conducted to prove that the cell is capable of containing this pressure.

The HRT cell was originally designed for an internal pressure of 15 psig with maximum stresses of 20,000 psi in the steel members. Since a test to 30 psig involved stresses which would possibly exceed the yield strength of the material, an air-pressure test was considered to be too hazardous. Consequently, it was decided to fill the cell with water and apply hydrostatic overpressure, although such a test does not completely simulate the conditions described above.

It was anticipated that the cell would adjust itself to the load during the test and, in so doing, would experience local yielding. However, it was desired to keep the general stress level below the yield point of the material. The lowest yield strength indicated by mill test reports was 34,960 psi. Two tensile specimens, taken from the cell wall and tested, showed the lower yield point to be about 91% (~31,800 psi) of the upper yield point. It was decided to permit steel stresses, both in tension and compression, to go to values near 32,000 psi.

The cell was instrumented with 80 strain gages located to indicate the stress at salient points in the north wall structure, which is the weakest portion of the cell. Two extensometers, consisting of waterproofed linear differential transformers, were used to measure the relative movement of opposite walls of the cell and to indicate whether the backfill concrete was supporting the east and west wall as had been assumed.

During the first phase of the test, the cell was filled with water and subjected to an overpressure of 10 psig. At this point it became evident that certain members would not be able to resist the stresses that would be expected at 30 psig and would have to be modified for the test to continue. The modification consisted of reinforcing 78 truss members and stiffening an 8 × 54 ft section of $\frac{5}{8}$-in. plate with channel bars.

Upon completion of the modifications, the test was resumed and the cell was successfully subjected to an overpressure of 26 psig, with a pressure of 36 psig at the bottom. The data taken during this run can be extrapolated to show that the cell is capable of containing a uniform gas pressure of 30 psig.

After the cell was drained, it was subjected to an air-pressure test of 15 psig to confirm that the data from a uniform loading by gas pressure paralleled the data from hydrostatic overpressure.

3. REACTOR COMPONENT DEVELOPMENT

C. B. Graham

L. J. Bell
R. Blumberg
J. S. Culver
K. E. Estes
H. L. Falkenberry[1]
C. H. Gabbard
L. F. Goode
B. A. Hannaford
P. H. Harley
P. F. Pasqua[2]
W. L. Ross
I. Spiewak
D. S. Toomb
H. D. Wills
W. B. Wilson

3.1 PUMP DEVELOPMENT

Tests of Westinghouse canned-rotor pumps 400A, 400B, 300A, and 230A continued during this period. General problems in the 400A, 230A, and 400B pump loops are discussed here; experience with the 300A HRT mockup pump is reported in Sec. 3.6.

3.1.1 400A Pump and Loop

The 400A pump was modified to use the new Westinghouse hollow thermal barrier. Temperatures behind the new thermal barrier were below 100°C; temperatures prior to the conversion had been as high as 180°C. After modification, the pump was run for 920 hr at approximately 285°C with a solution of approximately 0.04 *m* UO_2SO_4, 0.005 *m* $CuSO_4$, and 50 mole % excess H_2SO_4. Ionic concentrations during the run are shown in Fig. 3.1. The oxygen concentration was held at 400 ppm. This pump and its loop have been in operation for over 4200 hr as follows: approximately 600 hr on 0.04 *m* UO_2SO_4 with 10 mole % excess H_2SO_4; 2030 hr on 0.12 *m* UO_2SO_4 with 10 mole % excess H_2SO_4; 1080 hr on 0.04 *m* UO_2SO_4 with 50 mole % excess H_2SO_4; and the remaining time on water. The loop[3] and the early operation were described in detail previously.[4–6]

At the end of the run with the new thermal barrier, both the loop and the pump were dismantled for inspection. The loop, which had not been examined thoroughly since operation began, was in excellent condition with no observed excessive corrosion or pitting. Figure 3.2 shows three type 347 stainless steel orifice plates which were in the loop. Figure 3.3 shows a flange, weld joint, and pipe which were downstream from an orifice through which the flow had a velocity of 50 fps.

The pump was in good condition with the exception of the thermal barrier. The thermal-barrier hollow metallic O-ring was corroded at one place. The O-ring seating and adjacent surfaces were badly pitted. Some corrosion was evident in the case wear-ring section of the thermal barrier. This has been typical of these pumps. Photographs (Figs. 3.4 and 3.5) show the corrosion on the thermal barrier and motor ends of the pump. Figure 3.6 shows no excessive corrosion on the suction or front side of the impeller, although Fig. 3.7 shows some corrosion on the back hub of the impeller. This corrosion was observed following the 0.12 *m* UO_2SO_4 runs. Figure 3.8 shows no corrosion on the pump volute, front wearing ring, or diffuser. A break in the gold plate on the inner edge of the stainless steel gasket can be seen; however, no leakage was observed across the gasket.

3.1.2 230A Pump and Loop

The 230A pump was run on thorium oxide slurry which had a concentration of 1000 g of thorium per kilogram of water, and then the pump was removed from the loop for installation in the slurry mockup.

The slurry runs were unsuccessful in maintaining constant slurry concentrations, particularly at the beginning of each run. Plugged pressurizer lines, piping partially filled with slurry, plugged impeller balance ports, and erratic backwater injection rates were some of the difficulties encountered during the first run. The second thoria run, which lasted for a week, was made with a different batch of slurry. The concentration had decreased to 690 g of thorium per kilogram of water by the end of the run, as shown in Fig. 3.9. The water-injection rate to the back of the pump was limited to $\frac{1}{3}$ to $\frac{1}{2}$ gph by the pressure control system.

---

[1] On loan from TVA.

[2] Consultant.

[3] W. L. Ross *et al.*, *HRP Quar. Prog. Rep., July 31, 1954*, ORNL-1772, p 36.

[4] C. B. Graham *et al.*, *HRP Quar. Prog. Rep., Jan. 31, 1955*, ORNL-1853, p 26–30.

[5] C. B. Graham *et al.*, *HRP Quar. Prog. Rep., April 30, 1955*, ORNL-1895, p 28.

[6] C. B. Graham *et al.*, *HRP Quar. Prog. Rep., July 31, 1955*, ORNL-1943, p 25.

[redacted]

ORNL-LR-DWG 10324

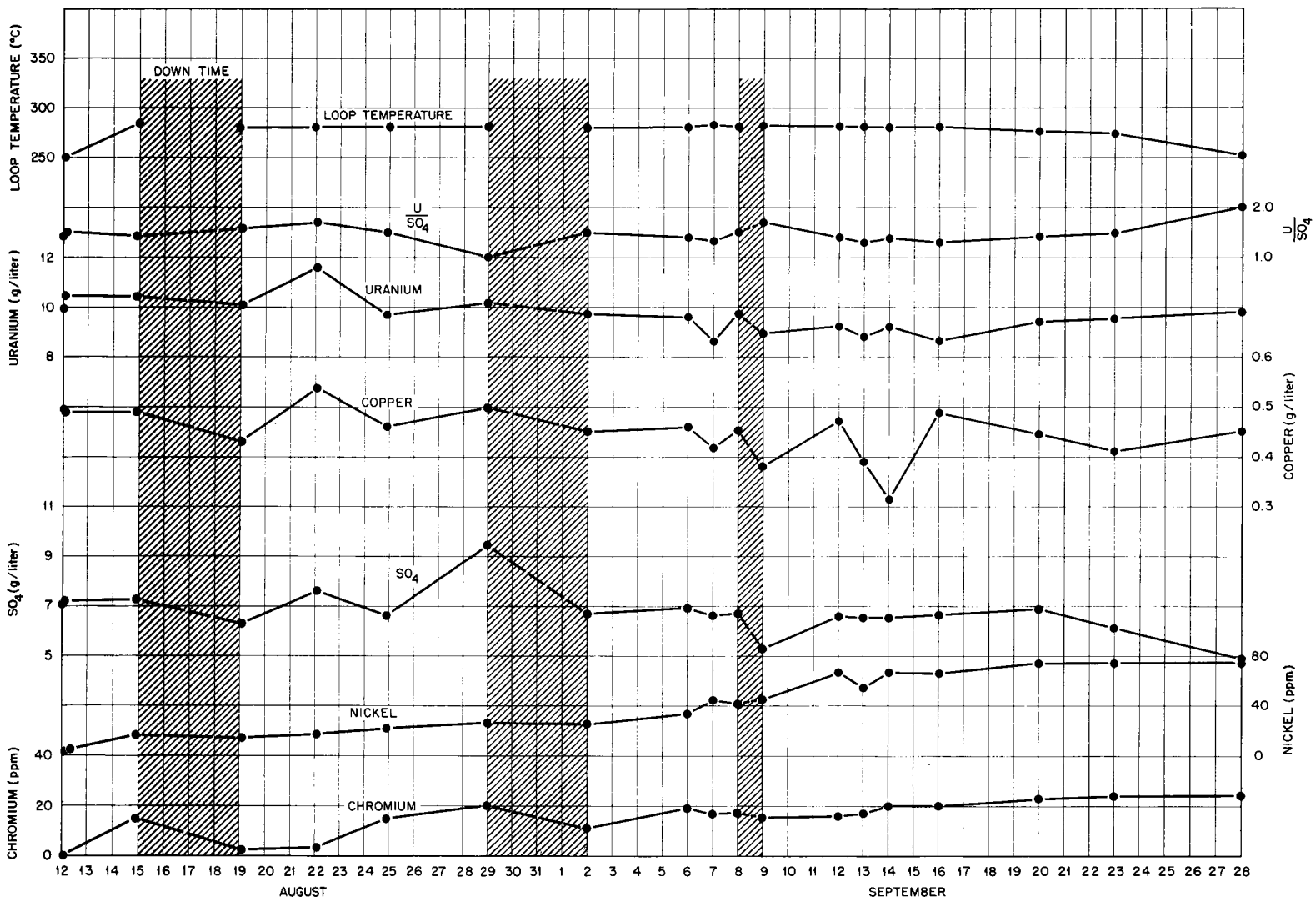

Fig. 3.1. 400A-Pump Test Loop.

UNCLASSIFIED
PHOTO 24824

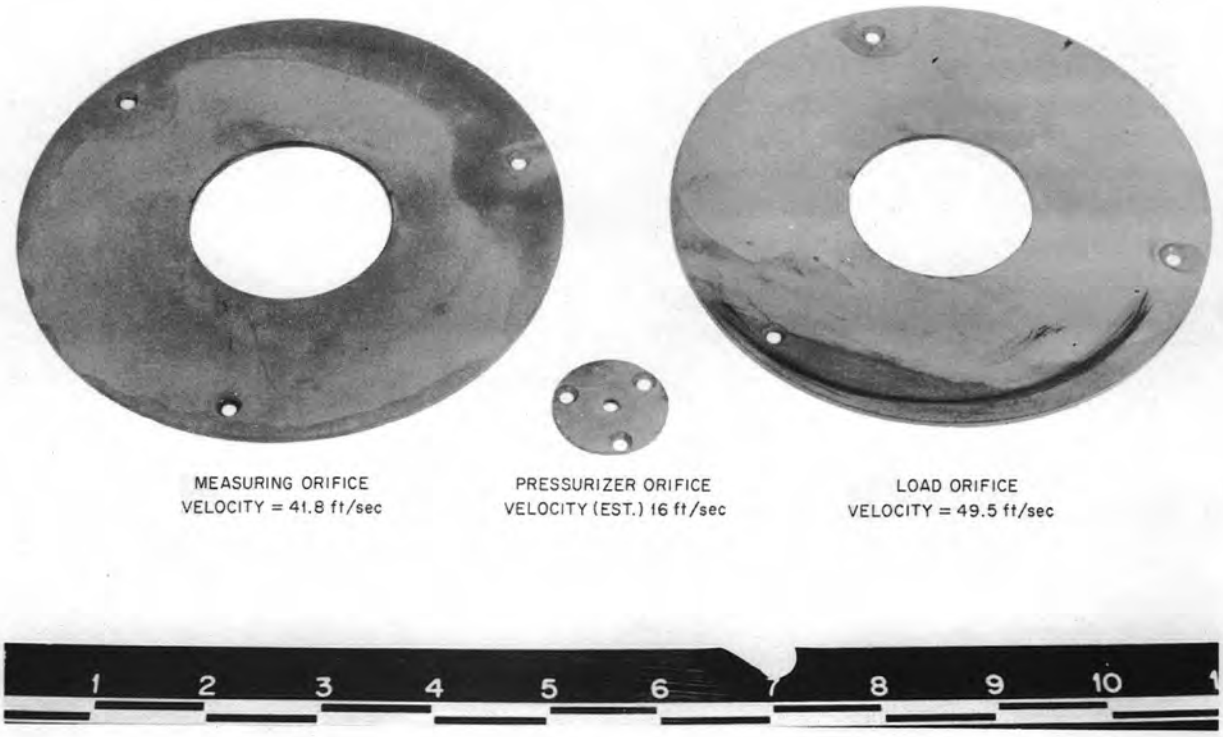

Fig. 3.2. Stainless Steel Orifice Plates from 400A Pump.

Fig. 3.3. Pipe Flange from 400A Loop.

No slurry caking or plugging of lines or impeller ports was observed when the pump and loop were disassembled after the second run; neither was excessive corrosion, erosion, or wear observed. Although some slurry was found in the back of the pump, the bearing surfaces appeared to be in good condition, with no measurable wear being observed. The pump has operated approximately 1100 hr on water and over 300 hr on thoria slurry. Photographs of the pump parts after 300 hr of slurry operation are shown in Figs. 3.10 and 3.11.

3.1.3 400B Pump and Loop

The 400B pump loop has been run on water only, prior to the installation of protective shields necessary for high-pressure operation. The system will undergo one water run at 250°C, and the pump will then be modified for use of the new Westinghouse thermal barrier.

Fig. 3.4. 400A-Pump Thermal Barrier.

3.2 FUEL AND BLANKET REACTOR PUMPS

There have been delays in delivery of the first two stainless steel HRT pumps. The 230-gpm pump failed during thermal-cycle tests and required repair. A journal bushing on the 400-gpm pump was found, during an inspection following its thermal-cycle tests, to have a small defect. After the bushing was replaced, the pump passed all tests and inspection and has been shipped to ORNL. The 230-gpm pump will be shipped early in November if performance tests are satisfactory.

Samples of titanium welding, submitted by Westinghouse and examined by ORNL, were found to be satisfactory for HRP requirements. The welding of titanium parts for the last two pumps has started.

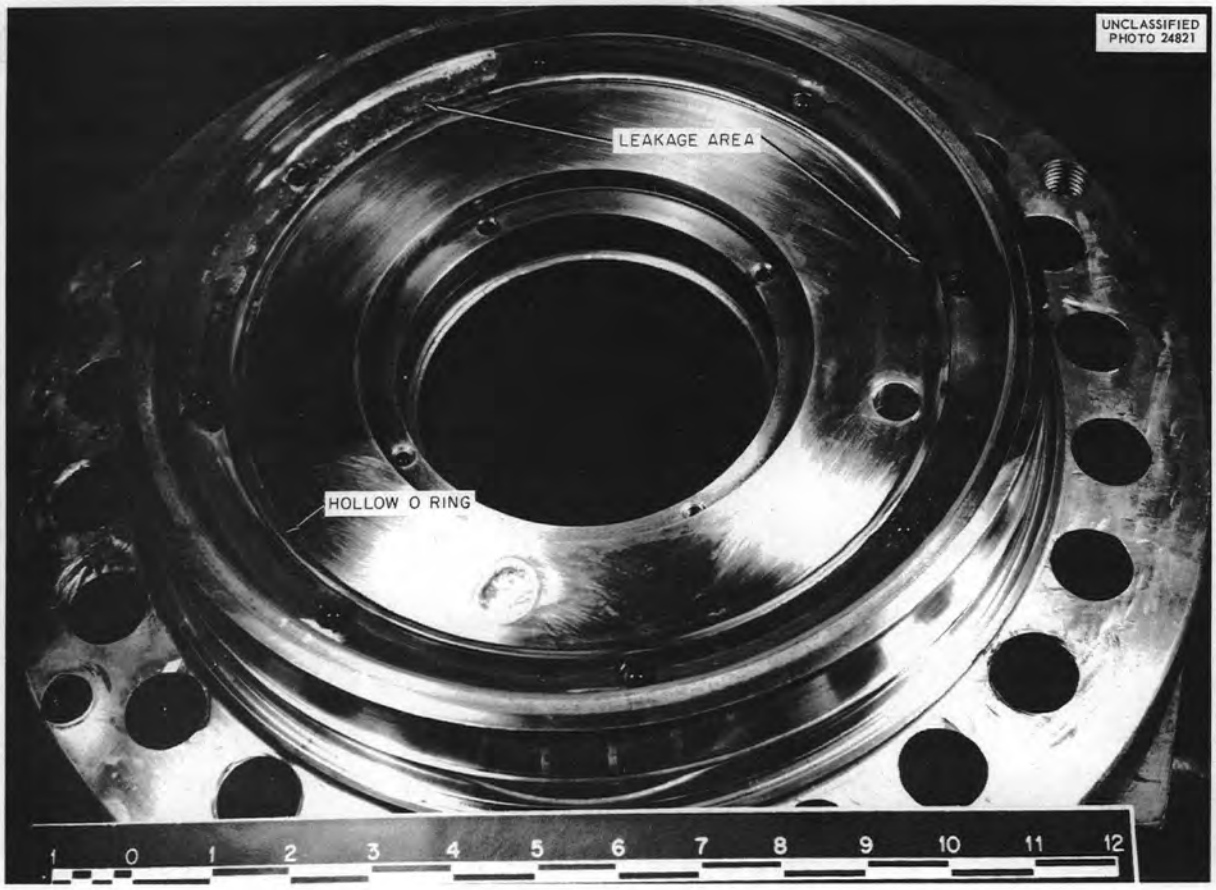

Fig. 3.5. 400A-Pump Motor End.

UNCLASSIFIED
PHOTO 24822

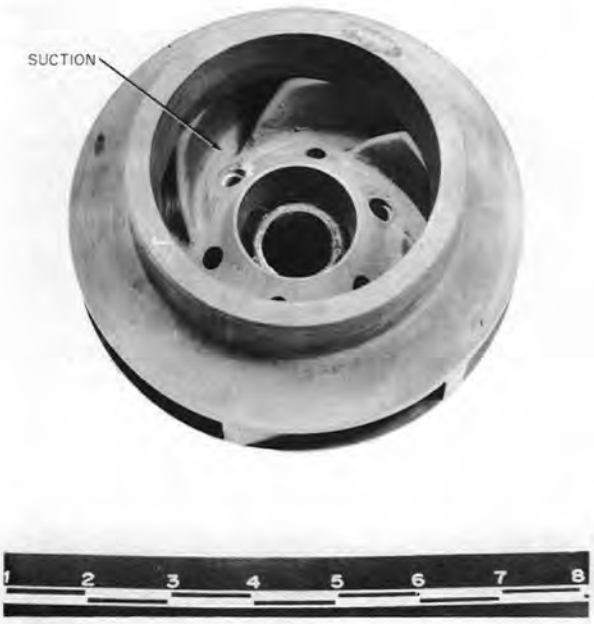

Fig. 3.6. 400A-Pump Impeller, Front Side.

UNCLASSIFIED
PHOTO 24823

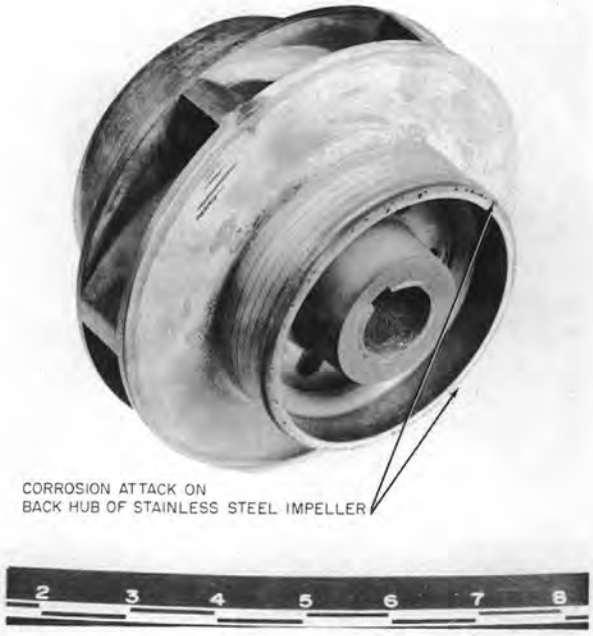

Fig. 3.7. 400A-Pump Impeller, Back Side.

3.3 HRT HEAT EXCHANGERS

Major fabrication of the two HRT heat exchangers was completed. Small leaks, which developed around the tube joints during the original thermal-cycle testing, were repaired and the units subjected to an additional ten cycles. If no additional leaks develop, the units will be subjected to a final cleaning and helium leak-testing.

Gasket leakage resulting from thermal cycling was stopped by using longer (more flexible) bolts, preheating the steam drum before cycling, and modifying the thermal-cycle specification. One unit was pressurized to 3750 psi after the thermal-cycle test before leakage was observed.

The Sarlun-type seal weld was fatigue-tested and found to be adequate. The only remaining difficulty is leakage across the pass-partition separating the inlet and outlet streams. Gold wire is being installed as a gasket to reduce the leakage at this point to an acceptable rate.

3.4 HRT DUMP TEST

A correlation has been found[7] which will predict the pressure-time curve for a reactor dump. The predicted curve closely approximates the results of the first HRT dump tests, in which the contents of a single-heated and pressurized vessel were dumped into a mockup of the HRT dump system.

The apparatus is nearly complete for the second phase of the dump test program, in which the contents of two concentric vessels simulating the core and blanket will be dumped simultaneously.

3.5 HRT DIAPHRAGM PUMP TESTING

The test model of the HRT purge pump has run for 1600 hr without trouble. Performance has been observed under varying conditions of inlet and outlet pressure, and the detailed results will be presented in a report to be issued soon.

A test to study the relation between pump and speed and output indicated that the most reliable operation was obtained with a motor driven at 850 rpm. Flow at 2000 psi is in excess of 15 gph.

A serious deficiency of the pump is its inability to restart at 2000 psi after becoming gas-bound. If continuity of purge is imperative in the reactor, a positive supply of condensate must be maintained, or, as an alternative, some means of venting

[7] P. F. Pasqua, *Report on Analysis of Data Obtained from the HRT Dump Test (Phase I)*, ORNL CF-55-10-14 (Oct. 6, 1955).

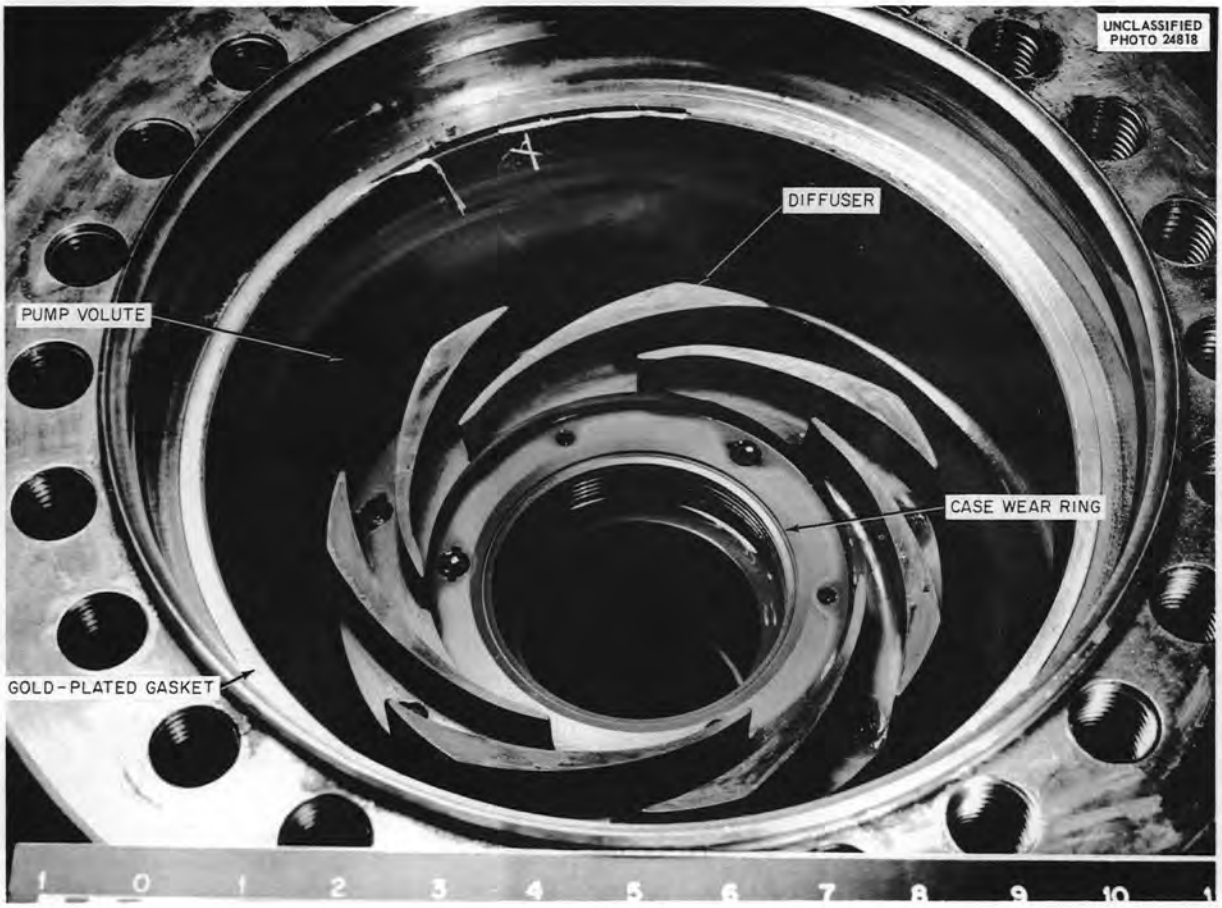

Fig. 3.8. 400A-Pump Volute.

the pump discharge must be supplied.

The major effort on the 1.5-gpm feed pumps has been on the HRT mockup pump. Here again, gas binding seems to be a problem. Operation in the mockup loop has not been so satisfactory as the original test results indicated,[8] since the pump occasionally fails to deliver the required flow or to operate continuously. The pump is under study for the cause of its erratic behavior to be ascertained.

3.6 HRT MOCKUP LOOP

Operation of the HRT mockup loop with water and three runs with UO_2SO_4 has been summarized previously.[9,10] In the past quarter the loop ran for 633 hr; 110 hr represented a continuous UO_2SO_4 run at 300°C and 2000 psi. The following equipment failures prevented longer continuous operation:

1. After modification of the Westinghouse 300A circulating pump to include the new thermal barrier and a gold-plated, flat, solid, stainless steel seal gasket, a new gasket leak appeared after several thermal cycles. When the pump was dismantled, it was noted that the gold plate had flaked from a large part of the gasket surface. An unplated gasket was substituted, but a leak showed again after two thermal cycles. The flange was retightened, and thermal insulation was removed. This appears to have eliminated the trouble.

[8] E. L. Youngblood, *Feed Pump Mockup*, ORNL CF-55-2-52 (Feb. 9, 1955).

[9] J. A. Hafford *et al.*, *HRP Quar. Prog. Rep., April 30, 1955*, ORNL-1895, p 33–37.

[10] C. B. Graham *et al.*, *HRP Quar. Prog. Rep., July 31, 1955*, ORNL-1943, p 28–31.

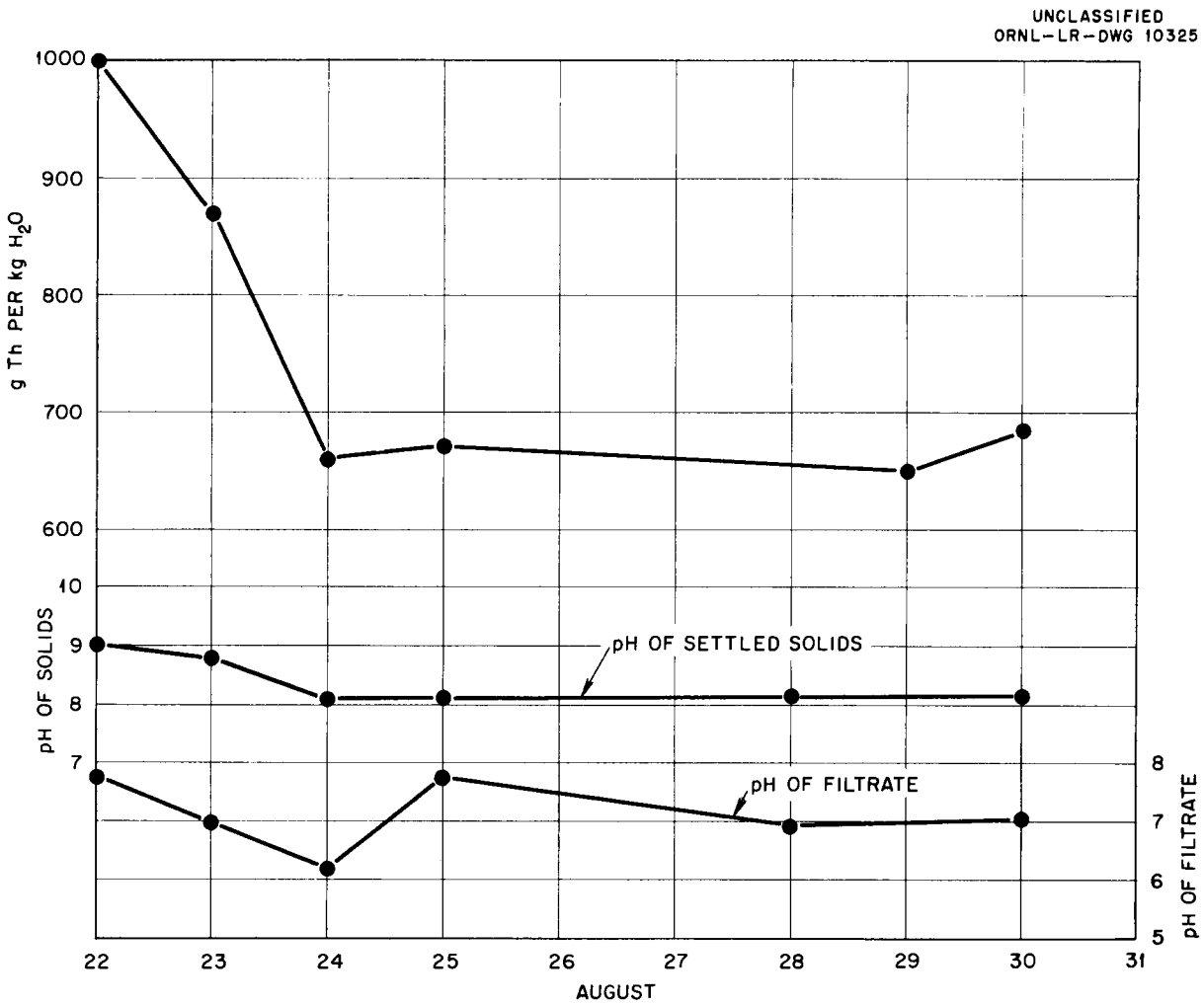

Fig. 3.9. Thorium Oxide Slurry Run, Westinghouse 230A-Pump Loop (August 22 to August 30, 1955).

2. The original Scott and Williams drive unit for the feed-pump heads was replaced by an HRT unit with a Denison variable-flow oil pump. Several rubber pulsators were ruptured during otherwise-normal operation of the feed pumps. Although several modifications were attempted, the trouble was not corrected until a new pumping head was installed. Later, a crack developed in a suction check-valve housing. The faulty valve has been replaced.

3. Leaks developed in two of the high-pressure stainless steel ring joint flanges after several thermal cycles. These leaks were caused by relaxation of the closure; that is, there was deformation in either the stainless steel flange, the stainless steel ring, or the low-alloy carbon steel bolts. These flanges were insulated, and, since they were in the vicinity of the pressurizer, they were slightly hotter than the other flanges in the system. The leaks were stopped by retightening of the joints, and did not reappear.

4. Numerous leaks appeared from time to time in tubing fittings, threaded joints, valve-bonnet joints, etc. Threaded joints have been back-welded where possible. Compression fittings, which were used originally, have been replaced with flare fittings for service in pulsating flow. The latter have the advantage that they can be retightened without interrupting loop operation.

UNCLASSIFIED
PHOTO 24720

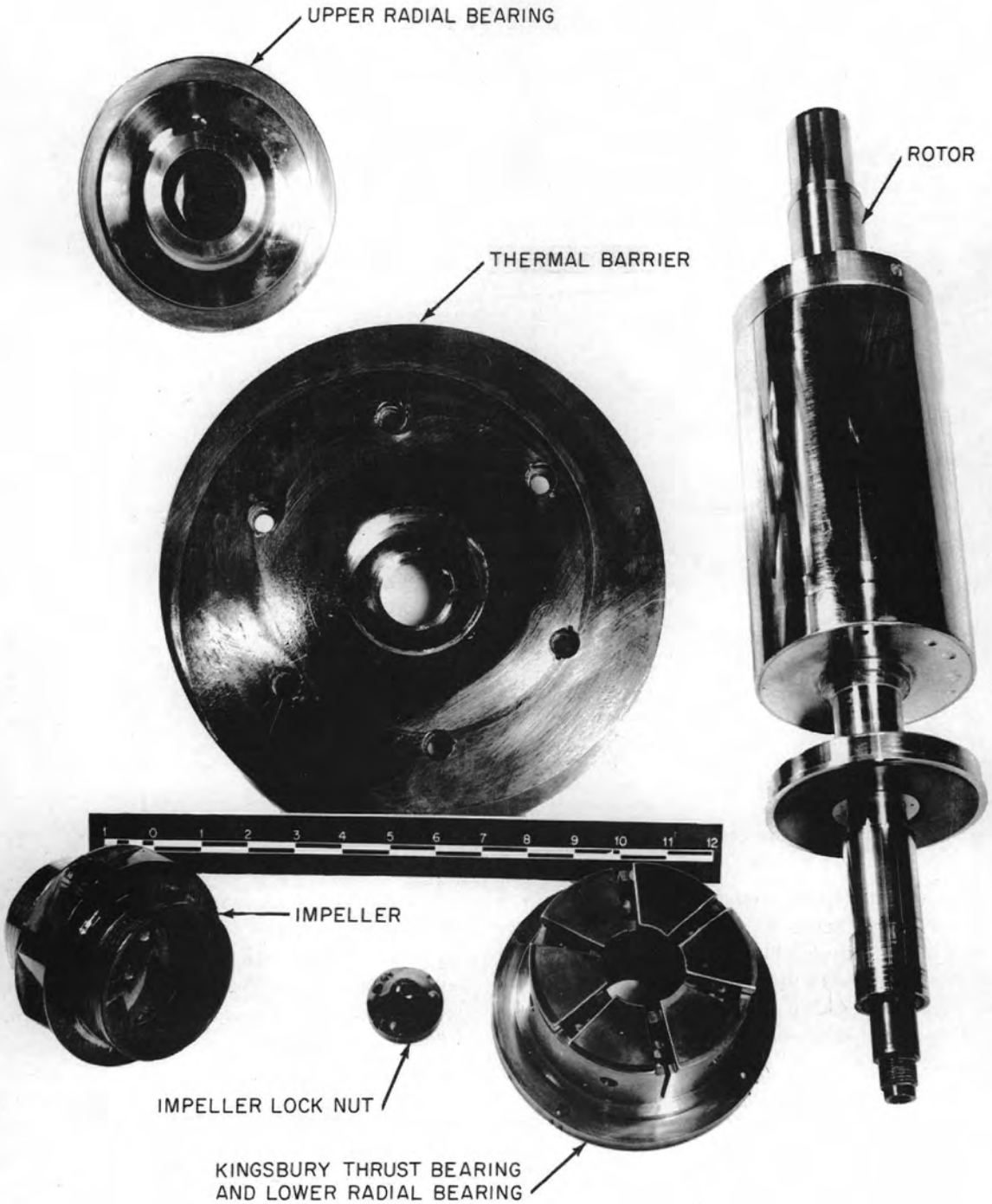

Fig. 3.10. 230A Slurry Pump Parts.

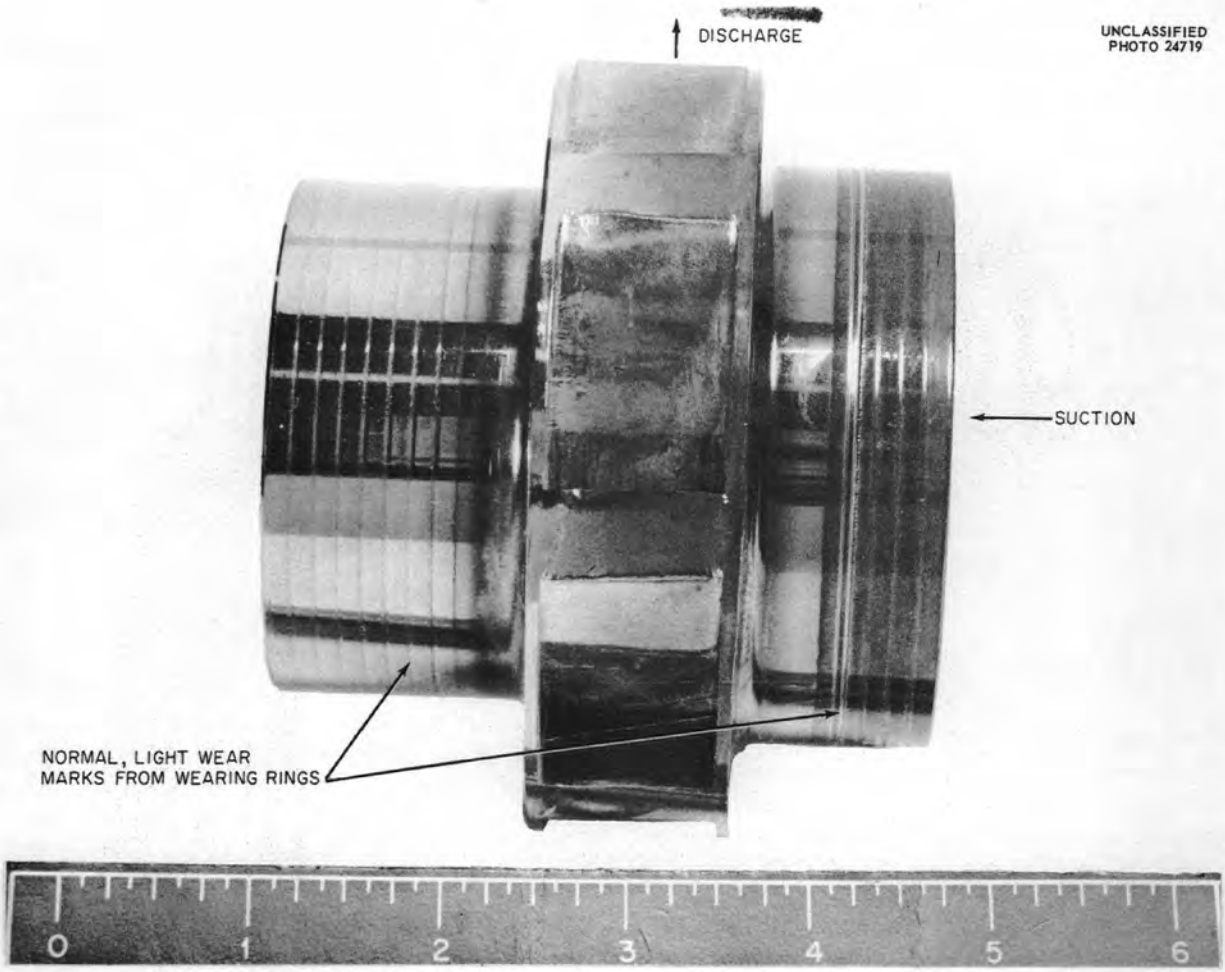

Fig. 3.11. 230A Slurry Pump Impeller.

After the above troubles were eliminated, the system was run at 300°C and 2000 psi with UO_2SO_4 at a uranium concentration of 10 g/kg, with 50 mole % excess H_2SO_4, 0.005 *M* $CuSO_4$, and 110 ppm O_2. The concentrations of the major constituents are plotted in Fig. 3.12. The rise in nickel concentration corresponds to a generalized corrosion rate of 35 mpy. This was accompanied by a gradual loss of uranium and copper; toward the end of the run, SO_4^{--} may have disappeared from solution.

When the loop was shut down, it was discovered that two of the three pressurizer legs were full of solids. There was also x-ray evidence of corrosion attack on the heater legs. The legs are currently being cut out for examination and will be replaced.

The next mockup run will be gas-pressurized, with all other variables held the same as in the previous run, to determine whether the pressurizer was the cause of the high corrosion rates and the uranium precipitation.

3.7 HRT SAMPLER[11]

In the course of further tests on the isolation chamber, two holes were drilled in the sleeve to improve venting action. This modification resulted in consistent samples at the design volume of 4.5 to 5.0 ml instead of the 3 to 4 ml reported previously.[12] The ability of the isolation chamber to

[11] R. B. Briggs, W. R. Gall, and C. L. Segaser, *HRT Design Request No. 5 – High Pressure and Low Pressure Sampling Systems for HRT*, ORNL CF-54-9-223, (Sept. 29, 1954).

[12] C. B. Graham *et al.*, *HRP Quar. Prog. Rep., July 31, 1955*, ORNL-1943, p 32.

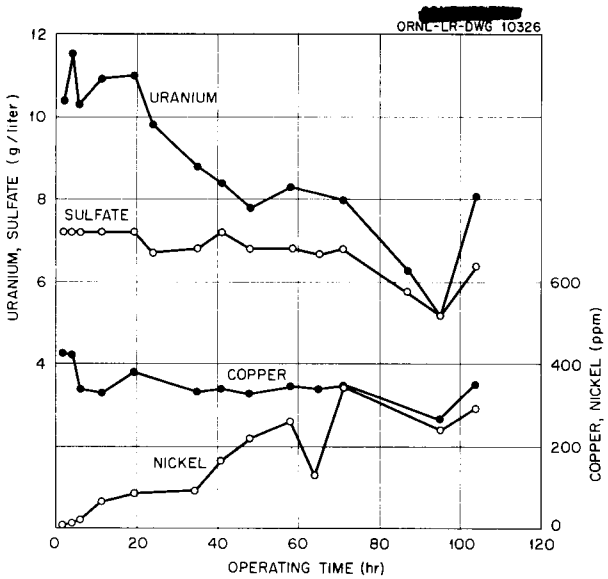

Fig. 3.12. Chemical Analyses of HRT Mockup Fuel (Runs 10-10-55 Through 10-14-55).

take a representative sample of suspended solids is, however, not so good as in the previous model. Samples are now 15 to 30% low in solids. The tests to date have been with a 0.1% slurry of thorium oxide having a particle size of 1 to 10 μ. It is expected that the reactor solids will be of smaller particle size and less difficult to sample.

3.8 HRT THERMAL INSULATION

Aluminum foil has been tested as an insulation material for the HRT.[13] It was found that nine layers of 0.0015-in.-thick kitchen foil, wrapped loosely around a 620°F pipe, enabled the heat losses to be reduced to 6% of the bare-pipe losses. This insulation material is cheap, readily installed, and suitable for reactor service. An estimate, based on bids received for radiation-resistant, waterproof insulation, indicates that use of the aluminum-foil insulation will result in a saving of approximately $20,000. Development of removable-flange insulation is contemplated.

3.9 REFLUX CONDENSER-RECOMBINER

Preliminary tests on the proposed reflux condenser-recombiner for the outer storage tanks have been described previously.[14]

A set of three catalyst baskets,[15] serving as flame igniters, was installed and tested in the reflux condenser. Explosions of varying severity occurred at 3- to 10-min intervals when H_2 and O_2 were added to the system. After several hours of operation, pulverized catalyst was found in the condensate drain. The arrangement was therefore unsatisfactory, and other methods must be developed. Several alternative solutions to this problem are being sought.

3.10 HRT FREEZE PLUG TEST

Models of the proposed freezing unit to be used on HRT piping have been constructed, and the necessary refrigeration equipment has been procured. Experiments will be run under water in a tank provided with observation windows. It is planned to test the various sizes of pipe (up to 3½ in.) which are to be sealed by freezing for maintenance. Methods for excluding water during removal of valves or components will be evaluated.

3.11 PRESSURE-BALANCING VALVE

A prototype of the spring-loaded relief valve, which will be used to equalize the pressure between the core and blanket systems, has been received. This valve, in the original condition, will be tested for seat leakage at elevated temperature and pressure. It will be operated a number of times with steam at elevated temperatures and again tested for leakage past the seat.

[13] I. Spiewak, *Aluminum Insulation (Report No. 2)*, ORNL CF-55-8-121 (Aug. 24, 1955).

[14] C. B. Graham *et al.*, *HRP Quar. Prog. Rep., July 31, 1955*, ORNL-1943, p 33.

[15] W. R. Gall and R. E. Aven, *Outer Dump Tank Recombiner Program*, ORNL CF-55-5-187 (May 13, 1955).

4. REACTOR CONTROLS AND INSTRUMENTATION

D. S. Toomb

A. M. Billings
J. R. Brown
C. H. Gabbard
R. L. Moore
L. R. Quarles[1]
W. P. Walker[1]
K. W. West

4.1 GENERAL STATUS

The effort of this quarter was spent mainly in cross-checking drawings, testing available components and installed systems, and in completing the layout and piping drawings for the shielded remote instrument cubicles. An estimated 75% of the main control-panel instruments were checked and sent to the HRT site for installation. The tank-weighing cells were installed in the low-pressure systems and calibration is in progress.

4.2 DIFFERENTIAL-PRESSURE TRANSMITTERS

Assembly of both the pneumatic and electric high-pressure differential-pressure transmitters has begun at the Foxboro Company. These weld-sealed transmitters are special adaptations of a standard design of the Foxboro Company. The electrical (variable inductance) transmitter shown in Fig. 4.1 has a range of 300 in. of water. One pressure chamber is evacuated and the diaphragm is returned to zero position by spring-loading. This arrangement permits use of the instrument as an absolute-pressure transmitter with minimum temperature-change error, and allows overranging to 2000 psi. A similar unit is used as a differential-pressure transmitter, with a range of 60 in. of water, by inserting a second pressure tap in the left side.

Figure 4.2 shows a pneumatic differential-pressure transmitter with a range of 50-0-50 psi. This transmitter is the sensing element for balancing the pressure between the reactor core and blanket systems.

[1]Consultant, University of Virginia.

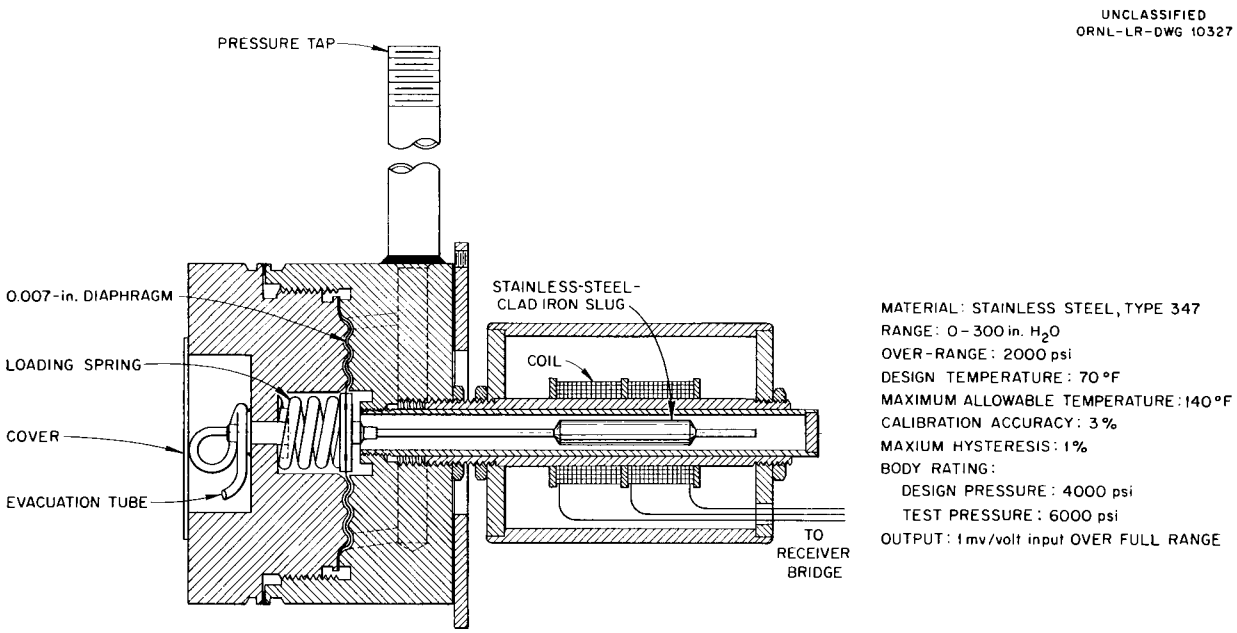

Fig. 4.1. Pressure Transmitter with a Range of 300 in. of Water.

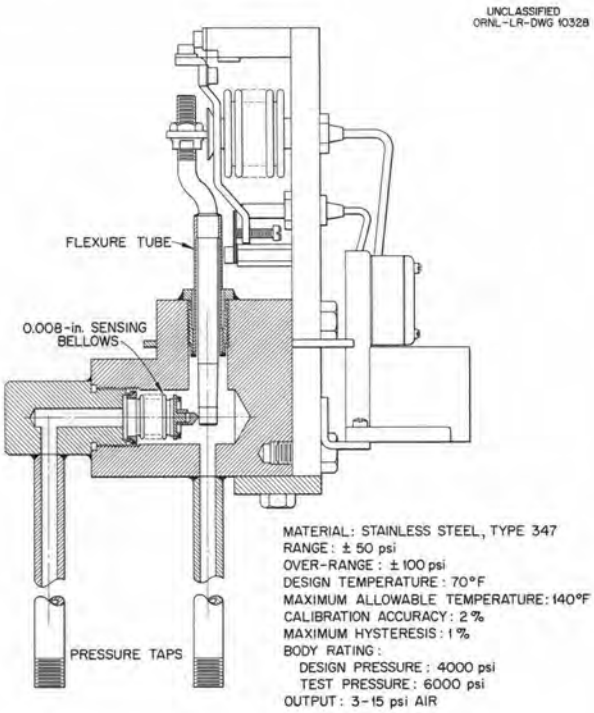

Fig. 4.2. Differential-Pressure Transmitter with a 50 psi – 0 – 50 psi Range.

4.3 LIQUID-LEVEL TRANSMITTER

The prototype of a displacement-type liquid-level transmitter[2] has proven insufficiently damped for satisfactory control of the letdown valve on the HRT mockup. Two similar transmitters incorporating damping mechanisms are being developed. One unit, with vanes for hydraulic damping, was bench-tested, and a design for a pressurizer-level controller, based on this principle, is being completed. The second unit, incorporating magnetic damping, was designed and is presently being assembled.

4.4 VALVES AND OPERATORS

4.4.1 HRT Low-Pressure Valves

Delivery and testing of the HRT low-pressure valves are 35% complete. All twenty-three of the hand-operated valves illustrated in Fig. 4.3 were accepted. Fabrication of the air-motor-operated valves is well under way at the vendor's plant.[3]

Fig. 4.3. HRT Low-Pressure Hand Valve.

Considerable difficulty was encountered in sealing both inner and outer diameters of the ring gasket to the ring-joint groove in the valve body. The vendor now has developed a tool and a gage for machining of the ring groove; their use has eliminated this trouble. Leakage past the sealing surfaces at both outer and inner diameters can be detected by applying pressure to the leak-detection hole (visible in Fig. 4.3) which connects the root of each ring groove.

Approval was given the vendor's proposal for measuring plug-to-seat leakage by heating the entire valve body to 100°C, applying 150 psi of helium under the seat, evacuating the valve body over the seat, and testing for leakage with a helium-leak detector of the mass-spectrometer type. Unusually low leakage rates (< 1 cfh at 1 μ pressure) were found in all valves tested to date.

[2] W. P. Walker *et al.*, *HRP Quar. Prog. Rep., July 31, 1955*, ORNL-1943, p 34.

[3] Fulton Sylphon Division, Robertshaw-Fulton Controls Company, Knoxville, Tenn.

4.4.2 HRT High-Pressure Valves

Approval of the vendor's[3] welding procedure was granted, and qualification of welders was completed. In view of the vendor's excellent welding facilities, 100% inspection of production welds by Oak Ridge National Laboratory is no longer required. However, radiographs of all welds will be reviewed by Oak Ridge National Laboratory. A high-pressure sampling valve is shown in Fig. 4.4 and a high-pressure throttling valve (the let-down valve) in Fig. 4.5.

UNCLASSIFIED
ORNL-LR-DWG 10329

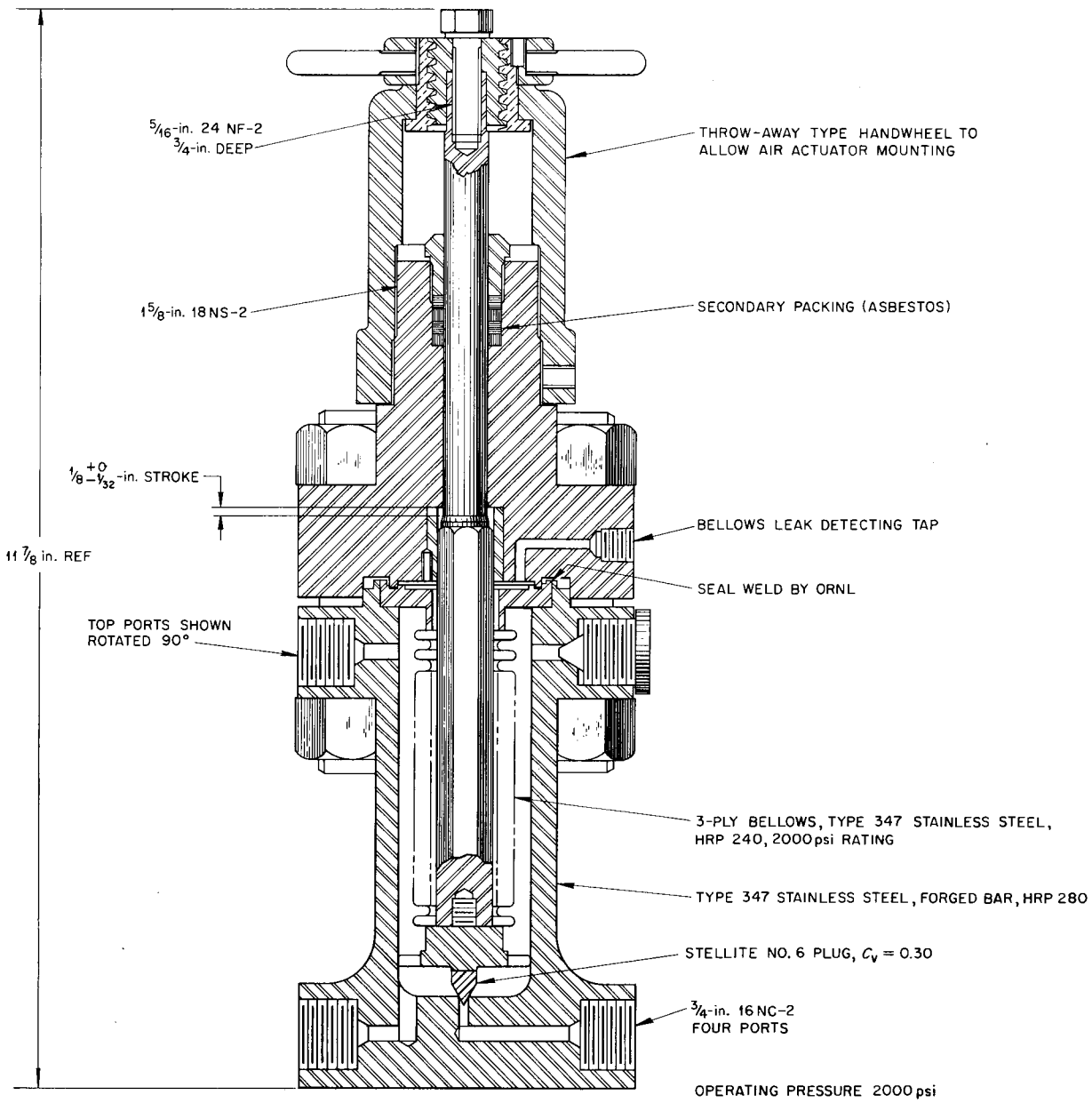

Fig. 4.4. High-Pressure Sampling Valve.

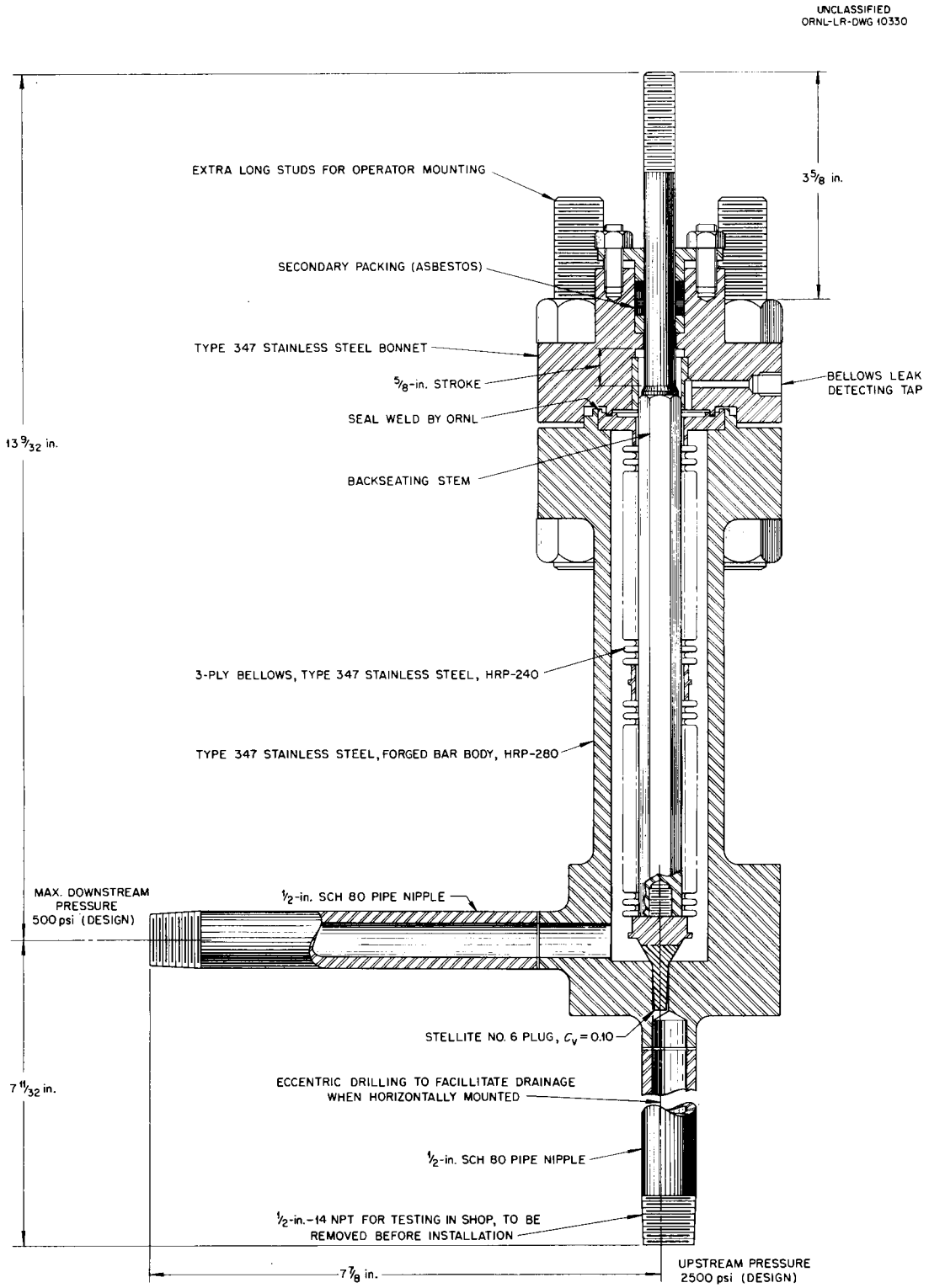

Fig. 4.5. HRT Letdown Valve.

4.4.3 HRT Auxiliary-System Valves

Procurement and testing were completed on all automatic valves for the steam, cooling-water, waste, and air systems.

4.4.4 Valve-Trim Testing Program

The valve-trim testing program, utilizing the valve-test loop,[4] has as its objective the determination of an optimum combination of material and geometry.

To establish a standard of evaluation, type 347 stainless steel plugs and 347 stainless steel seats are being tested. The first set of the type 347 stainless steel trim, which was subjected to 100 "dumps" of fuel solution at 2000 psi and 250°C, is pictured before test in Fig. 4.6. "Before" and "after" pictures of the plug are shown in Fig. 4.7 and Fig. 4.8, respectively. Similar pictures of the valve seat are Figs. 4.9 and 4.10. Wear of the seating region was insignificant and no difference in plug-to-seat leakage after the test was detected. Weight loss for the plug amounted to 0.0334 g and for the seat, 0.004 g.

Twenty-five sets of trim-containing material combinations, thought suitable for HR valve applications, are presently being fabricated and will be compared with the "standard" 347 stainless steel trim.

For more efficient utilization of the valve-test loop, two experimental valve bodies, designed for easy interchangeability of trim, are being fabricated in ORNL shops.

[4] C. B. Graham *et al.*, *HRP Quar. Prog. Rep., Oct. 31, 1954*, ORNL-1813, p 109.

Fig. 4.6. Valve Trim Before Test.

Fig. 4.7. Valve Plug Before Test.

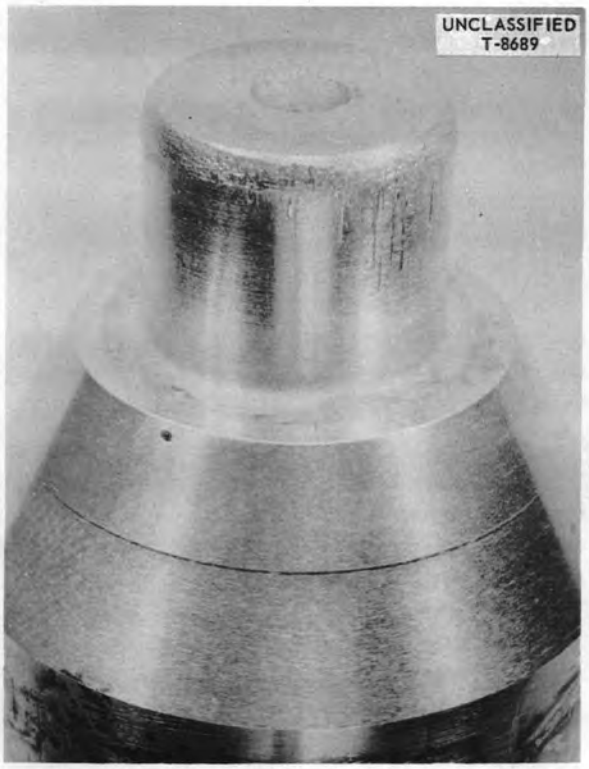

Fig. 4.8. Valve Plug After Test.

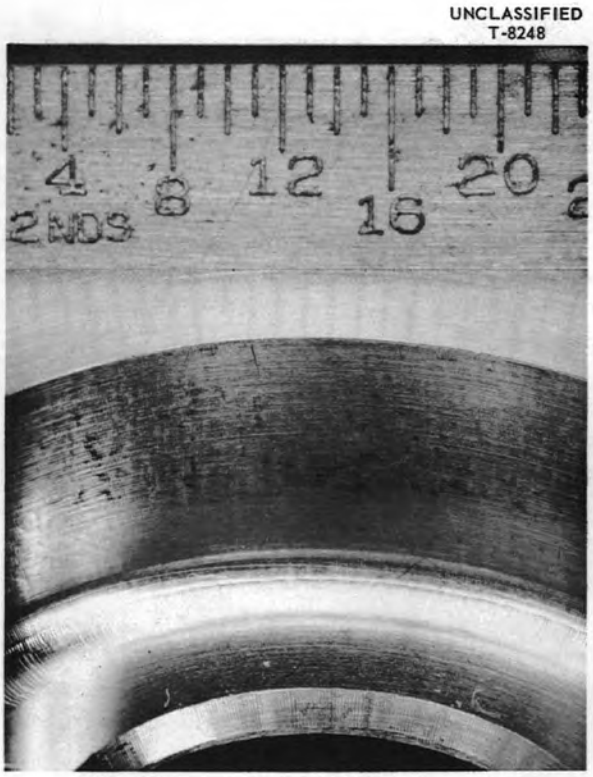

Fig. 4.9. Valve Seat Before Test.

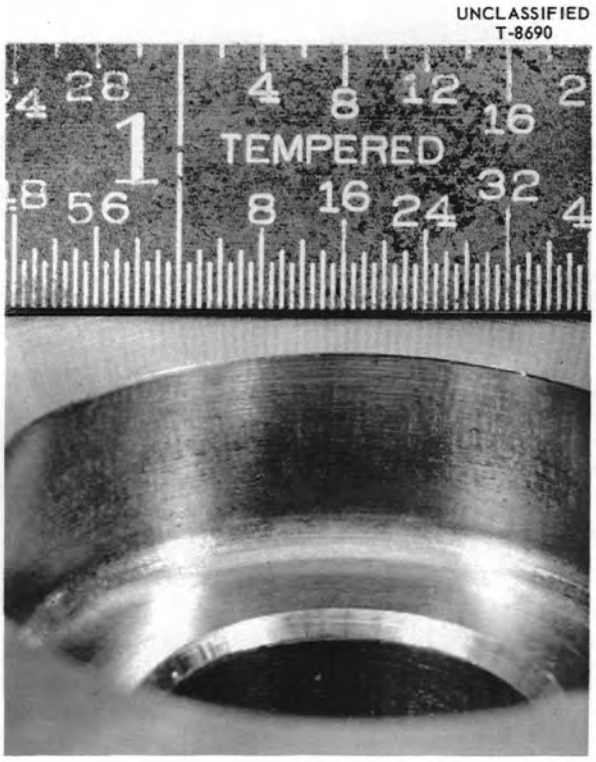

Fig. 4.10. Valve Seat After Test.

5. HRT FUEL PROCESSING PLANT

F. R. Bruce W. E. Unger

W. D. Burch B. H. Hamling A. M. Rom
W. L. Carter C. C. Haws H. O. Weeren
J. R. Engel R. B. Lindauer H. E. Williamson
G. W. Gray F. C. McCullough R. H. Winget
C. E. Guthrie E. O. Nurmi

5.1 DESIGN

The HRT-fuel-processing plant is an experimental facility designed to remove the insoluble fission and corrosion products from 0.25 to 1 gpm of reactor fuel which bypasses the reactor heat exchanger. The insoluble fission and corrosion products will be centrifuged from the fuel by a hydroclone and concentrated in about 2 gal of fuel; this fuel and the extracted products will be discharged periodically and the D_2O recovered by evaporation.

Originally, the D_2O was to be removed in an evaporator, which would also temporarily store the fission products until the preponderant energy of radioactive decay had been dissipated. It was planned that a 3-month accumulation of fission and corrosion products, concentrated by evaporation, would be dropped into a shielded carrier for final drying and removed in the shielded carrier to a solvent-extraction plant for recovery and decontamination of the associated uranium. This scheme now appears impractical. At 5 Mw power, the corrosion rate of zirconium may be 10 mpy, and that of stainless steel may be 1 mpy. At these assumed corrosion rates the reactor system may contribute 400 g per week of corrosion products, which will also be removed centrifugally from the reactor fuel. Very little concentration of the discharged underflow-pot contents is possible before a heavy sludge of corrosion products is formed. This sludge has poor fluid-flow properties, which would impair the operation of valves and contribute to the plugging of transfer lines. As indicated by the revised flowsheet, Fig. 5.1, evaporation is to be effected in the carrier. The contents of the underflow pot will now be discharged directly to the carrier, the heavy water driven off by evaporation, and the residual solids accumulated in the carrier, pending shipment to a solvent-extraction facility. A second identical carrier-evaporator will be used alternately with the first, to accumulate fission products while those accumulated in the first are decaying. Furthermore, provision will be made for either of the two carrier-evaporators in use to be replaced with a smaller, heavily shielded carrier of sufficient capacity to accommodate single underflow-pot batches. The increased shielding will permit the removal of single batches, within a relatively short time after discharge (about 7 days), to a sludge-processing facility for complete dissolution of the small-carrier contents and accurate sampling of the solution. Thus, the effectiveness of the solids-separation equipment could be determined by treatment of the entire batch rather than of a sample which might not be representative.

The effectiveness of the hydroclone in separating the insoluble fission and corrosion products might also be determined by analyses of samples taken from the clarified hydroclone-overflow stream and from the slurry in the underflow pot. Experience with high-temperature experimental loops, operated under simulated reactor conditions, has indicated that, while most of the particles are expected to be of the order of 1 μ, occasional flakes or agglomerates many times this size will be encountered. These apparently are spalled from the hot-pipe surfaces, upstream from the hydroclone, on which insoluble materials progressively deposit. The large particles complicate the problem of sampling the underflow receiver. Representative sampling of a finely divided slurry is difficult under the best of circumstances, but where relatively large and dense particles are involved, violent agitation is necessary to ensure even an approach to a representative sample.

In order to provide the best possible sample, the chemical plant flowsheet in Fig. 5.1 is arranged so that, after the period of operation is completed and the chemical plant is isolated from the reactor, the underflow-pot contents may be agitated by feed-pump circulation. Continued circulation through the heater and past the screen should be effective in comminuting loosely formed agglomerates. After a period of such recirculation, the sample will be isolated by simultaneously closing the sampler valves.

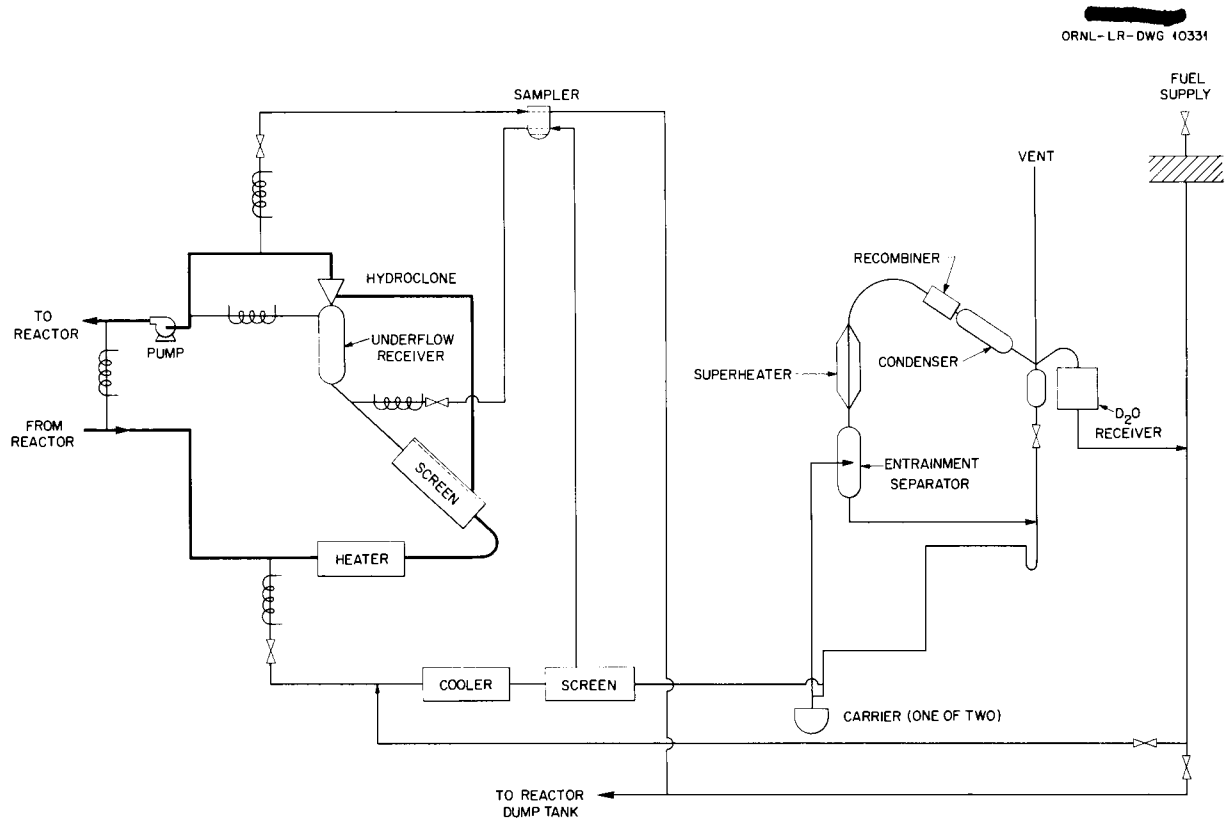

Fig. 5.1. Schematic HRT Chemical-Processing Flowsheet.

A homogeneous dispersion of solid particles in the underflow receiver will require a recirculation rate of at least 3 gpm. Slight modifications of the sampler components are required to decrease the pressure drop of the sampler and to enlarge the chamber clearances that might otherwise obstruct the passage of larger particles. Stokes' law computations for a 6-in.-dia underflow receiver and a 3-gpm recirculation rate indicate a sample analysis accuracy of ±10% for particles less than 10 μ in diameter. The reliability of this sampling system can be confirmed only by comparing the analytical results for the sample with the analysis of the complete charge after dissolution.

The remainder of the flowsheet is unchanged from that previously described in the HRP quarterly progress reports.

5.2 CONSTRUCTION

The contractor for the chemical plant construction has completed 90% of the plant. Welding and structural steel work within the two process cells was completed and the inner surfaces were coated with Amercoat (see Fig. 5.2). The concrete shield was finished on all sides of the tanks. The building extension is complete except for painting and finish-work in the office area.

Figure 5.3 is a view of the 300,000-gal waste-storage pond in which shield water from the chemical processing cells or reactor cells will be stored if radioactivity is present after repair operations.

5.3 COMPONENT DEVELOPMENT

5.3.1 Hydroclone Development

(a) Performance. – Tests were made in loop A to determine the distribution of precipitated neodymium sulfate when the preheater was at a temperature 25 to 30°C higher than that of the main circulating loop. Ten per cent of the precipitated solids appeared in the hydroclone underflow (Table 5.1). The solution in the underflow pot was concentrated to 4270 mg of $Nd_2(SO_4)_3$ per

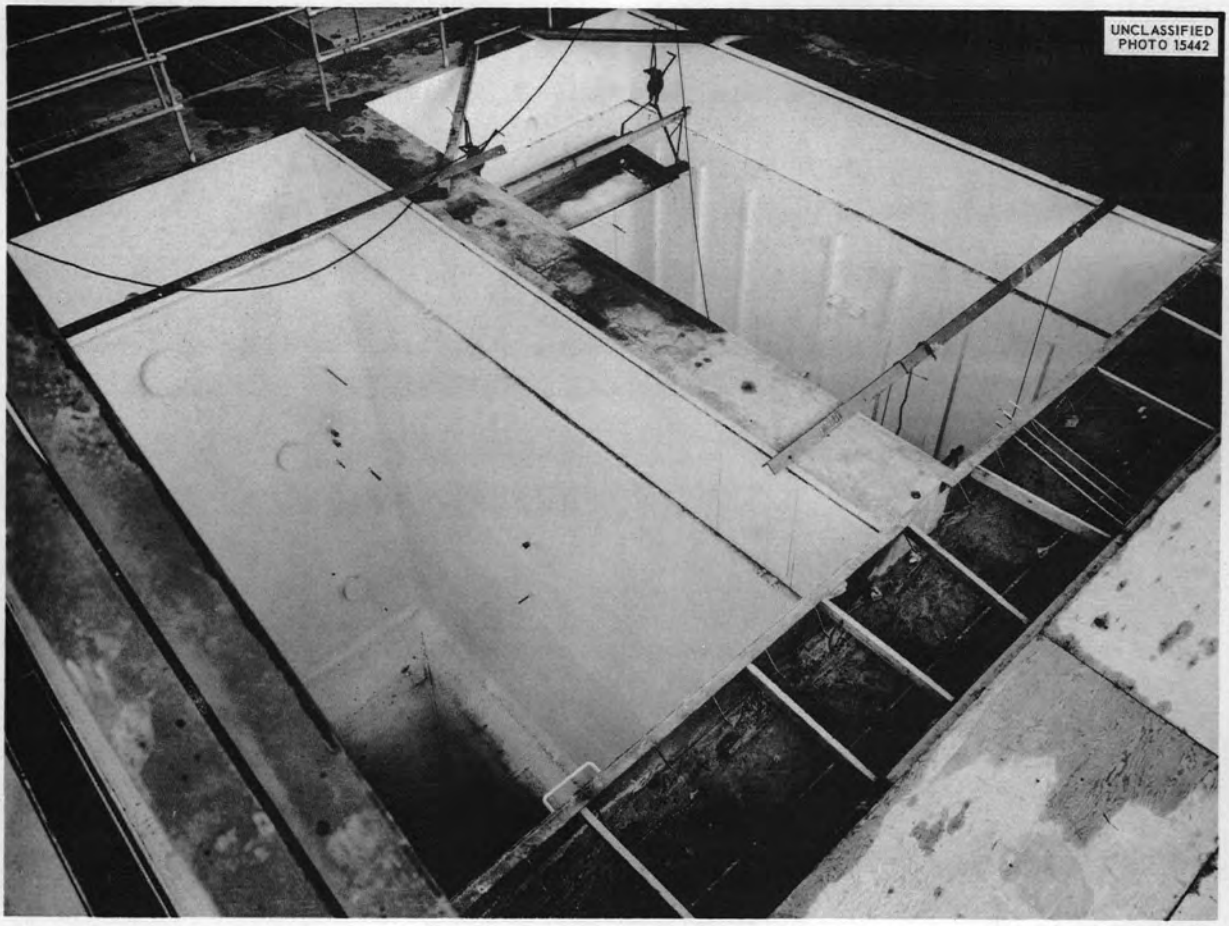

Fig. 5.2. Chemical-Processing Cells After Amercoating.

TABLE 5.1. DISTRIBUTION OF $Nd_2(SO_4)_3$ PRECIPITATE IN LOOP A TESTS

Fuel solution in loop: 0.04 *m* UO_2SO_4, 0.01 *m* H_2SO_4

Test No.	Temperature of Preheater (°C)	$Nd_2(SO_4)_3$ (mg)			
		In Hydroclone Pot	In Filter	In Preheater	In Main Loop
LR-34	325	117	None used	967	39
LR-35	325	1.3	461	29	3.7
LR-36	310	2.5	10	650	9

Fig. 5.3. Waste Storage Pond.

kilogram of H_2O, a factor of 65 times the average concentration of 65 mg of $Nd_2(SO_4)_3$ per kilogram of H_2O dissolved in the loop-circulating system during the test.

The hydroclone feed port plugged several times with, presumably, large particles of precipitated neodymium sulfate (since allowing the stream to cool 75 to 100°C dissolved the precipitate). When a filter was inserted in the system downstream from the preheater, essentially all the precipitated neodymium sulfate was retained in the heater and filter.

The hydroclone tested was 0.25 in. in diameter and had a 25-ml underflow pot. The filter was a 6-in. length of 0.25-in.-dia titanium tubing with 500 holes, 0.030 in. in diameter, drilled through the walls.

(b) Corrosion. – In high-temperature corrosion tests with simulated reactor fuel on two titanium-lined 0.4-in.-dia units, the region of most severe attack was on the walls near the underflow port. Wall thicknesses are being measured. The diameters of the underflow ports were not appreciably affected. These results indicate that the 3.14-in. length of the 0.4-in.-dia unit may not be optimum for extended operation. The characteristic flow pattern in a hydroclone is generally downward along the walls and upward along the axis toward the vortex finder. The evidence of high turbulence above the underflow port indicates that the turning point of the fluid stream is well up inside the hydroclone body. This is further borne out by the low underflow-to-feed ratio (1% for the 0.4-in.-dia hydroclone compared with 2 to 2.5% for the 0.25-in.-dia unit, which was optimized with respect to length) observed when these hydroclones are used in connection with an induced-underflow pot.

One hydroclone, which was sectioned after 460 hr, had been operated[1] under a wide variety of conditions in development loop B-2. No underflow pot had been used in this arrangement. Measurement of the pressure drop as a function of flow rate, after operation, indicated a decrease of 25 to 30% in the pressure required to produce any given flow over the entire range. Although a slight decrease in pressure drop is to be expected as a result of oxide film formation on the surfaces, a change of the magnitude observed here usually indicates extensive attack which makes further operation undesirable.

The second hydroclone was operated, under the conditions shown in Table 5.2, for 1366 hr with a 1.5-liter underflow pot. After an operation period of 200 hr, the pressure requirement decreased 15%. Subsequent tests showed no further change until the final measurement, after 1366 hr total operating time. The erratic pressure characteristics observed at this point were the cause for the termination of the test.

Three 0.25-in.-dia prototypes of the integrally flanged hydroclone, which is proposed for installation in the HRT processing plant, have been built for use in corrosion testing.

(c) Underflow-Pot Heat-Transfer Studies. – At the end of one week of operation, the HRT chemical plant underflow pot will contain fission products generating an estimated 3 kw of heat. The removal of this amount of heat is one of the design requirements for the hydroclone underflow pot. It was found that convective heat transfer was effective enough to permit use of a simple cylindrical tank with a cooling jacket.

The hydroclone-pot geometry and volume heating of fission products were simulated by heating, with electrical resistance, a 2-ft-high vertical cylinder of 0.04 *m* UO_2SO_4 solution in a 6-in.-dia pyrex pipe (Fig. 5.4). Cooling water entering at approximately 20°C flowed through a jacket around the pyrex pipe. Temperatures of the solution, which was open to atmospheric pressure, were measured by a thermocouple in a movable glass thermowell. The lower liquid viscosity and higher density at 250 to 300°C would make convective heat transfer more effective under HRT chemical plant conditions.

Power input rates of up to 2.1 kw were investigated; temperature gradients were less than 1°C across any pot diameter. A gradient of 9°C per foot at the pot center – or 30°C from electrode to electrode – existed for steady-state temperature at 2.1 kw heat input (see Fig. 5.5).

[1]P. A. Haas and R. W. Horton, *HRP Quar. Prog. Rep. July 31, 1955*, ORNL-1943, p 204.

TABLE 5.2. OPERATING CONDITIONS FOR CORROSION TEST OF 0.4-in.-dia TITANIUM-LINED HYDROCLONE

Feed flow rate: 1.0 gpm

Length of Run (hr)	Uranium Concentration (g/kg H_2O)	Temperature (°C)	Pressure (psi)
200*	15	250	1000
191*	10.2	300	1500
200	10.5	300	1500
100	10	300	1400
200*	40	300	1400
475*	300	250	1000

*Pressure drop vs flow rate measured at these times.

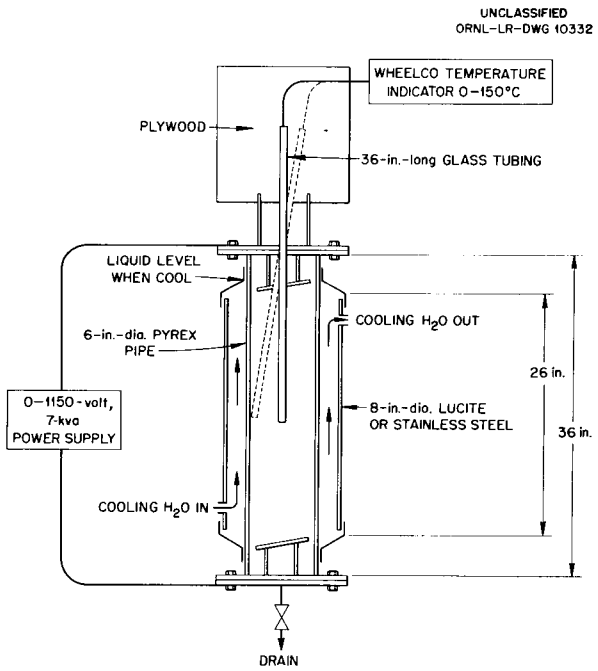

Fig. 5.4. Simulated Hydroclone Underflow Pot.

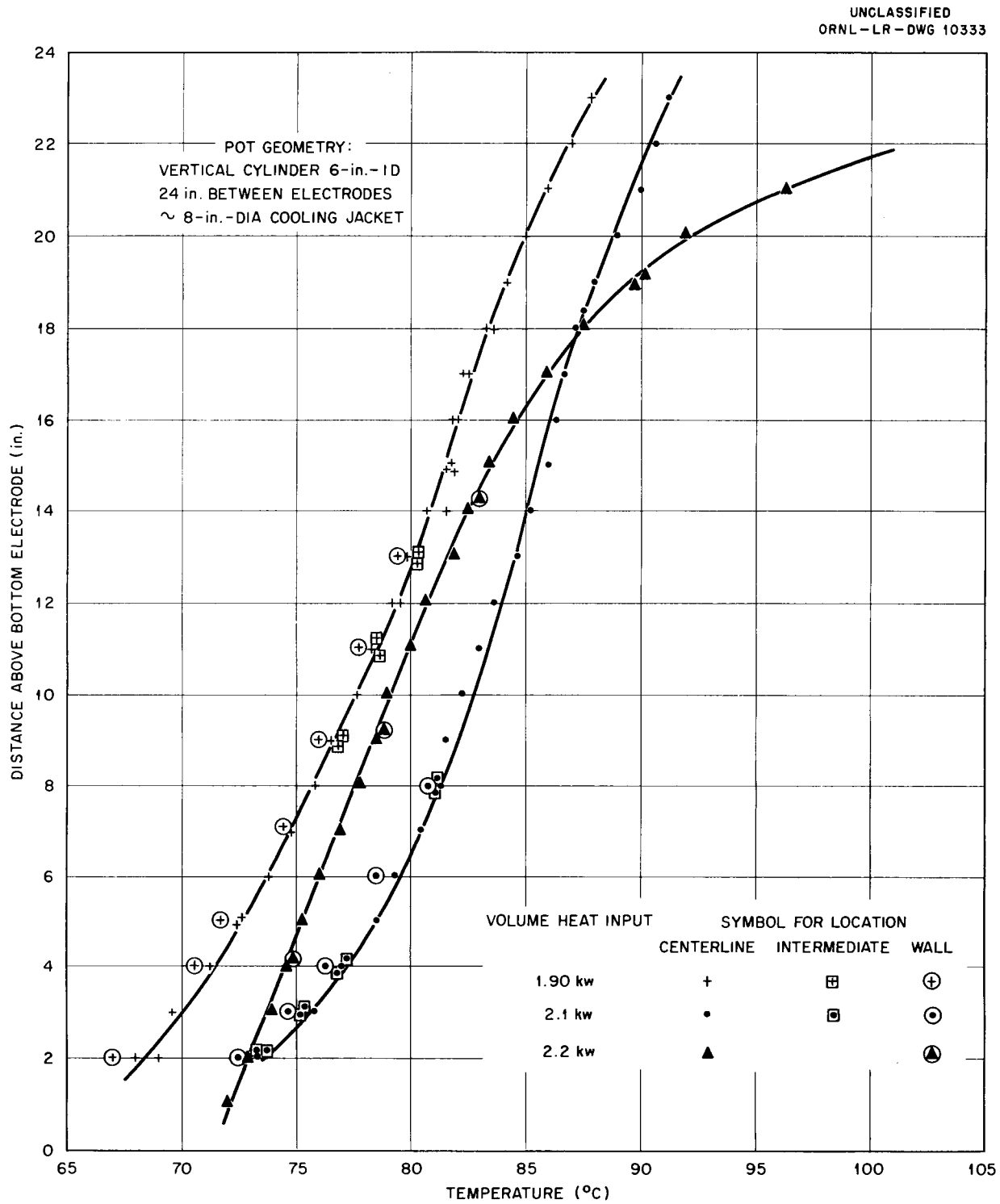

Fig. 5.5. Temperature Distribution in a Simulated Hydroclone Underflow Pot.

Convection currents were studied by observing suspended MnO_2. The flow pattern for the center two-thirds of the cylinder was a slowly rising column of liquid with an average velocity of about 2 in. per minute; there was a thin layer (about $^5/_{32}$ in. thick) falling near the cold walls with a velocity 10 to 15 times the center velocity. Near the ends the flow was eddying, with net flow, from the center to the wall at the top and from the wall to the center at the bottom. With the proposed pot geometry, convective heat transfer should permit easy removal of the fission-product heat (estimated at 3 kw or less) with less than a 50°C temperature difference between the hottest and coldest pot solution.

5.3.2 Evaporator

In evaporation tests a 0.04 *m* UO_2SO_4 solution, containing nonradioactive fission products and corrosion products, was evaporated to about 2 *m* before there was any foaming, splashing, or entrainment. As a dry condition was approached, a crumbly brown cake formed, spattering was frequent, and brown fumes were given off. With pure uranyl sulfate solutions, evaporation to about 3 *m* was possible without difficulty. The condensate uranium concentrations were 10^{-3} to 10^{-5}% of the evaporator concentrations.

Electrical resistance heating was used to simulate heating by radioactive fission products. Stainless steel end plates served as electrodes. The evaporator, made of pyrex glass, was horizontal, 7 ft long and 6 in. in diameter. The shape was similar to that proposed for the HRT chemical plant. An enlarged section of the vapor line contained York demisting mesh as an entrainment separator. Heat was supplied as 60-cycle alternating current at 0 to 900 v and 0 to 7 kva.

Since keeping the insoluble material suspended and transferring it were not feasible after only about a fourfold concentration had been obtained, it is now planned to evaporate the solution in the carrier in which it is collected, rather than in a separate evaporator from which the residue would have to be transferred (see Sec. 5.1).

5.3.3 Pumps

Two ORNL 5-gpm canned-rotor pumps were rewound to permit operation with 3-phase power supplies. The higher efficiency obtained from 3-phase winding, as compared with single phase, permits the application of more power to the pump and, hence, the achievement of higher pumping heads.

The first pump – the circulating pump on development loop A – has operated with a 3-phase stator for 266 hr on a current of 60 cps and for 48 hr at higher frequencies. Two single-phase stators were burned out on a current of 60 cps on this loop, one after 791 hr of operation and one after 338 hr. This pump is operated with 0.04 *m* UO_2SO_4 solution at 300°C and 2000 psi, and is mounted in a vertical position. Although the Stellite-Graphitar thrust bearing was not designed for operation in this position, no ill effects have been observed. When the pump was dismantled for inspection after 1129 hr, there were no obvious signs of wear, and careful measurement failed to show any attack. The pump has been reassembled and will be operated for extended periods at 70, 80, and 90 cps to ascertain the reliability at these frequencies and at high temperature and pressure.

5.3.4 Freeze Plugs

Design has been completed and construction started on a freeze-plug test loop, which will be installed as part of loop B. Test conditions will closely simulate reactor operating conditions.

Part II

REACTOR DESIGN AND ANALYSIS

J. A. Lane R. B. Briggs

6. THORIUM BREEDER REACTOR[1]

R. B. Korsmeyer

R. E. Aven
C. Michelson[2]
M. C. Lawrence[3]
M. I. Lundin
R. G. McGrath[4]
C. L. Segaser
W. F. Taylor[5]

6.1 TBR DESIGN

6.1.1 Reduced-Power Study

In order to reduce the effect of reactor-system-component failures upon plant on-stream efficiencies, modifications of the present TBR design are under study, wherein the main circulating loops are divided into several "part-capacity" loops. The first phase of this study involved consideration of a core system containing one pump that was circulating fluid through four heat exchangers in parallel,[6] each of these heat exchangers being of the same size as the blanket heat exchanger. By reducing the steam temperature and pressure as heat exchangers are isolated (on assumed failure), the power output, at constant reactor temperature, may be held above the proportionate amount otherwise carried by the heat exchangers remaining in service. The calculated relationship between reactor system and turbogenerator capabilities at reduced heat-exchanger area is shown in Fig. 6.1. In the figure the curves take into account the reduced thermal efficiencies at lower steam pressures and are adjusted for constant mechanical losses. The cross-plots show the power obtainable from the reactor with different numbers of the four core heat exchangers in service plus the single blanket heat exchanger. The true operating point in each case is, therefore, the intersection of the cross-plots with the turbogenerator curve. A comparison of the pertinent process flows, steam conditions, heat generation, and electrical output is given in Table 6.1 for the three intersections and the design point shown in Fig. 6.1. By reducing the steam temperature, the loss of one heat exchanger need result in a decrease of only 13% in total electrical output although 20% of the total heat-transfer surface is lost.

[1]The entire group listed below contributed part time.

[2]On loan from TVA.

[3]On loan from General Dynamics Corp.

[4]On loan from Westinghouse Electric Corporation.

[5]On loan from Pioneer Service & Engineering Co.

[6]W. F. Taylor and M. C. Lawrence, *Reduced Power Operation of Reactor Plant—Turbine-Generator Combination, TBR Memo No. 1*, ORNL CF-55-10-43 (to be issued).

TABLE 6.1. TBR REDUCED-POWER OPERATING CONDITIONS

	Design Conditions	Heat Exchangers		
		One Out	Two Out	Three Out
Reactor power, Mw (heat)	440	381	305	210
Fuel flow, lb/hr	11.4×10^6	10.1×10^6	8.25×10^6	4.85×10^6
Blanket flow, lb/hr	4.28×10^6	4.28×10^6	4.28×10^6	4.28×10^6
Δp in core circuit, ft of fluid	224	237	252	270
At Turbine				
Steam temperature, °F	427*	415	392	357
Steam pressure, psia	335	294	228	147
Electrical output, Mw	100	86.5	64	38.5

*Design boiling temperature at the heat exchanger is 437°F.

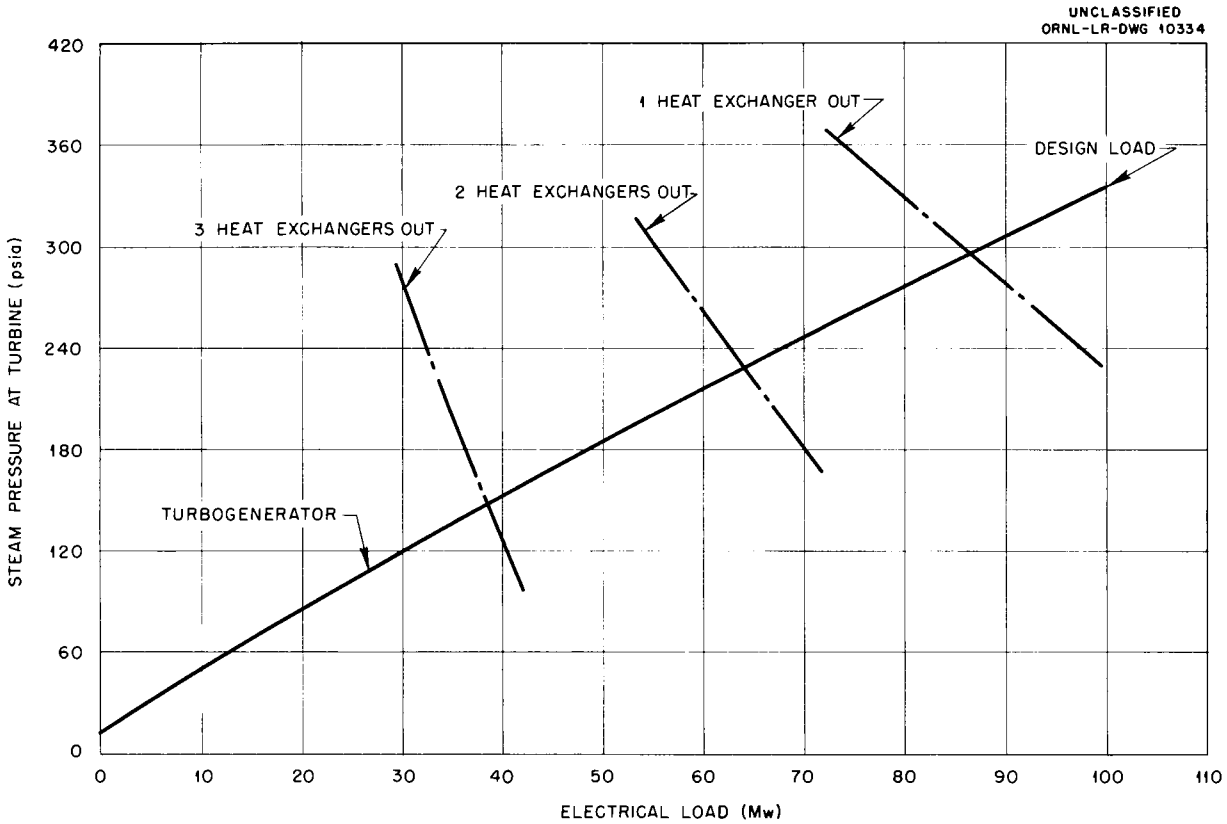

Fig. 6.1. Reactor Capability at Various Steam Pressures vs Turbogenerator Output.

6.1.2 Piping-Flexibility Analysis

The Oracle coding[7] for the three-plane piping stress analysis has been enlarged[8] to include the following items:

1. Provision for computation of deflections and rotations at any point in the piping system. (This is useful in hanger computations and in cases where piping passes through thin cell walls or shields.)
2. Revision of the basic equations to include effects (if desired) of rotation of the anchor points due to "external" movements. [This is necessary to analyze those cases in which equipment components (e.g., reactor vessel) are "floated" rather than anchored.]
3. Inclusion in the computations of secondary terms appearing when inclined straight members and circular members are subjected to transverse bending and torsional moments. (This revision permits a more accurate computation for short lines consisting of relatively large percentages of bends.)

[7]Oracle Code 139.

[8]Oracle Code 204.

6.2 TBR PILOT PLANT

6.2.1 Preliminary Considerations

Before the final design of a breeder power station can be undertaken, the breeding gain actually obtainable vs the calculated breeding gain must be established. This may be possible on a small scale; such a demonstration is part of the homogeneous reactor program. With this in mind and with the additional purpose of approaching the TBR design conditions, a preliminary study of critical fuel concentrations, reactor power, and conversion ratios for two-region thorium breeder reactors, suitable for installation in the present HRT facilities, has been completed. The nuclear calculations were coded for the Oracle, and the results were analyzed by the Reactor Analysis

Section. The data relating to core concentration, core diameter, blanket thickness, breeding ratio, ratio of wall-to-average core power densities, and power levels and inventories corresponding to core-wall power densities of 10, 25, and 50 kw/liter are shown in Table 6.2. The corresponding fluid flows, line sizes, pumping heads, heat-exchanger data, and component volumes are shown in Table 6.3.

To simplify the calculations, the following assumptions were made:

1. average temperature of 280°C for core and blanket,
2. 10% core poisons,
3. 1000 g of thorium per liter in the blanket,
4. no U^{233} in the blanket,
5. steam generated at 437°F (370 psi).

6.2.2 Letdown System

The feasibility of designing a gas letdown system is being investigated for 5-Mw and higher powered homogeneous reactors in which the pressure drop is taken across a fairly long tube and orifice (if necessary) rather than across a throttling valve. The scheme is to provide a group of small-diameter tubes in parallel and of suitable length, controlled by block valves at the high-pressure end and discharging into a suitable tank. The total flow is regulated incrementally by the valves being opened or closed. Thus the wear on the valve seat, characteristic of letdown throttle valves, should be reduced greatly. Since liquid is entrained in the gas stream as it leaves the gas separator, there is two-phase flow in the letdown line. The method of calculating the flow rates and the pressure drops involved is based on methods outlined by S. Mirshak.[9] Mirshak gives a graph for the water-steam system in which the critical mass velocity is plotted vs the energy content of the flowing, flashing fluid, with the critical downstream pressure, P_c, as a parameter. This critical pressure is assumed to be the pressure at the tube outlet,

[9] S. Mirshak, *Two-Phase Flow in Tubes with Outlet Orifices*, DP-109 (April 1955).

TABLE 6.2. TBR PILOT-PLANT REACTOR PARAMETERS

Power Density at Core Wall (kw/liter)	Power Level (Mw)	Breeding Ratio	Blanket Thickness (ft)	D_2O Inventory (lb)	Thorium Inventory (lb)	Uranium Inventory (g)
	Core Concentration, g of U^{233} per kg of D_2O: 5 Core Diameter, ft: 3.89 (Power Density at Core Wall)/(Average Power Density) = 0.387					
10	22.5	1.00	1.05	8,010	7,410	5,580
		1.10	1.52	10,900	11,260	5,580
25	56.3	1.00	1.05	8,920	7,410	8,250
		1.10	1.52	11,800	11,260	8,250
50	113	1.00	1.05	10,900	7,410	12,080
		1.10	1.52	13,760	11,260	12,080
	Core Concentration, g of U^{233} per kg of D_2O: 10 Core Diameter, ft: 3.10 (Power Density at Core Wall)/(Average Power Density) = 0.465					
10	9.5	1.00	1.14	5,310	5,480	5,470
		1.10	1.57	7,450	8,330	5,470
25	23.8	1.00	1.14	5,730	5,480	7,360
		1.10	1.57	7,860	8,330	7,360
50	47.6	1.00	1.14	6,730	5,480	11,900
		1.10	1.57	8,870	8,330	11,900

TABLE 6.3. TBR PILOT-PLANT DESIGN PARAMETERS

Power Density at Core Wall (kw/liter)	Average Power Density (kw/liter)	Flow (lb/hr)	Flow at 260°F (cfs)	Pump Head at 260°F (ft)	Line Diameter (in.)	Fluid Velocity (fps)	Heat Exchanger				Core-System Volume (liters)	Blanket-System Volume* (liters)		Estimated Volumes of Core-System Components (liters)					
							Area (ft^2)	Number of Tubes	Tube Length (ft)	Shell ID (in.)		Breeding Ratio, 1.00	Breeding Ratio, 1.10	Core	Heat Exchanger	Pump	Piping	Pressurizer	Total
Core Concentration, g of U^{233} per kg of D_2O: 5 Core Diameter, ft: 3.89																			
10	25.8	886,000	4.40	110	6	32.9–30.0	1018	608	18.2	17	1307	3361	5109	872	156	34	187	58	1307
25	64.6	2,210,000	11.04	80	10	29.8–27.2	2545	1521	18.2	26.5	1927	3361	5109	872	421	59	517	58	1927
50	129	4,430,000	22.08	110	14	34.6–31.6	5090	3042	18.2	37.5	2819	3361	5109	872	915	90	884	58	2819
Core Concentration, g of U^{233} per kg of D_2O: 10 Core Diameter, ft: 3.10																			
10	21.5	371,000	1.83	95	4	30.0–27.4	429	253	18.4	11.5	640	2483	3777	442	63	20	85	30	640
25	53.8	926,000	4.58	115	6	34.1–31.2	1073	631	18.5	17.5	860	2483	3777	442	166	35	187	30	860
50	108	1,850,000	9.17	60	10	24.7–22.6	2145	1263	18.5	24	1389	2483	3777	442	347	53	517	30	1389

*The blanket system has an external volume of 174 liters (same as that of the HRT). (No U^{233} in blanket.)

provided that it is greater than the pressure of the tank into which the fluid discharges. If an orifice is used, critical flow across the orifice is assumed.

The letdown stream from the HRT when it is operating at 5 Mw power has the following approximate composition at 300°C and 2000 psia:

	Wt %
$D_2 + \frac{1}{2}O_2$	3.7
D_2O vapor	13.2
D_2O liquid	83.1

The amount of material being let down is about 0.23 lb/sec.

If $\frac{3}{16}$-in. tubes (BWG 17, 0.072-in. ID) are used for letdown lines, then 12 tubes in parallel will be needed to handle the letdown stream, each line handling 0.019 lb/sec. The letdown gas stream plus entrainment enters a header at 2000 psia and passes through the letdown lines, which can be valved in or out as needed. A pressure profile of the letdown stream as it passes through these letdown lines is presented in Fig. 6.2. The final pressure immediately downstream of the letdown lines is 130 psia, which represents the critical pressure for this particular mass flow rate. The tubes discharge into a receiving tank which is at atmospheric pressure.

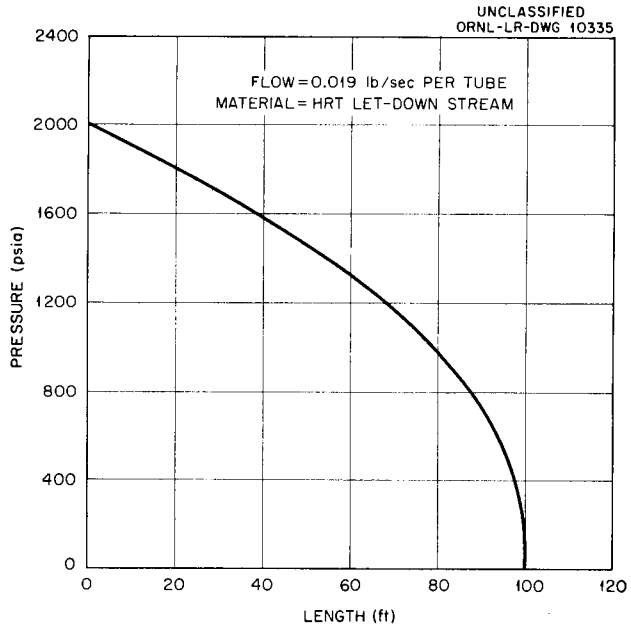

Fig. 6.2. Two-Phase Flow Pressure Drop Through $\frac{3}{16}$-in. Tubes.

7. REACTOR ANALYSIS

P. R. Kasten

H. C. Claiborne
T. B. Fowler
D. C. Hamilton
M. K. Hullings
C. W. Nestor, Jr.
M. W. Rosenthal
M. Tobias

7.1 THORIUM BREEDER REACTOR SAFETY

M. W. Rosenthal

Several possible incidents involving interruption of normal operation of the Thorium Breeder Reactor have been investigated. Two general types of events were considered – rapid changes in the rate of heat removal in the heat exchanger and sudden reduction in the flow rate of fuel solution. The following four examples, which represent extreme cases of conceivable occurrences, have been treated:

1. sudden cessation of heat removal in the heat exchanger,
2. sudden and complete stoppage of circulation in the core circuit,
3. circulating-pump failure,
4. rapid decrease in steam pressure.

The results of computations for the present TBR design[1] indicate that cases 1, 2, and 4 are potentially dangerous situations, whereas no hazard appears to be associated with case 3.

7.1.1 Case 1 – Cessation of Heat Removal

If heat transfer from the fuel solution of a homogeneous reactor to the heat exchanger should cease, the temperature of the core would rise rapidly and the negative temperature coefficient would cause the reactor to become subcritical. Analysis of the behavior of a subcritical reactor[2] can be greatly simplified by the valid approximation that the kinetics are controlled by the delayed neutrons; a single equation is then obtained which relates instantaneous fission power to the time-temperature history of the event. The decay of the several known groups of delayed-neutron precursors is represented by a single group having an average decay constant. An energy balance on the system couples the temperature of the fuel solution to total reactor power, that is, fission power plus heat released by fission-product decay. Simultaneous solution of the kinetic equation and the energy balance by numerical methods yields the core power and temperature as functions of time following the initiation of the incident.

The results of calculations concerning the behavior of the TBR following sudden interruption of heat removal in the heat exchanger are shown in Figs. 7.1 and 7.2. In this analysis, normal fluid flow is assumed to continue and the entire volume of the core circulating system is available for storage of energy. For this case the fission power decreases rapidly and, in about 60 sec, becomes negligible as compared with fission-product decay. However, the temperature of the fuel solution increases more than 30°C in the first minute and continues to rise afterwards at

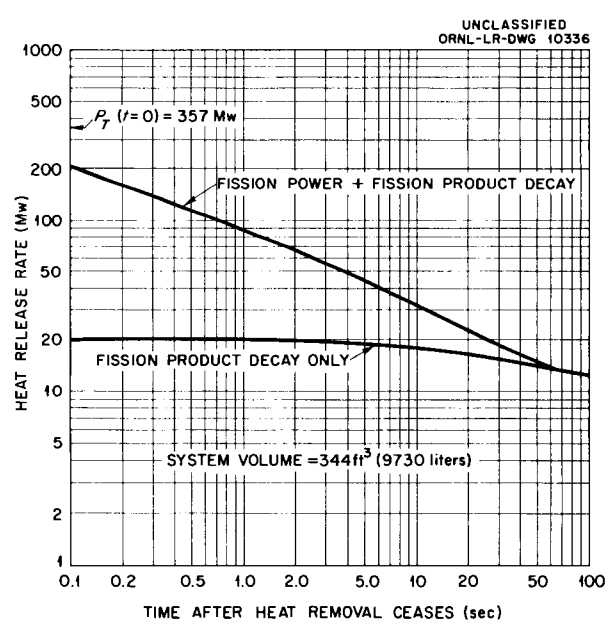

Fig. 7.1. Heat-Release Rate in TBR Core Circulating System Following Sudden Cessation of Heat Removal in Heat Exchanger.

[1] R. B. Korsmeyer *et al.*, *HRP Quar. Prog. Rep. April 30, 1955*, ORNL-1895, p 48–65.

[2] M. W. Rosenthal, *Power and Temperature of TBR Following Interruption of Normal Operation*, ORNL CF-55-9-120 (Sept. 27, 1955).

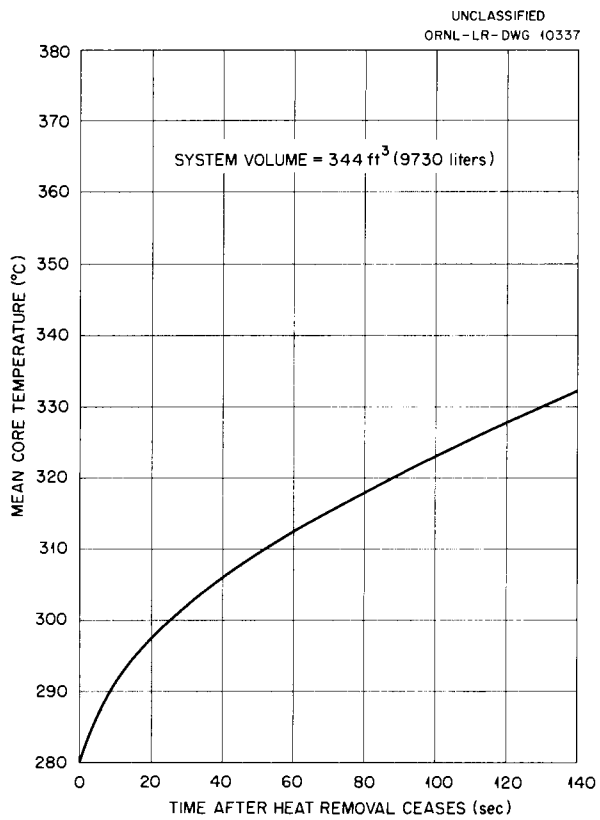

Fig. 7.2. Temperature of TBR Core Following Sudden Cessation of Heat Removal in Heat Exchanger.

a reduced rate from fission-product decay energy. The temperature of the entire system thus rapidly reaches a level at which phase separation of the fuel solution might occur. If the geometry of the systems were such that the fuel-rich phase could accumulate and attain criticality, a hazardous situation would exist.

While instantaneous cessation of heat removal is a more extreme event than might reasonably occur, a circumstance such as the draining of boiler water from the heat exchanger would still result in a rapid rise in solution temperature. Fission-product decay energy alone causes the temperature to rise at an initial rate of over 15°C per minute.

7.1.2 Case 2 – Interruption of Flow

Case 2, which would result from sudden and complete cessation of flow in the core circuit, is more extreme than that described in the preceding section, because only the solution in the core is available for storage of energy. Moreover, the fraction of delayed-neutron precursors which normally decay outside the core are retained within the core. These factors result in a more rapid rise in the core temperature than would result in the previous case, but the negative temperature coefficient causes fission power to decrease more quickly than before. The net result is a rise in core temperature of about 45°C in the first minute. The temperature continues to rise from fission-product decay at the same rate as shown in Fig. 7.2 for times in excess of 1 min.

7.1.3 Case 3 – Circulating-Pump Failure

The condition postulated in this case is that the core circulating pump stops suddenly but heat removal continues in the heat exchanger. Flow in the core circuit decelerates as the momentum of the fluid is dissipated, decreasing to the natural circulation rate in about 7 sec. The core temperature initially rises, since the decreased flow rate results in a lower rate of heat removal from the core; but this temperature rise results in the core becoming subcritical, and so the power decreases accordingly. Subsequently, the temperature decreases and an equilibrium power, of the order of 60 Mw, is reached; the reactor then remains critical, with fluid circulating at about 400 lb/sec. The momentary temperature rise is less than 10°C, and the behavior of the system following a pump failure does not appear to be hazardous as long as the stationary impeller does not offer a high resistance to flow.

7.1.4 Case 4 – Steam-Pressure Decrease

If the steam pressure on the shell side of the heat exchanger decreases rapidly, the temperature difference between fuel solution and boiler water is increased, resulting in a higher-than-normal rate of heat transfer. The temperature of the solution leaving the heat exchanger decreases, and there is a transient period in which this temperature changes with time. Cold liquid flows into the reactor core during this transient period and adds reactivity by means of the negative temperature coefficient, putting the reactor on a power excursion which causes a rapid rise of the pressure in the core.

The peak pressure rise which would occur during a power excursion in the TBR has been calculated

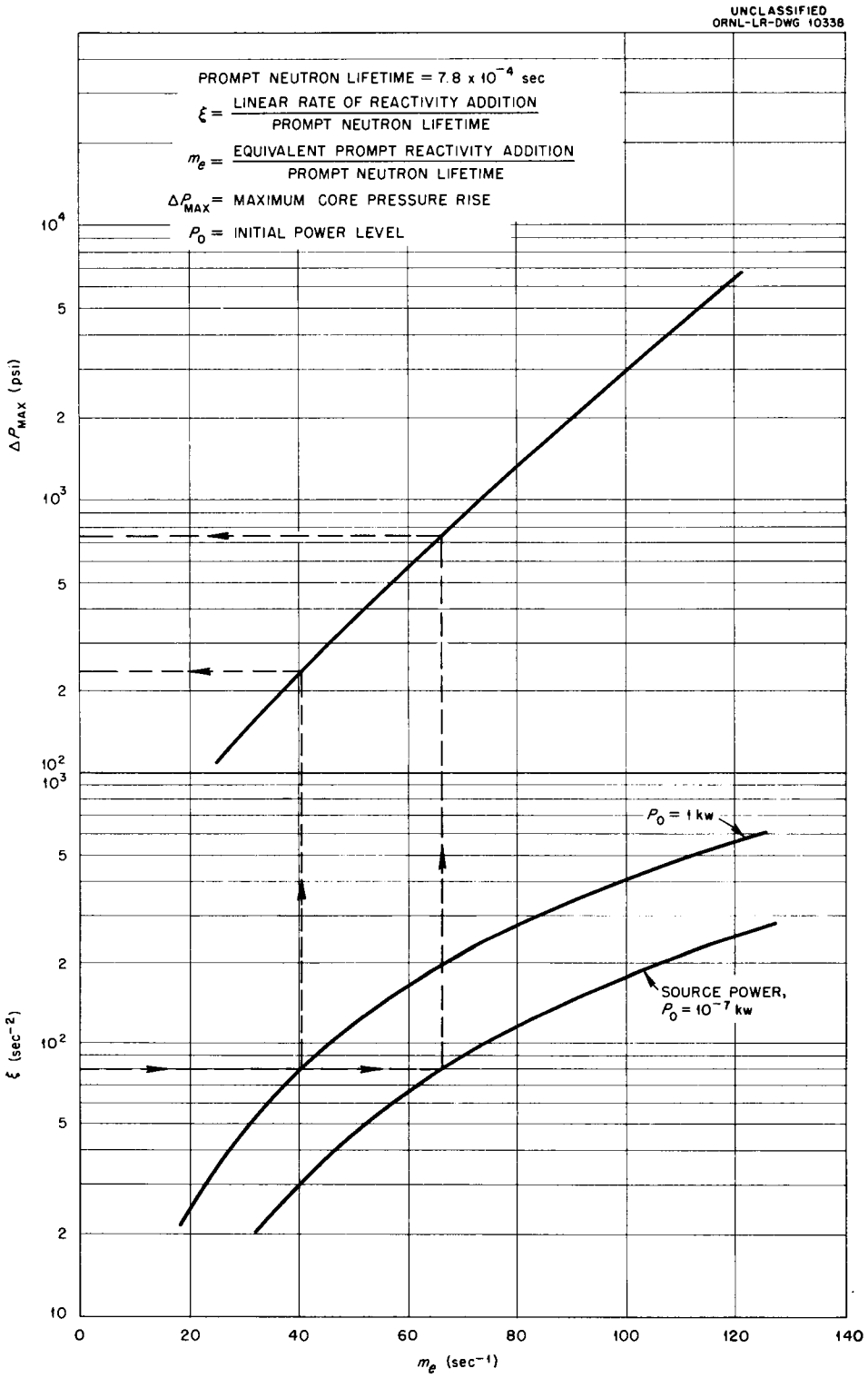

Fig. 7.3. Relationship Between Maximum Core Pressure Rise, Equivalent Prompt Reactivity Addition, and Rate of Reactivity Addition for TBR.

as a function of prompt reactivity addition, and the equivalent prompt addition has been related to the rate of reactivity addition and to the initial power level of the reactor.[3] The results of the calculation of pressure rise vs reactivity addition for the TBR are presented in Fig. 7.3. The rate of addition has been related to equivalent prompt addition for two initial power levels: 10^{-7} kw, corresponding to a source of 10^7 neutrons/sec, and 1 kw. Higher initial power levels result in less severe pressure surges, as indicated in Fig. 7.3.

As described above, reactivity can effectively be added to the reactor by lowering the steam pressure in the shell side of the heat exchanger. Since the shell-side steam temperature will closely follow the equilibrium relation between pressure and temperature for saturated steam, the temperature of the fuel fluid leaving the heat exchanger can be obtained as a function of time for given changes in shell-side pressure. Instead of considering the shell-side pressure, it is more convenient and just as useful to assume that the shell-side fluid temperature decreases linearly with time from 280 to 100°C. For a given rate of decrease in shell-side fluid temperature, dT_b/dt, the maximum rate of fall for the core fluid temperature can be obtained from a time-dependent energy balance over the reactor system. Combining this result with the value for the temperature coefficient of reactivity and the results presented in Fig. 7.3, the peak core pressure is obtained as a function of dT_b/dt. Figure 7.4 presents the net results in terms of peak core pressures vs dT_b/dt, with initial reactor power as a parameter.

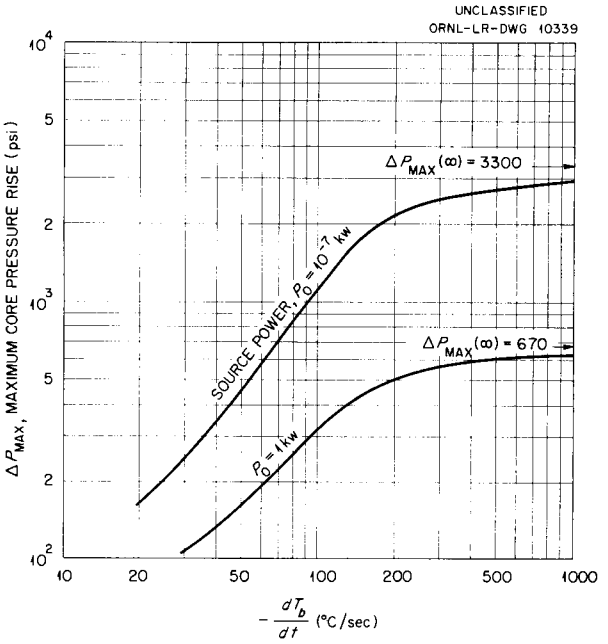

Fig. 7.4. Maximum Pressure Rise in Core of TBR vs Rate of Fall of Steam-Side Temperature in Heat Exchanger.

7.2 TEMPERATURE COEFFICIENT AND REACTOR SAFETY

P. R. Kasten M. W. Rosenthal

A high negative value for the temperature coefficient of reactivity is usually associated with a high degree of reactor safety. However, this is true only if reactivity is introduced by means other than the temperature coefficient itself. If reactivity is added by means of the temperature coefficient (e.g., by adding cold fluid to the reactor core), then the smaller the value of the temperature coefficient the smaller the reactivity addition. The introduction of cold fluid would add no reactivity to a system in which the temperature coefficient is zero. Thus, from this viewpoint, a small temperature coefficient would be desirable for a system in which the most hazardous reactivity addition is likely to occur by the introduction of cold fluid into the core. On the other hand, a large negative temperature coefficient is needed to keep the reactor near its design point under all operating conditions and to compensate for reactivity added by means other than that of changing the core fluid temperature. In reactors investigated so far, the most dangerous situation appears to be associated with cold-fluid addition to the core.

To evaluate the safety of reactors, specific cases are required. The parameters associated with the specific reactors investigated here are given in Table 7.1. The basis for selection of these particular reactors is that they appear at present to be the most economical of two types (viz., one region and two region) for producing 125 Mw of electrical energy (26% thermal efficiency). The safety is evaluated from the viewpoint of reactivity addition by means of a cooling incident;

[3] M. W. Rosenthal, *Pressure Rise in TBR Core Following Rapid Addition of Reactivity*, ORNL CF-55-10-45 (Oct. 14, 1955).

TABLE 7.1. PARAMETER VALUES OF REACTORS INVESTIGATED

Parameter	Two-Region Reactor	One-Region Reactor
Power level, Mw (heat)	480	480
Operating temperature, °C	280	280
Core diameter, ft	5	12
Core concentration		
g of U^{233} per kg of D_2O	2.48	5.82
g of U^{235} per kg of D_2O	0.30	0.56
g of uranium per kg of D_2O	8.3	13.42
g of thorium per liter	0	250
Core Thorex cycle time, days	336	400
Blanket thickness, ft	$2\frac{1}{4}$	0
Blanket concentration		
g of thorium per liter	1000	
g of U^{233} per kg of thorium	3	
Blanket Thorex cycle time, days	140	
Mean neutron lifetime, τ, sec	7.8×10^{-4}	3.25×10^{-4}
$\partial k_e/\partial T$, $°C^{-1}$ (temperature coefficient of reactivity)*	-1.5×10^{-3}	-3.73×10^{-3}
α_1, sec^{-1} (normalized friction coefficient)*	9	9
γ_2, $(sec\text{-}psi)^{-1}$ (dimensional reactor parameter)*	0.0155	0.0091
γ_3, sec^{-2} (dimensional reactor parameter)*	1260	53.6
ω_h^2, sec^{-2} (square of hydraulic frequency)*	24,000	1750

*P. R. Kasten, *Homogeneous Reactor Safety*, ORNL CF-55-5-51 (May 9, 1955).

that is, in each reactor, cool fluid at a given temperature is introduced at a given flow rate. For such an occurrence, the rate of reactivity addition in the one-region reactor would be lower than in the two-region reactor because of the smaller negative value of the temperature coefficient of reactivity and the larger core volume of the one-region reactor.

The relationship of interest in reactor safety considerations is the maximum pressure rise in the reactor core as a function of reactivity addition. The pressure rise can be subdivided into two effects: that due to the nuclear-physical system exclusive of the pressurizer volume and that due to the finite pressurizer volume itself. These two pressure effects are considered separately below.

The core pressure rise due to the first effect is related to the reactivity addition and the nuclear and physical parameter values. In the situation examined here, reactivity is added as a linear-rate function by cold fluid being added to the reactor core. The equivalent prompt reactivity addition, corresponding to a particular rate of reactivity addition, is a function of the initial power level of the reactor.[4]

For convenience in presentation, let

ξ = rate of reactivity addition divided by the mean lifetime of prompt neutrons,

P_0 = initial power level of the reactor,

[4]P. R. Kasten, *Homogeneous Reactor Safety*, ORNL CF-55-5-51 (May 9, 1955).

m_e = equivalent prompt reactivity addition divided by the mean lifetime of prompt neutrons,

Δp_{max} = maximum pressure rise within the reactor for a given reactivity addition.

The relations between ξ, P_0, m_e, and Δp_{max} are given in Figs. 7.5 and 7.6 for the reactors specified in Table 7.1 (ref. 5).

As shown in Fig. 7.5, if the largest permissible value of Δp_{max} is 200 psi, the limiting value of m_e is 56 sec^{-1}, or $\xi_2 = 108$ sec^{-2} when $P_0 = 1$ kw, where the subscript 2 refers to the two-region-reactor case. For the same rate of injection of cold fluid into the core region, the corresponding value of ξ_1 is 4.7. As given in Fig. 7.6, the resulting core-pressure rise of the one-region reactor would be only 110 psi. Thus, although the temperature coefficient is considerably smaller in the one-region machine, for the same cooling incident the core-pressure rise is about half that obtained in the two-region case.

In the preceding relations the volume of the pressurizer was treated as infinite; that is, the resistance to core-fluid expansion was assumed to result only from inertial and frictional effects. If the compression of vapor in the finite vapor volume of a pressurizer is considered, a core-pressure increase in addition to that calculated above must be included. This increase is to be added to values obtained from Figs. 7.1 and 7.2 and will be represented by Δp_p. For the two-region case, Δp_p is equal to 250 psi if the pressurizer volume is half the core volume. To obtain a value for Δp_p of 250 psi for the one-region reactor, the volume of the pressurizer would need to be 0.19 that of the core, corresponding to a pressurizer volume 5.25 times as large as that for the two-region reactor. However, increasing the size of the pressurizer probably has a negligible effect on over-all power costs, and so the above effect can be made as small as desired for either the one- or two-region reactor by means of physical design. The same is not true for Δp_{max}, since it is more dependent upon nuclear parameter values than is Δp_p. Physical design will also influence Δp_{max}, inasmuch as increasing the ratio of the cross-sectional area of the relief pipe to the core volume will increase ω_b^2 and decrease α_1. Both effects are desirable from a safety viewpoint. For the reactors considered here, the areas of the relief pipes were assumed to be equal.

The results given in Figs. 7.5 and 7.6 indicate that, when reactivity is added by extracting energy from the core heat exchangers, the reactor with the smaller absolute value of temperature coefficient of reactivity is the safer of the two. The above results, although obtained for one reactor of each type, could also be applied to a comparison of three two-region reactors with one one-region reactor if the total power were the same and the same cooling incident occurred. The cooling incidents would be comparable if both reactor systems had the same number of heat exchangers and if the number of heat exchangers failing at one time did not exceed the number attached to one two-region reactor. Thus, increasing the size of a reactor is actually desirable, from the standpoint of reactor safety, if the most dangerous situation corresponds to reactivity addition by means of the temperature coefficient itself. The actual case considered corresponds to adding 8.4% Δk_e per second in the two-region reactor. Such a rate appears to be extremely high, but it is associated with the parameter values chosen. Other parameter values do not appreciably change the relative safety of the two reactor types for the incident considered, although allowable rates of reactivity addition could differ significantly for the same pressure-rise limitation.

Although one- and two-region reactors are compared in the specific cases, the results in effect also provide a comparison of large and small reactors. The essential difference between the two-region reactor considered and a small, high-specific-power, one-region reactor would be in the value for $\partial k_e/\partial T$. If these reactors were compared on the same basis as outlined above, the two-region reactor would have a greater degree of safety than the small, high-specific-power, one-region reactor. However, the reactors treated in this comparison would not compete economically.

7.3 EFFECT OF Li_2SO_4 ON THE FUEL COST OF A PLUTONIUM-PRODUCING POWER REACTOR

H. C. Claiborne

The homogeneous reactor as a plutonium-producing power reactor requires uranium concentrations in

[5] P. R. Kasten and M. W. Rosenthal, *Temperature Coefficient and Reactor Safety*, ORNL CF-55-8-108 (Aug. 18, 1955).

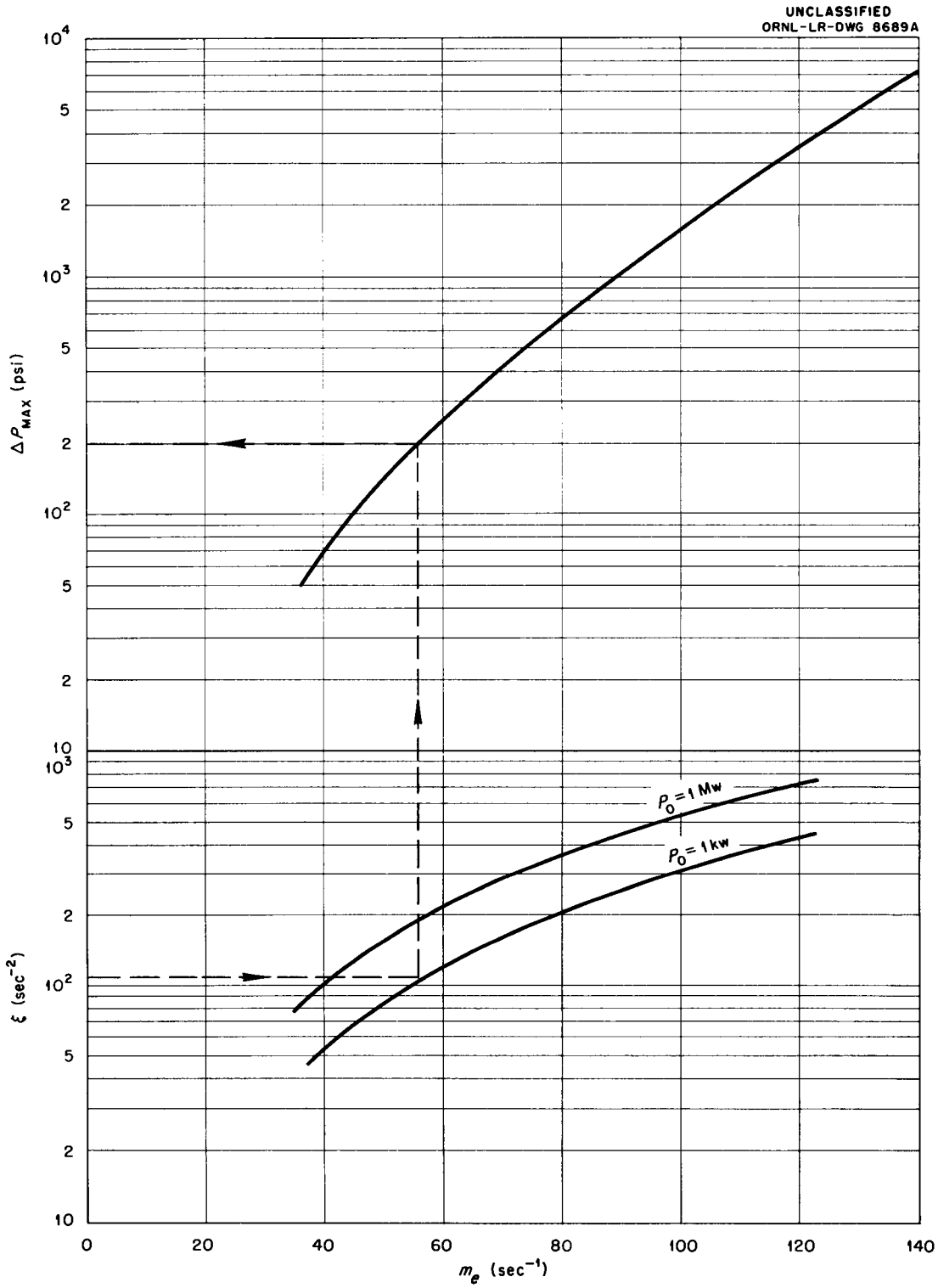

Fig. 7.5. Relationship Between Maximum Core Pressure Rise, Equivalent Prompt Reactivity Addition, and Rate of Reactivity Addition for the Two-Region Reactor.

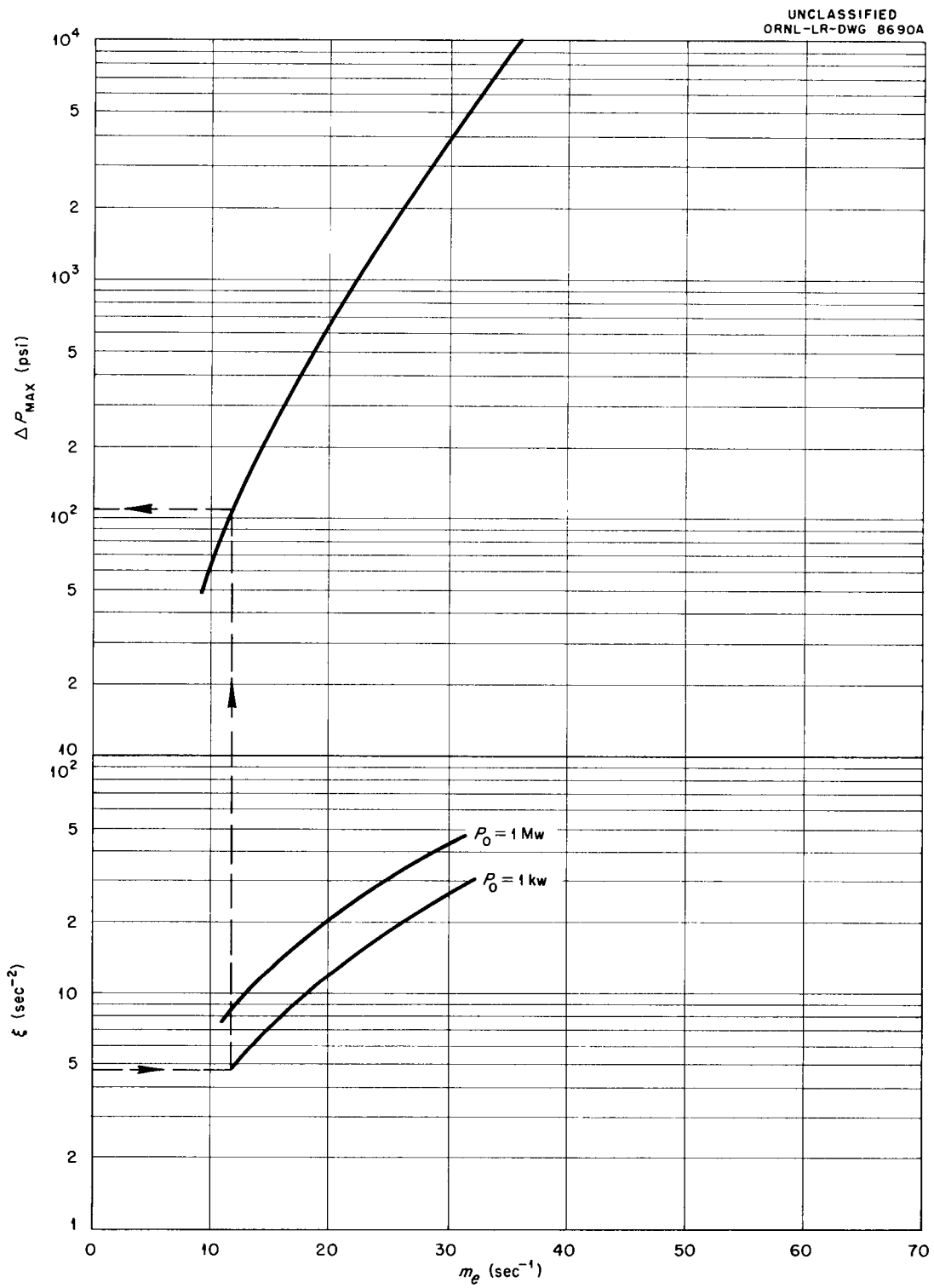

Fig. 7.6. Relationship Between Maximum Core Pressure Rise, Equivalent Prompt Reactivity Addition, and Rate of Reactivity Addition for the One-Region Reactor.

the order of a few hundred grams per liter. The most promising fuel for this purpose is a UO_2SO_4-D_2O solution. Unfortunately, a UO_2SO_4-D_2O solution of the required concentration is corrosive and forms two liquid phases at temperatures above 280°C; restriction of the temperature to below this value limits the thermal efficiency of the system.

It has been recently established that the addition of Li_2SO_4, in molar concentration equal to the uranium, will prevent phase separation for temperatures up to at least 350°C and also act as a corrosion inhibitor for stainless steel. The use of Li_2SO_4, therefore, would permit the attainment of higher thermal efficiences and might eliminate the otherwise-probable requirement of expensive titanium liners and pump parts.

The neutron-capture cross section of natural lithium is much too high (75 barns) for use. Consequently, Li^7 of high isotopic purity would be necessary. For an average cross section of 0.2 barn (which was assumed in this study), an isotopic purity of 99.98% Li^7 is required. Actually, a slightly lower purity probably would be sufficient for startup, since Li^6 would burn out due to neutron absorption.

The reactor system investigated was fueled with a UO_2SO_4-D_2O-Li_2SO_4 solution and required an enriched-uranium feed. It was assumed that high-quality plutonium (only 2 to 3% Pu^{240}) can be precipitated from the fuel solution and removed with hydraulic separators on about a one-day cycle. The effect of neptunium and plutonium solubility was ignored; the plutonium production represents the maximum value. For comparison purposes, calculations were also made for a UO_2SO_4-D_2O fuel solution. The calculations do not consider the temperature limitation imposed upon UO_2SO_4-D_2O solutions due to the formation of two liquid phases above 280°C. Characteristics of the system are presented below:

Electrical power, Mw	125
Heat generation, Mw	480
Diameter, ft	12
External power density, kw/liter	20
Average reactor temperature, °C	280
Reactor poisons, %	5
Chemical process rate, g of U^{235} per day	1000
Plutonium removal	Instantaneous
Isotopic purity of lithium, %	99.98

The results, as shown in Figs. 7.7 and 7.8 and Table 7.2, are based on a two-group calculation for a homogeneous, 12-ft, one-region, spherical reactor operating at an average temperature of 280°C and generating 125 Mw of electrical power at a net station efficiency of 26%.

The critical concentration and plutonium production are shown as a function of uranium concentration in Fig. 7.7. At concentrations over 600 g/liter, the Li_2SO_4 causes the required critical concentration to increase very rapidly. On the other hand, the effect of Li_2SO_4 on plutonium production diminishes when the uranium concentration increases. This is due to the displacement of D_2O by the Li_2SO_4, leading to an increase in resonance absorption in U^{238} at a given U^{238} concentration.

Figure 7.8 indicates that the addition of Li_2SO_4 to the fuel solution, in the same molar concentration as the uranium, adds about 0.8 mill/kwhr to the fuel cost near the optimum concentration of 500 g of uranium per liter (at reactor temperature). The negative fuel cost is the result of taking a credit of $40 per gram for the high-quality plutonium produced. Using a credit of $20 per gram, which is probably the highest credit possible for a "power-only" industry, the fuel cost increases to about 1.6 mills/kwhr. This would also lower the cost differential, due to the Li_2SO_4 addition, to about 0.4 mill/kwhr.

The 0.8 mill/kwhr increase due to Li_2SO_4 addition probably represents the maximum cost differential, since the two fuel solutions are compared at the same temperature. Addition of Li_2SO_4 would permit higher operating temperature with a corresponding increase in station efficiency. In addition, because of lowered corrosion rates and vapor pressure, savings on the cost of construction are probable.

A more thorough study, which includes the effects of reactor temperature and equipment costs, is required for a full evaluation of the economic effect of adding Li_2SO_4 to the fuel solution.

7.4 BREEDING RATIO AND FUEL-REMOVAL METHOD

P. R. Kasten

Companies operating future nuclear power stations may not wish to become involved in the chemical operations associated with continuous reprocessing of homogeneous fuel systems. Replacement of

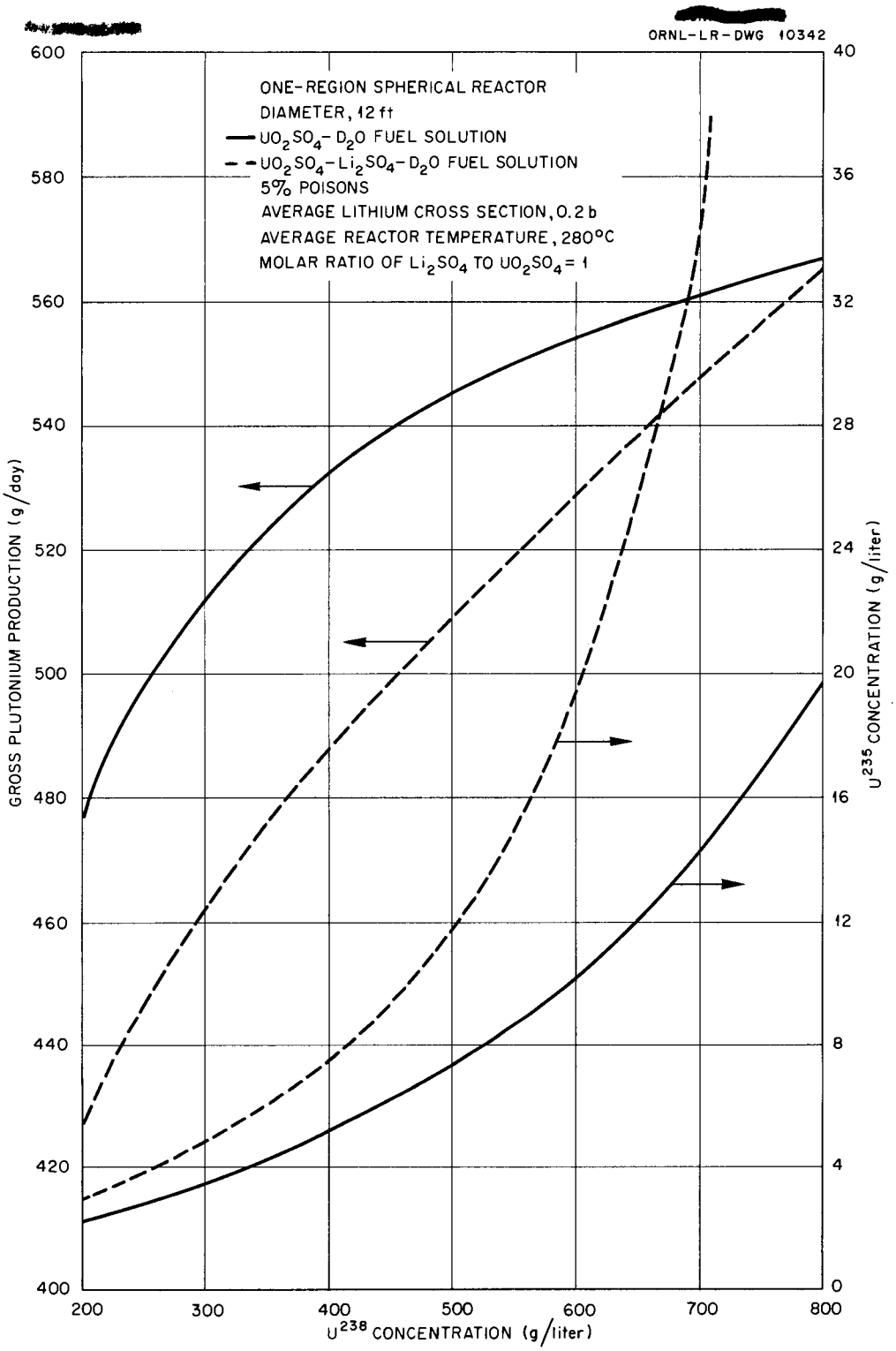

Fig. 7.7. Effect of Li_2SO_4 on the Critical Concentration and Plutonium Production.

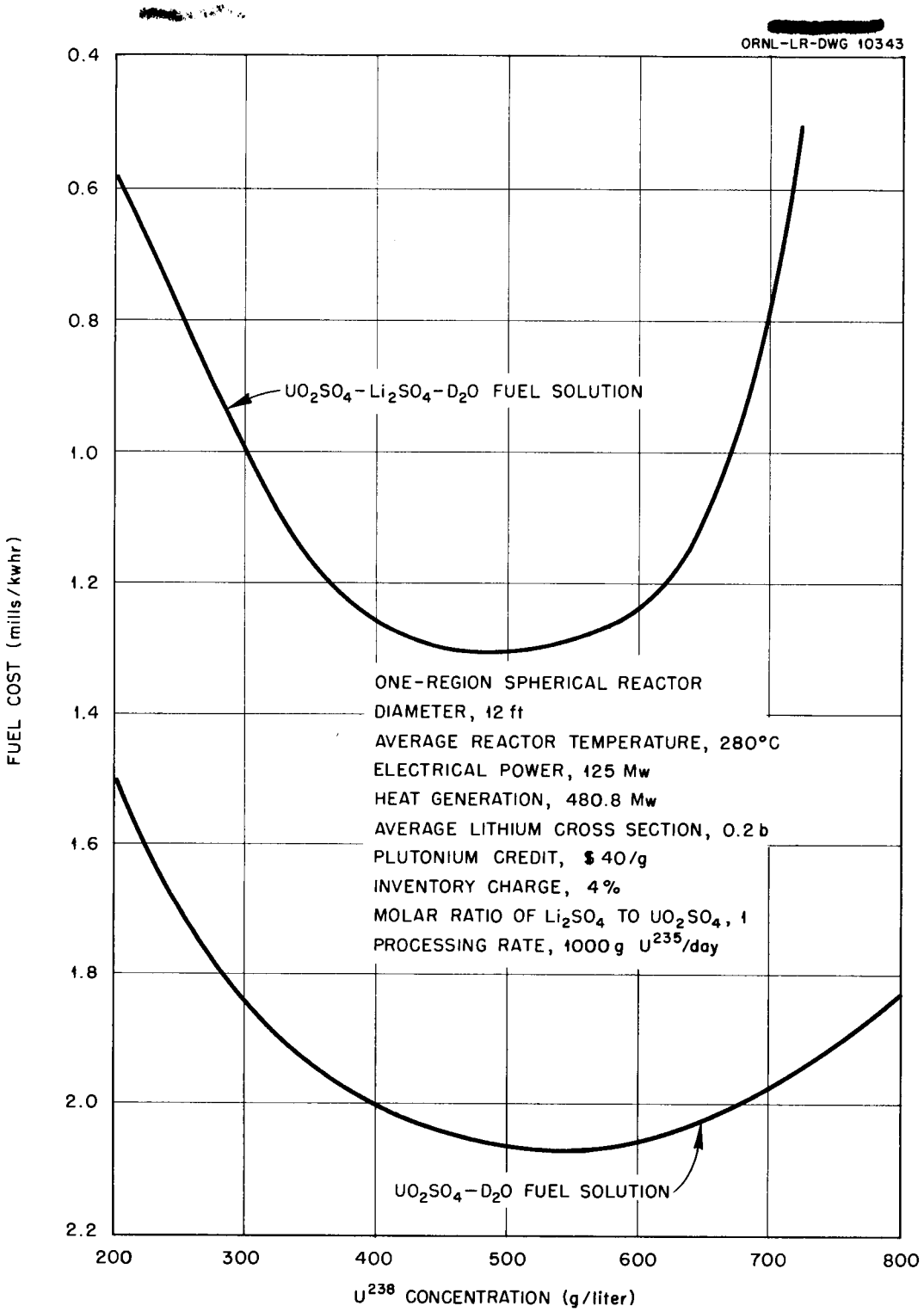

Fig. 7.8. Effect of Li_2SO_4 on the Fuel Cost of a Plutonium Producer–Power Reactor.

TABLE 7.2. SOME TYPICAL RESULTS FOR A ONE-REGION PLUTONIUM-PRODUCING POWER REACTOR*

Molar ratio of Li_2SO_4/UO_2SO_4	0	1	0	1	0	1
U^{238} concentration, g/liter	400	400	500	500	600	600
Reactor power density, kw/liter	18.8	18.8	18.8	18.8	18.8	18.8
Critical concentration, g of U^{235} per liter	5.27	7.5	7.4	11.8	10.2	19.3
Feed enrichment, wt fraction of U^{235}	0.021	0.030	0.024	0.037	0.027	0.050
Operating enrichment, wt fraction of U^{235}	0.013	0.018	0.015	0.023	0.017	0.031
Gross plutonium production, g/day	532	488	545	509	554	526
Net feed cost, mills/kwhr	3.43	3.53	3.49	3.65	3.55	3.72
Fuel inventory, mill/kwhr	0.17	0.26	0.23	0.40	0.32	0.65
Li_2SO_4 inventory, losses, mill/kwhr	0	0.007	0	0.008	0	0.009
D_2O inventory, losses, mill/kwhr	0.35	0.35	0.35	0.35	0.35	0.35
Chemical processing cost, mills/kwhr	1.15	1.10	1.13	1.10	1.12	1.09
Plutonium credit, mills/kwhr	7.09	6.51	7.27	6.79	7.39	7.05
Fuel cost, mills/kwhr	−2.00	−1.26	−2.07	−1.30	−2.06	−1.24
Plutonium credit required for fuel cost to be zero	28.70	33.00	29.30	33.10	29.50	34.00

*Electrical power, 125 Mw; heat generation, 480.8 Mw; reactor diameter, 12 ft; total system volume, 49,700 liters; poisons, 5%; average reactor temperature, 280°C; chemical processing rate, 1000 g of U^{235} per day; cost of D_2O, $28 per pound.

the fuel on a batch cycle would allow the power-production operation to be independent of the major fuel-processing operation. However, the processing method ultimately employed will be based upon economic factors. One facet in the economic picture is the breeding ratio associated with reactor operations. This study is concerned with the effect of the fuel-replacement method upon the breeding ratio, and so the average cycle time is assumed to be the same for both batch and continuous cycles. For either method it is assumed that fission gases and precipitated fission products (in the case of fuel solutions) might be removed continuously with equal facility; therefore the term "batch" or "continuous" as used here refers only to the method of removing those fission-product poisons which are not removed by gas separation and hydroclones.

Specific one-region and two-region homogeneous reactors were investigated. The particular reactors chosen were based upon economic studies[6] and represented minimum-cost electrical-power-producing reactor systems in which the fuel is continuously reprocessed. The one-region reactor considered has a 12-ft spherical core region, operates at a power density of ~20 kw/liter, contains about 6 g of fissionable material per liter of fluid and about 250 g of thorium per liter, has a continuous fuel-reprocessing cycle time of 400 days, contains 5.5% poisons, and has a breeding ratio of 1.012. The two-region reactor consists of a 5-ft spherical core surrounded by a 2¼-ft blanket containing 1000 g of thorium per liter. The core region generates 400 Mw of thermal energy; contains 6% poisons, about 2.3 g of fissionable material per liter of fluid, and about 6.6 g of uranium per liter; and operates on a reprocessing cycle time of 340 days. The blanket region generates 80 Mw of thermal energy, contains 3 g of U^{233} per kilogram of thorium and about 3% poisons, and operates on a reprocessing cycle time of 140 days.

An indication of the effect on breeding ratio is furnished by a comparison of the average poison cross sections of reactors operated on batch and

[6]H. C. Claiborne and M. Tobias, *Some Economic Aspects of Thorium Breeder Reactors*, ORNL-1810 (Oct. 12, 1955).

continuous processing cycles. As pointed out by Young,[7] the average poison cross section in a reactor operated on a batch cycle is smaller than the poison cross section in a continuously processed reactor if the fuel-processing time is the same in the two cases. Such a result indicates that a reactor operating on a batch fuel-replacement cycle may have a greater breeding ratio than the corresponding reactor operating on a continuous cycle. Rather than the average poison cross section itself, however, the breeding ratio is influenced by the average value of the product of the poison cross section and the flux. Since the flux varies with time in a reactor operating on a batch process and since the specific variation is dependent upon the particular reactor system, an a priori statement cannot be made as to the desirability of batch processing. To indicate that the batch operation is indeed better, calculations were made for one- and two-region reactor systems.[8]

7.4.1 One-Region Reactor

For a large, bare, homogeneous reactor, the macroscopic fuel-absorption cross section is given by

$$\Sigma_f = a + b\Sigma_p \ , \tag{1}$$

where

Σ_f = macroscopic fuel absorption cross section, cm^{-1},

Σ_p = macroscopic poison cross section, cm^{-1},

a, b = constants dependent upon nuclear constants, reactor geometry, and size.

The assumption of constant power appears to be logical for a power-producing one-region reactor. Thus the same number of neutrons will be available for absorption in fertile material and poisons for either batch or continuous fuel replacement, since any change in leakage and parasitic losses would be negligible. A comparison of neutron absorptions in poisons for the two cases will therefore show which fuel-replacement method results in the higher breeding ratio.

For the single-region reactor under consideration, the ratio of absorptions in poisons for the batch-to-continuous cases is given by

$$\frac{A^b}{A^c} < \frac{\int_0^T S(x)\,[1-(x/T)]\,dx}{\int_0^\infty S(x)\,e^{-x/T}\,dx} \left(\frac{\phi^b}{\phi^c}\right)_{max} , \tag{2}$$

where

A = total neutron absorption by poisons in cycle time T,

$S(x)$ = microscopic poison cross section as a function of time,

b, c = superscripts referring to batch and continuous fuel replacement, respectively,

T = average fuel-replacement cycle time,

ϕ = average neutron flux.

Inserting the value for $S(x)$, as given by Sampson *et al.*,[9] for the reactor conditions stated previously, the above inequality becomes

$$\frac{A^b}{A^c} \approx 0.7 \ . \tag{3}$$

The breeding ratio will thus be slightly greater for the batch process. Specifically, the breeding ratio will increase from 1.012 for continuous reprocessing to about 1.03 for batch reprocessing. The important point is that no breeding-ratio penalty is incurred because of batch replacement of the fuel.

7.4.2 Two-Region Reactor

For the core region the problem is similar to the one-region reactor, except that the core power changes with time for the case of batch operation. With this stipulation, insertion of the appropriate poison cross-section data gives

$$\frac{A^b}{A^c} < 0.9 \ . \tag{4}$$

Since relatively fewer neutrons are absorbed by fission products when the batch fuel-replacement method is used, more neutrons will leak into the blanket and be absorbed by fertile material, leading to a higher breeding ratio.

[7] G. Young, *On the Formulation of the Fission Product Poisoning Problem*, CL-GY-1 (Dec. 4, 1946).

[8] P. R. Kasten, *Breeding Ratio and Chemical Processing Method*, ORNL CF-55-9-4 (Sept. 1, 1955).

[9] J. B. Sampson, W. L. Robb, J. R. Stehm, and J. K. Davidson, *Poisoning in Thermal Reactors Due to Stable Fission Products*, KAPL-1226 (Oct. 4, 1954).

For the blanket region, the blanket power will vary from zero to an appreciable magnitude if batch fuel replacement is used. If, for the batch case, the blanket power is assumed to vary linearly with time, the reactor conditions previously specified give A^b/A^c to be

$$\frac{A^b}{A^c} \approx 0.77 \quad . \tag{5}$$

Therefore, considering the blanket alone, the average breeding ratio over time T would be greater for the batch fuel-replacement method.

Thus, for both the one- and two-region reactors studied, the batch fuel-replacement method results in a higher breeding ratio than would continuous reprocessing. The increase in the breeding ratio appears to be in the range 0.01 to 0.03. A detailed investigation pertaining to the time behavior of critical reactor systems is now proceeding, and the purpose is to determine the over-all economic features associated with batch chemical processing.

[10] T. B. Fowler, *Oracle Code for a General Two-Region, Two-Group Spherical Homogeneous Reactor Calculation*, ORNL CF-55-9-133 (Sept. 22, 1955).

7.5 MATHEMATICS AND COMPUTATIONS

T. B. Fowler
D. C. Hamilton
C. W. Nestor, Jr.
M. K. Hullings

A general code has been written for the Oracle for the solution of a spherical, homogeneous, two-region reactor by the two-group method.[10] The calculation can accommodate two fuel components plus seven other nuclear components in the blanket, and it can accommodate two fuel components, poisons, moderator, and four other nuclear components in the core. The reactor may or may not contain a core tank separating the two regions. This code will compute for a non-steady-state reactor the stable reactor period, effective multiplication constant, mean lifetime of prompt neutrons, and temperature coefficient of reactivity, as well as for a critical steady-state reactor the fuel concentration, flux, and neutron balance.

An Oracle code has also been written for reactors having cylindrical geometries. Among the quantities calculated are neutron bookkeeping, flux distributions, critical concentrations, mean lifetime of prompt neutrons, and reactivity coefficients. Except for several Bessel function subroutines, the code is complete.

Part III

ENGINEERING DEVELOPMENT

J. A. Lane

8. DEVELOPMENT OF FUEL-SYSTEM COMPONENTS

C. B. Graham

J. S. Culver
L. F. Goode
B. A. Hannaford
P. H. Harley
P. P. Holz
I. K. Namba
W. L. Ross
I. Spiewak
D. S. Toomb
H. D. Wills

8.1 RECOMBINER DEVELOPMENT

8.1.1 High-Pressure Recombiner Loop

Severe stress-corrosion cracking was observed in portions of the loop in contact with superheated vapors.[1] It was believed that chloride present in the loop was responsible. In order to establish this, it is necessary to repeat the run in the absence of halogens.

Chloride was originally introduced in the caustic of the electrolytic cells. Reagent-grade KOH normally contains about 100 ppm Cl^-. Attempts to remove the Cl^- by $AgNO_3$, by silver-electrode electrolysis, and by H_2O_2 treatment were unsuccessful. Ion-exchange methods were not feasible because of the pH conditions. The best KOH prepared (50 ppm Cl^-) was from metallic potassium. However, $Ba(OH)_2$ was found to contain only 7 ppm Cl^-. Its electrical conductivity is probably adequate. The loop is being rebuilt, and a low-halogen run will be carried out.

8.1.2 Natural-Circulation Catalytic Recombiner

A low-pressure natural-circulation recombiner was designed and fabricated. Tests have indicated the feasibility of the design.

The test unit, Fig. 8.1, contains a 4-in. stainless steel chimney 6 ft high, inside a 12-in. sched 40 pipe. The catalyst medium is 6 in. of platinized Yorkmesh. Jacketed electrical heaters are placed under the catalyst to start thermal convection and maintain a dry catalyst for startup. The system has an air-cooled condenser containing 29.1 ft of $\frac{5}{8}$-in.-OD copper tubing. A liquid-level probe is provided to maintain a predetermined water level. Thermocouples are placed at various points in the unit for control purposes and temperature recording.

The system was operated with steam diluent at 100 psia and with air diluent at atmospheric pressure.

To simulate off-gas introduction, a metered quantity of H_2 and O_2 was fed in at approximately the midsection of the unit. With steam being used as a diluent, the unit operated satisfactorily with an H_2 flow of 1.064 cfm, which was the maximum flow attainable with the rotameter. For the initial run, H_2 and O_2 were added in small quantities

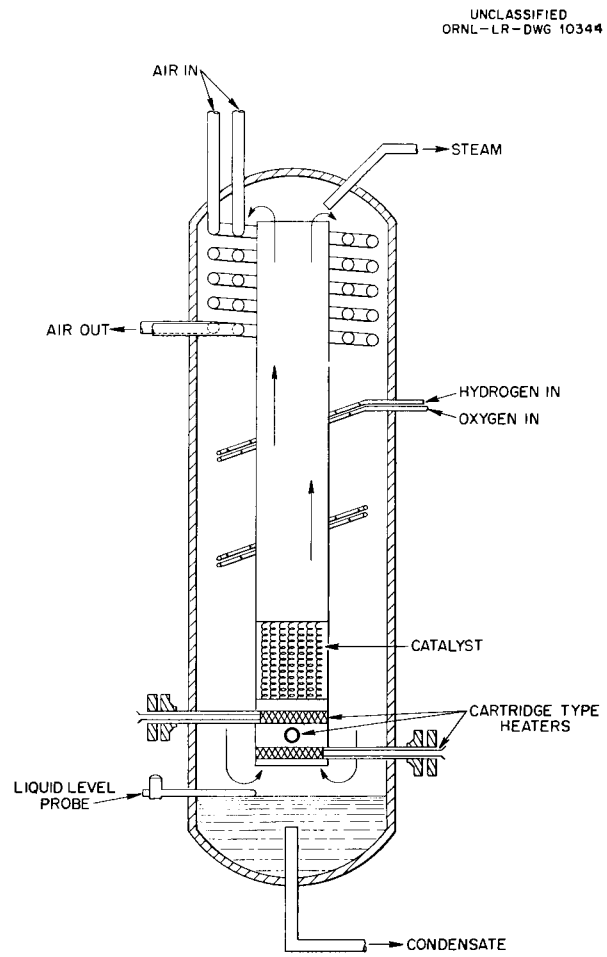

Fig. 8.1. Natural-Circulation Catalytic Recombiner.

[1] C. B. Graham *et al.*, *HRP Quar. Prog. Rep. July 31, 1955*, ORNL-1943, p 153–154.

(0.266 and 0.133 cfm, respectively), and the rates were gradually increased. On subsequent runs, the maximum flow rate was introduced at once, without causing flashbacks. The maximum temperature attained in the chimney was 792°F.

With air as a diluent, the unit operated satisfactorily with H_2 flow up to 0.20 cfm. A further increase in H_2 flow caused flashbacks to occur at an H_2 concentration of 3.5 mole %. The maximum temperature in the chimney was 597°F when air was used as a diluent.

8.1.3 Battelle and Syracuse Subcontracts

Battelle Memorial Institute has completed its investigations on the solubility of gases in uranyl sulfate solutions. A summary report is being prepared which will give the solubilities of O_2, H_2, He, and Xe at temperatures up to 550°F in solutions of concentrations up to 243 g of uranium per liter.

Explosion-limit determinations in autoclaves of several sizes have indicated that the limits are very strongly influenced by geometry and also are considerably lower in large systems than was previously believed. For example, for stoichiometric $2H_2 + O_2$ in steam at 480°F, the reaction limit in a 1.5-in.-dia bomb was 22.6 mole % gas; in a 2.5-in. bomb, 11.6 mole %; and in a 3-in. bomb, around 2 mole %.[2] The leaner gas mixtures were more difficult to spark-ignite.

Investigations of detonation pressures, damping of explosion waves, and transient loading of containers are under way. Some experimental results on detonation pressures have been reported. The presence of steam reduces the explosion pressures considerably. For example, pressures of 9880 psi were developed from the following detonations: $2H_2 + O_2$ at 25°C and 294 psia; $2H_2 + O_2$ at 150°C and 467 psia + 69-psi water vapor; and $2H_2 + O_2$ at 200°C and 671 psia + 226-psi water vapor.[3]

Syracuse University has completed its investigations of the PVT relations, heat capacity, and composition of steam-helium and steam-oxygen mixtures.[4,5] The conclusions were that Dalton's law correlated these properties quite well. The work on viscosity of these mixtures should be completed soon.

It is difficult to draw any conclusions concerning the safety of high-pressure recombiners at this stage of the investigations. However, it does seem likely that reactors can be designed so that an accidental explosion will not cause any damage except to the internal parts of the high-pressure recombiner.

8.2 SMALL REACTOR COMPONENTS

8.2.1 20-cfm Canned-Rotor Gas Circulator

The layout drawing and bill of materials for a 20-cfm gas circulator were approved. This unit is suitable for operation in the HRT or larger reactors to supply vapor circulation in high-pressure recombiner systems. Allis-Chalmers Mfg. Co. is completing details and procuring materials to fabricate the unit.

8.2.2 ORNL Gas Circulator

The ORNL gas circulator, a converted 5-gpm ORNL pump, suffered an electrical failure due to either the windings becoming wet or the insulation being mechanically broken. The unit has not gone back into operation. This unit was tested to indicate problems which would be encountered in the development of a gas circulator for reactor use.

8.2.3 Small Circulating Pumps

After repeated interruptions due to small leaks, a thorough helium leak test was performed on the 2000-psi 5-gpm canned-rotor pump loop. All detected defects were repaired, and subsequent operation was satisfactory. An asbestos gasket was substituted for the metal-casing gasket in the pump. The asbestos gasket was too thin and did not allow sufficient clearance between the impeller shroud and the scroll face; rubbing of metal surfaces occurred. The problem was solved with a gasket consisting of metal sandwiched between two layers of asbestos. The unit has accumulated 2400 hr of operation with water at 300°C.

---

[2] Letter from E. F. Stephan, Battelle Memorial Institute, to I. Spiewak, Sept. 28, 1955.

[3] P. L. McGill, *Research on Thermodynamic Properties of Gaseous Mixtures. Measurement of the Detonation Pressure of Hydrogen, Oxygen, and Steam Mixtures*, Progress Report, Syracuse University Research Institute, June 1955.

[4] J. A. Luker and T. Gniewek, *Saturation Composition of Steam-Helium-Water Mixtures. P-V-T Data and Heat Capacity of Superheated Steam-Helium-Water Mixtures*, Syracuse University Research Institute, Ch.E. 273-557F, July 29, 1955.

[5] J. A. Luker and T. Gniewek, *Determination of P-V-T Relationships and Heat Capacity of Steam-Oxygen Mixtures*, Syracuse University Research Institute, Ch.E. 273-558F, Aug. 2, 1955.

The 1000-psi 5-gpm canned-rotor pump has accumulated 9400 hr of operation with 250°C water. The stator has operated for 4500 hr since the last failure.

The 5-gpm canned-rotor pump, rewired with windings in series to increase stator life, has operated over 5000 hr with water. Operation has been normal, and no failures have occurred on this unit.

8.3 4000-gpm LOOP[6]

High-pressure oil traps were installed on the discharge line of both new Scott & Williams feed pumps to keep oil out of the loop in the event of pulsator failures. Minor loop revisions completed preparations for the series of runs on uranyl sulfate solutions.

The loop was operated with oxygenated water at 1000 psi and 250°C for approximately 150 hr before UO_2SO_4 was added. The current UO_2SO_4 run is reported in Sec. 10.1.1*c*.

At the conclusion of this run, the Byron Jackson pump will be disassembled for inspection. The 18-8 stainless steel bolts which were installed in the stator assembly during the last inspection period will be removed and replaced with bolts made from 17-4 PH stainless steel.

8.4 TITANIUM-LINED EQUIPMENT

A contract has been made with Crane Co. to produce test lengths of 20- and 3½-in.-dia steel pipe lined with titanium. Design calculations are already under way; however, fabrication will not be completed for several months.

A contract has been made with The Pfaudler Co. for construction of a small titanium-lined heat exchanger, which should be completed and ready for testing early in 1956. Both the pipe and heat exchanger will be used for testing only and will serve as a means of perfecting fabrication techniques for this type of construction.

A third contract is to be awarded to the Armour Research Foundation for developing a method of metallurgically cladding titanium on steel. This contract will run for six months starting March 1, 1956.

[6] J. R. McWherter *et al.*, *HRP Quar. Prog. Rep. March 15, 1951*, ORNL-1221, p 18.

9. DEVELOPMENT OF BLANKET-SYSTEM COMPONENTS

R. N. Lyon

A. S. Kitzes, W. Q. Hullings, C. G. Lawson, J. D. Perret, L. F. Parsly, H. D. Wills, R. H. Nimmo, L. E. McTaggart, M. Richardson, P. R. Crowley, R. P. Wichner, D. G. Davis

9.1 WESTINGHOUSE 200A SLURRY PUMP

W. Q. Hullings H. D. Wills

A total of 787 hr of slurry operation has now been logged by the Westinghouse 200A slurry pump loop. A number of bearing failures have been experienced, but these are attributed to curable causes. In all cases, some slurry was found in the motor cavity of the pump after a run. For this reason, tests were made for determining the amount of condensate flow required to keep the motor cavity free from solids. The experiments have been completed, but the results have not yet been analyzed.

During one run with unusually high solids content in the motor cavity, the motor-cooling coil became plugged; this permitted the motor cavity temperature to rise above the desirable limit for the Graphitar bearings. The pump has now been revised so that the flow of the cooled stream and the temperature in the motor cavity can be measured. Experiments showed that the Kingsbury bearing became noisy when the cooled flow was reduced to less than 0.5 gpm.

It was also found that the temperature in the motor cavity rises rapidly from the usual temperature of about 120°F to temperatures above 212°F when the pump is stopped with the system temperature at 300°C.

The 200A pump and others of this general model are designed so that a seal weld is used to close the casing. Since in developmental work with the pump it is desirable to open the casing frequently, attempts have been made to secure a reliable closure with gaskets. So far no gasket has proved to be completely satisfactory, although a pure-gold O-ring gasket and an annealed-stainless-steel teardrop gasket have produced the most trouble-free seals to date. At present a custom-built seal-weld cutter is on order. When this is received in December, it is believed that sealing the casing will no longer be a problem.

In the most recent run, very serious caking of thorium oxide occurred, with a major portion of the suspended solids being deposited on the walls in cakes which became as much as $\frac{1}{4}$ in. thick in less than 150 hr. This caking has not yet been satisfactorily explained, but a careful investigation has begun and experiments are already under way to test some of the proposed explanations.

9.2 DUMP TANK–EVAPORATOR TESTS

M. Richardson

Four dump-tank systems, which look promising for use in the HRT blanket, are being investigated in small steel or glass models (Fig. 9.1).

1. Filter Plate. – A Micro Metallic Corp. stainless steel filter is welded to the bottom of the dump tank to form a steam chest (*a*, Fig. 9.1). At a pressure of 2 to 3 psi, sufficient steam passes through the filter plate to keep the solids suspended as they are circulated by boiling-convection. In tests with slurry, excessive foaming occurred as a result of the minute bubbles formed as the steam passed through the filter plate. No acceptable method for minimizing foaming has yet been found.

2. Race Track. – The use of a longitudinal barrier to form a continuous slurry-circulation path, that is, "race track," in combination with an air-sparging system was operated successfully with slurry (*b*, Fig. 9.1). The driving force created by the two opposing thermal legs circulated slurry around the vertical barrier mounted in the center of the tank. Without the sparging system, solids settled out in the less-turbulent areas.

3. Vertical Gas Lift. – A slurry containing 1000 g of thorium per kilogram of H_2O was circulated at room temperature in a vertical-gas-lift system for two weeks without any appreciable change in concentration occurring (*c*, Fig. 9.1). The system was shut down for varying lengths of time up to two weeks. No difficulty was encountered in resuspending the solids. After the two-week shutdown, with the bed approximately 2 ft deep, an air pressure of 8 psig was required to set the bed in motion. Once the bed was in motion, only 0.3 cfm of 2.5-psig air was required to keep the solids suspended in 12 liters of slurry.

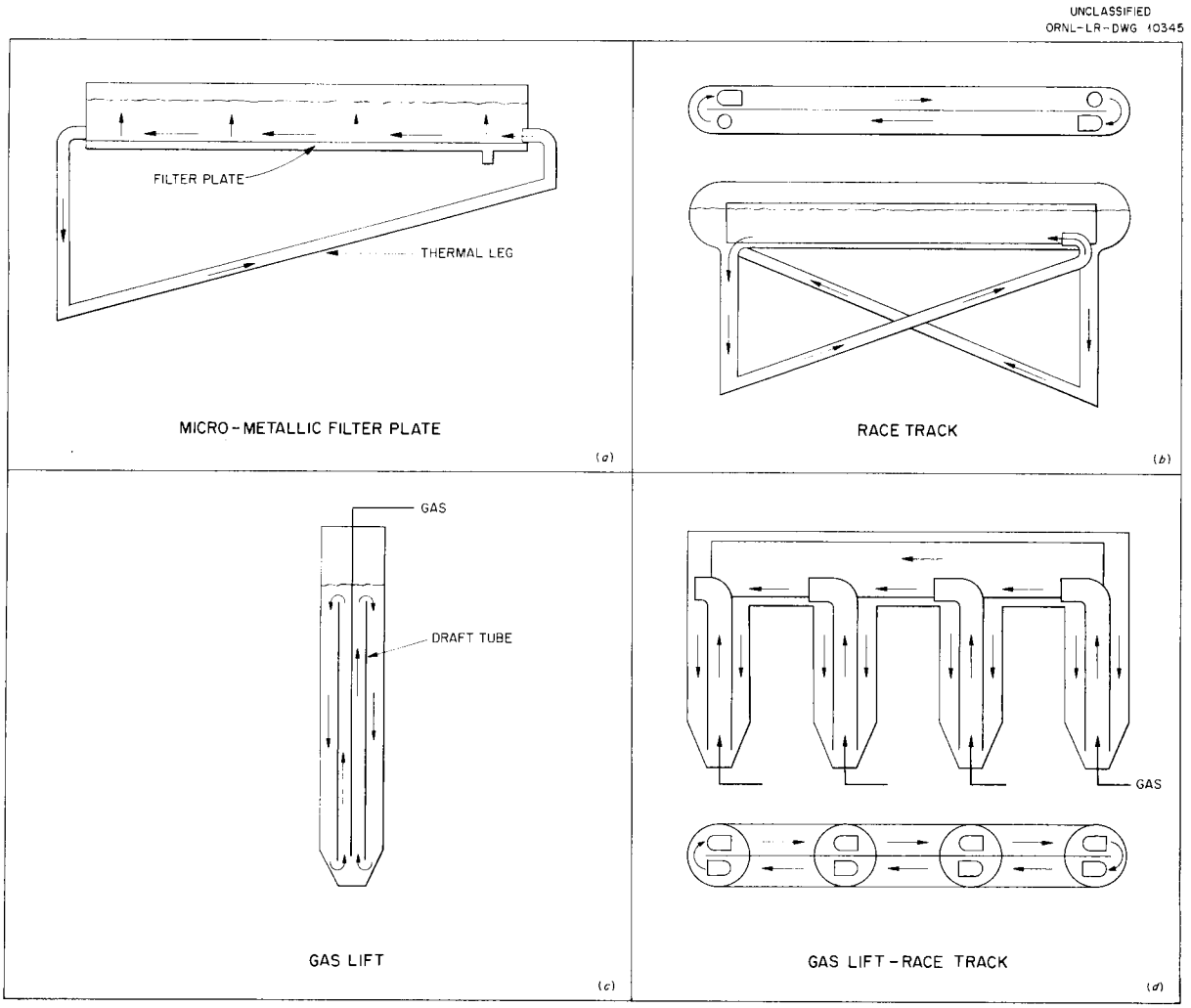

Fig. 9.1. Direction of Flow in Dump-Tank Models.

The system operated normally with 0.3 cfm of air at 2.5 psig. A slight accumulation of solids at the top of the column was observed.

4. Vertical Gas Lift–Race Track System. – This system combines the high velocities of the race track with the circulation efficiency of the gas lift (*d*, Fig. 9.1). A test is now in progress in which a slurry containing 600 g of thorium per kilogram of H_2O is being circulated in a 6-in.-dia prototype; no settling of the solids has been observed.

Of the four systems, the gas lift–race track combination looks most promising. A steel mock-up, half HRT scale and using steam instead of air, is now being designed.

9.3 RHEOLOGICAL PROPERTIES OF SLURRY SYSTEMS

P. R. Crowley

Construction of the high-temperature pipeline viscometer is complete. Calibration of the system with a high-grade lubricating oil is now in progress.

The system shown in Fig. 9.2 consists of two pots connected by a length of small-diameter heavy-walled tubing. The slurry, made to flow from one tank to the other under the action of a differential pressure, is stirred in the supply reservoir, a modified 5-gpm pump being used as the agitator.

End effects have been minimized by shaping the entrances and exits of the various tubes to conform

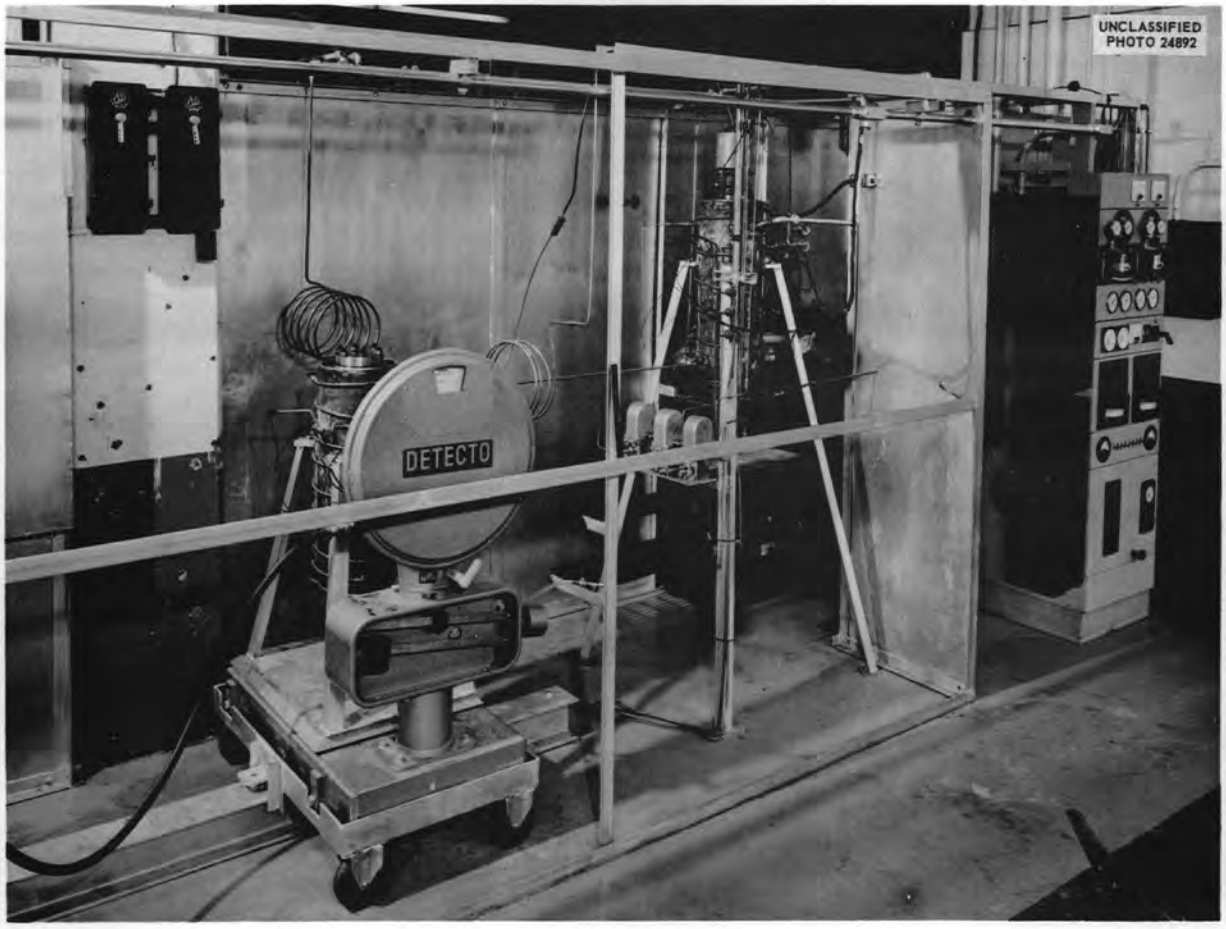

Fig. 9.2. High-Temperature Pipeline Viscometer.

to the geometry of a venturi; for these sections the tubing, therefore, is essentially an extended section of the throat of a venturi.

To maintain constant temperature and to minimize temperature gradients along the length of tubing, the tubes will be heated.

The rheological properties of thorium oxide slurries containing 500 to 1000 g of thorium per kilogram of H_2O will be measured over a temperature range from ambient to 300°C. By varying the diameter and length of the pipes, thixotropy will be studied. Shear diagrams at elevated temperatures will be extended into the turbulent region so that turbulent viscosities of the various slurries can be determined.

[1] C. G. Lawson, *A State-of-the-Art Survey on Engineering Calculations for Slurry Systems*, ORNL CF-55-9-165 (Sept. 22, 1955).

9.4 HEAT-TRANSFER STUDIES

C. G. Lawson R. P. Wichner

For Newtonian or nearly Newtonian slurries, the Dittus-Boelter equation or modified forms of this equation can be used to predict turbulent heat-transfer coefficients. The same equations can probably be used[1] for Bingham-type plastic slurries if the ratio of yield stress to shear at the pipe wall τ_y/τ_w is less than 0.1. These relationships, however, have not been applied to Bingham plastics with a yield value above 0.1 lb/ft^2; no data are available.

Since, under some conditions, thorium oxide slurries behave as Bingham plastics with yield values exceeding 0.1 lb/ft^2, heat-transfer studies were initiated. A low-pressure (150-psi), low-temperature (150°C) loop has been assembled to

measure simultaneously the heat-transfer characteristics and rheological properties of slurries containing from 500 to 1000 g of thorium as the oxide per kilogram of water (Fig. 9.3). Calibration of the system is now in progress.

9.5 SLURRY-TRANSPORT VELOCITIES

J. D. Perret

Pickup velocities or minimum bulk fluid velocities, necessary to resuspend a settled slurry, were measured in a glass system for circulating thorium oxide slurries (Fig. 9.4). Minimum transport velocities necessary to ensure homogeneity of the circulating slurry were also determined at room temperature.

A series of runs with varying slurry concentrations was completed in which ¾-in.-ID glass pipe was used. Sedimentation and wall velocities were visually determined by following the motion of small (<200-mesh) graphite particles in the slurry. Results are shown in Table 9.1.

The resuspension of slurry from a sedimented bed on the bottom of a pipe was observed to follow a definite pattern. As the bulk velocity of the slurry flowing over the bed was increased, the bed thickness decreased, until a velocity was reached at which the remaining sediment became a moving bed along the bottom of the pipe. The velocity at which this phenomenon occurred was designated as the lower critical bulk velocity, V_{cl}. At the lower critical velocity, solids did not deposit in the straight section of smooth pipe; this velocity, however, was not sufficient to ensure a uniform concentration throughout the pipe, and any small obstruction did cause sedimentation. As the bulk velocity was further increased, the moving bed was reduced in size, and the velocity at which the moving bed disappeared completely was called the upper critical bulk velocity, V_{cu}. At velocities higher than the upper critical bulk velocity, the suspensions were homogeneous for all slurry concentrations.

The data will be extended to include determination of pickup and transport velocities for circulating slurries containing 200 to 1000 g of thorium per kilogram of H_2O in pipes ranging in diameter from ⅜ to 3 in.

TABLE 9.1. TRANSPORT VELOCITIES AT ROOM TEMPERATURE FOR ThO_2 SLURRIES IN ¾-in. GLASS PIPE

Slurry Concentration (g of Th per kg of H_2O)	Density (g/cc)	Bulk Critical Velocity (fps)	
		Lower, V_{cl}	Upper, V_{cu}
265	1.26	1.4	
425	1.41	1.7	
490	1.47	2.0	
600	1.56	2.3	
690	1.65	2.4	3.7
825	1.76	1.6	3.5
910	1.84	1	3.7
1030	1.94	0	4.5
1180	2.05	0	5.2
1325	2.17	0	5.5
1490	2.29	0	6.3
1645	2.43	0	7.4

9.6 SLURRY BLANKET MOCKUP

L. F. Parsly, L. E. McTaggart, R. H. Nimmo, D. G. Davis

At the end of the report period, construction of the mockup was approximately 95% complete. All process piping and 95% of the auxiliary piping had been installed. Instrument piping and tubing connections were approximately 20% complete. Figure 9.5 shows a general view of the installation above the track floor in Building 9204-1. Figure 9.6 gives a view of the instrument panel, and Fig. 9.7 shows the piping at the bottom of the pressurizer.

Corrosion tests on the type 54S aluminum test-core-tank material have indicated that it may be unsuited for service in flowing slurry at 200°C. Accordingly, a stainless steel replacement has been designed. It should still be possible to utilize the aluminum core for preliminary tests at temperatures up to 100°C.

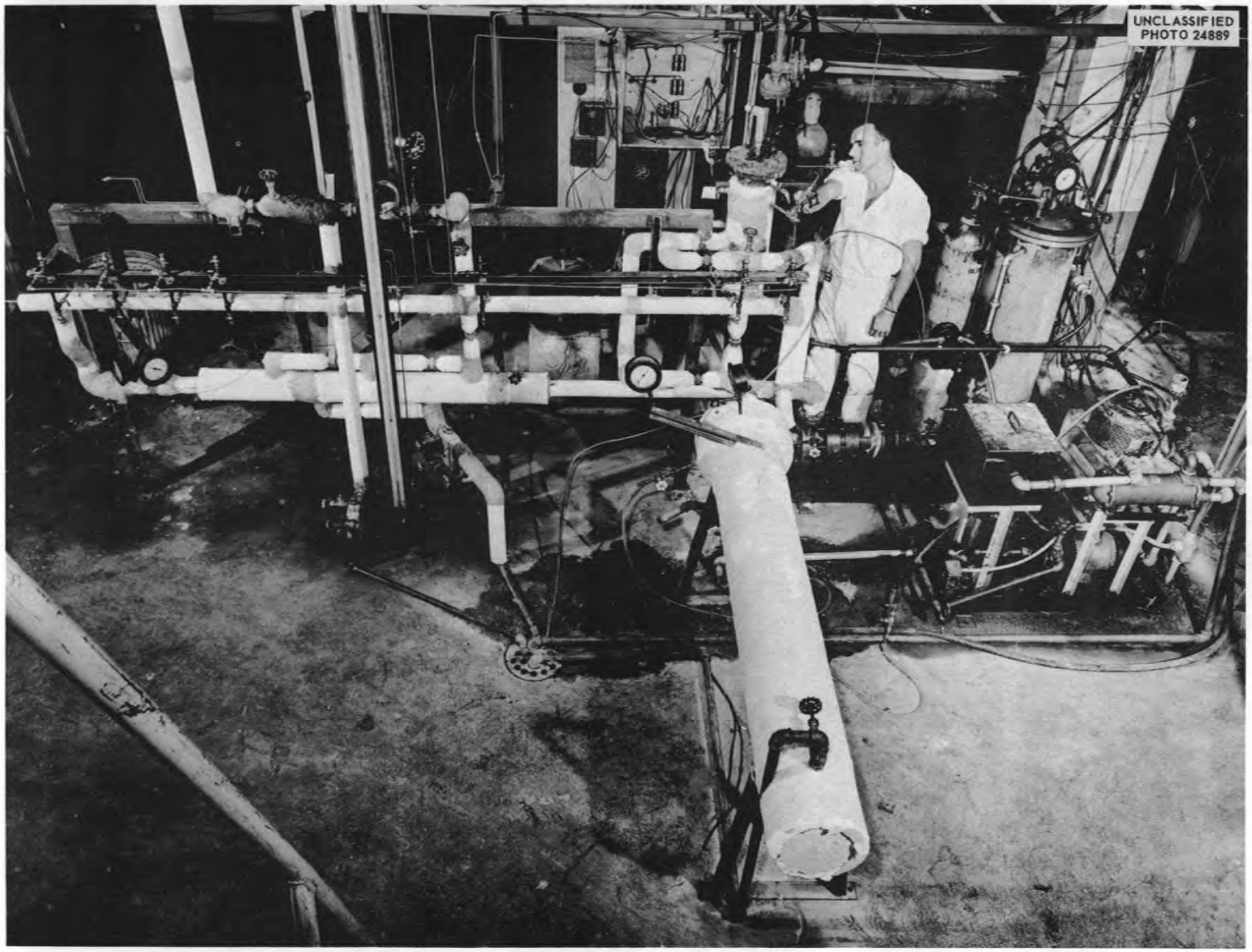

Fig. 9.3. Loop for Heat-Transfer and Pressure-Drop Measurements.

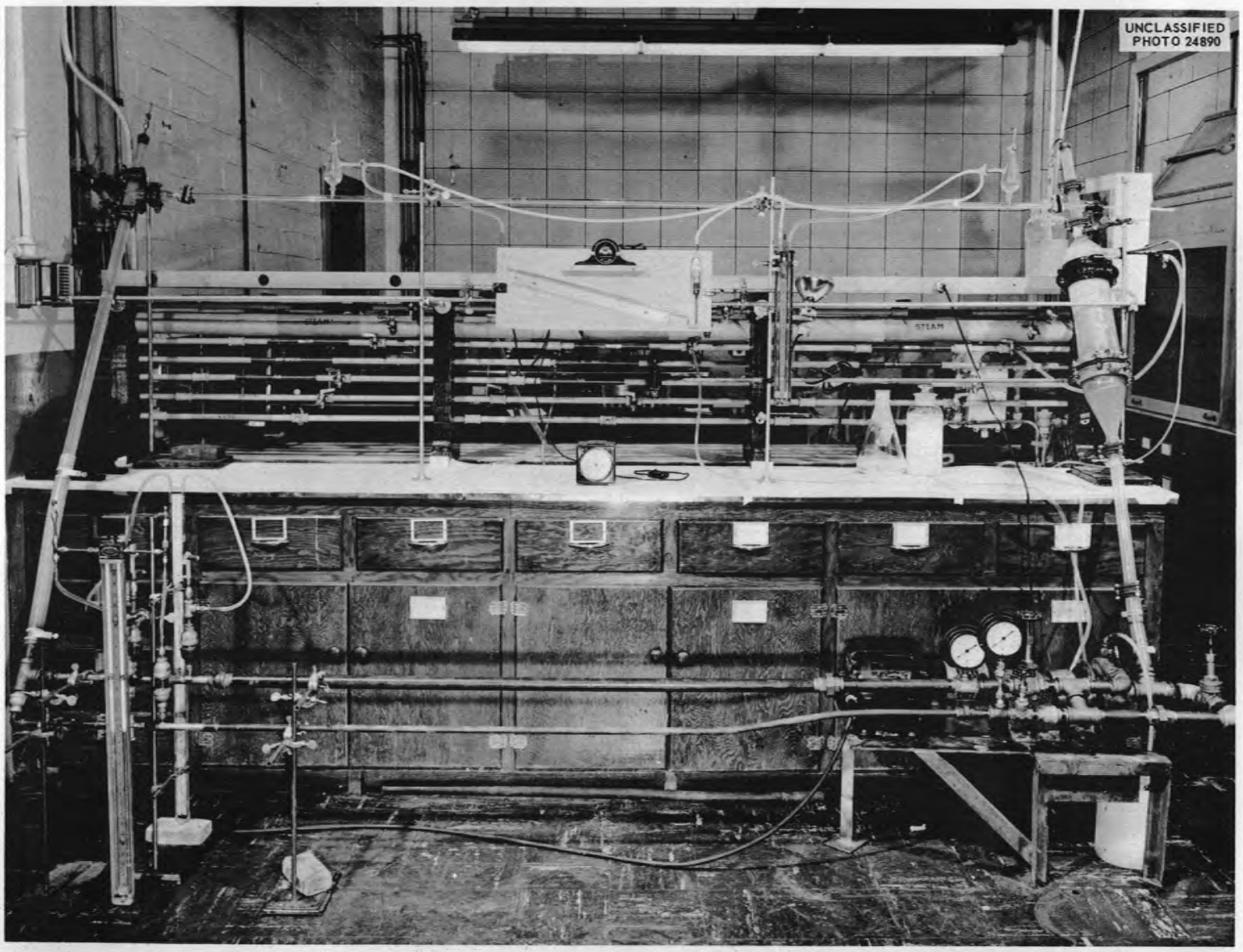

Fig. 9.4. System for Slurry Pickup and Transport Velocity Measurements.

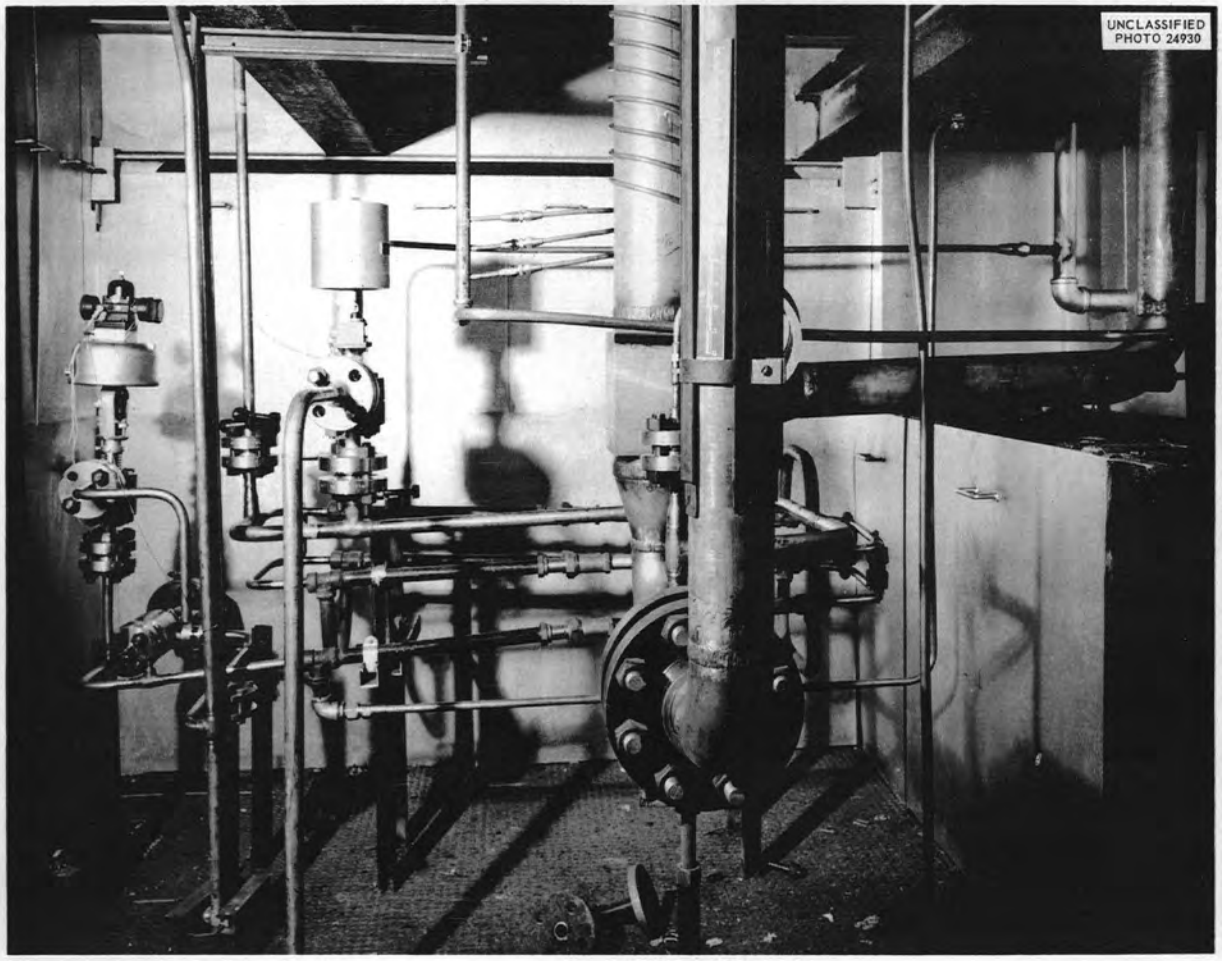

Fig. 9.5. View of Lower End of Blanket Mockup Pressurizer with Associated Equipment.

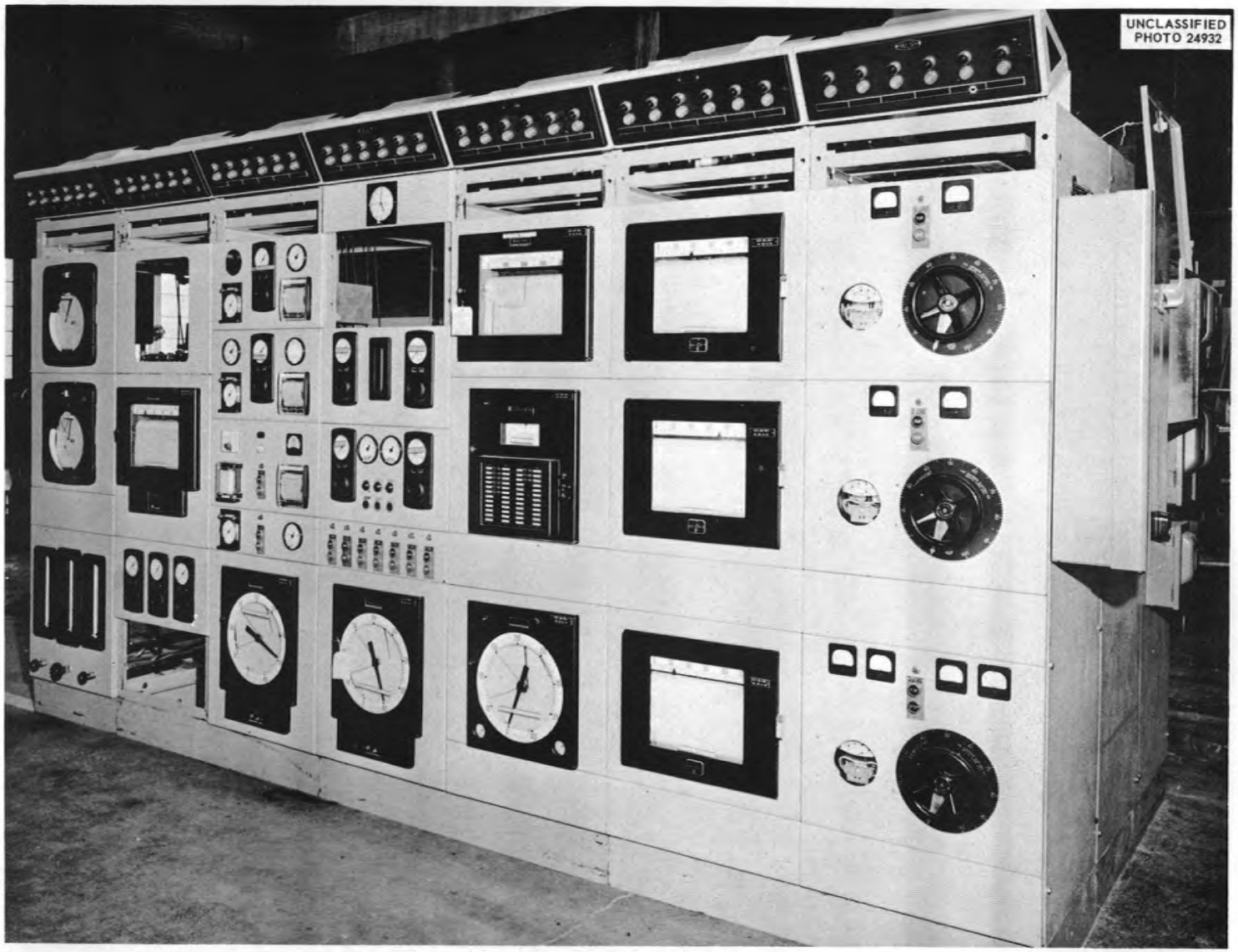

Fig. 9.6. Panel Board for Blanket Mockup.

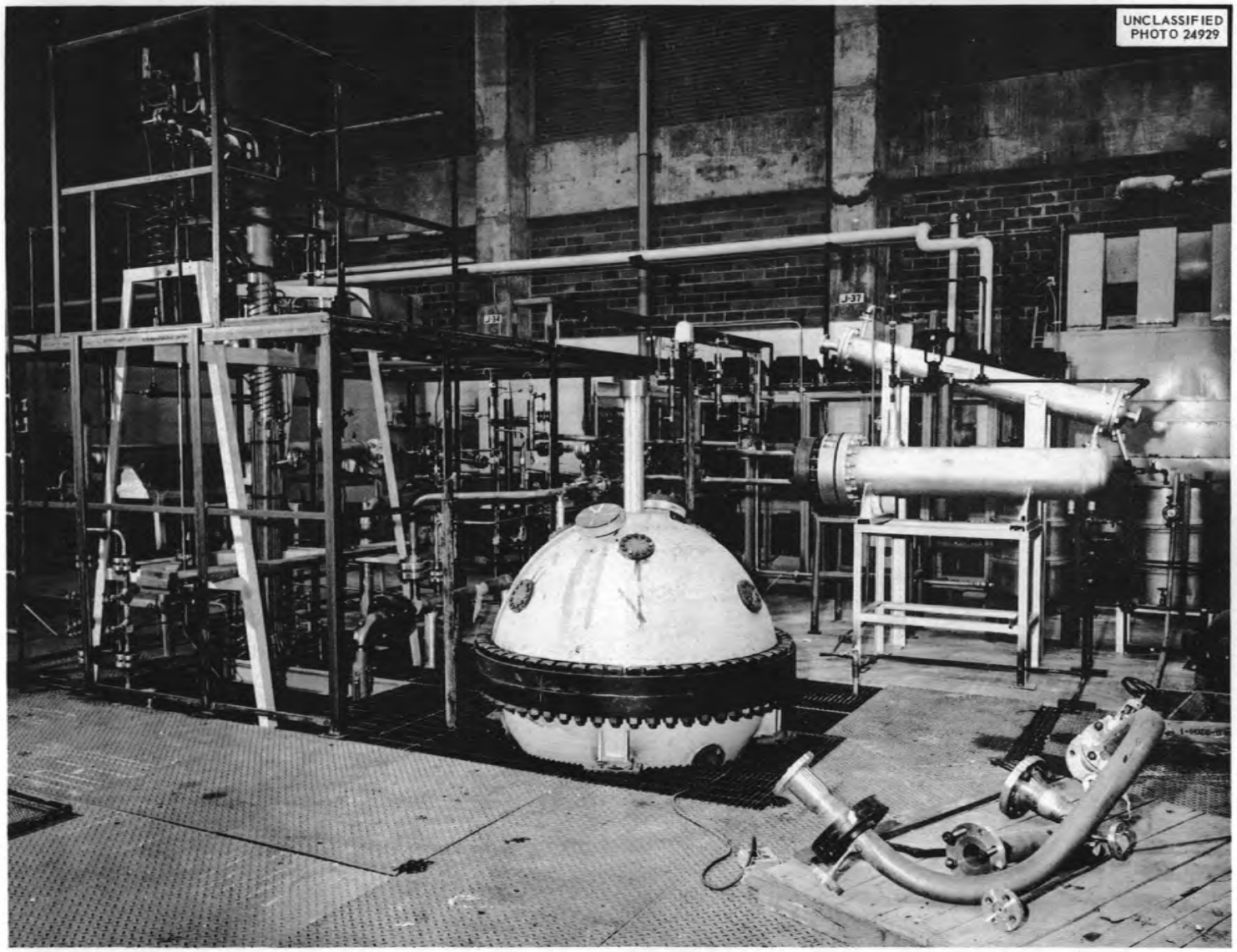

Fig. 9.7. Upper Level of Mockup.

Part IV

CORROSION AND MATERIALS

E. G. Bohlmann

10. SOLUTION CORROSION TESTS

J. C. Griess H. C. Savage
S. R. Buxton R. S. Greeley
G. K. Ellis S. A. Reed
J. L. English R. M. Warner

10.1 PUMP LOOPS

H. C. Savage J. C. Griess
S. R. Buxton R. S. Greeley
G. K. Ellis S. A. Reed
R. M. Warner

10.1.1 Operation and Maintenance

(a) General. – Operation of 11 dynamic-corrosion test loops is continuing. As previously reported,[1] test loops K, L, and M were being operated on a long-term basis to measure corrosion by uranyl sulfate solution of the composition originally planned (0.04 *m* UO_2SO_4, 0.006 *m* H_2SO_4, 0.005 *m* $CuSO_4$) for use in the HRT and to determine the stability of the solution. Evidence of solution instability in loops K and M, which were operating at 300 and 250°C, respectively, has caused the program to be interrupted. Operation of the three loops will be resumed with fresh uranyl sulfate solution containing 0.015 *m* sulfuric acid. In the future long-term runs, loop K will contain an experimental hydroclone of the type to be used in the HRT chemical processing plant. This hydroclone, designed and built by the Chemical Technology Division, will be evaluated for the effects of corrosion after long-term operation at 300°C with the uranyl sulfate solution presently planned for the HRT.

(b) Heat-Exchanger Test. – A single tube-and-shell type of test heat exchanger, previously described,[2,3] was used to determine the effect of corrosion and/or film formation by uranyl sulfate solution on the over-all heat transfer coefficient. A previous long-term test[3] had been made with a 0.17 *m* uranyl sulfate solution at 250°C. These conditions were those of the HRE; it was reported[3] that no loss of over-all heat-transfer coefficient resulted during the longest period of operation (1600 hr).

Since the acidity and uranium content of the uranyl sulfate solution planned for the HRT differed substantially from that of the solution used in the HRE and since, in addition, the operating temperature was increased from 250 to 300°C, another heat-transfer test was incorporated in the long-term run in loop K. Preliminary test results on two type 347 stainless steel heat-exchanger tubes, ¼-in.-OD by 0.049-in. wall, have been obtained during the 8515 hr of operation.

For tube 1 the over-all heat-transfer coefficient appeared to decrease from approximately 1300 to approximately 900 Btu/hr·ft^2·°F over a period of 6500 hr of operation. The coefficient for tube 2 has decreased from approximately 1200 to approximately 1000 Btu/hr·ft^2·°F after 2000 hr of operation. For calculations of the over-all heat-transfer coefficient the properties of the uranyl sulfate were assumed to be those of water. For tube 1 the data are probably less reliable than those on tube 2. Some thermocouple difficulties were encountered in the early temperature readings on tube 1, and very few measurements were made in the period from 100 to 3000 hr. For tube 2 more reliable data were probably obtained, as evidenced by cross-checking the heat removal from the uranyl sulfate solution against that from the shell-side cooling water. Additional measurements are being made. Tube 2 will be left in loop K when operation is resumed. A brief summary of the test heat-exchanger operating conditions is given below:

Tube size	¼-in. OD 0.049-in. wall ~30 in. long
Tube material	Type 347 stainless steel
Tube side	0.04 *m* UO_2SO_4 0.006 *m* H_2SO_4 0.005 *m* $CuSO_4$ 1000 ppm O_2

[1] H. C. Savage and F. J. Walter, *HRP Quar. Prog. Rep. April 30, 1955*, ORNL-1895, p 69.

[2] H. C. Savage, R. A. Lorenz, and D. Schwartz, *HRP Quar. Prog. Rep. Jan. 1, 1953*, ORNL-1478, p 63, Fig. 26.

[3] H. C. Savage and R. A. Lorenz, *Over-all Heat Transfer Coefficient – Uranyl Sulfate Solution in Tube Type Heat Exchanger*, ORNL CF-54-7-136 (July 8, 1954).

Shell side	Steam
Tube-side flow rate	~0.78 gpm
Shell-side flow rate	Static
Approximate heat removal rate	12,000 Btu/hr
Inlet temperature	~300°C
Outlet temperature	~280°C
Log mean ΔT, uranyl sulfate–steam	~38°C

(c) 4000-gpm Loop. – The 4000-gpm loop,[4] designed and constructed by the Engineering Development and Design Sections, is now in operation to obtain corrosion and solution stability data under operating conditions proposed for the HRT startup.[5] The loop contains standard pin and coupon corrosion specimens in a bypass line for correlation with loop corrosion. Because of loop design limitations, operation is at 250°C instead of at the 280°C specified.[5] All other portions of the HRT startup procedure are being adhered to as closely as possible. Table 10.1 shows the operating schedule being followed.

TABLE 10.1. SOLUTION COMPOSITION AND TIME SCHEDULE FOR HRT STARTUP

U^{238} Concentration (m)	Cumulative Time at 280°C (hr)	$CuSO_4$ (m)	H_2SO_4 (m)	O_2 (ppm)
0	50	0	0	50–100
0.004	150	0	0.004	50–100
0.01	250	0	0.004	50–100
0.02	350	0.005	0.006	50–100
0.04	550	0.005	0.015	50–100

(d) Westinghouse Model 100A Pump Bearings. – Graphitar as a bearing material is of interest in that the circulating pump presently proposed for the HRT and almost all other pumps in use in the development program of the HRP contain bearings made of this material. The Westinghouse model 100A pumps in use in the dynamic corrosion test loops are equipped with Graphitar No. 14 bearings, supplied by the United States Graphite Co., and Stellite 98M2 journal bushings. Recently a survey was made to determine the operating life of the Graphitar No. 14 bearings as used in the model 100A pumps circulating uranyl sulfate solutions over a wide range of conditions in the dynamic corrosion test loops.

To date the survey has included the pumps used in 5 of the 13 test loops, involving a total cumulative operating time in excess of 80,000 hr. Temperatures of the circulating solution varied between 100 and 300°C, and the concentration of uranyl sulfate varied from 0 to 1.3 m. In general the front bearings have worn out much faster than the rear bearings, the average life of the rear bearing being approximately three times as great. Among the reasons for this may be the following: higher bearing load, higher solution temperature because the front bearing is just behind the thermal barrier, and loss of hydraulic thrust balance (which always produces wear on the thrust surface of the front bearing, necessitating replacement).

For the pumps surveyed, a maximum life of approximately 8000 hr was observed in one front Graphitar No. 14 bearing (circulating 0.17 m UO_2SO_4 solution usually at 250°C). A number of bearings lasted only a few hundred hours. There does not appear to be any great difference in bearing life with different uranyl sulfate concentrations or loop operating temperatures (most of the operating temperatures were between 250 and 300°C).

The maximum life of a rear Graphitar bearing was approximately 17,000 hr, with a large proportion having a life of more than 4000 hr.

A breakdown of the duration of the Graphitar No. 14 bearing within various time ranges is shown in Table 10.2. In a few cases the bearing failure could be attributed to cracking of the Stellite journal bushing or to the dynamic unbalance of the pump rotor. However, this type of failure was included in the breakdown.

Since most of the runs in the dynamic corrosion test loops are of 200 to 500 hr, replacement of the pump bearings has not been a serious problem. Frequent pump inspections are normally made, and replacement of a worn bearing is a relatively simple operation. However, for experimental

[4] Shown in Fig. 8, p 19, in *HRP Quar. Prog. Rep. Nov. 15, 1951*, ORNL-1221; for additional information, see *HRP Quar. Prog. Reps.* for March 15, 1952, Oct. 1, 1952, and from Jan. 1, 1953, through July 31, 1955.

[5] E. L. Compere and E. G. Bohlmann, *HRT Uranyl Sulfate Start-up Procedure*, ORNL CF-55-9-27 (Sept. 7, 1955).

TABLE 10.2. DURATION OF GRAPHITAR BEARING IN WESTINGHOUSE MODEL 100A PUMPS

Operating Time (hr)	Bearing Life			
	Front		Rear	
	No.	%	No.	%
<1,000	7	27	1	9
1,000– 2,000	7	27	2	18
2,000– 4,000	5	19	2	18
4,000– 6,000	5	19	3	28
6,000–10,000	2	8	1	9
>10,000	0	0	2	18
Total	26	100	11	100

purposes, bearings and journal bushing blanks of pure sintered aluminum oxide have been ordered and will be tested in the model 100A pumps. This material has been used as bearing and journal material with some success in the ORNL 5-gpm pumps installed in the in-pile loops.

10.1.2 Data and Discussion

(a) General. – The 100A loop program has continued along somewhat the same lines as last quarter. Among the problems investigated were the effects of acid in 0.04 *m* uranyl sulfate solution, both on solution stability and corrosion, and the suppression of corrosion of stainless steel by the addition of lithium sulfate to uranyl sulfate solutions. Also, a long-term run was completed, and one case of very severe attack of titanium was observed.

The results of the above investigations are reported in the following sections.

(b) General Corrosion Rates. – Table 10.3 lists the pin data obtained during the quarter from runs in the dynamic loops. The form of the table is the same as it has been in previous reports,[6] and the precautions given before still apply.

(c) Long-Term Run with Simulated HRT Solution at 300°C. – A long-term run, K-14, with a proposed HRT solution (0.04 *m* uranyl sulfate, 0.005 *m* copper sulfate, 0.006 *m* sulfuric acid) at 300°C was terminated after 8515 hr. The shutdown was made in order to change to a solution containing more acid so that the solution will be hydrolytically stable. Table 10.3 contains the final pin data. Preliminary results of the weight losses after 2865 and 6539 hr and a discussion of the solution instability were given in a previous report.[7]

The run since the shutdown at 6539 hr was without incident except for the previously noted decrease in uranium and copper concentration. However, the oxygen concentration was reduced from the 1000–2000 ppm maintained during the former part of the run to 100–500 ppm. This decrease in oxygen concentration did not change the rate of increase of nickel, but it did prevent the chromium concentration from increasing as rapidly as it had previously. Based on the rate of increase of the nickel in solution, the generalized corrosion rate of the system was 0.06 mpy.

At the conclusion of the run a small amount of a crystalline, rustlike material was found in the pressurizer. Chemical analysis showed this material to contain 68.7% uranium, 6.22% copper, and only traces of other elements. These percentages correspond to a molar ratio of 3/1 for uranium/copper. However, the x-ray pattern of the material did not correspond to any known uranium or copper compounds. Since the material could not be collected quantitatively, it is not known whether it could account entirely for the uranium and copper lost from solution during the run.

Comparison of the scrubbed weights of the specimens after 2865, 6539, and 8515 hr showed that in almost all cases the various stainless steel and zirconium pins did not change appreciably after the initial 2865 hr; that is, the corrosion rates were essentially zero after the initial oxide film had formed. On the other hand, most of the titanium specimens continued to corrode at a low rate throughout the run. This was particularly true of the Ti-Al-Cr and the Ti-Al-Sn alloys, although even in the extreme case the corrosion rate did not exceed 0.3 mpy. As has been observed previously, there was little tendency for the oxides of iron and chromium to be transported at 300°C; as a result, the titanium and zirconium pins had practically no films of stainless steel corrosion products.

[6] J. C. Griess, J. M. Ruth, and R. W. Wacker, *HRP Quar. Prog. Rep. Jan. 1, 1953*, ORNL-1478, Table 8, p 65; see also *HRP Quar. Prog. Reps.* from March 31, 1953, through July 31, 1955.

[7] J. C. Griess and R. S. Greeley, *HRP Quar. Prog. Rep. July 31, 1955*, ORNL-1943, p 84–86.

TABLE 10.3. CORROSION RATES OF PIN-TYPE CORROSION SPECIMENS IN URANYL SULFATE SOLUTIONS

Run No.	Test Conditions					Pin Material	Number of Pins	Corrosion Rate (mpy)		
	UO_2SO_4 Concentration (m)	Temperature (°C)	Time (hr)	Additions	Flow Rate (fps ± 10%)			Minimum	Average	Maximum
A-85	0.04	300	656	0.02 m H_2SO_4 0.005 m $CuSO_4$ ~1000 ppm O_2	18	304L SS	4	0.65	0.84	0.93
						309 SCb SS	3	2.0	2.2	2.3
						347 SS	4	1.6	1.3	0.83
						Titanium 75A	2	0.14	0.14	0.14
						Zircaloy-2	1		[a]	
					30	304L SS	5	0.67	1.3	1.5
						309 SCb SS	4	2.7	3.3	3.8
						316L SS	3	1.3	1.5	1.7
						321 SS	3	0.73	0.80	0.91
						347 SS	7	1.1	2.5	3.6
						Platinum	1		0.04	
						Titanium 75A	1		0.14	
						Titanium RC-55	1		0.23	
						Zircaloy-2	1		[a]	
A-86	0.04	300	33[b]	0.02 m H_2SO_4 0.005 m $CuSO_4$ ~1000 ppm O_2	18	304L SS	4	13	19	22
						309 SCb SS	3	34	36	39
						347 SS	4	22	27	35
						Titanium 75A	2	0.93	0.93	0.93
						Zircaloy-2	1		[a]	
					30	304L SS	5	14	27	50
						309 SCb SS	4	57	73	110
						316L SS	3	31	42	56
						321 SS	3	30	45	68
						347 SS	8	40	119	500
						Platinum	1		0.59	
						Titanium RC-55	1		2.8	
						Titanium 75A	1		0.93	
						Zircaloy-2	2		[a]	

TABLE 10.3. (continued)

Run No.	Test Conditions: UO_2SO_4 Concentration (m)	Temperature (°C)	Time (hr)	Additions	Flow Rate (fps ± 10%)	Pin Material	Number of Pins	Corrosion Rate (mpy): Minimum	Average	Maximum
A-87	0.04	300	200	0.02 m H_2SO_4 0.005 m $CuSO_4$ ~1000 ppm O_2	18	304L SS	4	1.7	2.8	3.9
						309 SCb SS	3	5.0	5.1	5.4
						347 SS	4	3.0	3.8	4.8
						Titanium 75A	2	0.61	0.61	0.61
						Zircaloy-2	1		0.22	
					29	304L SS	5	4.4	5.0	5.9
						309 SCb SS	4	4.2	8.9	16
						316L SS	3	5.5	6.7	7.2
						321 SS	3	3.8	5.7	7.3
						347 SS	7	5.8	8.2	11
						Platinum	1		0.07	
						Titanium RC-55	1		0.77	
						Titanium 75A	1		0.77	
						Zircaloy-2	2	0.32	0.38	0.43
A-88	0.04	300	200	0.02 m H_2SO_4 0.005 m $CuSO_4$ ~1000 ppm O_2	18	304L SS	3	1.8	2.3	2.6
						309 SCb SS	3	5.5	5.8	6.4
						347 SS	3	4.3	4.3	4.4
						Frogalloy[c]	1		2.6	
						Incoloy	2	3.2	4.1	4.9
						Titanium 75A	1		0.15	
						Zircaloy-2	1		[a]	
					30	304L SS	6	2.0	3.3	3.9
						309 SCb SS	6	6.5	7.4	8.5
						347 SS	7	4.6	5.3	5.9
						Incoloy	4	5.5	6.0	6.3
						Platinum	1		0.97	
						Titanium 75A	2	0.30	0.40	0.45
						Zircaloy-2	2	[a]	0.11	0.22

TABLE 10.3. (continued)

Run No.	Test Conditions: UO_2SO_4 Concentration (m)	Temperature (°C)	Time (hr)	Additions	Flow Rate (fps ± 10%)	Pin Material	Number of Pins	Corrosion Rate (mpy): Minimum	Average	Maximum
D-50	2.9	300	157	3.2 m Li_2SO_4 200–400 ppm O_2	18	304L SS	2	2.9	6.5	10
						309 SCb SS	2	2.7	6.4	10
						321 SS	2	5.0	9.5	14
						347 SS	5	2.9	12	18
						Titanium 75A	1		0.39	
						Titanium 100A	1		0.39	
						Zircaloy-2	1		*a*	
					68	304L SS	2	360	360	360
						309 SCb SS	3	490	820	1000
						347 SS	4	230	380	470
						Gold	1		0.41	
						Titanium 75A	1		1.2	
						Titanium 100A	1		1.1	
						Zircaloy-2	1		*a*	
D-51	2.9	200	63	3.2 m Li_2SO_4 250–500 ppm O_2	17	304L SS	2	11	14	16
						309 SCb SS	2	9.3	9.4	9.5
						321 SS	2	15	21	26
						347 SS	5	13	15	19
						Titanium 75A	1		0.49	
						Titanium 100A	1		0.98	
						Zircaloy-2	1		*a*	
					68	304L SS	2	8.4	8.7	9.0
						309 SCb SS	3	4.9	5.3	5.7
						347 SS	4	10	12	13
						Gold	1		*a*	
						Titanium 75A	1		*a*	
						Titanium 100A	1		0.49	
						Zircaloy-2	1		*a*	

TABLE 10.3. (continued)

Run No.	Test Conditions: UO_2SO_4 Concentration (m)	Temperature (°C)	Time (hr)	Additions	Flow Rate (fps ± 10%)	Pin Material	Number of Pins	Corrosion Rate (mpy): Minimum	Average	Maximum
D-52	1.9	200	200	2.2 m Li_2SO_4 250–500 ppm O_2	18	304L SS	2	12	14	17
						309 SCb SS	2	8.4	26	43
						321 SS	2	12	13	13
						347 SS	5	12	13	14
						Titanium 75A	1		0.30	
						Titanium 100A	1		0.15	
						Zircaloy-2	1		*a*	
					107	304L SS	2	21	41	61
						309 SCb SS	3	7.7	8.2	9.0
						347 SS	4	11	13	16
						Gold	1		*a*	
						Titanium 75A	2	0.15	0.63	1.1
						Zircaloy-2	1		*a*	
D-53	3.0	250	193	3.4 m Li_2SO_4 250–500 ppm O_2	18	304L SS	2	130	150	160
						309 SCb SS	2	130	130	130
						321 SS	1		96	
						347 SS	4	59	62	69
						Incoloy	1		190	
						Titanium (3% Al, 5% Cr)	1		0.16	
						Titanium 75A	1		0.32	
						Titanium 100A	1		0.32	
						Zircaloy-2	1		*a*	
					105	304L SS	2	230	250	260
						309 SCb SS	2	300	350	390
						347 SS	4	220	320	490
						Gold	1		0.19	
						Incoloy	1		280	
						Titanium 75A	1		0.48	
						Titanium 100A	1		0.32	
						Zircaloy-2	1		*a*	

TABLE 10.3. (continued)

Run No.	Test Conditions: UO_2SO_4 Concentration (m)	Temperature (°C)	Time (hr)	Additions	Flow Rate (fps ± 10%)	Pin Material	Number of Pins	Corrosion Rate (mpy): Minimum	Average	Maximum
D-54	4.4	300	200	4.4 m Li_2SO_4 200–500 ppm O_2	17	304L SS	2	2.3	9	15
						309 SCb SS	2	4.9	7	11
						321 SS	1		22	
						347 SS	4	3.1	9.6	17
						Incoloy	1		13	
						Titanium (3% Al, 5% Cr)	1		6.6	
						Titanium 75A	1		1.4	
						Titanium 100A	1		1.5	
						Zircaloy-2	1		*a*	
					36	304L SS	2	80	81	81
						309 SCb SS	2	39	47	54
						347 SS	4	10	47	74
						Gold	1		0.21	
						Incoloy	1		320	
						Platinum	1		0.13	
						Titanium 75A	1		1.5	
						Titanium 100A	1		1.7	
						Zircaloy-2	1		0.22	
E-44	0.17	250	200	0.17 m $MgSO_4$ 0.04 m H_2SO_4 ~1000 ppm O_2	17	304L SS	4	5.3	16	30
						309 SCb SS	3	6.1	7.6	8.4
						347 SS	4	5.8	26	38
						Titanium 75A	2	*a*	0.08	0.15
						Zircaloy-2	1		*a*	
					36	304L SS	2	110	140	170
						309 SCb SS	1		110	
						316L SS	1		120	
						321 SS	3	87	150	200
						347 SS	4	110	110	120
						Platinum	1		0.19	

TABLE 10.3. (continued)

Run No.	Test Conditions: UO_2SO_4 Concentration (m)	Temperature (°C)	Time (hr)	Additions	Flow Rate (fps ± 10%)	Pin Material	Number of Pins	Corrosion Rate (mpy): Minimum	Average	Maximum
E-44	0.17	250	200	0.17 m $MgSO_4$ 0.04 m H_2SO_4 ~1000 ppm O_2	36	Titanium RC-55	1		0.15	
						Zircaloy-2	1		*a*	
E-45	0.17	250	200	0.17 m $MgSO_4$ 0.02 m H_2SO_4 ~1000 ppm O_2	17	304L SS	4	1.7	3.9	8.9
						309 SCb SS	3	2.5	7.6	11
						347 SS	4	1.7	7.8	14
						Titanium 75A	2		*a*	
						Zircaloy-2	1		*a*	
					31	304L SS	2	90	94	97
						309 SCb SS	1		83	
						316L SS	1		84	
						321 SS	3	88	88	88
						347 SS	4	90	92	93
						Gold	1		0.15	
						Titanium RC-55	1		*a*	
						Zircaloy-2	1		*a*	
E-46	0.04	300	200	0.04 m $MgSO_4$ 0.02 m H_2SO_4 0.005 m $CuSO_4$ ~1000 ppm O_2	18	304L SS	3	1.2	1.4	1.5
						309 SCb SS	2	2.2	2.3	2.4
						321 SS	2	1.3	1.3	1.3
						347 SS	5	0.84	1.4	1.8
						Titanium 75A	1		1.5	
						Zircaloy-2	1		*a*	
					68	304L SS	3	9.3	9.4	9.4
						309 SCb SS	2	16	17	17
						321 SS	2	9.3	10	10
						347 SS	4	15	16	18
						Titanium 75A	1		8.4	
						Zircaloy-2	2	4.3	4.8	5.3

TABLE 10.3. (continued)

Run No.	Test Conditions: UO_2SO_4 Concentration (m)	Temperature (°C)	Time (hr)	Additions	Flow Rate (fps ± 10%)	Pin Material	Number of Pins	Corrosion Rate (mpy): Minimum	Average	Maximum
E-47	0.04	250	200	0.04 m $MgSO_4$	14	304L SS	3	1.7	3.3	6.2
				0.02 m H_2SO_4		309 SCb SS	2	8.7	9.1	9.4
				0.005 m $CuSO_4$		321 SS	2	2.2	4.0	5.8
				~1000 ppm O_2		347 SS	5	5.2	6.7	8.0
						Titanium 75A	1		*a*	
						Zircaloy-2	1		*a*	
					68	304L SS	3	120	130	130
						309 SCb SS	2	110	110	110
						321 SS	2	120	120	130
						347 SS	4	110	130	150
						Titanium 75A	1		4.8	
						Zircaloy-2	2	10	11	11
E-48	0.04	300	200	0.04 m Li_2SO_4	15	304L SS	3	1.1	1.2	1.3
				0.02 m H_2SO_4		309 SCb SS	2	1.5	1.6	1.7
				0.005 m $CuSO_4$		321 SS	2	1.4	1.5	1.6
				~1000 ppm O_2		347 SS	4	0.42	1.2	1.5
						Incoloy	1		2.8	
						Titanium 75A	1		0.15	
						Zircaloy-2	1		*a*	
					68	304L SS	3	7.0	9.1	11
						309 SCb SS	2	14	15	15
						321 SS	2	18	32	45
						347 SS	4	11	12	13
						Incoloy	1		13	
						Titanium 75A	1		1.4	
						Zircaloy-2	1		0.76	
F-61	0.04	250	200	0.02 m H_2SO_4	12	304L SS	4	4.6	6.4	7.5
				0.005 m $CuSO_4$		309 SCb SS	3	13	13	13
				~1000 ppm O_2		347 SS	4	5.4	7.3	12
						Titanium 75A	2	*a*	0.15	0.31
						Zircaloy-2	1		*a*	

TABLE 10.3. (continued)

Run No.	Test Conditions: UO_2SO_4 Concentration (m)	Temperature (°C)	Time (hr)	Additions	Flow Rate (fps ± 10%)	Pin Material	Number of Pins	Corrosion Rate (mpy): Minimum	Average	Maximum
F-61	0.04	250	200	0.02 m H_2SO_4 0.005 m $CuSO_4$ ~1000 ppm O_2	68	304L SS	3	96	100	100
						309 SCb SS	3	86	92	98
						316L SS	2	100	110	110
						347 SS	4	85	98	110
						Titanium 75A	1		0.15	
						Zircaloy-2	1		*a*	
F-62	0.04	250	200	0.01 m H_2SO_4 0.005 m $CuSO_4$ ~1000 ppm O_2	13	304L SS	4	1.3	2.7	3.2
						309 SCb SS	3	4.0	4.1	4.1
						347 SS	4	3.8	4.1	4.3
						Titanium 75A	2	0.46	0.46	0.46
						Zircaloy-2	1		*a*	
					68	304L SS	3	15	18	22
						309 SCb SS	3	60	62	65
						316L SS	2	62	63	64
						347 SS	4	18	47	72
						Titanium 75A	1		0.77	
						Zircaloy-2	1		*a*	
F-63	0.04	250	200	0.15 m H_2SO_4 0.005 m $CuSO_4$ ~1000 ppm O_2	13	304L SS	4	2.0	3.8	4.7
						309 SCb SS	3	6.3	6.5	6.7
						347 SS	4	5.9	6.1	6.6
						Titanium 75A	2	0.15	0.23	0.30
						Zircaloy-2	1		*a*	
					68	304L SS	4	25	26	28
						309 SCb SS	3	66	82	110
						347 SS	5	28	47	52
						Titanium 75A	1		0.15	
						Zircaloy-2	1		*a*	
H-75	1.6	300	555	1.7 m Li_2SO_4 ~1000 ppm O_2	16	304L SS	4	15	16	18
						309 SCb SS	3	12	14	14
						347 SS	4	4.2	16	23
						Titanium 75A	2	0.83	1.0	1.2
						Zircaloy-2	1		*a*	

TABLE 10.3. (continued)

Run No.	Test Conditions: UO_2SO_4 Concentration (m)	Temperature (°C)	Time (hr)	Additions	Flow Rate (fps ± 10%)	Pin Material	Number of Pins	Corrosion Rate (mpy): Minimum	Average	Maximum
H-75	1.6	300	555	1.7 m Li_2SO_4 ~1000 ppm O_2	68	304L SS	2	510	520	520
						309 SCb SS	1		670	
						316L SS	1		330	
						321 SS	3	460	650	900
						347 SS	4	510	520	550
						Platinum	1		36[d]	
						Titanium RC-55	1		37[d]	
						Zircaloy-2	1		63[d]	
H-76	1.5	300	340	2.0 m Li_2SO_4 ~1000 ppm O_2	17	304L SS	2	4.2	4.9	6.1
						309 SCb SS	1		8.5	
						321 SS	2	7.0	7.2	7.4
						347 SS	4	7.1	9.0	11
						Gold	1		[a]	
						Platinum	1		[a]	
						Titanium RC-55	1		0.09	
						Titanium 75A	1		0.27	
						Zircaloy-2	1		[a]	
					68	304L SS	3	25	240	350
						309 SCb SS	3	470	480	490
						347 SS	4	280	290	300
						Gold	1		10[c]	
						Platinum	1		18[c]	
						Titanium 75A	1		16[c]	
						Zircaloy-2	1		26[c]	
H-78	1.5	200	200	1.7 m Li_2SO_4 ~1000 ppm O_2	14	304L SS	2	12	12	12
						309 SCb SS	1		7.8	
						321 SS	2	12	17	21
						347 SS	4	10	12	14
						Gold	1		0.36	
						Platinum	1		1.9	
						Titanium 75A	1		0.46	
						Zircaloy-2	1		0.54	

TABLE 10.3. (continued)

Run No.	Test Conditions: UO_2SO_4 Concentration (m)	Temperature (°C)	Time (hr)	Additions	Flow Rate (fps ± 10%)	Pin Material	Number of Pins	Corrosion Rate (mpy): Minimum	Average	Maximum
H-78	1.5	200	200	1.7 m Li_2SO_4 ~1000 ppm O_2	68	304L SS	3	38	49	63
						309 SCb SS	3	30	37	50
						347 SS	4	38	43	54
						Gold	1		25[d]	
						Platinum	1		53[d]	
						Titanium 75A	1		34[d]	
						Zircaloy-2	1		58[d]	
H-79[e]	1.5	250	200	1.7 m Li_2SO_4 ~1000 ppm O_2	14	304L SS	2	64	66	67
						309 SCb SS	2	33	35	37
						347 SS	4	34	38	46
						Incoloy	1		63	
						Gold	1		0.07	
						Titanium 75A	1		0.46	
						Titanium (5% Al, 2.5% Sn)	1		0.77	
						Titanium (6% Al, 4% V)	1		1.5	
						Zircaloy-2	1		*a*	
					68	304L SS	2	190	200	210
						309 SCb SS	2	180	190	200
						347 SS	4	160	190	210
						Gold	1		0.65	
						Incoloy	1		200	
						Titanium 75A	1		2.1	
						Titanium (5% Al, 2.5% Sn)	1		1.4	
						Zircaloy-2	1		*a*	
K-14[f]	0.04	300	8515	0.006 m H_2SO_4 0.005 m $CuSO_4$ ~1000 ppm O_2	9	302B SS	2	0.16	0.24	0.33
						304 SS[g]	1		0.10[b]	
						304L SS	4	0.08	0.09	0.12

TABLE 10.3. (continued)

Run No.	Test Conditions: UO_2SO_4 Concentration (m)	Temperature (°C)	Time (hr)	Additions	Flow Rate (fps ± 10%)	Pin Material	Number of Pins	Corrosion Rate (mpy): Minimum	Average	Maximum
K-14[f]	0.04	300	8515	0.006 m H_2SO_4 0.005 m $CuSO_4$ ~1000 ppm O_2	9	309 SCb SS	3	0.07	0.11	0.13
						316 SS[g]	1		0.16	
						316L SS	1		0.09	
						347 SS[g]	1		0.002[b]	
						347 SS	8	0.03[b]	0.10	0.11
						Titanium 75A	1		0.03[b]	
						Titanium 100A	1		0.03	
						Titanium (5% Al, 2.5% Sn)	1		0.10[b]	
						Zirconium, crystal bar	1		*a, b, i*	
						Zirconium, 2.5% Sn	1		*a, b, i*	
						Zircaloy-2	2		*a, b*	
					19	302B SS	1		0.19	
						304 SS[g]	1		0.09[b]	
						304 SS[j]	1		0.27	
						304L SS[k]	2	0.41	0.52	0.63
						304L SS[l]	2	0.41	0.54	0.67
						304L SS	3	0.01[b]	0.11	0.12
						309 SCb SS	3	0.02[b]	0.14	0.14
						347 SS[g]	1		0.01[b]	
						347 SS	10	0.05[b]	0.11	0.12
						Titanium RC-55	1		0.03	
						Titanium 150A	1		0.09	
						Titanium (3% Al, 5% Cr)	1		0.29[b]	
						Zirconium, crystal bar	1		*a, b, i*	
					33	304L SS	2	0.03[b]	0.06	0.09
						309 SCb SS	2	0.10[b]	0.13	0.16
						347 SS[m]	3	0.09	0.11	0.13

TABLE 10.3. (continued)

Run No.	Test Conditions: UO_2SO_4 Concentration (m)	Temperature (°C)	Time (hr)	Additions	Flow Rate (fps ± 10%)	Pin Material	Number of Pins	Corrosion Rate (mpy): Minimum	Average	Maximum
K-14[f]	0.04	300	8515	0.006 m H_2SO_4	33	347 SS[n]	3	0.09	0.10	0.12
				0.005 m $CuSO_4$		347 SS	4	0.05[b]	0.12	0.13
				~1000 ppm O_2	37	302B SS	2	0.37	0.40	0.43
						304 SS[g]	1		0.12	
						304L SS[k]	2	0.39	0.62	0.84
						304L SS[l]	2	0.35	0.39	0.43
						304L SS	2	0.15	0.16	0.16
						309 SCb SS	2	0.14	0.16	0.17
						347 SS[g]	1		0.10	
						347 SS	8	0.11	0.14	0.16
						Titanium RC-55	1		0.03	
						Titanium 75A	1		0.03	
						Titanium (5% Al, 2.5% Sn)	1		0.13	
						Titanium (3% Al, 5% Cr)	1		0.29	
						Zirconium, crystal bar	1		*a, b, i*	
						Zirconium, 2.5% Sn	1		*a, b, i*	
						Zircaloy-2	1		*a, b*	
N-5	0.04	300	417	0.01 m H_2SO_4	17	304L SS	4	0.57	0.61	0.62
				0.005 m $CuSO_4$		309 SCb SS	3	0.85	0.91	1.0
				~1000 ppm O_2		347 SS	4	0.69	0.77	0.81
						Titanium 75A	2	0.08	0.12	0.15
						Zircaloy-2	1		*a*	
					75	304L SS	3	0.98	1.2	1.3
						309 SCb SS	3	1.7	2.5	2.9
						316L SS	2	1.4	1.4	1.4
						347 SS	4	1.3	1.6	1.8

TABLE 10.3. (continued)

Run No.	Test Conditions: UO_2SO_4 Concentration (m)	Temperature (°C)	Time (hr)	Additions	Flow Rate (fps ± 10%)	Pin Material	Number of Pins	Corrosion Rate (mpy): Minimum	Average	Maximum
N-6	0.04	300	425	0.015 m H_2SO_4 0.005 m $CuSO_4$ ~1000 ppm O_2	16	304L SS	3	0.72	0.76	0.80
						309 SCb SS	3	1.2	1.3	1.4
						316 SS	2	0.92	0.94	0.96
						347 SS	4	1.2	1.3	1.4
						Titanium 75A	1		*a*	
						Zircaloy-2	1		*a*	
					70	304L SS	4	1.4	1.6	1.7
						309 SCb SS	3	3.3	3.5	3.8
						347 SS	4	2.8	3.1	3.4
						Titanium 75A	1		0.08	
						Zircaloy-2	1		*a*	
N-7	0.04	225	200	0.02 m H_2SO_4 0.005 m $CuSO_4$ ~1000 ppm O_2	16	304L SS	3	15	19	24
						309 SCb SS	3	23	28	31
						347 SS	4	24	29	35
						Incoloy	2	50	59	68
						Titanium 75A	1		0.15	
						Zircaloy-2	1		0.11	
					67	304L SS	3	120	150	180
						309 SCb SS	3	130	130	130
						347 SS	3	130	150	160
						Incoloy	2	160	190	220
						Titanium 75A	2	0.15	0.30	0.46
						Zircaloy-2	1		0.43	
N-8	0.04	225	200	0.015 m H_2SO_4 0.005 m $CuSO_4$ ~1000 ppm O_2	16	304L SS	3	13	15	15
						309 SCb SS	3	17	20	24
						347 SS	4	19	20	21
						Incoloy	2	36	56	75
						Titanium 75A	1		*a*	
						Zircaloy-2	1		0.31	

TABLE 10.3. (continued)

Run No.	Test Conditions: UO_2SO_4 Concentration (m)	Temperature (°C)	Time (hr)	Additions	Flow Rate (fps ± 10%)	Pin Material	Number of Pins	Corrosion Rate (mpy): Minimum	Average	Maximum
N-8	0.04	225	200	0.015 m H_2SO_4 0.005 m $CuSO_4$ ~1000 ppm O_2	68	304L SS	3	120	130	140
						309 SCb SS	3	110	110	120
						347 SS	3	120	130	140
						Incoloy	2	150	160	170
						Titanium 75A	2	0.15	0.30	0.46
						Zircaloy-2	1		[a]	

[a]Showed no weight change or only slight weight gain.
[b]A shutdown occurred during this run. The relatively high corrosion rates may be due to the hot liquid standing in contact with the specimens.
[c]A speciol melt containing 19% Cr, 9% Ni, 4.8% Mn, 0.7% C, balance Fe.
[d]High corrosion rates believed to be due to erosion by particles of oxide film sloughed off loop walls.
[e]A hydroclone was installed on the loop for this run to separate suspended oxide particles.
[f]Shut down twice during the run at 2865 and 6539 hr for examination of the specimens.
[g]Cast.
[h]Corrosion rates based on scrubbed weights; pin carried over to next run.
[i]The black oxide film showed some white areas.
[j]Sensitized.
[k]Heat-treated in moist hydrogen at 1900°F for 1 hr.
[l]Heat-treated in moist hydrogen at 1900°F for 1 hr. The alloy contained a small amount of cerium.
[m]Welded (oxyweld 60).
[n]Welded (oxyweld 60); heat-treated at 1000°F for 6 hr.

The type 304L stainless steel pins which had been pretreated in moist hydrogen at 1900°F to form a surface film rich in chromic oxide showed the highest corrosion rates. Also, a small amount of cerium in some of these pretreated pins did not improve their corrosion resistance. Evidently, at 300°C the chromic oxide film was fairly soluble in the uranyl sulfate solution. At a lower temperature, where Cr(III) is not oxidized to the soluble Cr(VI), the pretreatment probably would have been beneficial.

Six welded stainless steel pins in this run showed low corrosion rates and a complete absence of any localized attack either in the heat-affected zone or in the weld metal itself.

The type 347 stainless steel coupons exposed in a venturi type of holder at velocities of 15 to 70 fps showed a pitting attack at velocities above 50 fps, as was previously noted.[8] When first examined after 2865 hr, the coupons showed a few triangular pits. Upon examination after 6539 hr the areas of the pits were found to be larger but the number of pits had not increased. During the final part of the run the areas of the pits became elongated and even larger but did not increase appreciably in depth. At the end of the run the maximum pit depths were between 25 and 30 mils. The coupons exposed at flow rates less than 50 fps showed very little weight change and no evidence of pitting. Table 10.4 gives the weight changes and corrosion rates for these coupons.

The pump and loop showed no signs of localized attack either in the pump housing or on the impeller. All parts of the loop were covered with a thin, adherent black film. One section of pipe in this loop had been transferred from the old B loop and prior to this run had been exposed to

[8] J. C. Griess and R. S. Greeley, *HRP Quar. Prog. Rep. Jan. 31, 1955*, ORNL-1853, p 74.

TABLE 10.4. WEIGHT CHANGES AND CORROSION RATES OF TYPE 347 STAINLESS STEEL COUPONS IN RUN K-14

Conditions: 0.04 *m* UO_2SO_4
0.005 *m* $CuSO_4$
0.006 *m* H_2SO_4
~ 1000 ppm O_2
300°C

Velocity at Leading Edge (fps)	Weight Loss (mg/cm^2)				Corrosion Rate (mpy) for Defilmed Specimen After 8515 hr
	Scrubbed Specimen After			Defilmed Specimen After 8515 hr	
	2865 hr	6539 hr	8515 hr		
14	4.3	3.7	3.9	9.9	0.093
20	4.6	3.8	4.0	10	0.094
30	6.5	6.1	6.2	13	0.12
45	16	23	28	36	0.34*
64	140	200	330	340	3.2*
73	45	80	120	130	1.2*
64	34	40	49	56	0.53*
45	5.3	4.5	5.3	12	0.11
30	4.3	3.4	5.2	12	0.11
20**	3.2	2.4	4.0	12	0.11

*Pitted coupons.

**Velocity at trailing edge was 14 fps.

the following solutions: 0.43 *m* uranium at 100°C for 1772 hr; 0.02 *m* uranium plus 0.005 *m* sulfuric acid at 250°C for 6229 hr. After the run this section of pipe looked like the rest of the loop and showed no evidence of localized or severe generalized attack. During shutdown it was removed from the loop for sectioning.

(d) Stability of 0.04 molal Uranyl Sulfate Solutions. – As noted above and in the previous report,[9] the solution originally proposed for use in the HRT (0.04 *m* uranyl sulfate, 0.005 *m* copper sulfate, 0.006 *m* sulfuric acid) was not chemically stable in long runs at 250 and 300°C. Uranium and copper were gradually lost from solution, probably by hydrolytic precipitation. For example, at 300°C over a period of 2865 hr the concentration decreased from 10 to 9.4 g of uranium per liter, the copper concentration from 325 to 200 ppm, and the pH from 2.2 to 1.8. Several runs were made therefore with various amounts of acid to determine the amount necessary to prevent hydrolytic precipitation.

A solution of 0.04 *m* uranyl sulfate and 0.005 *m* copper sulfate containing 25 mole % excess sulfuric acid (0.010 *m*) lost no uranium or copper within the limits of analytical precision during a 400-hr run at 300°C. However, the pH decreased during the run from 1.9 to 1.7. Solutions containing 38 mole % excess acid (0.015 *m*) and 50 mole % acid (0.020 *m*) appeared to be stable analytically also and in addition showed no pH change for 400- and 650-hr runs, respectively. Thus it appears that at least 25 and probably 35 mole % acid is required to prevent hydrolytic precipitation of uranium and copper at 300°C.

The addition of the larger amounts of acid increased the corrosiveness of the solution and decreased the critical velocity. Figure 10.1 illustrates the effect of 25, 38, and 50 mole % acid on the weight losses of type 347 stainless steel coupons at 300°C. It can be noted that the low-velocity weight losses roughly doubled with each increase in concentration and that the critical velocity decreased from greater than 80 fps with 0.010 *m* acid to 50–60 fps with 0.015 *m* acid and to 30–40 fps with 0.020 *m* acid.

At 250°C a similar increase in corrosiveness and a decrease in the critical velocity with added acid occurred as shown in Fig. 10.2. Note that

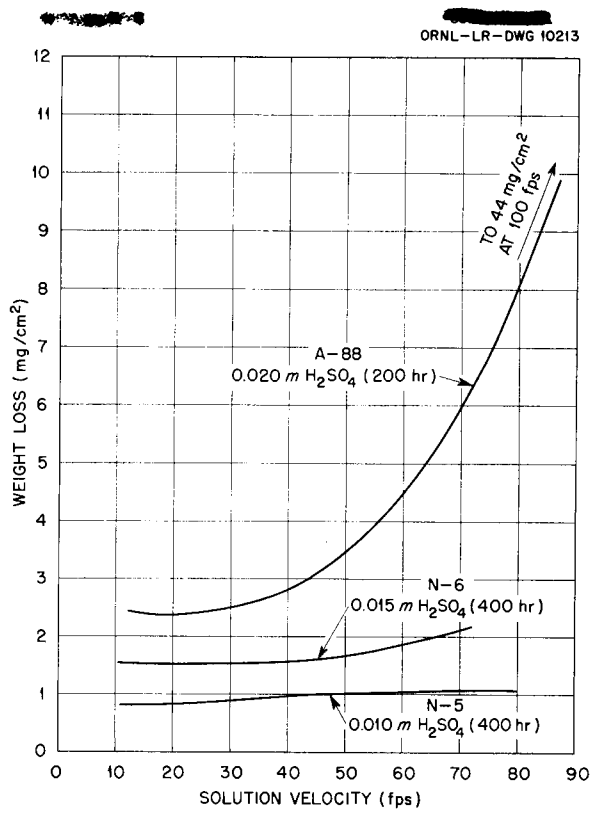

Fig. 10.1. Weight Loss vs Velocity for Type 347 Stainless Steel Coupons in 0.04 *m* UO_2SO_4, 0.005 *m* $CuSO_4$ Plus Various Amounts of Acid at 300°C.

the weight loss scale is different from the scale in Fig. 10.1. Corrosion of type 347 stainless steel coupons was worse at 250°C than at 300°C and the critical velocities were lower. With 0.020 *m* acid the critical velocity is very low – about 10 fps.

At 225°C two runs have been made: one with 0.020 *m* and one with 0.015 *m* added acid. Figure 10.3 shows that corrosion is slightly worse than at 250°C and that the critical velocities are as low as they were at 250°C, or even lower.

These series of runs indicate that a solution of 0.04 *m* uranyl sulfate plus 0.005 *m* copper sulfate containing 0.015 *m* (38 mole %) sulfuric acid is probably optimal with respect to hydrolytic stability and corrosion. The pin data for all these runs are included in Table 10.3. They indicate that types 304L and 309 SCb stainless steels are roughly similar to type 347 stainless steel in corrosion resistance to these solutions. Titanium

[9] J. C. Griess and R. S. Greeley, *HRP Quar. Prog. Rep. July 31, 1955*, ORNL-1943, p 85.

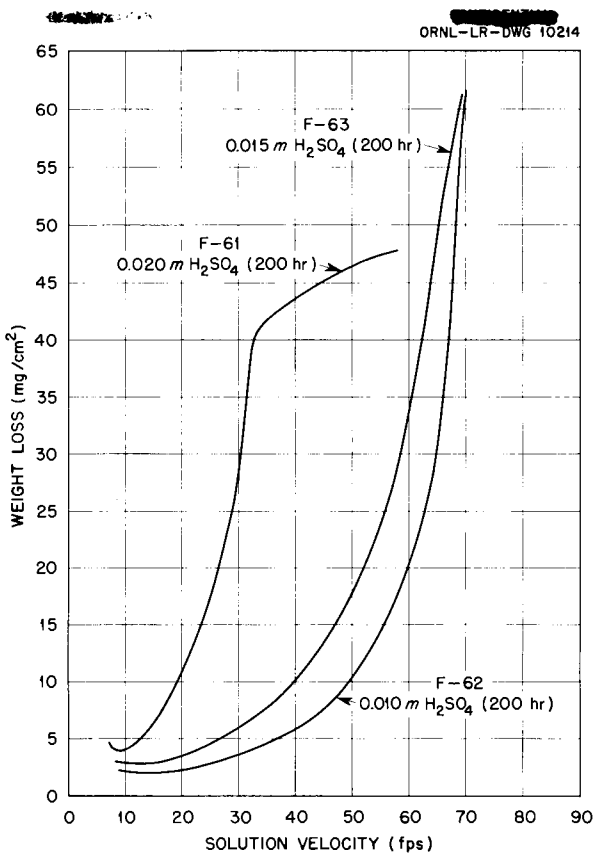

Fig. 10.2. Weight Loss vs Velocity for Type 347 Stainless Steel Coupons in 0.04 *m* UO_2SO_4, 0.005 *m* $CuSO_4$ Plus Various Amounts of Acid at 250°C.

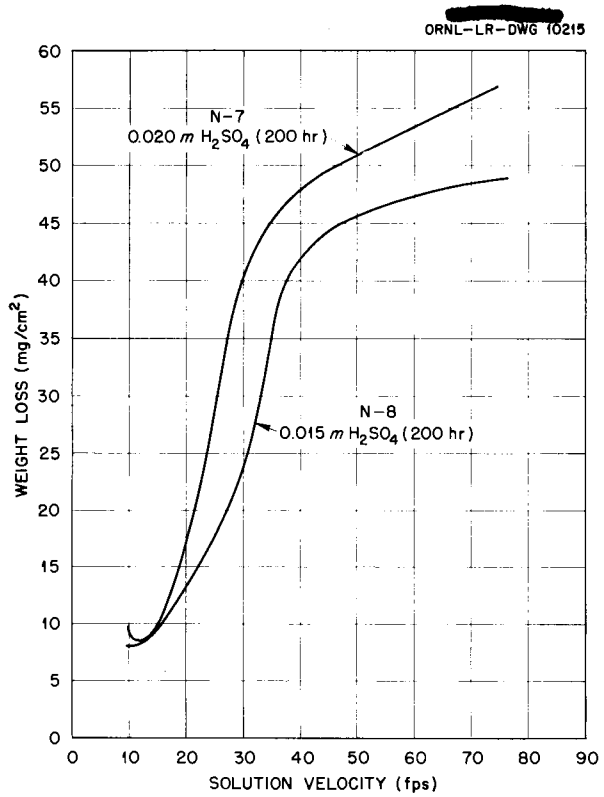

Fig. 10.3. Weight Loss vs Velocity for Type 347 Stainless Steel Coupons in 0.04 *m* UO_2SO_4, 0.005 *m* $CuSO_4$ Plus Various Amounts of Acid at 225°C.

75A and Zircaloy-2 in general showed excellent resistance at all acid concentrations. It should be noted that run A-86 was very short (33 hr), and hence the relatively high low-velocity corrosion rates reported are initial rates, which would decrease in time to the values reported in runs A-85, A-87, and A-88.

(e) Uranyl Sulfate Solutions Containing Added Sulfates. – It was reported in the last two quarterly reports[10] that the incorporation of either lithium or magnesium sulfates in dilute uranyl sulfate solutions substantially reduced the corrosiveness of such solutions over that of similar solutions without the added sulfate salts. However, it was also noted that at temperatures of 250 and 300°C these solutions were not completely stable and that magnesium or lithium, uranium, and copper slowly precipitated from solution.

Runs E-44 and E-45 were made in order to determine whether the addition of 0.04 *m* (E-44) or 0.02 *m* (E-45) sulfuric acid to a solution containing 0.17 *m* uranyl sulfate and 0.17 *m* magnesium sulfate would stabilize the solution at 250°C and still yield a solution having a low corrosion rate. The solution containing 0.02 *m* sulfuric acid (E-45) was not stable, and both uranium and magnesium slowly precipitated from solution. For example, during the 199-hr run, the uranium concentration decreased from 39 to 34 g/liter (25°C) and the magnesium from 3.9 to 3.2 g/liter (25°C). In this run, corrosion of the specimens was somewhat lower than is usually observed in 0.17 *m* uranyl sulfate, but the results were erratic. It can be seen from Table 10.3 that at a flow rate of 17 fps the corrosion rates of the pins varied

[10] J. C. Griess and R. S. Greeley, *HRP Quar. Prog. Rep. April 30, 1955*, ORNL-1895, p 84; and *HRP Quar. Prog. Rep. July 31, 1955*, ORNL-1943, p 70.

by as much as a factor of 7. The critical velocity in run E-45 was the same (~20 fps) as is usually observed in 0.17 *m* uranyl sulfate at 250°C, although both above and below the critical velocity the corrosion rates were reduced by a factor of about 2.

In run E-44, in which the system contained 0.17 *m* uranyl sulfate, 0.17 *m* magnesium sulfate, and 0.04 *m* sulfuric acid at 250°C, the solution was stable. While the corrosion rate observed on stainless steel specimens was lower than in 0.17 *m* uranyl sulfate at 250°C, the difference was only a factor of about 2, and there was no change in the critical velocity.

Runs E-46 through E-48 were made in order to determine the stability of 0.04 *m* uranyl sulfate containing either lithium sulfate or magnesium sulfate and sulfuric acid. Generally the results paralleled those obtained at the 0.17 *m* level. For example, in both runs at 300°C in which the solution contained 0.04 *m* uranyl sulfate, 0.02 *m* sulfuric acid, and 0.005 *m* copper sulfate in addition to 0.04 *m* magnesium sulfate (in run E-46) and 0.04 *m* lithium sulfate (in run E-48), the solutions were not stable; either magnesium or lithium, plus uranium and copper, were slowly lost from solution. The corrosion results were not significantly improved in either case.

In run E-47, which was identical to E-46 except that the temperature was 250°C, the solution was stable but again there was no improvement corrosionwise.

The results obtained at the concentrations of 0.04 and 0.17 *m* uranyl sulfate containing an equimolal amount of either lithium sulfate or magnesium sulfate indicated that hydrogen ions promoted and sulfate ions inhibited corrosion of stainless steel by uranyl sulfate solutions. Unfortunately, if sufficient concentrations of sulfate ions are added to reduce corrosion appreciably, the solution is not phase-stable.

The use of lithium sulfate in concentrated uranyl sulfate solutions to reduce corrosion has been investigated further. In loop D a series of runs was made in order to determine the effect of temperature in the range 200 to 300°C on the corrosion of stainless steel, zirconium, and titanium in solutions containing about 3 *m* uranyl sulfate and an equivalent amount of lithium sulfate. The solution contained 690 g of uranyl sulfate, 226 g of lithium sulfate, and 650 g of water per liter of solution at 25°C and had a density of 1.6 g/cm^3. The pin data can be seen in Table 10.3 (runs D-50 through D-53). In all cases titanium and zirconium showed low corrosion rates, but stainless steel specimens showed appreciable corrosion rates. However, it must be remembered that the reported rates are average for the entire run and that the runs were of short duration. Since corrosion rates are high during the period of film formation and decrease rapidly as the film forms, the reported corrosion rates probably would have been lower had the run been of longer duration. In all cases at low flow rates, the specimens were covered with a heavy black film.

Figure 10.4 shows the data obtained from the coupons and shows corrosion, expressed as weight loss, as a function of flow rate. At 200°C no critical velocity was observed, and at all flow rates corrosion was slight. At 250°C the critical velocity was about 25 fps and at 300°C about 45 fps.

Runs H-74 through H-76 show the effect of time on the extent of corrosion by a solution containing 1.6 *m* uranyl sulfate and 1.7 to 2.0 *m* lithium sulfate at 300°C. Run H-74 was reported

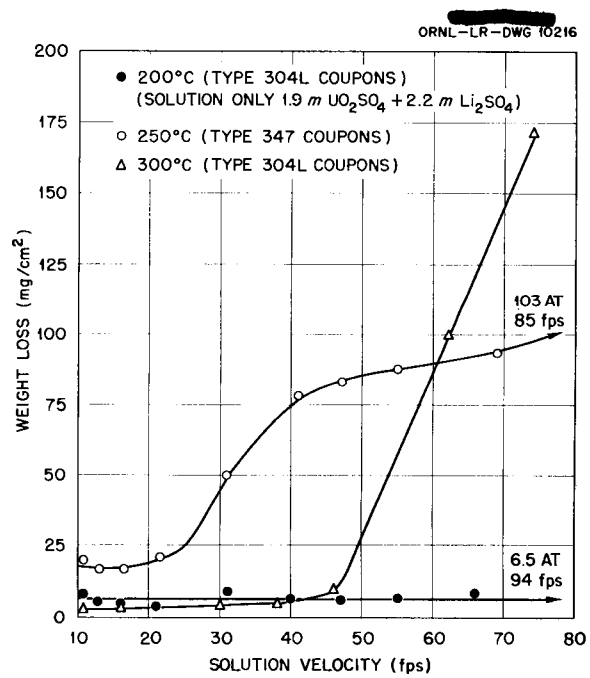

Fig. 10.4. Weight Loss vs Velocity for Stainless Steel Coupons in 2.9 *m* UO_2SO_4 Plus 3.2 *m* Li_2SO_4.

in the last quarterly report.[11] The concentrations for runs H-65 through H-68 and for run H-74 were reported incorrectly and are herewith corrected.[12] The results obtained on the pin-type specimens are shown in Table 10.3, and the results from the type 347 stainless steel coupons exposed at different flow rates are shown in Fig. 10.5. Note that at low flow rates the specimens showed no corrosion after the first 174 hr, whereas at high flow rates the extent of corrosion was approximately proportional to the exposure time. The critical velocity was about 30 fps.

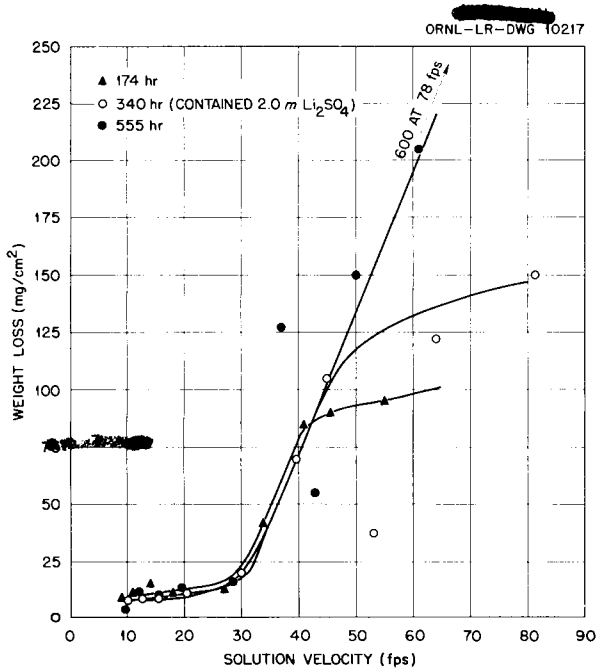

Fig. 10.5. Weight Loss vs Velocity for Type 347 Stainless Steel Coupons in 1.6 *m* UO_2SO_4 Plus 1.7 *m* Li_2SO_4 at 300°C.

The combination of runs H-75, H-76, H-78, and H-79 was made so as to show the effect of temperature in the range 200 to 300°C on the corrosion of stainless steel in a solution of 1.5 to 1.6 *m* uranyl sulfate and 1.7 *m* lithium sulfate (2.0 *m* for run H-76). The results obtained were almost identical to those shown in Fig. 10.4. At 250°C the critical velocities were the same at the two concentrations, but at 300°C the critical velocity appeared to be higher in the more concentrated solution (30 fps compared with 45 fps).

Platinum, gold, titanium, and zirconium exposed at 68 fps, runs H-75, H-76, and H-78 in Table 10.3, showed high corrosion rates. During these runs some scale from the interior of the loop flaked off, and, as a result, the solution contained a considerable quantity of suspended solids. Based on the appearance of the pins, the attack appeared to be more mechanical than chemical. To check this point, a hydroclone was used to remove the solids from solution in run H-79. From Table 10.3 it can be seen that, in the absence of the solids, gold, platinum, zirconium, and titanium showed low corrosion rates even at the highest velocity. It should be noted that relatively high corrosion rates for titanium, zirconium, and platinum were reported for runs H-65, H-66, H-68, and H-74 in the last quarterly report.[11] It now seems probable that the high rates were due to the suspended solids abrading the surfaces of the pins.

In view of the relatively low corrosion rates obtained in 1.5 to 2.9 *m* uranyl sulfate solutions containing an equivalent amount of lithium sulfate, a 4.4 *m* uranyl sulfate solution, containing the same molality of lithium sulfate, was prepared. This solution contained 730 g of uranium per liter and had a density of 2.2 g/cm^3 at room temperature. Quartz tube experiments showed no phase changes in this solution at temperatures as high as 390°C.

By use of an autoclave equipped with a pressure gage the vapor pressure of the above solution was determined approximately. Figure 10.6 shows that the vapor pressure of the solution was very substantially lower than that of pure water.

The above-mentioned solution was circulated in loop D at 300°C for 200 hr. The data obtained from the pin-type specimens are shown in Table 10.3 (run D-54). Figure 10.7 illustrates the weight losses of the coupons vs solution velocity in comparison with runs of lower concentration. The fact that the critical velocity in the 1.6 *m* solution was 10 to 15 fps lower is unexplained; but it is interesting to note that for a threefold change in

[11] J. C. Griess and R. S. Greeley, *HRP Quar. Prog. Rep. July 31, 1955*, ORNL-1943, Table 8.2, p 78.

[12] The corrected concentrations are: H-65: 1.2 *m* UO_2SO_4 + 1.4 *m* $MgSO_4$; H-66: 1.5 *m* UO_2SO_4 + 1.5 *m* Li_2SO_4; H-67: 1.0 *m* UO_2SO_4 + 1.1 *m* $MgSO_4$; H-68: 1.2 *m* UO_2SO_4 + 1.2 *m* Li_2SO_4; H-74: 1.6 *m* UO_2SO_4 + 1.7 *m* Li_2SO_4.

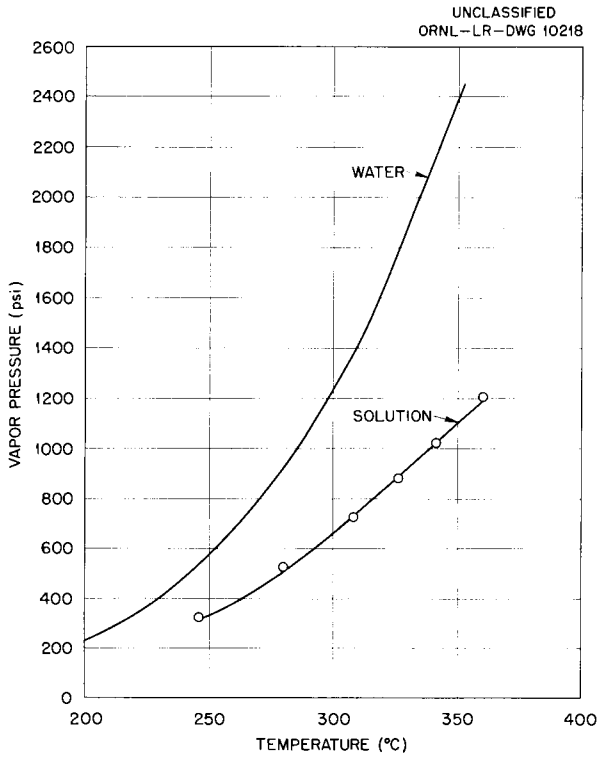

Fig. 10.6. Vapor Pressure vs Temperature for a Solution of 4.4 *m* UO_2SO_4 Plus 4.4 *m* Li_2SO_4.

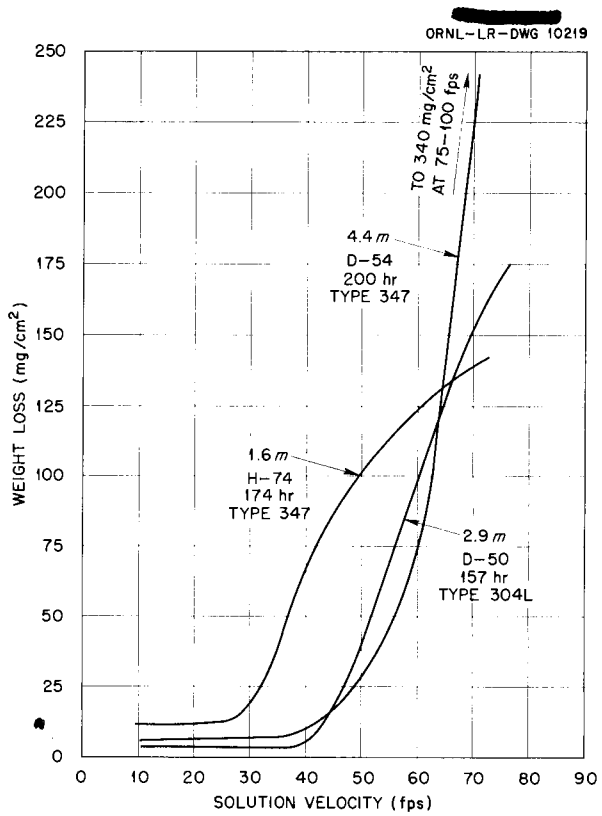

Fig. 10.7. Weight Loss vs Velocity for Stainless Steel Coupons at 300°C in Equimolal UO_2SO_4–Li_2SO_4 Solutions with 100 to 500 ppm O_2.

concentration the changes in corrosion and critical velocity were relatively slight. The room temperature pH's of the solutions were 1.4, 1.2, and 0.8; the concentrations were 300, 450, and 730 g of uranium per liter at room temperature; and the densities were 1.4, 1.6, and 2.2 for runs H-74, D-50, and D-54, respectively.

One characteristic of these concentrated solutions with added lithium sulfate is their high oxidizing power. At 300°C the Cr(VI) concentration increases rapidly during a run, reaching 500 to 1000 ppm in 200 hr, depending on the oxygen concentration and the previous history of the loop. Even at 200°C, where no hexavalent chromium formation has been observed previously, 100 ppm was found after 200 hr in runs D-52 (1.9 *m*) and H-78 (1.6 *m*). Such amounts of Cr(VI) undoubtedly affect the corrosion rates of stainless steel, probably accounting, at least partially, for the favorable corrosion results observed. It is also possible that the oxidizing character of the lithium sulfate–uranyl sulfate solutions may change the chemistry of plutonium and of some of the fission products. Stabilization of plutonium in the Pu(VI) should be more likely, for example.

(f) Damage to a Titanium Impeller. – During a run in the all-titanium loop, loop G, with 0.11 *m* uranyl sulfate at 250°C under a partial pressure of about 400 psi oxygen, the rear hub of the titanium impeller and the seal and spacer rings (Rem-Cru 70 titanium with 0.3% carbon) were severely damaged. Visual, microscopic, and metallographic examinations indicated that very intensive oxidation had occurred. X-ray diffraction studies showed that the major product was TiO. Figure 10.8 shows the appearance of the rear hub, and Fig. 10.9 is a photograph of the seal and spacer rings as removed from the thermal spacer of the pump. All other parts of the impeller were free of damage. The impeller had been in use for more than 12,000 hr under a variety of conditions, and all indications from the operation of the pump were that the impeller was functioning properly

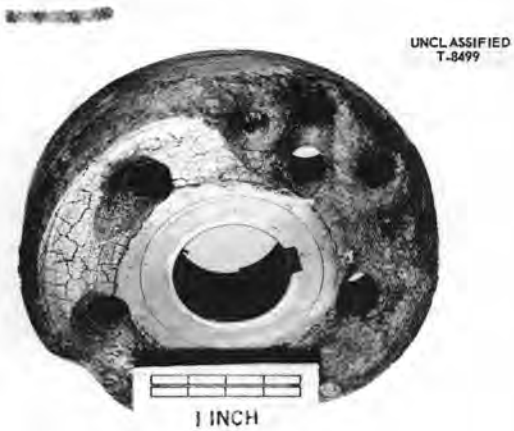

Fig. 10.8. Hub of Titanium Impeller No. 1 After Damage by Oxidation.

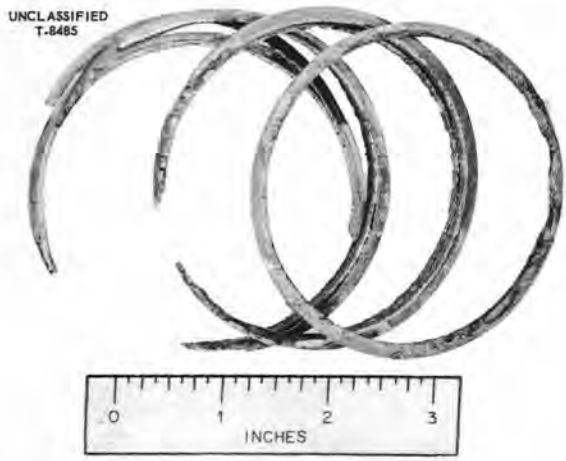

Fig. 10.9. Titanium Seal and Spacer Rings Used with Titanium Impeller No. 1.

and had not undergone extensive corrosion until the time of failure.

Two hours after startup of the run it was noticed that the pump was vibrating, so the run was terminated and the pump disassembled. The front Graphitar bearing was found to be badly worn; evidently, wear of this bearing allowed the impeller hub to rub the seal rings. The rubbing action probably removed the protective oxide film on the titanium and raised the surface temperature sufficiently to permit very rapid oxidation of the metal by the solution and/or oxygen.

The oxidation must have been very rapid and intense, since portions of the oxidized titanium were melted and thrown from the hub. Moreover, the surface and parts of the rings were partially fused. It therefore seems probable that the surface temperature rose to the neighborhood of 2000°C. The rapid oxidation of the titanium in the oxygen-water mixture presumably produced the great increase in temperature (the heat of formation of TiO is approximately 135 kcal/mole at room temperature). The reaction very likely proceeded until the water and oxygen, in the limited space enclosing the hub, were consumed or until the layer of molten or semimolten titanium-oxygen alloy smothered the reaction.

Conclusive evidence that oxidation and high temperatures occurred in the titanium was given by photomicrographs. They showed that the heavily corroded surfaces consisted of transformed beta-titanium (the alpha-beta transformation temperature for pure titanium is 885°C) with a region of high-oxygen material at the surface. This high-oxygen region consisted of four layers: alpha-titanium plus transformed beta; alpha-titanium stabilized by oxygen; alpha-titanium plus TiO; and TiO (on the surface). A more complete discussion has been prepared.[13]

(g) Corrosion Resistance of Incoloy. – Incoloy, a 20% chromium–35% nickel steel alloy, is of possible interest for some reactor applications, and in previous tests,[14] unlike other high nickel alloys it showed a corrosion resistance similar to that shown by type 347 stainless steel. Table 10.3 gives the results of further tests on Incoloy in runs A-88, D-53, E-48, H-79, and N-7. In general, the corrosion rates of Incoloy were very slightly higher than those of the other austenitic stainless steels tested. In run N-7, however, in 0.04 *m* uranyl sulfate plus 0.005 *m* copper sulfate with 0.02 *m* sulfuric acid at 225°C, the Incoloy pins at low velocity corroded about twice as fast as the steels.

A run was made with Incoloy coupons in 0.17 *m* uranyl sulfate at 250°C in order to compare the critical velocity of Incoloy with type 347 stainless

[13] J. C. Griess, T. M. Kegley, and J. L. Gregg, *Report on Corrosion of Titanium Impeller No. 1*, ORNL CF-55-9-65 (Sept. 15, 1955).

[14] J. C. Griess and R. S. Greeley, *HRP Quar. Prog. Rep. April 30, 1955*, ORNL-1895, Table 3.2, p 76–82, Runs I-23 through I-26.

steel. The critical velocity was 15 to 20 fps, in contrast to 20 to 30 fps for type 347 stainless steel. Also, the corrosion rate of the Incoloy coupons below the critical velocity was somewhat higher than with type 347 stainless steel coupons.

10.2 LABORATORY STUDIES

J. L. English J. C. Griess

10.2.1 Corrosion of Type 303 Stainless Steel High-Pressure Valves by Sulfuric Acid and Uranyl Sulfate Solutions at Room Temperature

The corrosion behavior of ¼-in. stainless steel high-pressure valves was examined for 1000 hr in nonaerated sulfuric acid and uranyl sulfate solutions at room temperature in connection with the use of the valves for adding reagents to an in-pile corrosion-test loop during operation. The valves employed for the corrosion study were standard, 30,000-psi, two-way straight and right-angle valves as supplied by Autoclave Engineers, Inc. The valve bodies were fabricated from type 303 stainless steel, and the valve stems were hardened type 420 stainless steel.

The test solutions were sulfuric acid in concentrations of 0.08, 0.8, and 12.2 *m*; and 0.17 *m* uranyl sulfate plus 0.03 *m* copper sulfate solution containing, in addition, various concentrations of chromic and sulfuric acids. The valves were dismantled prior to exposure, and the bodies and stems were immersed separately in the test solutions. The tests were run for as long as 1000 hr at room temperature and without solution replacement or aeration. With the exception of those tests which were terminated very early because of very severe initial corrosion attack, the valve components were removed from the test solutions for examination and weight measurements after total elapsed times of 24, 72, 500, and 1000 hr. The final observations and corrosion results are reported in Table 10.5.

The behavior of types 303 and hardened 420 stainless steel was found – with one exception – to be completely unsatisfactory in the nonaerated sulfuric acid solutions at room temperature (tests I-56, I-57, and I-58); corrosion rates were 500 mpy and greater. The exception to this behavior was a type 303 stainless steel valve body which was corroded at the very low rate of 0.3 mpy after 68 hr in 0.08 *m* sulfuric acid (test I-58).

The corrosion resistance of type 303 stainless steel valve body material was quite acceptable in all 0.17 *m* uranyl sulfate plus 0.03 *m* copper sulfate solutions containing different concentrations of chromic and sulfuric acids. After 1000 hr of exposure the corrosion rates were less than 1.0 mpy for those valve bodies showing a weight loss. In a few instances, weight gains were observed on the valve bodies. The behavior of the hardened type 420 stainless steel stems was markedly different, however. Corrosion rates varied between 4 and 370 mpy, as indicated in Table 10.5. One exception to this behavior was the stem exposed in 0.17 *m* uranyl sulfate, 0.03 *m* copper sulfate, 0.8 *m* sulfuric acid, and 0.004 *m* chromic acid solution (test I-99), where the observed rate was less than 0.1 mpy. It was noted also that copper-colored deposits were present on four of the six hardened stainless steel stems at the completion of the initial 24-hr exposure. The deposits appeared as smooth, platelike areas randomly distributed over the surface of the metal. The effect was not observed on specimens exposed in two of the solutions: (1) 0.17 *m* uranyl sulfate plus 0.03 *m* copper sulfate solutions containing 12.2 *m* sulfuric acid plus 0.04 *m* chromic acid (test I-98) and (2) 0.8 *m* sulfuric acid plus 0.004 *m* chromic acid (test I-99). During continued exposure the platelike deposits disappeared. Final solution analyses disclosed no depletion in copper content from the originally determined values.

In conclusion, the behavior of the type 303 stainless steel bodies and of the hardened type 420 stainless steel valve stems was found to be satisfactory in one solution only, namely, a solution consisting of 0.17 *m* uranyl sulfate, 0.03 *m* copper sulfate, 0.8 *m* sulfuric acid, and 0.004 *m* chromic acid. The corrosion rates for the body and the stem were less than 0.1 mpy, and no copper-colored deposits were observed on either of the valve components during the course of the 1000-hr test.

10.2.2 Corrosion of Cast Zirconium Alloys

A series of cast zirconium alloys was prepared (see Sec. 13.3.4, this report) by the Metallurgy Division and submitted for exposure in static uranyl sulfate solutions at elevated temperature. The immediate objective of the test program was a preliminary evaluation of the high-temperature corrosion behavior of cast zirconium as influenced by the presence of specific alloying elements in the metal. The cast specimens included alloys

TABLE 10.5. CORROSION OF TYPE 303 STAINLESS STEEL VALVE BODIES AND HARDENED TYPE 420 STAINLESS STEEL VALVE STEMS BY IN-PILE LOOP SOLUTIONS AT ROOM TEMPERATURE

Test No.	Solution Composition (*m*)				Valve Component	Total (hr)	Corrosion Rate (mpy)	Final Appearance of Specimen
	UO_2SO_4	$CuSO_4$	H_2SO_4	CrO_3				
I-56			12.2		Body	3	3640	Dull black; severe general attack
					Stem	3	6140	Dull black; very severe general attack
I-57			0.8		Body	30	470	Gray-black; moderate general attack
					Stem	30	3310	Dark gray; severe general attack
I-58			0.08		Body	68	0.3	Lustrous metallic gray; very light general attack
					Stem	68	2280	Dark gray; severe general attack with pitting
I-59	0.17	0.03	12.2		Body	1000	0.3	Bright and metallic; very light general attack
					Stem	1000	21*	Dark gray; mild general attack
I-96	0.17	0.03	0.8		Body	1000	Gain	Bright and metallic; negligible attack
					Stem	1000	370*	Dark gray; moderate general attack
I-97	0.17	0.03	0.08		Body	1000	Gain	Bright and metallic; negligible attack
					Stem	1000	5.8*	Lustrous gray; mild general attack
I-98	0.17	0.03	12.2	0.04	Body	1000	0.8	Dark-black luster; light general attack
					Stem	1000	48	Dark black; mild general attack
I-99	0.17	0.03	0.8	0.004	Body	1000	<0.1	Bright and metallic; negligible attack
					Stem	1000	<0.1	Bright and metallic; negligible attack
J-1	0.17	0.03	0.08	0.0004	Body	1000	Gain	Bright and metallic; negligible attack
					Stem	1000	3.7*	Lustrous dark gray; mild general attack

*Copper-colored deposits observed during initial 24-hr run; deposits disappeared during continued exposure.

of zirconium with aluminum (Zircaloy-2X), chromium, columbium, cesium, cerium, silver, tin (Zircaloy-2), and yttrium. The compositions of the alloys are shown in Table 10.6. Specimens of crystal-bar zirconium and titanium 75A were also included in the study for comparative purposes.

The specimens were prepared by a vacuum arc-melting process. The resulting "finger" castings, weighing approximately 50 g or less, were sectioned into suitable corrosion test specimens having an apparent surface area between 2 and 12 cm^2. The flat surfaces of the specimens were given a No. 180 grit finish by mechanical abrasion on a belt sander. The corrosion tests were run at 300°C in 0.04 *m* uranyl sulfate solution containing 0.005 *m* copper sulfate and either 0.004 or 0.02 *m* (10 or 50 mole %) sulfuric acid. The specimens were exposed individually in nitric acid–pretreated, 225-ml-capacity stainless steel autoclaves, using 125 ml of the test solution. Sufficient 30% hydrogen peroxide was added to the uranyl sulfate test solution at room temperature to produce approximately 150 psi of oxygen pressure at 300°C by thermal decomposition of the peroxide.

TABLE 10.6. CORROSION OF CAST ZIRCONIUM ALLOYS BY OXYGENATED 0.04 *m* UO_2SO_4–0.005 *m* $CuSO_4$ SOLUTION AT 300°C

Test No.	Alloying Element (wt %)	H_2SO_4 (*m*)	Total (hr)	Corrosion Rate (mpy)	Final Appearance of Specimen
K-86	None*	0.004	430	0.1	Lustrous dark gray-black thin film
K-97	None*	0.02	50	1.3	Lustrous gray-green thin film
K-82	1.5 Sn**	0.004	430	0.1	Lustrous dark gray-black thin film; few scattered white corrosion products
K-98	1.5 Sn**	0.02	50	0	Lustrous dark gray-black thin film
K-85	0.7 Cr	0.004	430	0	Lustrous dark gray-black thin film
K-81	1.4 Cr	0.004	430	<0.1	Lustrous dark gray-black film with scattered pink corrosion products
K-87	3.5 Cr	0.004	430	0.9	Dull gray-white with random white corrosion products
K-80	53.0 Cr	0.004	430	Gain	Dull dark black; nonuniform bulky black corrosion products
K-83	1.9 Al 1.0 Sn	0.004	430	121	Heavy deposits of white scale; surfaces badly etched
K-99	2.0 Cb	0.02	50	14.5	Dull light-gray film with green-colored corrosion products
L-1	5.0 Cb	0.02	50	Gain	Spotty black film with random gray-green corrosion products
L-2	7.5 Cb	0.02	50	Gain	Lustrous blue-gray thin film with dark black streaks
L-3	15.0 Cb	0.02	50	<0.1	Uniform dull gray-white film
L-4	3.0 Ce	0.02	50	1.2	Lustrous thin purple film
L-5	2.25 Cs	0.02	50	124	Heavy white-and-tan corrosion scale
L-6	5.0 Y	0.02	50	550	Dull gray; bulky white products
L-7	7.75 Ag	0.02	50	87	Dull light-gray; surface attack
K-84	Ti-75A	0.004	430	<0.1	Highly lustrous mottled blue thin film

*Crystal bar zirconium.
**Zircaloy-2.

The corrosion rates, based on as-scrubbed weight losses, and the final condition of the test specimens after 50- and 430-hr exposures are summarized in Table 10.6.

An examination of the data in Table 10.6 shows that, other than the crystal-bar zirconium and the Zircaloy-2 specimens, the only alloys of zirconium which exhibited promising corrosion behavior in 0.04 *m* uranyl sulfate at 300°C were the 0.7 and 1.4 wt % chromium alloys and possibly the 3.0 wt % cerium alloy. The remaining alloys with higher chromium contents and with columbium, aluminum, cesium, silver, and yttrium were considered unsatisfactory because of excessive corrosion rates and/or the presence of significantly large quantities of corrosion products. Exposure of the more promising alloys will be continued.

11. SLURRY CORROSION TESTS

E. L. Compere H. C. Savage
S. R. Buxton G. E. Moore
S. A. Reed R. M. Warner

11.1 PUMP LOOPS

H. C. Savage
S. R. Buxton S. A. Reed
R. M. Warner

11.1.1 Operation and Maintenance

(a) 100A Pump Loops. – A number of additional short-term runs were made during the quarter in 100A pump loop CS,[1] designed to obtain dynamic-corrosion data with thorium dioxide slurries. In runs CS-4 through CS-9, previously reported,[2] difficulties were experienced by caking of the thorium dioxide and in maintaining the desired thorium concentrations in the circulating system. Consequently, the short test runs in loop CS were made primarily for determining loop operating conditions required for long-term dynamic-corrosion studies. In particular, conditions were sought which would afford the pumping of high-concentration thoria slurries, that is, 1000 to 1200 g of thorium per kilogram of water, without the formation of cakes and/or loss in concentration which were observed in runs CS-4 through CS-9.

Six test runs, CS-10 through CS-14 and CS-16, were carried out; five were with the loop and pressurizer at approximately the same temperature, 300°C, and with an oxygen overpressure of 150 to 400 psi. One run, CS-16, was made with the pressurizer 15 to 20°C above the loop temperature (300°C in the loop, 315 to 320°C in the pressurizer) to provide steam pressurization. In all cases the concentration of thorium in samples removed from the circulating stream of the loop was less than the thorium concentration charged to the system. However, the highest concentration of thorium, in samples removed from the loop, averaged 1030 g of thorium per kilogram of water in run CS-16 with steam pressurization. In this run the theoretical thorium concentration charged to the loop was 1200 g of thorium per kilogram of water. Results of runs CS-10 through CS-14 and CS-16 are summarized in Table 11.1.

[1] H. C. Savage, F. J. Walter, and R. M. Warner, *HRP Quar. Prog. Rep. Oct. 31, 1954*, ORNL-1813, Fig. 3.1, p 65, and Fig. 3.2, p 66.

[2] H. C. Savage and F. J. Walter, *HRP Quar. Prog. Rep. July 31, 1955*, ORNL-1943, p 64–70.

TABLE 11.1. SUMMARY OF RUNS WITH THORIUM OXIDE SLURRY

Run No.	Thorium Concentration (g/kg of H_2O)		Time (hr)	Temperature (°C)	Calcination Temperature (°C)	Comments
	Charged	Sampled				
CS-10	538	211–448	200	300	950 (D-30)	
CS-11	1100	708–740	115	300	950 (D-30)	Some caking; pump bearing failure
CS-12	1100	637–780	214	300	650 (D-17)	Caking in pressurizer, tapered coupon holder, and mixing line
CS-13	1100	628–692	99	300	800 (D-38)	No caking observed
	*					
CS-14	1000	608–745	44	300	800 (D-38)	No caking observed; pump bearing failure
CS-16	1200	965–1120	75	300 (loop) ~315 (pressurizer)	800 (D-38)	No caking observed; pump bearing failure

*Attempt was made to increase the concentration by adding additional thorium oxide slurry to system. Slurry could not be resuspended after this addition.

Numerous changes were made in the loop geometry and flow during the course of these runs in an attempt to bring the thorium concentration of the circulating slurry up to the concentration charged to the loop and to minimize or eliminate caking of the slurry. A brief outline of each run illustrates these changes.

In runs CS-10 and CS-11 a slurry of thorium oxide calcined at 950°C was used instead of the 650°C calcined material used in runs CS-4 through CS-9. Runs CS-10 and CS-11 were made with the system operating under isothermal conditions with oxygen overpressure. Run CS-10, charged to provide a thorium concentration of 538 g of thorium per kilogram of water, was terminated at 200 hr without incident except that the thorium concentration of the circulating slurry was uniformly lower, averaging 386 g of thorium per kilogram of water. In run CS-11, charged to give a thorium concentration of 1100 g of thorium per kilogram of water, plugging of the tapered coupon holder (which has an opening of approximately 0.026 in.) caused difficulty. This plugging is believed to have been caused by foreign material in the thorium dioxide. In addition it was necessary to replace the Graphitar bearings in the 100A pump because of excessive wear.

Prior to run CS-12 the system was modified by the addition of two extra bypass lines to the pressurizer (see Fig. 11.1) in an attempt to minimize caking and/or concentration gradients by increasing the pressurizer flow. No improvement was observed under isothermal conditions with the loop charged at 1100 g of thorium

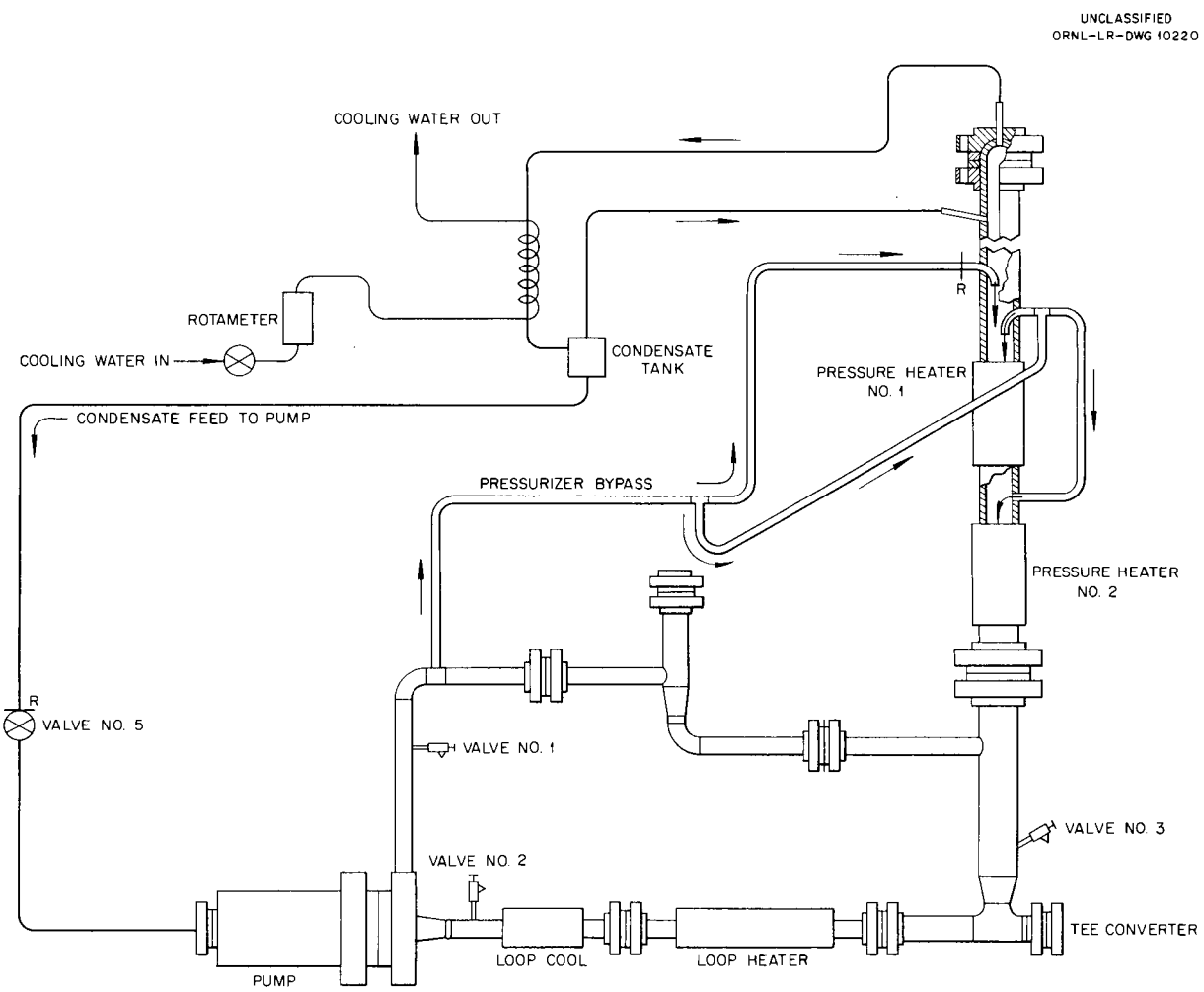

Fig. 11.1. Schematic Diagram – Slurry Loop CS.

per kilogram of water with thorium oxide calcined at 650°C. The run was terminated because of plugging of the bypass lines and tapered coupon holder and because of evidence of caking in the pressurizer.

The tapered coupon holder was replaced with a standard pin-type holder, and the flow through the three pressurizer bypass lines was increased by removing restrictors. The slurry concentration charged to the system for run CS-13 was 1100 g of thorium per kilogram of water, made from thorium dioxide calcined at 800°C. No caking was observed in this run but, as indicated by samples, theoretical thorium concentration was not obtained in the circulating stream.

On the assumption that the observed loss of thorium concentration in the loop was the result of material holdup in dead spots in the loop, three of the five sample barrel holders in the loop[3] were removed in an attempt to reduce the total number of dead spaces around the sample units.[4] In addition, the flow through each of the two remaining sample barrels was increased to the maximum obtainable (~40 gpm, ~75 fps velocity past the sample pins). When a thorium oxide slurry made from material calcined at 800°C was used, no improvement in thorium concentration in the circulating stream, compared with the charge concentration, was observed. The Graphitar bearings in the model 100A pump were excessively worn and had to be replaced at the end of this run.

Run CS-16 was made in order to duplicate as nearly as possible the operating conditions of slurry loops operated by the Engineering Research Section. The thorium oxide slurry charged to the system was the same as in run CS-14 (D-38, calcined at 800°C) except that a thorium concentration of 1200 g of thorium per kilogram of water was charged to the system. Operation was at 300°C in the loop with steam pressurization (pressurizer at 310 to 320°C). The thorium concentration in the circulating stream was increased to approximately 1030 g of thorium per kilogram of water but was still below the concentration charged to the system. The run was terminated after 75 hr because of excessive pump-bearing wear.

The loop is now being modified so as to improve the system of water addition to the rear of the pump. At present, long-term runs cannot be made because of pump-bearing failures. Installation of a more reliable system with increased flow rate of water to keep the pump bearings free of slurry should prolong pump bearing life. In addition, provisions are being made to increase further the flow of slurry through the pressurizer in an attempt to improve the control of concentration in the circulating slurry. Because of the heating requirements for steam pressurization at large flow rates through the pressurizer, isothermal operation with gas pressurization of the loop will probably be required. From the standpoint of obtaining corrosion data, isothermal operation is more desirable than steam pressurization in that loop operation is somewhat simplified.

(b) In-Pile Loop. – During the quarter, work was continued with the experimental in-pile slurry loop[5] in an attempt to develop an operable loop and pressurizer assembly. The results of runs made with both water and thorium oxide slurry under various operating conditions indicate the advisability of redesigning the pressurizer and condensed-vapor system, which feeds clear water to the rear of the pump can, in order to prevent or minimize bearing wear.

While it was doubtful that the flow of condensed vapor could be completely eliminated without pump-bearing damage, a run with 500 g of thorium per kilogram of water (prepared from D-17 oxide which had been recalcined at 800°C) was made so as to verify this point. The pump was a 5-gpm canned-rotor double-bearing pump containing 17-4 PH stainless steel journals and Graphitar No. 14 bearings. At the end of approximately 3 hr of operation with no condensed vapor flow, the run was discontinued because of noisy pump operation. Examination of the pump parts following disassembly showed the 17-4 PH journals to be in excellent condition but that the Graphitar No. 14 bearings were damaged beyond further use. As a result of this run and of previous runs made with extremely low condensed-vapor feed rates to the rear of the pump, it has been concluded that the 5-gpm canned-rotor pump with Graphitar bearings cannot circulate 500 g of thorium per kilogram of water slurry unless the rear of the

[3] *Ibid.*, Fig. 8.3, p 65.

[4] H. C. Savage, F. J. Walter, and R. M. Warner, *HRP Quar. Prog. Rep. Oct. 31, 1954*, ORNL-1813, Fig. 3.1, p 65.

[5] G. H. Jenks *et al.*, *HRP Quar. Prog. Rep. April 30, 1955*, ORNL-1895, Fig. 4.2, p 95–96.

pump is kept flushed relatively free of oxide particles.

A previous run performed with relatively high condensed-vapor flow rates (800 cc/hr) resulted in a porous cake forming in the pressurizer[6] as a result of excessive evaporation. This run was made with only a portion of the main loop flow going through the pressurizer side inlet. The system flow pattern was revised to permit all the main loop flow to be introduced into the side and to pass out the bottom of the pressurizer. Also, at this time a calibrated rotameter was installed in the condensed-vapor line between the condenser and the pump to provide a more accurate measurement of this flow. Runs with water employing this scheme of operation illustrated the necessity of revising the pressurizer and condensed-vapor system to provide water to the pump-bearing area. Observed condensate flow rates were erratic and unreliable.

At present the entire pressurizer section of the in-pile loop is being revised to permit more condensate to be removed. Also, in an attempt to counteract the difficulties which have been experienced with the Graphitar bearings, the pump is now being fitted with sintered aluminum oxide bearings and journals.

It may be noted that the difficulties of slurry operation in the small in-pile type of loop are similar to those experienced in 100A pump loop CS mentioned above. Both loops are being worked on concurrently.

11.1.2 Data and Discussion

Corrosion data collected during this period were obtained during a series of short-term test runs made primarily to check out the operational characteristics of the dynamic test loop CS with high-concentration thorium oxide slurries. These tests are described in Sec. 11.1.1*a*. Pin-type specimens and, when possible, coupon-type specimens of various materials were exposed in these runs.

All tests were made at 300°C. No additions were made to the slurries other than the gaseous oxygen added to the loop pressurizer to provide loop overpressure and/or to maintain approximately 1000 ppm of dissolved oxygen at temperature. The average corrosion rates of pin-type corrosion specimens exposed in the tests are presented in Table 11.2. Results of chemical analyses of samples withdrawn from the loop during each test are shown in Table 11.3.

Three different thorium oxide preparations were tested. They were ORNL production batches D-17, D-30, and D-38, calcined at 600, 950, and 800°C, respectively.

Batch D-17 thoria, which had been tested previously,[2,7] was replaced early in the period by batch D-30, the 950°C calcined material, to determine the effect of firing temperature on pumping characteristics.

The first test, run CS-10, was with D-30 oxide, ran for 225 hr, and employed a nominal slurry charge concentration of 500 g of thorium per kilogram of water. The system was operated isothermally; that is, the loop and pressurizer were operated at the same temperature and an attempt was made to maintain a uniform slurry concentration throughout the system. However, the concentration, falling after the first 75 hr, fluctuated between 447 and 220 g of thorium per kilogram of water during the test. Data from weight losses of defilmed type 347 stainless steel coupons exposed in the test showed an apparent critical velocity at approximately 30 fps. The over-all corrosion rate, calculated from nickel analyses, was 0.1 mpy.

The D-30 oxide was used again in run CS-11. The loop, operated isothermally, was charged to give a slurry concentration of 1100 g of thorium per kilogram of water. During the startup procedure, the double-tapered coupon holder was plugged by foreign material, which necessitated stopping the run to unplug the barrel. The run was started again and continued for an additional 107 hr. Slurry samples withdrawn from the loop during this period contained additional foreign matter. A portion of this material, submitted for chemical analysis, was found to be composed principally of calcium, magnesium, silica, and sulfate, presumably from the furnace used in calcination. The slurry concentration, based on one set of duplicate samples taken after approximately 50 hr of operation, was 740 g of thorium per kilogram of water. Due to the foreign matter found in batch D-30, no further tests were made with the material.

[6] G. H. Jenks *et al.*, *HRP Quar. Prog. Rep. July 31, 1955*, ORNL-1943, p 108–109.

[7] J. C. Griess and S. A. Reed, *HRP Quar. Prog. Rep. July 31, 1955*, ORNL-1943, p 91–100.

TABLE 11.2. CORROSION RATES OF PIN-TYPE SPECIMENS (RUNS CS-10 THROUGH CS-16)

Run No.	Test Conditions: ThO_2 Slurry Concentration (g/kg of H_2O)[a]	Temperature (°C)	Time (hr)	Additions	Flow Rate (fps ± 10%)	Pin Material	Number of Pins	Corrosion Rate (mpy): Minimum	Average	Maximum
CS-10	211–448 Av 386	300	226	1000 ppm O_2	8	322 W SS[b]	1		0.5	
						322 W SS[c]	1		1	
						347 SS	2	0.38	0.4	0.38
						Gold	1		0.1	
						Platinum	1		0.1	
						Stellite 1	1		7	
						Stellite 2	1		9	
						Stellite 3	1		7	
						Stellite 25	1		4	
						Stellite 98M2	1		18	
						Thorium oxide[d]	1		Disintegrated	
						Titanium 75A	1		0.1	
						Zirconium[e]	1		/	
					20	304L SS	1		2	
						309 SCb SS	2	1.6	1.8	2.1
						347 SS	2	2.6	2.6	2.6
						347 SS[c]	2	1.6	2.0	2.4
						Gold	1		2	
						Platinum	1		2	
						Thorium oxide[d]	1		Disintegrated	
						Titanium alloy[g]	1		2	
						Titanium alloy[h]	1		3	
						Titanium alloy[i]	1		3	
						Zirconium[e]	1		1	
					30	304L SS	2	6.3	6.5	6.6
						309 SCb SS	2	3.3	4.7	6.0
						347 SS	2	6.1	7.0	7.9
						443 SS	1		5	
						446 SS	1		5	
						Gold	1		7	

TABLE 11.2 (continued)

Run No.	Test Conditions: ThO_2 Slurry Concentration (g/kg of H_2O)[a]	Temperature (°C)	Time (hr)	Additions	Flow Rate (fps ± 10%)	Pin Material	Number of Pins	Corrosion Rate (mpy): Minimum	Average	Maximum
CS-10	211–448 Av 386	300	226	1000 ppm O_2	30	Inconel X	1		17	
						Platinum	1		7	
						Thorium oxide[d]	1		Disintegrated	
						Titanium 75A	1		6	
						Zirconium[e]	1		3	
CS-11	740	300	115	1000 ppm O_2	9	322 W SS[b]	1		0.1	
						322 W SS[c]	1		0.1	
						347 SS	2	0.59	0.67	0.74
						Gold	1		0.3	
						Platinum	1		0.4	
						Stellite 1	1		12	
						Stellite 3	1		12	
						Stellite 6	1		11	
						Stellite 25	1		13	
						Stellite 98M2	1		34	
						Thorium oxide[d]	1		Disintegrated	
						Titanium 75A	1		1	
						Zirconium	1		0.0	
					21	304L SS	1		6	
						309 SCb SS	2	6.0	8	10.2
						347 SS	4	4.4	5	6.0
						Gold	1		5	
						Platinum	1		5	
						Thorium oxide[d]	1		Disintegrated	
						Titanium alloy[g]	1		6	
						Titanium alloy[h]	1		6	
						Titanium alloy[i]	1		4	
						Zirconium[e]	1		3	
					29	304L SS	2	14.1	15.4	16.7
						309 SCb SS	2	10.8	12.9	14.9

TABLE 11.2 (continued)

Run No.	Test Conditions: ThO_2 Slurry Concentration (g/kg of H_2O)[a]	Temperature (°C)	Time (hr)	Additions	Flow Rate (fps ± 10%)	Pin Material	Number of Pins	Corrosion Rate (mpy): Minimum	Average	Maximum
CS-11	740	300	115	1000 ppm O_2	29	347 SS	1		13	
						443 SS	1		14	
						446 SS	1		13	
						Gold	1		17	
						Inconel X	1		28	
						Platinum	1		16	
						Rhodium[j]	1		8	
						Titanium 75A	1		14	
						Zirconium[e]	1		11	
CS-12	632–780[k]	300	214	1000 ppm O_2	35	304L SS	1		22	
	Av 713		(total)			309 SCb SS	2	23	26	28
CS-13	640–652[l]					347 SS	5	11	16	19
	Av 650					Gold	1		3	
						Platinum	1		5	
						Titanium alloy[g]	1		5	
						Titanium alloy[h]	1		7	
						Titanium alloy[i]	1		6	
						Zircaloy-2	1		6	
					43	304L SS	2	43	44	44
						309 SCb SS	2	30	38	45
						347 SS	2	34	40	45
						443 SS	1		58	
						446 SS	1		54	
						Gold	1		8	
						Inconel	1		49	
						Platinum	1		1	
						Rhodium[j]	1		61	
						Titanium 75A	1		11	
						Zircaloy-2	1		12	

TABLE 11.2 (continued)

Run No.	Test Conditions: ThO_2 Slurry Concentration (g/kg of H_2O)[a]	Temperature (°C)	Time (hr)	Additions	Flow Rate (fps ± 10%)	Pin Material	Number of Pins	Corrosion Rate (mpy): Minimum	Average	Maximum
CS-12	632–780[k]	300	119	1000 ppm O_2	68	322 W SS[b]	1		22	
CS-13	640–652[l]	300	96	1000 ppm O_2		322 W SS[c]	1		28	
CS-14	725–745	300	44	2400 ppm O_2		347 SS	3	14	24	29
			259			Gold	1		9.2	
						Platinum	1		7.2	
						Stellite 1	1		31	
						Stellite 2	1		30	
						Stellite 3	1		36	
						Stellite 25	1		29	
						Stellite 98M2	1		170	
						Titanium 75A	1		15	
						Zircaloy-2	1		7.6	
CS-16	965–1120[l]	298	76	~200 ppm O_2	75	322 W SS	1		110	
	Av 1030	310				347 SS	9	69	106	120
						Gold	2	35	32	38
						Platinum	2	48	52	55
						Stellite 1	2	350	380	410
						Stellite 3	2	230	290	360
						Stellite 6	2	290	295	300
						Stellite 25	2	210	215	220
						Stellite 98M2	2	510	600	690
						Titanium 75A	2	48	50	51
						Zircaloy-2	2	30	32	33

[a]See Table 11.3, col. 5.
[b]Hardened.
[c]Annealed.
[d]Contained 0.5% CaO as binder, which was thought to be preferentially leached out.
[e]Crystal bar.
[f]Defilmed but still showed weight gain due to incomplete removal of oxide.
[g]A titanium alloy containing 3% aluminum and 5% chromium.
[h]A titanium alloy containing 5% aluminum and 2.5% tin.
[i]A titanium alloy containing 6% aluminum and 4% vanadium.
[j]Rhodium-plated type 347 stainless steel.
[k]Batch D-17 thoria.
[l]Batch D-38 thoria.

TABLE 11.3. CHEMICAL ANALYSES OF SLURRY SAMPLES FROM RUNS CS-10 THROUGH CS-16

Run No.	Temperature (°C)	Loop Charge Concentration (g per kg of H_2O)	Pumping Time (hr)	Solid Phase: Thorium (g per kg of H_2O)	Solid Phase: Corrosion Products (μ per g of slurry) Fe	Cr	Ni	Aqueous Phase: Conductivity $\times 10^5$ (mho/cm)	pH	ThO_2 Used in Preparing Slurry (ORNL Batch No.)*
CS-10	300	585	3	438	59	14	8	0.46	6.55	D-30
			26	440	108	20	9	0.56	6.65	
			50	432	145	32	25	6.1	6.00	
			75	447	194	39	29	6.6	6.20	
			122	340	214	46	34	6.3	6.85	
			225	220	180	37	16	4.7	5.50	
		av	386							
CS-11	300	1100	29	740	167	27	30	9.2	6.50	D-30
CS-12	300	1100	20	780	117	33	<5	5.3	7.10	D-17
			45	632						
			118	728	394	99	34		5.55	
CS-13	300	1100	20	652	340	70	58	0.11	7.95	D-38
			44	649						
CS-14	300	1000	24	745	175	37	23	9.4	7.85	D-38
			47	725	559	130	103	0.11	7.10	
CS-16	300	1200	3	1120	99	30	16	8.5	8.05	D-38
			20	965						
			21	920	458	131	98	3.2	6.15	
			22	995						
			68	1060	915	266	163	4.6	6.00	
			74	1120	980	275	177	5.6	5.80	

*Final calcination temperature: D-17, 650°C; D-30, 950°C; D-38, 800°C.

The pin-type specimens, inspected after the run, were badly scratched and appeared to have been severely abraded on the upstream side. Thin oxide films were formed on all coupon-type specimens. However, deep scratches had penetrated the films, exposing bare metal.

Batch D-17 thoria was used in run CS-12, and the system, operated isothermally at 300°C, was charged to give a slurry concentration of 1100 g of thorium per kilogram of water. Thorium concentrations of samples taken from the flowing stream during operation varied between 632 and 780 g per kilogram of water. The run was terminated after 118 hr operation because the bypass lines became plugged. Corrosion specimens were not removed from the system until run CS-13 was completed.

Because the supply of D-17 thoria had been depleted, the 800°C calcined batch D-38 was used in run CS-13. The charge concentration and operating conditions were identical to those in run CS-12. No plugging or caking was evident during the test, but the concentration of slurry again was low, approximating 650 g of thorium per kilogram of water. The test was stopped after approximately 90 hr of operation, and an additional quantity of thoria was added in an effort to increase the concentration to 1000 g of thorium per kilogram of water. However, the thoria could not be resuspended, and the test was terminated after a total circulation time of 99 hr.

Coupon-type specimens of type 347 stainless steel exposed during the two tests appeared to be uniformly attacked, and all specimens were covered with a thin adherent corrosion film. No definite critical velocity was observed. The over-all loop corrosion rate for the combined runs, CS-2 and and CS-13, was 8.8 mpy.

After three of the five sample barrels were removed and after the flow characteristics of the loop were adjusted for higher flow rates, the loop was charged to a concentration of 1000 g of thorium per kilogram of water with batch D-38 thoria for run CS-14. The original oxygen pressure was 130 psi, corresponding to 2400 ppm. The loop was operated isothermally for 44 hr at 300°C. Operation was stopped because of a leak in a tube fitting. The slurry could not be resuspended when the pump was restarted, and the run was terminated. The generalized loop corrosion rate for this run was 7.7 mpy. One set of pin-type specimens was exposed at 68 ± 7 fps.

An electrical short in the pump stator 4 min after startup terminated run CS-15. No corrosion data were obtained.

The loop was cleaned out and then recharged with 1200 g of thorium per kilogram of water slurry, and an attempt was made to run with steam pressurization (see Sec. 11.1.1*a*). Run CS-16, a 75-hr run, was achieved before excessive bearing wear forced termination. An average concentration of 1030 g of thorium per kilogram of water with the batch D-38 thoria was used.

Two sets of pin-type specimens were exposed to the slurry at velocities of 75 ± 7 fps. All specimens were severely attacked. Attack on two lead pins of type 347 stainless steel was uniform, and each specimen was covered with a thin oxide film. Specimens of the same material, located farther downstream in the specimen holder, had no films and appeared to be badly abraded. All gold and platinum specimens were deeply scratched and abraded on the upstream side. Zircaloy-2 and titanium 75A specimens were uniformly attacked. Their surfaces were highly polished but had no abraded areas. The over-all loop corrosion rate, calculated from nickel analyses, was 4.4 mpy.

It may be seen from the assembled data in Table 11.2 that the corrosion rate of all materials tested depended strongly on velocity. Thus, on type 347 stainless steel at 300°C at a concentration of approximately 650 to 750 g of thorium per kilogram of water, the corrosion rate was 0.67 mpy at 9 fps, 5 mpy at 21 fps, and 40 mpy at 43 fps. Other stainless steels exhibited similar behavior. In general, gold, platinum, Zircaloy-2, and the various titanium alloys were the most resistant to corrosion. The Stellites, as a group, appeared to be the most severely attacked, with Stellite 98M2 showing the highest rate. Pins of thorium oxide containing 0.5% CaO binder disintegrated in each of several tests.

11.2 TOROIDS

H. C. Savage E. L. Compere
R. M. Warner G. E. Moore

11.2.1 Operation and Maintenance

During the quarter, revisions were made to the drive motor and speed control on two of the five 4-toroid rotators used to make corrosion studies with thorium oxide slurries. In both cases the ¼-hp a-c motor and Variac speed-control system

was replaced with a ½-hp variable-speed d-c motor and a G-E Type H-1 Thy-Mo-Trol drive to improve operating reliability. This drive employs a rectification circuit to convert the a-c power supply to the dc required by the motors and permits accurate electrically controlled speed adjustment over a wide range. Preliminary tests indicate that the revised rotators will be capable of operating continuously under full load over an 86- to 1725-rpm range; this range is equivalent to flow velocities of 2.3 to 45 fps in the toroids. The a-c motor and Variac speed-control system was limited to a 500- to 1100-rpm range. Also, it is believed that the service life of the larger variable-speed d-c motors will be more satisfactory than that of the ¼-hp a-c motors.

11.2.2 Data and Discussion

(a) General. – Study of the effect, on a number of materials of interest, of circulating thorium oxide slurries at temperatures from 200 to 250°C by use of toroids has continued.

Because a large quantity of thorium oxide was available from the Feed Materials Processing Center at Fernald, Ohio, the attack rates on type 347 stainless steel, titanium 75A, and Zircaloy-2 by circulating slurries of this oxide were determined.

It has been proposed that the mockup of the HRT core vessel be used in the slurry blanket mockup in order to make possible certain slurry engineering studies.[8] The HRT core vessel mockup had been fabricated of 54S aluminum (actual analysis, 3.33% Mg, 0.25% Cr, 0.27% Fe, balance aluminum) by the Newport News Shipbuilding & Dry Dock Co., since this alloy at room temperature shows properties similar to Zircaloy-2 at the design temperature of 600°F.[9] The corrosion resistance of 54S aluminum to distilled water and circulating thorium oxide slurries under conditions expected in the slurry mockup has been investigated.

(b) Fernald Thorium Oxide Tests. – A laboratory evaluation by the Chemical Technology Division had already shown that, except for fluoride content, a refired thorium oxide produced by the Feed Materials Processing Center at Fernald, Ohio, met the proposed specifications for slurry material for use in the loop and blanket mockup studies.[10] Attack rates in toroids on type 347 stainless steel, titanium 75A, and Zircaloy-2 by a circulating slurry of the Fernald oxide have now been determined. The rates were not significantly different from those obtained under similar experimental conditions with an oxide produced at ORNL (D-17).

Properties of the ORNL-produced D-17 and the Fernald thorium oxides are shown in Table 11.4. The D-17 thorium oxide was recalcined at 800°C, so that the maximum calcination temperatures of the two oxides were the same; the calcination did not affect the particle-size distribution. The attack rates by aqueous slurries of the two oxides were determined in toroids by circulation at 26 fps relative velocity for 200 hr at 255 ± 15°C. Concentrations of 1000 g of thorium per kilogram of water with excess oxygen were used. The results are summarized in Table 11.5.

[8] L. F. Parsly *et al.*, *HRP Quar. Prog. Rep. Jan. 31, 1955*, ORNL-1853, p 150.

[9] R. B. Briggs *et al.*, *HRP Quar. Prog. Rep. Oct. 31, 1954*, ORNL-1813, p 24.

[10] V. D. Allred, J. P. McBride, and C. E. Schilling, *Laboratory Evaluation of Thorium Oxide Produced by the Feed Materials Processing Center at Fernald, Ohio*, ORNL CF-55-8-182 (Aug. 23, 1955).

TABLE 11.4. PROPERTIES OF THORIUM OXIDES PRODUCED AT ORNL (D-17) AND AT THE FEED MATERIALS PROCESSING CENTER, FERNALD, OHIO

	D-17	Fernald
Maximum calcination temperature (°C)	650	800
Thorium (%)*	86.7	86.7
Iron (ppm)	25	40
Chromium (ppm)	10	9
Nickel (ppm)	9	8
Sulfate (ppm)	<100	1350
Carbon (ppm)	1400	530
Aluminum (ppm)		62
Particle size distribution** (wt %)		
0–1 μ	23	20
1–3 μ	36	35
3–10 μ	26	28
>10 μ	15	17

*After drying at 110 to 150°C.

**As determined by gravitational sedimentation in 0.005 *M* $Na_4P_2O_7$ (see G. W. Leddicotte and H. H. Miller, *Anal. Chem. Semiann. Prog. Rep. Oct. 20, 1954*, ORNL-1788, p 21).

TABLE 11.5. COMPARISON OF AQUEOUS SLURRIES PREPARED FROM FERNALD FMPC AND ORNL THORIUM OXIDES BY CIRCULATION IN STAINLESS STEEL TOROIDS

Slurry concentration: 1000 g of Th per kg of H_2O
Relative velocity, fps: 26
Temperature, °C: 240 to 270
Oxygen pressure, psi: 90 (250°C)
Duration of test, hr: 200

	Toroid			
	M	N	O	P
Thorium oxide[a]	Fernald	Fernald	Fernald	ORNL D-17
Maximum calcination temperature (°C)	800	800	800	800
Thorium drained at room temperature after run (%)	2	0	0	71
Slurry appearance after run	White, thick	Cream-colored, thick	Cream-colored, thick	Cream-colored, thick
Pin attack rate (mpy)				
Type 347 stainless steel[b]	3.5	2.9	3.1, 3.7	6.0, 6.1
Titanium 75A[c]	5.1	5.0	5.3	7.7
Zircaloy-2[c]	1.0	1.6	1.5	1.7
Toroid attack rate (mpy)				
Type 347 stainless steel[d]	0.4	0.5	0.5	1.0

[a]Properties summarized in Table 11.4.
[b]Defilmed.
[c]Scrubbed.
[d]As-run, from slurry analysis.

The slurries of Fernald thorium oxide could not be poured from the toroids at room temperature after circulation, whereas the D-17 800°C thorium oxide slurry poured as a thick suspension. Slurries of both oxides gave about the same attack rates on pin-type corrosion specimens: from 3 to 6 mpy for type 347 stainless steel, 5 to 8 mpy for titanium 75A, and 1 to 2 mpy for Zircaloy-2. The as-run attack rate of the type 347 stainless steel toroids, calculated from the analysis of the slurry for stainless steel corrosion products, was from 0.5 to 1.0 mpy.

(c) 54S Aluminum Tests. – Since it was proposed that the HRT core vessel mockup (fabricated of 54S aluminum) be used in the slurry blanket mockup, the resistance of 54S aluminum to circulating thorium oxide slurries was investigated. Under experimental conditions in toroids as close to anticipated mockup operating conditions as possible, circulating thorium oxide slurries severely attacked 54S aluminum pin specimens.

Four toroids were operated at 26 fps relative velocity and 195 ± 10°C for 56 hr in order to determine the attack on 54S aluminum by oxygenated (70 psi) water and thorium oxide slurries. Distilled water (pH 6.0, specific resistance 160,000 ohm-cm, 2 ppm total solids primarily as sulfate) produced an attack rate of approximately 700 mpy on the 54S aluminum pin specimens. There was an intensification of attack near the root end of the pins, and a considerable quantity of brown solids was present; analyses are incomplete. The pH after the run was 8.0. The presence of 10 ppm Ni(II) as nickelous sulfate in the circulating, oxygenated water greatly reduced the attack on the 54S aluminum pins: duplicate specimens showed a slight weight gain and a slight weight loss, the latter yielding an attack rate of about 5 mpy. The pH at the end of the run was 6.7. A slurry of Fernald 800°C thorium oxide at a concentration of 1000 g thorium per kilogram of water destroyed the exposed part of the 54S aluminum pins; only the stubs of the specimens, where they were protected by the Teflon insulators, remained

after the 56-hr test. The pH of the slurry at the end of the test was 7.1. A duplicate slurry containing 400 ppm Ni(II) (thorium oxide basis) also consumed the exposed, unprotected portions of the 54S aluminum pins.

In static autoclave tests vapor- and solution-phase specimens of 54S aluminum have shown little attack by distilled water with 250 psi oxygen after 315 hr exposure at 200°C (about 4 hr was at 270°C due to failure of the temperature controller on the furnace). The specimens have shown a mild general etch, slight weight gains, and small amounts of white corrosion products on the surfaces. Specimens of 54S aluminum, exposed to oxygenated distilled water containing 10 ppm Ni(II), have thus far shown little difference from those exposed to oxygenated water alone.

Table 11.6 summarizes the available data on the 54S aluminum tests; analyses are not complete. Photographs of typical 54S aluminum pin specimens from the toroid runs are shown in Fig. 11.2.

The Ni(II) additions were suggested by the work of Draley and Ruther.[11]

[11] J. E. Draley and W. E. Ruther, *Corrosion Resistant Aluminum Above 200°C*, ANL-5430 (July 15, 1955).

TABLE 11.6. SUMMARY OF STATIC AND DYNAMIC (TOROIDS) CORROSION TEST ON 54S ALUMINUM AT APPROXIMATELY 200°C

Test Conditions							Specimen Condition
Velocity (fps)	Solution			pH		Duration (hr)	
	Ni(II) (ppm)	Th (g per kg of H_2O)	O_2 at 200°C (psi)	Original	Final		
				Autoclave Test			
0	0	0	250	5.98	6.5	315[a]	Vapor and solution specimens showed mild general etch, slight weight gains, white corrosion products
0	10	0	250	6.68	3.7[b]	315[a]	Perhaps slight improvement in appearance of solution specimen
				Toroid Test			
26	0	0[c]	70	5.98	8.0	56	Severe attack, ~700 mpy attack rate
26	10	0[c]	70	6.68	6.7	56	Mild general etch; slight impact attack on upstream surface; apparent attack rate, <5 mpy
26	0	1000[d]	70		7.06	56	Exposed part of pins destroyed; only protected stubs of pin specimens remain
26	400[e]	1000[d]	70		7.20	56	Exposed part of pins destroyed; only protected stubs of pin specimens remain

[a]Also 4 hr at 270°C.
[b]Approximately 20 ppm Cr(VI) present in each of three runs to date; source unknown.
[c]Some thorium oxide may be present as result of residual oxide from previous run.
[d]Fernald 800°C thorium oxide (see Table 11.1).
[e]Thorium oxide basis.

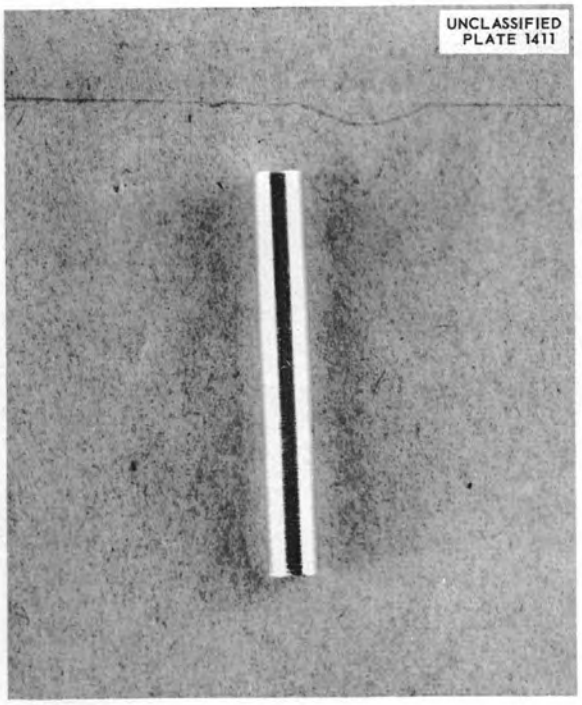

UNEXPOSED

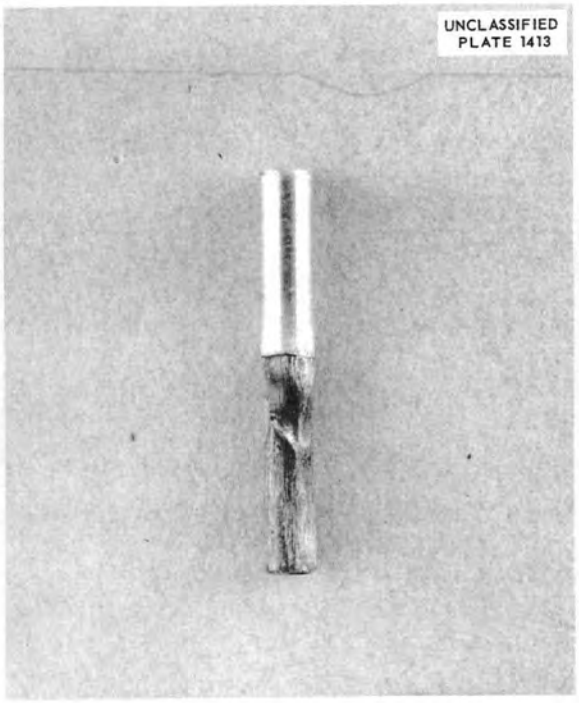

EXPOSED TO DISTILLED WATER, pH 6.0.

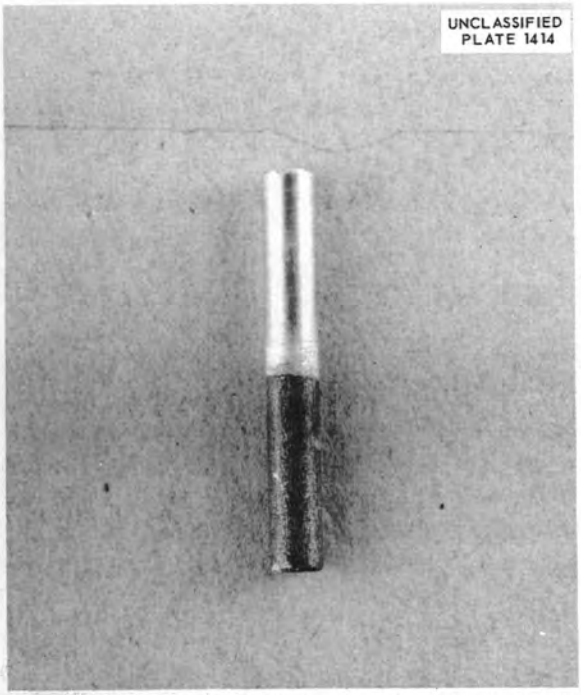

EXPOSED TO DISTILLED WATER + 10 ppm Ni(II), pH 6.7.

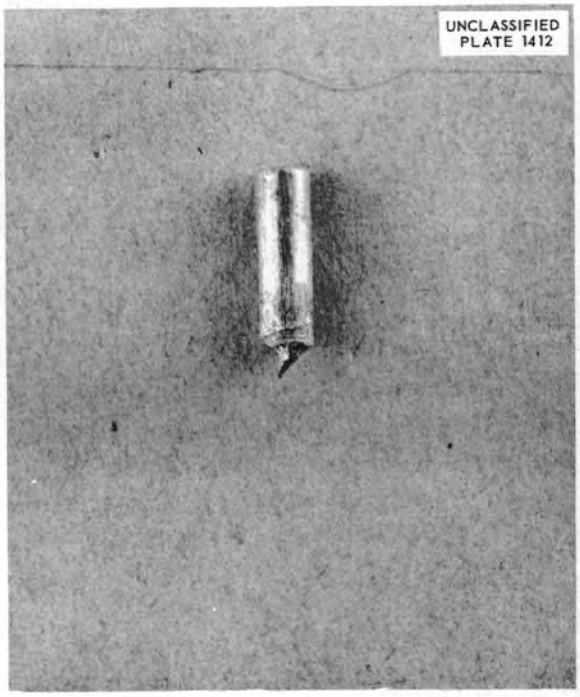

EXPOSED TO 1000 g OF THORIUM PER kg OF H_2O.
FERNALD THORIUM OXIDE (800°C, pH 7.1)

Fig. 11.2. 54S Aluminum Pin Corrosion Specimens. 3X. Reduced 23%.

12. RADIATION CORROSION

G. H. Jenks

A. L. Bacarella
J. E. Baker
W. N. Bley
N. C. Bradley
W. E. Clark
R. J. Davis
H. O. Day
H. A. Fisch
B. O. Heston
D. T. Jones
H. C. Savage
R. A. Lorenz
J. R. McWherter
A. R. Olsen
M. D. Silverman
H. H. Stone
F. J. Walter
R. M. Warner
K. S. Warren
L. F. Woo
W. C. Yee

12.1 IN-PILE LOOP

G. H. Jenks
H. C. Savage
J. E. Baker
W. N. Bley
N. C. Bradley
D. T. Jones
R. A. Lorenz
A. R. Olsen
F. J. Walter
R. M. Warner

12.1.1 Development and Construction

(a) **HB-4 Mockup.** – The fabrication and performance testing of in-pile loop L-4-11 was completed during the past quarter. The circulating pump is a modified ORNL 5-gpm model with pure sintered aluminum oxide bearings and journal bushings identical to the one used in loop L-4-8. The pump used in loop L-4-8 operated satisfactorily in excess of 1600 hr after installation of the loop in beam hole HB-4 of the LITR, but the run had to be terminated at that time because of a pump failure due to a locked rotor. This was the longest in-pile run of the five made to date.

In loop L-4-11 the tapered coupon holders in both the core and in-line position were replaced with holders with a straight channel flow section so that there is no velocity gradient over the corrosion test coupons. The specimen holders are made of Zircaloy-2. The core specimen holder contains twenty-four $\frac{1}{2} \times \frac{1}{4} \times 0.060$ in. corrosion specimens and is surrounded by eighty-eight $\frac{1}{2} \times \frac{1}{2} \times 0.060$ in. corrosion specimens mounted on type 347 stainless steel rods and separated by type 347 stainless steel tubular spacers. The arrangement of the specimens surrounding the holder was arrived at in consultation with the Mathematics Panel (see Fig. 12.1).

In addition to the in-line corrosion specimen holder, a special in-line holder contains duplicates of the rod and coupon specimen materials contained in the core position (see Fig. 12.2). Also, two specimens of sapphire are mounted in special brackets in the core position (see Fig. 12.3). Light-transmission measurements of these sapphire pieces, before and after exposure, will evaluate this material for possible use as a transparent window; its use as an insulator is also of interest.

Loop L-4-11 contains a variety of materials for radiation-corrosion evaluation. In addition to the synthetic sapphire mentioned above, the following were included for evaluation: platinum; crystal bar zirconium; Zircaloy-2, with and without added hydrogen; 18 special alloys of zirconium; types 347, 316, 304, 443, 446, 309 SCb, and 350A stainless steel; eight different titanium alloys; Incoloy; and sintered Al_2O_3.

(b) **LITR – HB-2–Loop Package.** – Construction of in-pile loop L-2-10 has been completed, and preliminary testing with water has been completed at pressures up to 1950 psia and loop temperatures up to 305°C. The pressurizer was operated at 325°C. With the exception of a 5-hr, 5% HNO_3 run and a 20-hr, 3% trisodium phosphate run, all testing was done with the use of water with added oxygen. The total testing time has been 125 hr, the last 20 hr being at approximately 300°C. During the last 20 hr of operation the pump power increased and finally the rotor locked; the reason is discussed below.

(c) **In-Pile Pumps.** – As reported previously,[1] the new outboard-bearing 5-gpm pump with sintered aluminum oxide bearings was installed in loop L-4-8. The experiment was terminated during the quarter because a pump failed. Cursory examination of the contaminated pump in a hot cell revealed that the rear bearing assembly had slipped forward; this caused the pump to lose end-play, and the rotor became jammed. At the time of failure, total operating time on the pump was approximately 2400 hr. As near as could be determined by shaft manipulation in the hot cell, the pump from L-4-8 experienced no undue bearing wear.

[1] G. H. Jenks *et al.*, *HRP Quar. Prog. Rep. July 31, 1955*, ORNL-1943, p 107.

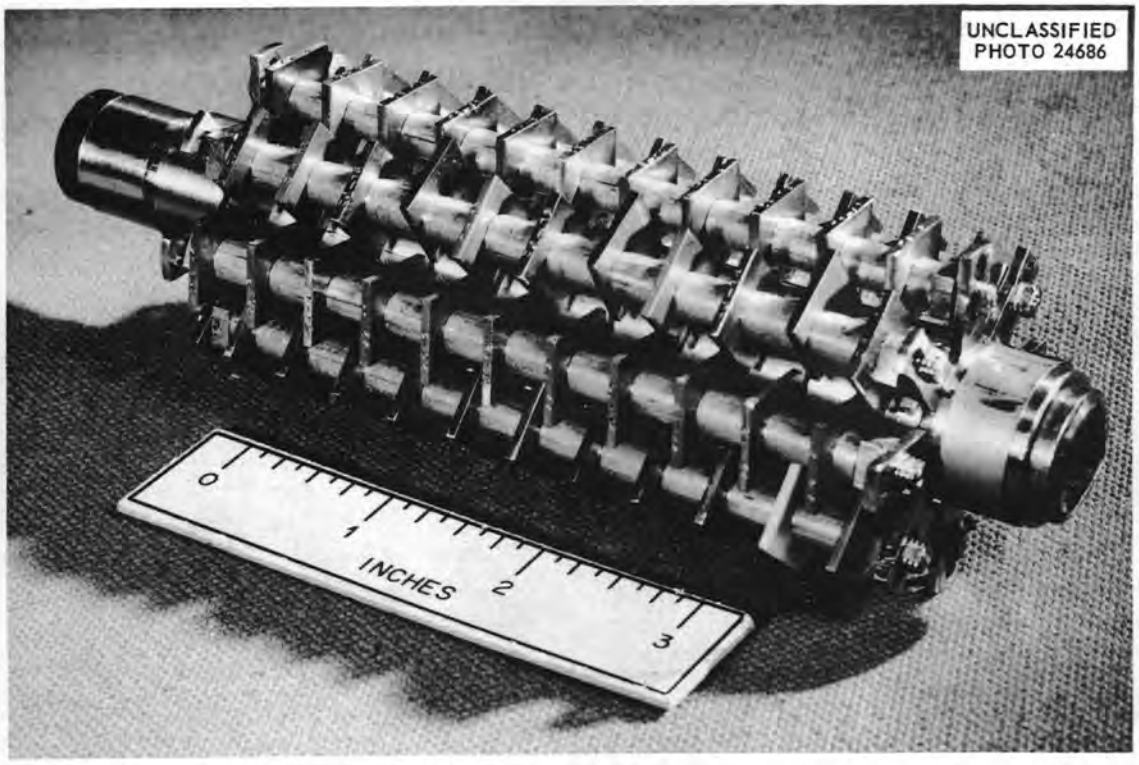

Fig. 12.1. Core Corrosion Specimen Assembly, Loop L-4-11.

It was found upon examination of the 2000-psi pump from in-pile loop L-2-10, mentioned above, that the rear bearing housing had also slipped forward and had locked the rotor. In the future all rear bearing housings in the outboard-bearing type of pump will be installed with an interference fit and a locking pin to eliminate this possibility of bearing housing slippage. The examination of the 2000-psi pump also indicated that the strength weld, used in place of bolted flanges and a seal weld in the 1000-psi pumps, did not warp the pump scroll or housing assembly or affect pump operation. Figure 12.4 is an assembly drawing of the 2000-psi pump design.

In order to reduce pump power and the high electrical load imposed on the stator by the electrical inefficiency of this design pump, it was found desirable to reduce the pump operating voltage to 105 v instead of operating at 117 v as had formerly been done. Pump head is not materially affected by this change, but pump amperes are decreased from 16.2 to 14.2 and pump power from 1050 to 850 w in the 1000-psi model at a 5-gpm output. The 2000-psi model is even more inefficient as a result of increased can thickness, and the pump amperes are decreased from 18.2 to 16.2 when the voltage is lowered to 105 v. Pump power is decreased from 1270 to 1050 w. It is expected that decreasing the operating voltage will lengthen the stator life.

The Byron Jackson pump for use in in-pile loops, mentioned in an earlier report,[1] has been repaired by the Byron Jackson Co. and is being returned to Oak Ridge for further testing. Inspection of the pump revealed that the rotor assembly had rubbed on the rear end of the rotor housing because of the change in hydraulic thrust balance, which was brought about by the lower density of high-temperature water at 300°C. The Byron Jackson Co. has added a rear thrust bearing to prevent the rotor from contacting the rear housing. The pump formerly had only one thrust bearing in the forward direction. The bearing and journal material in this pump is pure sintered aluminum oxide.

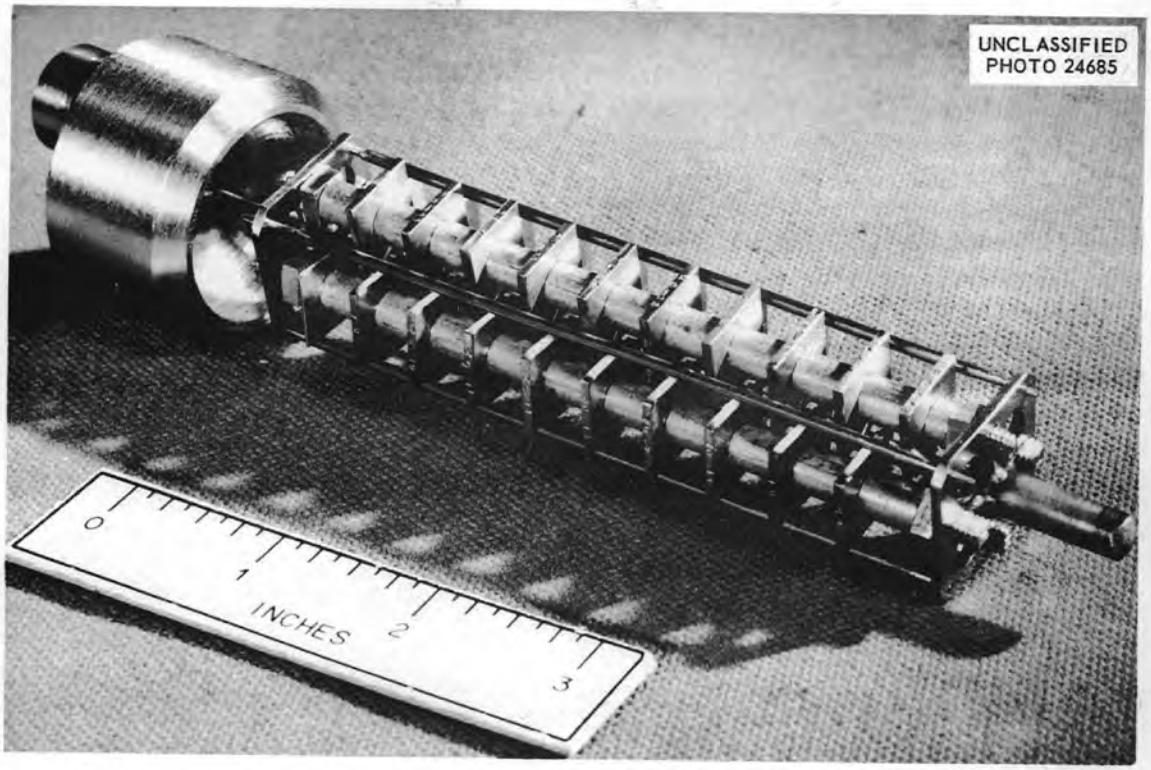

Fig. 12.2. Special In-Line Corrosion Specimen Assembly, Loop L-4-11.

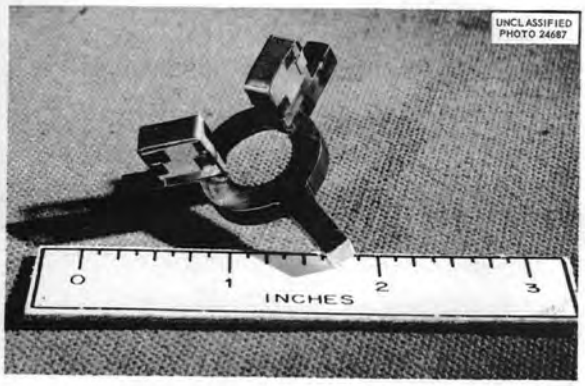

Fig. 12.3. Core Sapphire Specimens, Loop L-4-11.

12.1.2 LITR Operation – In-Pile Loop EE Corrosion Test

(a) Introduction. – A fourth in-pile loop (EE) experiment, designed to determine the effect of reactor radiations on the corrosion of Zircaloy-2, type 347 stainless steel, and titanium by uranyl sulfate solutions at 250°C, has been completed. Operating conditions were essentially the same as those for the previous loop,[2] except that for loop EE no chromium was added to the solution. The methods and procedures followed in this experiment were similar to those previously reported for the first three experiments,[2–4] and reference is made to the previous reports for details not included here. The experiment was terminated by failure of the circulating pump.

(b) Construction and Preparation of Loop. – The structure of the loop was identical to that of the previous loops. The specimen types, locations, and materials have been reported previously[3] but, for convenience, are reviewed briefly in the following.

As mentioned above, three different materials were tested in this loop: type 347 stainless steel, Zircaloy-2, and titanium. The titanium was of the 55AX type. The specimen types employed were coupon, stress, and couple.

---

[2] *Ibid.*, p 109.

[3] G. H. Jenks *et al.*, *HRP Quar. Prog. Rep. Jan. 31, 1955*, ORNL-1853, p 88.

[4] G. H. Jenks *et al.*, *HRP Quar. Prog. Rep. April 30, 1955*, ORNL-1895, p 94.

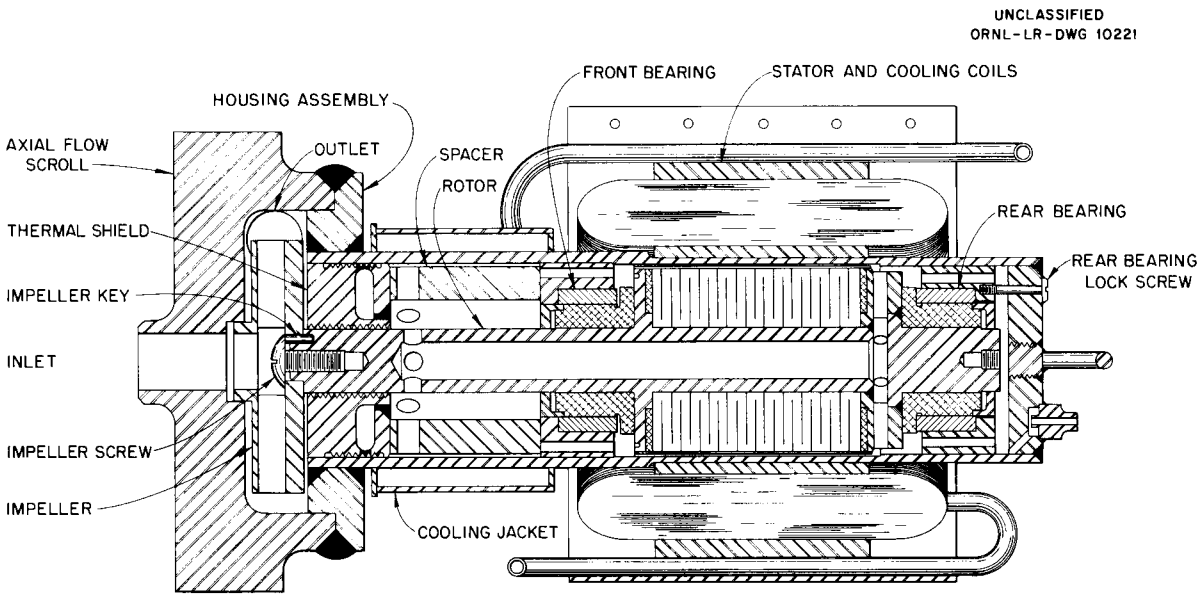

Fig. 12.4. 2000-psi, 5-gpm In-Pile Pump.

The coupon specimens were of the type that have been used in previous loops and, as before, were located in a core holder and in an in-line holder. However, the coupon dimensions were adjusted so that each holder accommodated 24 specimens rather than 12 as in the previous loops. Eight of the specimens in each holder were of type 347 stainless steel, eight of titanium, and eight of Zircaloy-2. The holder material was Zircaloy-2. The relative locations of materials within a holder are shown in Fig. 12.5*a*.

The couple specimens were employed in a test of possible galvanic couple action under irradiation. The specimens were in the form of two assemblies, each comprised of nine pairs of contacting coupons held on a rod and separated by spacers. In one assembly, the rod and spacers were of type 347 stainless steel and, in the other, of Zircaloy-2. The arrangements of the specimens within the assemblies are shown in Fig. 12.5*b* and 12.5*c*. Both assemblies were mounted in spiders, together with the stress specimens, around the coupon holder in the core.

The stress specimens were in the form of six assemblies, each comprised of two specimens, $\frac{3}{8}$ in. in width, $3\frac{1}{2}$ in. in length, and $\frac{1}{16}$ in. in thickness, stressed over a center fulcrum and held at each end by screws in a special bracket. Two assemblies of each of the three different materials

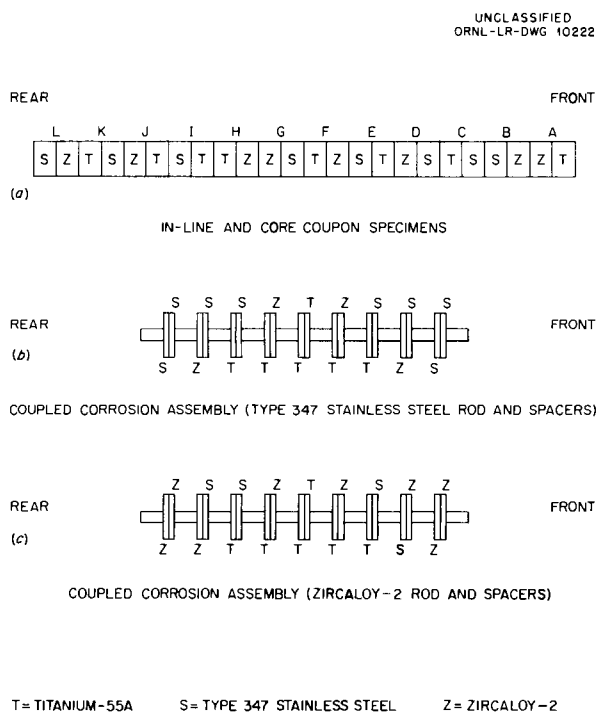

Fig. 12.5. Loop EE Specimen Distribution. (*a*) In-line and core coupon specimens. (*b*) Coupled corrosion assembly (type 347 stainless steel rod and spacers). (*c*) Coupled corrosion assembly (Zircaloy-2 rod and spacers).

were employed. A given assembly was constructed of the same material throughout. The specimens were stressed at room temperature to approximately 80% of the 250°C yield strength of the material. The assemblies were located in the core as described above.

Loop EE specifications are given below:

Loop volume, including pressurizer (cc)	1511
Pressurizer volume (cc)	520
Empty core volume (cc)	375
Loaded core volume (cc)	303
Flow rates	
Pressurizer (cc/sec)	5
Core (gpm)	5.5
Pump bearing material	Graphitar No. 14
Pump journal material	Hardened 17-4 PH stainless steel
Pressure at which system was checked (psi)	1200
Corrosion sample materials	
Corrosion coupons	Type 347 stainless steel, Zircaloy-2, Titanium 55AX
Coupled specimen assemblies	Type 347 stainless steel, Zircaloy-2, Titanium 55AX
Stress specimens	Type 347 stainless steel, Zircaloy-2, Titanium 55AX
In-line holder	Zircaloy-2
Core holder	Zircaloy-2
Minimum clearance (in.)	
Core holder	0.048
In-line holder	0.046

Loop EE areas exposed to high-temperature solutions are given below:

Component	Area (cm^2)
Type 347 Stainless Steel	
Total main circulation lines (not including pump and core)	1553
Pressurizer	
Total	(706)
Area wetted when filled with 335 ml of solution	455
Pressurizer lines	300
Core	445
Pump	
Scroll	272
Impeller	159
In-line specimen coupons, 8	11.4
Core specimen coupons, 8	11.4
Coupled specimens, 12	13.8
Coupled specimen spacers, 10	29.4
Stress specimens, 4	78.0
Stress specimen holders, 4	40.0
Stress specimen anvils, 2	3.8
Screws, 4	4.0
Nuts, 4	3.3
	3379
Zircaloy-2	
Core holder	162
In-line holder	162
In-line specimen coupons, 8	11.2
Core specimen coupons, 8	11.2
Coupled specimens, 12	13.8
Coupled specimen spacers, 10	29.4
Stress specimens, 4	78.0
Stress specimen holders, 4	40.0
Stress specimen anvils, 2	3.8
Screws, 4	4.0
	515
Titanium	
In-line specimen coupons, 8	11.4
Core specimen coupons, 8	11.4
Coupled specimens, 12	13.8
Stress specimens, 4	78.0
Stress specimen holders, 4	40.0
Stress specimen anvils, 2	3.8
Screws, 4	4.0
	162

The loop preparatory operations are summarized in Table 12.1. A tabulation of the results of solution analyses during these operations is given in Table 12.2.

A pretreatment of the loop with 5% nitric acid indicated that there was excessive corrosion. From previous experience, localized attack of the impeller screw was suspected. The pump seal weld was cut out and the pump removed for replacement of this screw, which was indeed badly corroded. A Huey test indicated that the replacement screw was from a better material.

Following this pump repair, a second 3% trisodium phosphate rinse and a third 5% nitric acid pretreatment gave satisfactory results. Following 41 hr of operation with water and oxygen at 250°C

TABLE 12.1. SUMMARY OF PREPARATORY OPERATIONS FOR LOOP EE

Time (hr)	Conditions
4.6	3 wt % trisodium phosphate + He, 100°C
17.4	5 wt % HNO_3 + He, 100°C
21.0[a]	5 wt % HNO_3 + He, 100°C
0.5	3 wt % trisodium phosphate + He, 100°C
19.2	5 wt % HNO_3 + He, 100°C
41.1[b]	H_2O + O_2, 250°C
16.7	5 wt % HNO_3 + He, 100°C
19.1	H_2O + O_2, 250°C
36.3[c]	0.17 *m* UO_2SO_4 (normal) + 0.031 *m* $CuSO_4$ + 0.006 *m* H_2SO_4 + O_2, 250°C
90.6	0.17 *m* UO_2SO_4 (normal) + 0.031 *m* $CuSO_4$ + 0.006 *m* H_2SO_4 + O_2, 250°C

[a]Pump removed and new impeller screw installed after this treatment.

[b]Found leak through core reducer following this run.

[c]Main loop heater failed at this point; replaced with new heater. Replaced uranyl sulfate solution for next treatment.

and 1000 psia, a routine leak check of the loop with helium revealed a leak in the core-reducer section similar to the leak in loop FF.[4] This fault was repaired by grinding almost through the reducer wall and then rewelding. The fourth nitric acid pretreatment was made following the repair of the reducer. This was followed by a water and oxygen run at 250°C.

After approximately 35 hr of operation with uranyl sulfate solution, the main loop heater burned out. A new heater was installed, and operation with uranyl sulfate was continued to completion of mockup operation, without the repetition of pretreatment.

It is believed that most of the corrosion attack indicated by nickel accumulation during these operations was on the screw holding the pump impeller on the original pump and on the replaced heater portion of the main circulating system.

(c) General Operating Conditions and Procedures. – The solution, which was initially charged to the loop for in-pile operation, was of the following composition: UO_2SO_4, 0.17 *m* (U^{235} per total U = 0.89); $CuSO_4$, 0.031 *m*; H_2SO_4, 0.008 *m*.

A solution of the same composition, with the exception of the H_2SO_4, which was 0.04 *m*, was used to replace liquid withdrawn from the loop during sampling operations.

In-pile operation of the loop with enriched solution was for a period of 594.3 hr. The total circulation time for this solution was 630.3 hr. The energy output of the LITR during this time was 1610.4 Mwhr, and essentially all the energy was liberated at the 3 Mw level. The reactor operating schedule for the exposure is shown in Fig. 12.6.

The schedule for solution sampling is also shown in Fig. 12.6. One sample of about 2 ml was taken for each sampling. Following the original reactor startup, all samples, with the exception of EE-1-94, EE-1-96, and EE-1-102, were withdrawn while the reactor was at power. The three exceptions were withdrawn after the reactor had been at zero power for 1.8, 2.1, and 1.9 hr, respectively.

After 400 hr of smooth operation the circulation pump began using greater amounts of power for short periods of time. Power consumption increased erratically from the normal 1025 w to 1040–1050 w during these periods. At 630.2 hr, high pump-power demand resulted in a scram of the reactor. There was noticeable mechanical noise at this time, which continued for another 6 min, and then the pump seized. The experiment was terminated at this time.

(d) Results of Solution Analyses, Oxygen Consumption, and Fission Power in Loop. – The results of solution analyses for constituents other than products of irradiation are tabulated in Table 12.3. As was observed during all previous experiments, the reported values for the uranium, copper, and SO_4^{--} content of the samples from this loop were found to be, in general, appreciably lower than the calculated values for the constituents. As was the case with loop GG,[2] sample dilution factors were obtained by adding lithium sulfate to the wash water and analyzing for this tracer in the samples. When the reported results were corrected for dilution as indicated by the amount of lithium, the "corrected" concentrations were, in most cases, in fair agreement with the calculated concentrations for the loop solution. The reported, corrected, and calculated values

TABLE 12.2. ANALYSES OF SAMPLES FROM LOOP INVENTORY DURING PREPARATORY OPERATIONS*

Treatment Conditions	Total Circulation Time for Each Solution (hr)	Inventory at Time of Sampling (ml)	Uranium		Sulfate		Copper		Cobalt		Nickel		Chlorine		Chromium		Iron		Aluminum		pH
			Conc (mg/ml)	Total (g)	Conc (mg/ml)	Total (g)	Conc (μg/ml)	Total (mg)	Conc (μg/ml)	Total (mg)	Conc (μg/ml)	Total (mg)	Conc (μg/ml)	Total (mg)	Conc (μg/ml)	Total (mg)	Conc (μg/ml)	Total (mg)	Conc (μg/ml)	Total (mg)	
3% TSP, He, 100°C	4.6	1250																			
5% HNO_3, He, 100°C	17.4	1300					12	16			272	354	<1	<1	632	822	2249	2924	-		
5% HNO_3, He, 100°C	21.0	1300					<1	<1			5	7	1	1	6	8	36	47			
3% TSP, He, 100°C	0.5	1300					<1	<1			6	8	<1	<1	4	5	41	53	9	12	
5% HNO_3, He, 100°C	19.2	1300																			
H_2O, O_2, 250°C	41.1	1100									<1	<1			1	1	<1	<1			
5% HNO_3, He, 100°C	16.7	1200					<1	<1			1	1	1	1	2	2	1	1			
H_2O, O_2, 250°C	19.1	1080																			
0.17 *m* UO_2SO_4 (normal) + 0.03 *m* $CuSO_4$ + 0.006 *m* H_2SO_4 (O_2, 250°C)	36.3	1100	38.1	42.0	18.6	20.0	2050	2255	1.0	1.0	5	6	3	3	18	20	17	19			2.4
0.17 *m* UO_2SO_4 (normal) + 0.03 *m* $CuSO_4$ + 0.006 *m* H_2SO_4 (O_2, 250°C)	90.6	1110	37.4	42.0	18.8	21.0	1750	1943	2.0	2.0	79	88			65	72	2	2			2.1

*Constituent concentrations and totals shown are not cumulative but represent the quantities present for operation with each solution.

TABLE 12.3. ANALYSIS OF SAMPLES FROM LOOP INVENTORY DURING ENRICHED SOLUTION OPERATIONS[a]

Sample	Total Circulation Time (hr)	Accumulated LITR Energy (Mwhr)	Elapsed Time from LITR Shutdown to Sampling (hr)	Inventory Volume at Time of Sampling, 25°C (ml)	Sample Dilution Factor	Uranium			Sulfate			Copper			Cobalt		Nickel		Chlorine		Chromium		Iron		Aluminum		Zirconium		Manganese		Titanium		pH	Specific Gravity
						Rep (mg/ml)	Cor (mg/ml)	Calcd[b] (mg/ml)	Rep (mg/ml)	Cor (mg/ml)	Calcd[c] (mg/ml)	Rep (mg/ml)	Cor (mg/ml)	Calcd[d] (mg/ml)	Rep (mg/ml)	Calcd Total[e] (g)	Rep (mg/ml)	Calcd Total[e] (g)	Rep (mg/ml)	Calcd Total[f] (g)	Cor (mg/ml)	Calcd Total[f] (g)	Cor (mg/ml)	Calcd Total[f] (g)	Rep (mg/ml)	Calcd Total[e] (g)	Cor (mg/ml)	Calcd Total[f] (g)	Rep (mg/ml)	Calcd Total[e] (g)	Rep (mg/ml)	Calcd Total[f] (g)		
EE-1-90[g]	0.0	0.0	0.0		1.00	38.59	38.59	38.59	20.91	20.91	20.91	1.756	1.756	1.756	(ND)[b]	(ND)	(ND)	(ND)	(ND)	(ND)	(ND)	(ND)	(ND)	(ND)	(ND)	(ND)	(ND)	(ND)	(ND)	(ND)	(ND)	1.70	1.055
EE-1-91[i]	0.0	0.0	0.0		1.00	38.31	38.31	38.31	24.28	24.28	24.28	1.665	1.665	1.665	(ND)	(ND)	(ND)	(ND)	(ND)	(ND)	(ND)	(ND)	(ND)	(ND)	(ND)	(ND)	(ND)	(ND)	(ND)	(ND)	(ND)	(ND)	1.30	1.054
EE-1-92[j]	33.3	0.0	0.0	1057	1.20	36.4	43.7	38.5	17.5	19.6	20.8	1.47	1.75	1.75	(ND)	(ND)	(ND)	(ND)	(ND)	(ND)	(ND)	(ND)	(ND)	(ND)	(ND)	(ND)	(ND)	(ND)	(ND)	(ND)	(ND)	(ND)	1.75	
Reactor started up	36.0	0.0																																
EE-1-93	54.8	56.0	0.0	1058	1.12	36.5	40.9	38.5	18.1	19.5	20.9	1.52	1.70	1.75	(ND)	(ND)	0.006	0.007	(ND)	(ND)	(ND)	(ND)	0.011	0.013	(ND)	(ND)	(ND)	(ND)	(ND)	(ND)	(ND)	(ND)	1.95	
EE-1-94[j]	76.3	107.4	1.8	1059	1.14	34.6	39.4	38.5	18.4	20.1	20.9	1.43	1.63	1.75	(ND)	(ND)	0.053	0.064	(ND)	(ND)	(ND)	(ND)	(ND)	(ND)	(ND)	(ND)	0.040	0.048	(ND)	(ND)	(ND)	(ND)	2.05	
EE-1-95	148.1	298.6	0.0	1057	1.17	34.8	40.7	38.5	18.4	20.3	21.0	1.47	1.71	1.75	(ND)	(ND)	0.118	0.147	(ND)	(ND)	(ND)	(ND)	0.010	0.012	(ND)	(ND)	0.020	0.024	(ND)	(ND)	(ND)	(ND)	2.05	
EE-1-96[j]	172.6	358.3	2.1	1056	1.10	36.2	39.8	38.5	17.9	19.1	21.0	1.59	1.75	1.75	(ND)	(ND)	0.144	0.172	(ND)	(ND)	0.015	0.017	0.011	0.13	(ND)	(ND)	0.027	0.032	(ND)	(ND)	0.005	0.006	1.90	
EE-1-97	196.7	428.3	0.0	1055	1.12	33.3	37.3	38.5	19.0	20.6	21.1	1.43	1.59	1.75	(ND)	(ND)	0.179	0.220	(ND)	(ND)	(ND)	(ND)	0.013	0.016	(ND)	(ND)	0.034	0.040	(ND)	(ND)	(ND)	(ND)	2.00	
EE-1-98	244.6	562.8	0.0	1055	1.24	31.3	38.8	38.5	17.1	19.5	21.2	1.33	1.65	1.75	(ND)	(ND)	0.189	0.265	(ND)	(ND)	0.008	0.011	0.065	0.084	(ND)	(ND)	0.045	0.059	0.032	0.042	0.049	0.064	2.05	
EE-1-99	316.6	766.7	0.0	1057	1.19	34.2	40.7	38.4	18.4	20.6	21.3	1.52	1.80	1.75	(ND)	(ND)	0.371	0.496	(ND)	(ND)	(ND)	(ND)	0.003	0.143	(ND)	(ND)	(ND)	(ND)	0.037	0.049	(ND)	(ND)	2.05	
EE-1-100	364.3	870.1	0.0	1058	1.18	34.5	40.7	38.4	18.7	20.8	21.5	1.36	1.60	1.75	(ND)	(ND)	0.307	0.439	(ND)	(ND)	(ND)	(ND)	0.008	0.010	(ND)	(ND)	0.019	0.023	0.031	0.042	0.040	0.048	2.00	
EE-1-101	412.4	1003.8	0.0	1058	1.21	32.2	39.0	38.4	18.6	21.1	21.5	1.59	1.93	1.75	(ND)	(ND)	0.333	0.491	(ND)	(ND)	(ND)	(ND)	0.005	0.006	(ND)	(ND)	0.006	0.007	0.037	0.052	(ND)	(ND)	2.10	
EE-1-102[j]	484.4	1211.5	1.9	1058	1.22	31.2	38.1	38.4	18.1	20.6	21.5	1.59	1.94	1.75	(ND)	(ND)	0.261	0.409	(ND)	(ND)	(ND)	(ND)	0.011	0.014	(ND)	(ND)	0.055	0.071	0.045	0.064	(ND)	(ND)	2.10	
EE-1-103	532.2	1334.2	0.0	1058	1.16	33.0	38.3	38.4	18.9	20.9	21.6	1.41	1.63	1.75	(ND)	(ND)	0.364	0.526	(ND)	(ND)	0.002	0.002	0.016	0.020	(ND)	(ND)	0.054	0.067	0.043	0.059	(ND)	(ND)	1.95	
EE-1-104	580.5	1463.8	0.0	1059	1.14	30.6	34.9	38.4	19.4	21.1	21.6	4.19	4.76	1.75	(ND)	(ND)	0.469	0.652	(ND)	(ND)	(ND)	(ND)	0.015	0.018	(ND)	(ND)	0.031	0.037	0.051	0.069	(ND)	(ND)	2.00	
Reactor down	630.2	1610.4		1057				38.4			21.6																							
Circulation pump down	630.3	1610.4		1057				38.4			21.6																							

[a]Where no values are given, either an analysis was not requested or the analytical results were not reliable.
[b]Determined from calculated uranium and inventory balance.
[c]Determined from calculated sulfate and inventory balance.
[d]$\frac{\text{(Original concentration)} \times \text{(calculated uranium concentration at time of sample)}}{\text{Original uranium concentration}}$
[e]Corrected for sample dilution and for amounts withdrawn in previous samples.
[f]From calculated inventory and from concentration corrected for sample dilution.
[g]Original solution.
[h](ND) not detected.
[i]Makeup solution.
[j]Taken with reactor down.

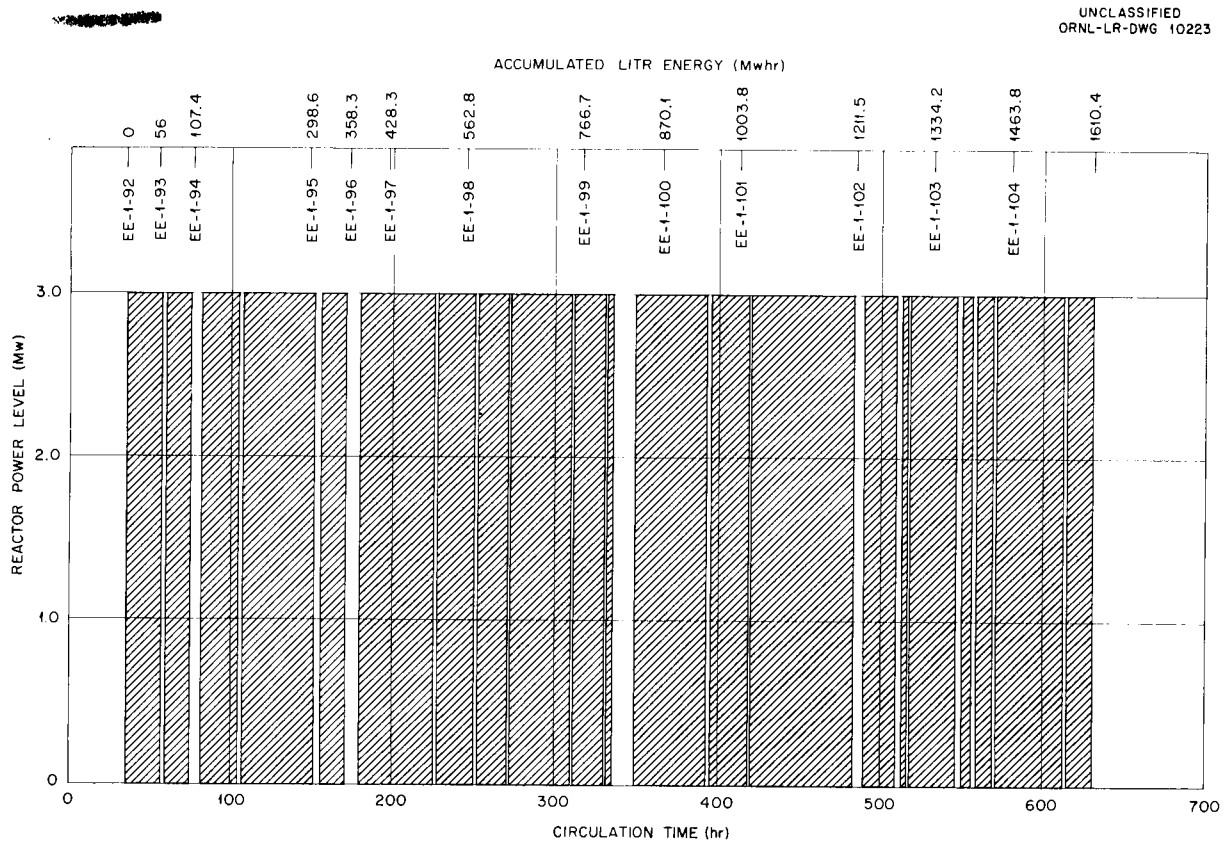

Fig. 12.6. Reactor Operating Schedule During In-Pile Operation.

for the uranium, copper, and SO_4^{--} concentrations are compared graphically in Fig. 12.7. The calculated values for the other elements listed in Table 12.3 and the corrected values for total fissions in Table 12.4 have been obtained through use of the listed dilutions. The values for nickel, chlorine, aluminum, manganese, and total fissions have also been corrected for the amount of material withdrawn in sampling. No correction was applied to pH measurements.

The results of oxygen depletion measurements are shown in Table 12.5. For conversion from gas volumes to pressures in the loop at operating temperature, the factor, 100 psi is equivalent to 120 cc at STP, is applicable. The values for corrosive penetration listed in the final column of Table 12.5 were calculated with the usual assumptions that all stainless steel surfaces, in contact with high-temperature solution, corroded uniformly and that oxygen was lost in the corrosion of steel only.

Values for fission power generated in the loop, calculated from total fissions observed in the loop solution samples based on Cs^{137} analysis, are presented in Table 12.4. The samples were allowed to cool for three months before they were analyzed so as to provide time for the 15-day Cs^{136} to decay. The values for fission power were calculated from the corrected cesium analytical results. Thus, the values represent the average power from the start of irradiation to the time of sampling.

The electrical power required to maintain loop temperature with the reactor at power and that required when the reactor was not at power differed by an average of 837 w. There was no significant change during the run. The maximum deviation from the average was about 6%.

Neutron fluxes at various specimen positions in the core were determined from comparison of the induced activities of these specimens with those of control specimens which had been irradiated

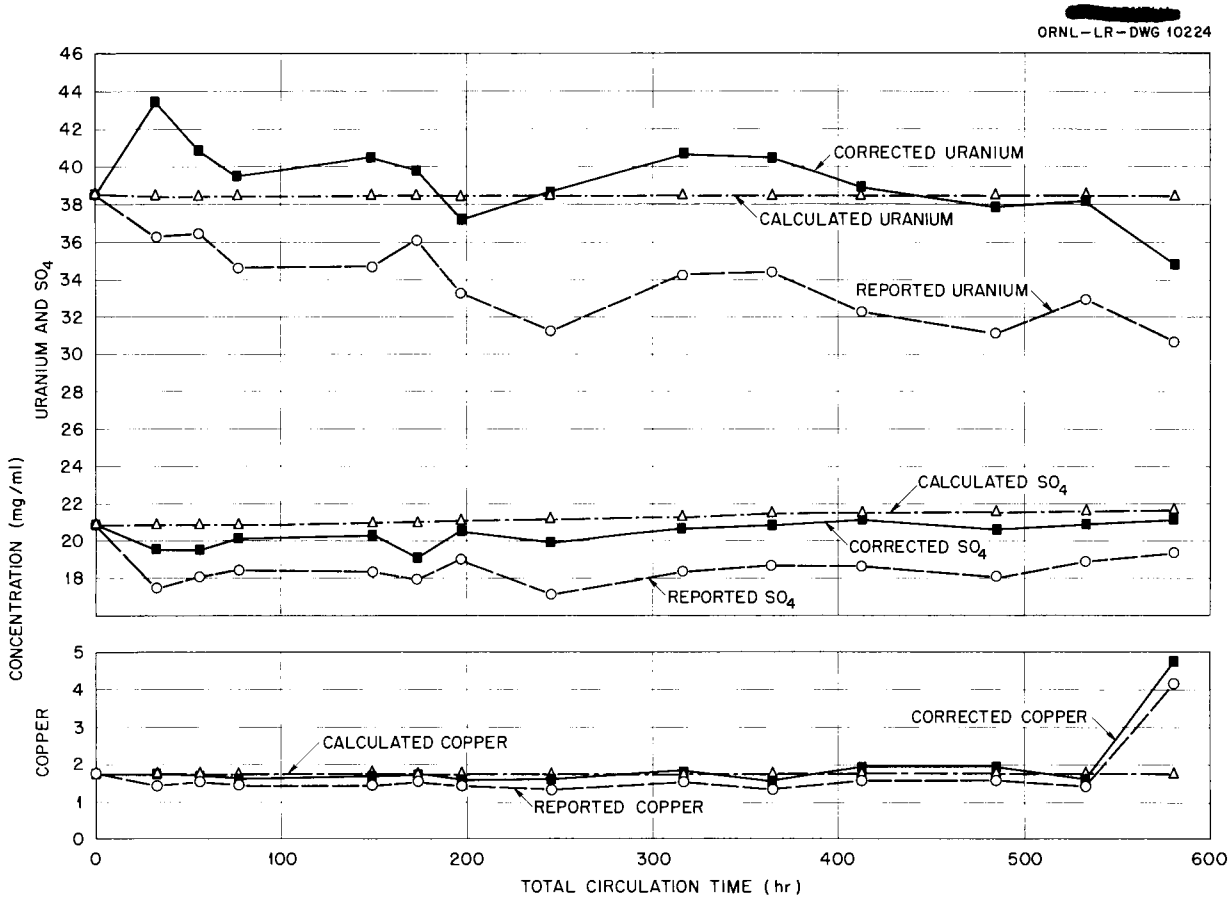

Fig. 12.7. Concentration of U, SO_4^{--}, and Cu in Solution Samples.

for a known nvt in the ORNL Graphite Reactor.

Representative stainless steel specimens were taken from the core coupon array, from the stainless steel spacers of the coupled specimen assembly, and from the core walls. Similarly, Zircaloy-2 specimens were taken from the coupon array and from Zircaloy-2 spacers of the coupled specimen assembly. The specimens were decontaminated prior to counting by the methods described previously.[2,3] As before, the Cr^{51} activity was employed for the steel measurements and the Zr^{95}-Nb^{95} activity was employed for the Zircaloy-2 measurements.

The results of the analyses for induced activity are shown in Table 12.6. The control specimens were irradiated for 315 hr in an average flux of 7.08×10^{11} neutrons/cm^2/sec. Elapsed time between termination of exposures and counting is shown in Table 12.6.

Figure 12.8 is a plot of the neutron flux for the type 347 stainless steel and Zircaloy-2 specimens vs the axial position of the specimens in the core. The location of the leading edge of the first core coupon is designated as zero distance. It is of interest to note that the flux values for the coupled assembly spacers and for the core walls fit the curve with little more scatter than do the values for the core coupons. This fact indicates that, within experimental limits, there is no radial flux gradient in the area occupied by the core specimens and core walls.

The value for total fission power, calculated from solution analyses for Cs^{137}, is about 30% lower than that found in the previous experiment. Approximately one-third of this difference can be accounted for by the volume of solution in the core of this loop being about 10% less than that in the previous loop. Another one-sixth of the

TABLE 12.4. FISSIONS IN LOOP SOLUTION

Sample No.	Accumulated LITR Energy (Mwhr)	Inventory Volume at Time of Sample (ml at 25°C)	Calculated Uranium Concentration (mg/ml)	Total Fissions per ml × 10^{-15}		Total Fission Power in Loop Solution at 3 Mw (w)
				Analysis	Corrected*	
EE-1-92	0.00	1057	38.5	0.00	0.00	0.00
93	56.0	1058	38.5	0.90	1.01	508
94	107.4	1059	38.5	1.74	2.01	528
95	298.6	1057	38.5	4.95	5.84	551
96	358.3	1056	38.5	6.12	6.81	534
97	428.3	1055	38.5	6.58	7.60	498
98	562.8	1055	38.5	9.12	11.9	594
99	766.7	1057	38.4	9.41	12.3	451
100	870.1	1058	38.4	12.8	16.6	538
101	1003.8	1058	38.4	15.4	20.4	573
102	1211.5	1058	38.4	16.7	22.5	523
103	1334.2	1058	38.4	18.4	23.9	505
104	1463.8	1059	38.4	21.5	27.4	528

*Corrected to include amounts withdrawn in previous samples and for sample dilution.

difference can be ascribed to an approximately 5% lower average neutron flux in the core of this loop. The remaining one-half of the difference is unaccounted for.

(e) Uranium Balance. – Amounts of uranium charged to and removed from the loop are shown below:

	Weight of Uranium (g)
Charged to Loop	
Original solution charged in	40.98
Additions during operation	13.07
Total in	54.05
Recovered from Loop	
Solution samples	9.82
Balance of inventory	43.11
Total out	52.93

Unlike the preceding loops, the resulting value for the total weight of uranium removed is less than the value for the charged weight.[2-4] The material balance for the loop was 2% low.

(f) Radiolytic Gas Pressures. – The steady-state pressures of radiolytic gas observed during this experiment were essentially constant at about 4.5 psi.

(g) Performance of Equipment. – As with the previous experiment, a decrease in the rate of flow of solution through the pressurizer was noted during the experiment. The flow, as measured by pressurizer heater requirements, remained fairly constant at 4.5 cc/sec for the first 350 hr of circulation. After this time the rate was observed to decrease gradually; at a time just prior to the termination of the experiment, it was about 3.5 cc/sec. With the exception of the pump, noted previously, the general performance of the equipment was satisfactory.

12.1.3 Remote Dismantling and Inspection of Loop EE

(a) Dismantling. – Two major difficulties with equipment were encountered during dismantling operations: the disk changer for remote replacement of cutting wheels failed when the nut holding

TABLE 12.5. OXYGEN CONSUMPTION IN LOOP EE

	Sample No.	Accumulated LITR Energy (Mwhr)	Total Solution Circulation Time (hr)	O_2 Additions to Loop (cc at STP)	O_2 Withdrawn from Loop* (cc at STP)	Total O_2 Charged to Loop Less O_2 Withdrawn in Sampling (cc at STP)	O_2 Volume at Time of Sampling (cc at STP)	O_2 Consumed Since Last Sampling (cc at STP)	Cumulative Amount of O_2 Consumed (cc at STP)	Calculated Corrosion Penetration of Type 347 Stainless Steel (mils)
Original filling		0.0	0.0	795	0	795	795	0	0	0
O_2 addition (EE-2)		0.0	21.5	839	0	1634	1601		33	
	EE-1-92	0.0	33.3	0	0	1634	1583	51	51	0.003
Reactor started		0.0	36.2	0	6	1628	1572		56	
	EE-1-93	56.0	54.8	0	0	1622	1432	139	190	0.01
	EE-1-94	107.4	76.3	0	7	1616	1272	154	344	0.02
	EE-1-95	298.6	148.1	0	6	1610	868	418	762	0.04
	EE-1-96	358.3	172.6	0	4	1606	786	58	820	0.04
	EE-1-97	428.3	196.7	0	6	1600	698	82	902	0.05
	EE-1-98	562.8	244.6	0	10	1590	529	159	1061	0.05
O_2 addition (EE-3)			251.3	986	8	2567	1490		1077	
	EE-1-99	766.7	316.6	0	0	2567	1253	253	1314	0.07
	EE-1-100	870.1	364.3	0	15	2553	1093	146	1460	0.07
	EE-1-101	1003.8	412.4	0	5	2548	933	155	1615	0.08
	EE-1-102	1211.5	484.4	0	4	2544	657	272	1887	0.09
	EE-1-103	1334.2	532.2	0	3	2542	484	171	2058	0.10
O_2 addition (EE-4)			557.5	917	2	3457	1310		2147	
	EE-1-104	1463.8	580.5	0	0	3457	1205	194	2252	0.11
End of run		1610.4	630.3	0	5	3451	977	222	2474	0.12

*Calculated amount removed as O_2 dissolved in sample.

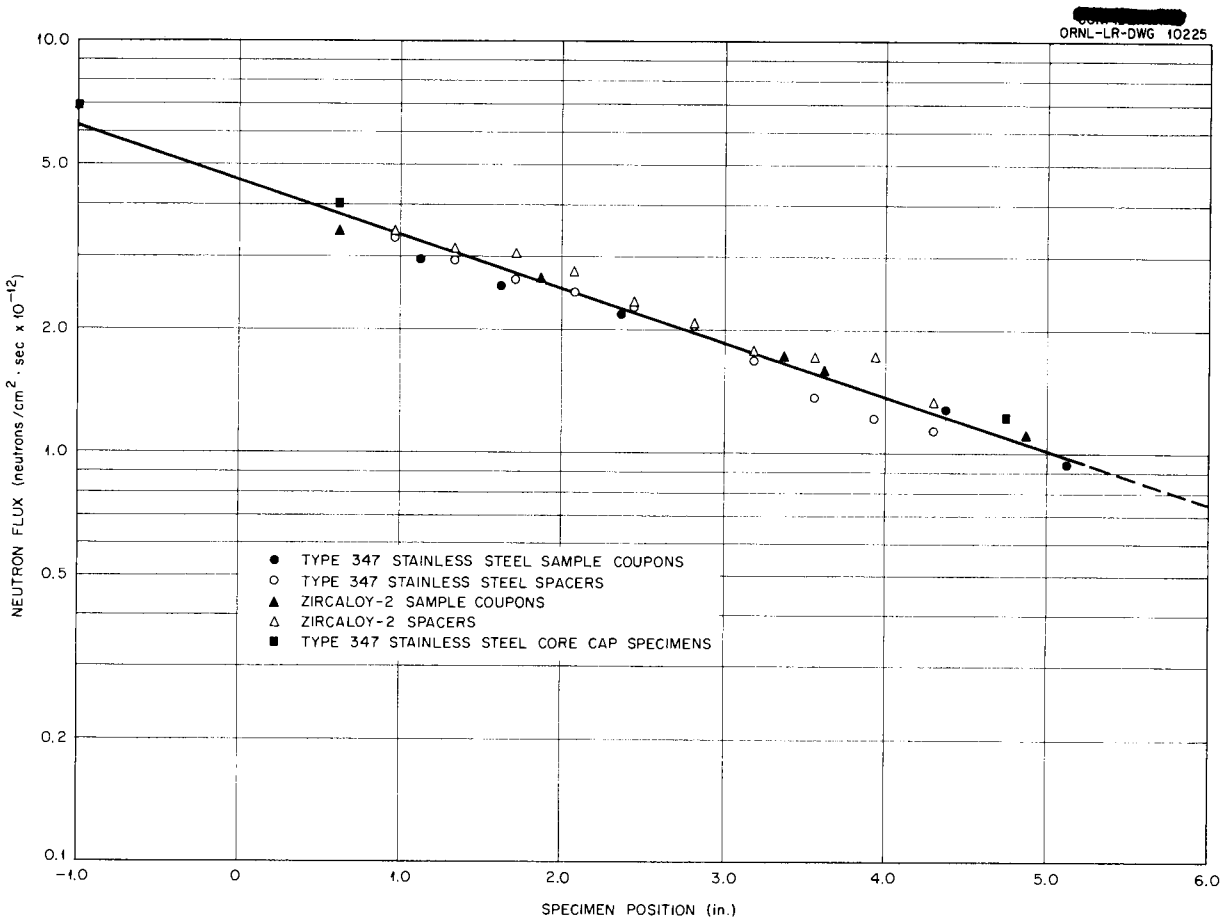

Fig. 12.8. Neutron Flux vs Specimen Position in Core.

the wheel to the motor jammed during an attempted removal of a worn wheel, and the centrifuge used for dust separation failed to operate. Both failures occurred during the latter stages of dismantling, so that it was possible to remove the remaining loop pieces and to decontaminate the cell for corrective maintenance. Heavier equipment was installed on the disk changer, and the defective rotor on the centrifuge was replaced with a perforated sheet model, which will probably prove more dependable. During the shutdown a slow leak on the inside of the main viewing window was repaired and an adapter installed to permit dismantling of the shorter HB-2 loops.

As with past loops, the core, the in-line sample holder, the pressurizer, a portion of the pressurizer heater, a sample of the piping, and the pump were transferred to the Solid State Division hot cells. The remainder of the loop package was sent to the burial ground.

Disassembly, sectioning, and examination of the various components were successful, with the exception of the pump. To date, it has not been possible to inspect the bearings and rotor of any pump. The equipment available in the Corrosion Examination Facility should remedy this situation. This facility is expected to be in operation early in the next quarter.

(b) Qualitative Results of Inspection and Evaluation. – As with previous loops,[2-4] all surfaces outside the core were covered with a rustlike scale and there was no apparent localized attack on any of the components inspected. In the core area all the stainless steel components were covered with a similar rustlike scale, although the scale was somewhat less bulky. The various titanium specimens were covered with a very thin

rust[redacted]e, which, in general, became more bulky with decreasing flux. In contrast to previously reported findings, not all the Zircaloy-2 surfaces in the higher flux regions were free from the rustlike scale. The core coupon holder and the stress specimens, which were mounted in the spider around the coupon holder, were free from bulk oxide deposits in the higher flux regions. The Zircaloy-2 coupons inside the tapered holder, the coupons in the couple assemblies, and the spacers in the Zircaloy-2 couple assembly were coated with some deposited bulk scale in even the highest flux region. The amount of this deposit, however, appeared to be inversely proportional to the flux. A description of each of the various specimens is included with the weight data in Table 12.7.

A photograph of the core assembly as removed from the loop is shown in Fig. 12.9. The stainless steel couple assembly, a titanium stress assembly, and the Zircaloy-2 couple assembly are shown in the foreground. As noted in Table 12.7, each titanium stress specimen exhibited a peculiar color pattern in the neighborhood of the fulcrum. This pattern can be seen in the photograph. The gradation of the quantity of scale with flux can also be seen in the photograph of the titanium specimen in Fig. 12.9.

Microscopic examination of all the surfaces of all the stress specimens revealed no sign of stress-corrosion cracking in the type 347 stainless steel, Zircaloy-2, and titanium 55AX tested during this run. A metallographic examination of these specimens will be made.

Figure 12.10 is a photograph of the core coupon array as removed from the loop. Unfortunately, some of the coupons were loosened during handling and could not be included. The first three stainless steel coupons in positions 4, 5, and 7 showed a concentration of attack in the exposed areas, with the clamped edges being protected. There was no such pattern of attack on the Zircaloy-2 or titanium coupons.

Surface examination of the various couple assemblies showed no pattern which would indicate an electrolytically enhanced corrosion rate for any of the six combinations tested. There were, however, indications of increased attack in crevice

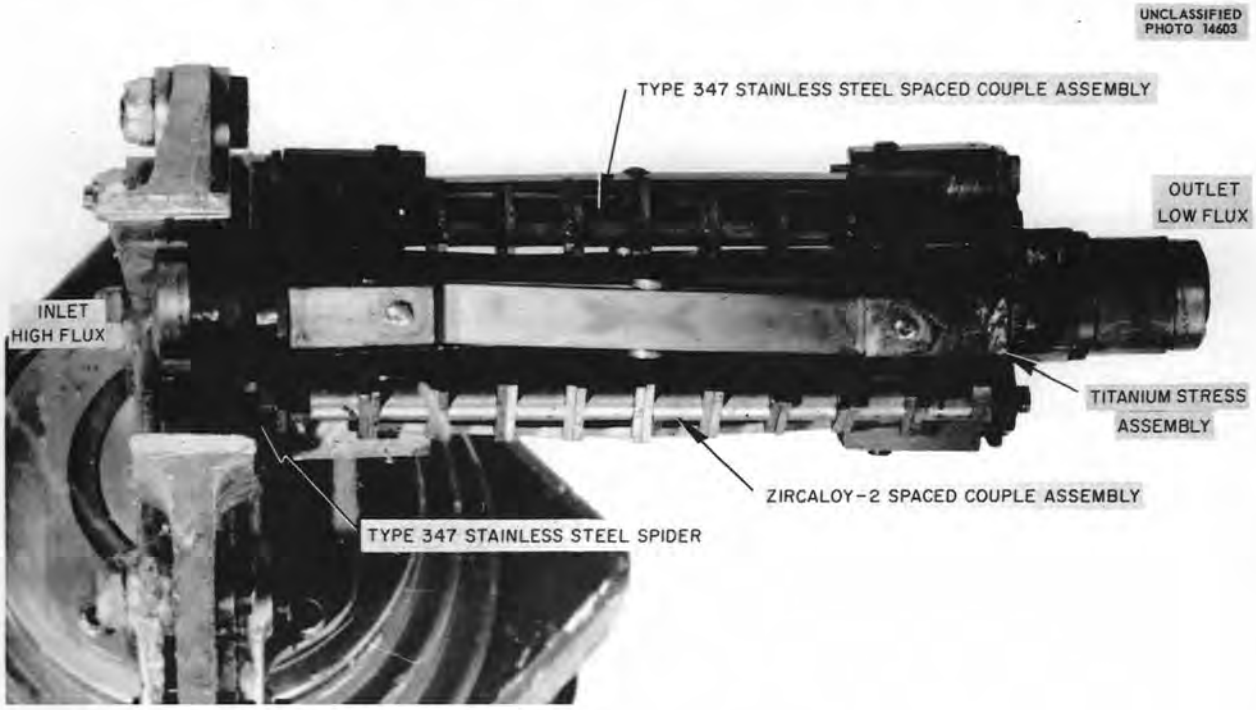

Fig. 12.9. HRP In-Pile Loop EE Core Specimen Assembly.

TABLE 12.6. INDUCED ZIRCONIUM-NIOBIUM AND CHROMIUM ACTIVITY IN SPECIMENS

Specimen Number	Cleaned Weight When Counted (g)	Relative Zr-Nb Activity (0.76-Mev gamma)		Relative Cr^{51} Activity		Neutron Flux at 3 Mw (neutrons/cm^2/sec × 10^{-12})	Power Density at 3 Mw* (w/ml)	Exposure Time for Type 347 Stainless Steel Control (hr)	Exposure Time for Zircaloy-2 Control (hr)	Exposure Time for Specimens (hr) (1 hr = 3 Mwhr)	Cooling Time Before Analysis (hr)
		Counts/min/coupon	Counts/min/g	Counts/min/coupon	Counts/min/g						
Core Corrosion Sample Coupons											
Type 347 stainless steel											
744 A	0.847			4.34	5.12	2.97	3.84	315		536.8	1584
745 A	0.838			3.67	4.38	2.54	3.28	315		536.8	1560
746 A	0.956			3.60	3.77	2.18	2.82	315		536.8	1584
784 A	0.956			2.11	2.21	1.28	1.66	315		536.8	1584
785 A	0.960			1.55	1.62	0.94	1.21	315		536.8	1584
Zircaloy-2											
Z-20	0.759	7.53	9.92			3.45	4.46		315	536.8	1536
Z-21	0.767	5.88	7.67			2.67	3.45		315	536.8	1536
Z-26	0.778	3.82	4.91			1.71	2.21		315	536.8	1536
Z-27	0.762	3.45	4.53			1.58	2.04		315	536.8	1536
Z-31	0.759	2.41	3.18			1.10	1.43		315	536.8	1536
Coupled Corrosion Specimen Spacers											
Type 347 stainless steel											
S-1	0.582			3.33	5.72	3.32	4.29	315		536.8	1560
S-2	0.602			3.06	5.08	2.95	3.81	315		536.8	1560
S-3	0.605			2.76	4.56	2.65	3.42	315		536.8	1560
S-4	0.547			2.35	4.30	2.49	3.22	315		536.8	1560
S-5	0.588			2.30	3.91	2.27	2.93	315		536.8	1560
S-6	0.547			1.93	3.53	2.05	2.65	315		536.8	1560
S-7	0.567			1.65	2.91	1.69	2.18	315		536.8	1560
S-8	0.550			1.30	2.37	1.37	1.77	315		536.8	1560
S-9	0.575			1.20	2.09	1.21	1.57	315		536.8	1560
S-10	0.545			1.07	1.97	1.14	1.47	315		536.8	1560
Zircaloy-2											
Z-1	0.514	5.10	9.92			3.45	4.46		315	536.8	1536
Z-2	0.506	4.57	9.03			3.14	4.06		315	536.8	1536
Z-3	0.507	4.43	8.74			3.04	3.93		315	536.8	1536
Z-4	0.513	4.08	7.95			2.77	3.58		315	536.8	1536
Z-5	0.494	3.29	6.66			2.32	2.99		315	536.8	1536
Z-6	0.494	2.94	5.96			2.07	2.68		315	536.8	1536
Z-7	0.478	2.45	5.13			1.78	2.31		315	536.8	1536
Z-8	0.517	2.55	4.94			1.72	2.22		315	536.8	1536
Z-9	0.516	2.53	4.90			1.71	2.21		315	536.8	1536
Z-10	0.507	1.96	3.86			1.34	1.74		315	536.8	1536
Type 347 Stainless Steel Core Cop Specimens											
A	0.318			3.81	12.00	6.96	8.99	315		536.8	1584
C	0.595			4.13	6.94	4.03	5.20	315		536.8	1584
D	0.491			1.04	2.12	1.23	1.59	315		536.8	1584
Standards											
Type 347 stainless steel											
	0.965			1.0	1.04	0.708		315			1368 for spacers and core coupon 745 A; 1392 for core coupons and core cap specimens
Zircaloy-2											
	0.766	1.0	1.31			0.708			315		1344

*Uranium concentration, 38.45 mg/ml; 88.78% enrichment.

TABLE 12.7. SPECIMEN DATA FOR LOOP EE

Sample No.	Position	Distance from Front of Core Holder to Center of Specimen (in.)	Flow Velocity at Leading Edge (fps)	Initial Weight (g)	As-Removed Weight (g)	Defilmed Weight (g)	Weight Change (mg)	Exposed Specimen Area (cm^2)	Corrosion Penetration (mils)	Corrosion Rate* (mpy) 630.3** (hr)	Corrosion Rate* (mpy) 536.8** (hr)	Total Specimen Area (cm^2)	Corrosion Penetration (mils)	Corrosion Rate* (mpy) 630.3** (hr)	Corrosion Rate* (mpy) 536.8** (hr)	Neutron Flux at 3 Mw (neutrons/cm^2/sec $\times 10^{-12}$)	Power Density at 3 Mw (w/ml)	Surface Appearance: As Removed	Surface Appearance: After Defilming
24 Core Sample Coupons																			
Type 347 Stainless Steel Coupons																			
743 A	4	0.88	11.8	0.9512	0.8465	0.8457	−105.5	1.40	3.70	51.3	59.9	2.1	2.47	34.2	39.9	3.52	4.55	Heavy rough scale on all surfaces	Thin film, pickled appearance; clamped edges were protected
744 A	5	1.13	13.1	0.9483	0.8514	0.8503	−98.0	1.40	3.44	47.4	55.6	2.1	2.29	31.6	37.1	2.97	3.84	Heavy rough scale on all surfaces	Thin film, pickled appearance; clamped edges were protected
745 A	7	1.63	16.3	0.9474	0.8422	0.8413	−106.1	1.40	3.72	51.2	60.2	2.1	2.48	34.2	40.1	2.54	3.28	Heavy rough scale on all surfaces	Thin film on one side, heavy pickled appearance; clamped edges were protected
746 A	10	2.38	26.0	0.9630	0.9583	0.9582	−4.8	1.40	0.17	2.3	2.8	2.1	0.11	1.6	1.8	2.18	2.82	Heavy rough scale on all surfaces	Thin film, some scale; machine marks visible
747 A	13	3.13	39.2	0.9545	0.9521	0.9520	−2.5	1.40	0.09	1.2	1.5	2.1	0.06	0.8	1.0	1.79	2.31	Spotty brown scale on all surfaces	Thin film on most of the surface, pickled appearance along one edge
784 A	18	4.38	22.3	0.9583	0.9581	0.9576	−0.7	1.40	0.02	0.3	0.3	2.1	0.01	0.2	0.2	1.28	1.66	Flaky scale on all surfaces	Film on all surfaces; machine marks visible
785 A	21	5.13	14.4	0.9615	0.9621	0.9614	−0.1	1.40	0.004	0.1	0.1	2.1	0.003	0.04	0.05	0.94	1.21	Spotty brown scale on all surfaces	Thin film on all surfaces; machine marks visible
787 A	24	5.88	10.4	0.9627	0.9640	0.9626	−0.1	1.57	0.003	0.04	0.05	2.1	0.002	0.03	0.03	0.78	1.01	Heavy dark-brown scale on all surfaces	Thin film on all surfaces; machine marks visible
Zircaloy-2 Coupons																			
Z 19	2	0.38	9.9	0.7638	0.7591	0.7587	−5.1	1.40	0.22	3.1	3.6	2.1	0.15	2.0	2.4	4.10	5.30	Heavy red-brown film on all surfaces	Thin film on all surfaces, light etching; machine marks visible
Z 20	3	0.63	10.7	0.7672	0.7629	0.7623	−4.9	1.40	0.21	2.9	3.4	2.1	0.14	1.9	2.3	3.45	4.46	Heavy red-brown film on all surfaces	Thin film on all surfaces, light etching; machine marks visible
Z 21	8	1.88	18.6	0.7738	0.7695	0.7698	−4.0	1.40	0.17	2.3	2.8	2.1	0.11	1.6	1.8	2.67	3.45	Heavy brown film on all surfaces	Dark film on all surfaces; machine marks visible
Z 24	11	2.63	34.0	0.7754	0.7712	0.7725	−2.9	1.40	0.13	1.8	2.1	2.1	0.09	1.2	1.4	2.09	2.70	Mottled brown scale on all surfaces	Some scale retained in spots on all surfaces
Z 26	14	3.38	42.5	0.7728	0.7698	0.7698	−3.0	1.40	0.13	1.8	2.1	2.1	0.09	1.2	1.4	1.71	2.21	Spotted brown scale on all surfaces	Thin dark scale on all surfaces
Z 27	15	3.63	47.8	0.7671	0.7641	0.7645	−2.6	1.40	0.11	1.5	1.8	2.1	0.07	1.0	1.2	1.58	2.04	Dark-gray film on all surfaces	Thin dark film on all surfaces; some white spots visible
Z 31	20	4.88	16.1	0.7626	0.7611	0.7609	−1.7	1.40	0.07	1.0	1.1	2.1	0.05	0.6	0.8	1.10	1.43	Heavy spotty film on all surfaces	No apparent film; machine marks clearly visible
Z 37	23	5.63	11.5	0.7639	0.7624	0.7623	−1.6	1.40	0.07	1.0	1.1	2.1	0.05	0.6	0.8	0.84	1.32	Heavy gray-brown film, some white deposits on all surfaces	Thin dark film on all surfaces; machine marks visible

*Corrosion rates have been calculated both for the nominally exposed and the total specimen areas.

**Two corrosion rates are presented: one based on the total operation time of 630.3 hr and one based on the total radiation time of 536.8 hr (3 Mwhr of reactor time equivalent to 1 hr of total radiation time).

TABLE 12.7 (continued)

Sample No.	Position	Distance from Front of Core Holder to Center of Specimen (in.)	Flow Velocity at Leading Edge (fps)	Initial Weight (g)	As-Removed Weight (g)	Defilmed Weight (g)	Weight Change (mg)	Exposed Specimen Area (cm^2)	Corrosion Penetration (mils)	Corrosion Rate* (mpy) 630.3** (hr)	Corrosion Rate* (mpy) 536.8** (hr)	Total Specimen Area (cm^2)	Corrosion Penetration (mils)	Corrosion Rate* (mpy) 630.3** (hr)	Corrosion Rate* (mpy) 536.8** (hr)	Neutron Flux at 3 Mw (neutrons/cm^2/sec $\times 10^{-12}$)	Power Density at 3 Mw (w/ml)	Surface Appearance: As Removed	Surface Appearance: After Defilming
Titanium Coupons																			
T 8	1	0.13	9.2	0.5433	0.5431	0.5428	−0.5	1.57	0.03	0.4	0.5	2.1	0.02	0.3	0.4	4.40	5.66	Thin rust-red film on all surfaces	Very thin film on all surfaces; machine marks visible
T 9	6	1.38	14.4	0.5397	0.5392	0.5392	−0.5	1.40	0.03	0.4	0.5	2.1	0.02	0.3	0.3	3.04	3.93	Thin brown film on all surfaces	Thin oxide film on all surfaces; machine marks visible
T 11	9	2.13	21.7	0.5452	0.5445	0.5447	−0.5	1.40	0.03	0.4	0.5	2.1	0.02	0.3	0.3	2.41	3.12	Heavy scale on all surfaces	Film on all surfaces; machine marks visible
T 12	12	2.88	36.2	0.5390	0.5388	0.5376	−1.4	1.40	0.09	1.2	1.5	2.1	0.06	0.8	1.0	1.92	2.48	Heavy film on all surfaces	Very thin film on all surfaces; machine marks visible
T 13	16	3.88	34.1	0.5367	0.5364	0.5348	−1.9	1.40	0.12	1.7	1.9	2.1	0.08	1.1	1.3	1.42	1.84	Flaky brown scale on all surfaces	No apparent film; machine marks visible
T 14	17	4.13	26.9	0.5429	0.5425	0.5415	−1.4	1.40	0.09	1.2	1.5	2.1	0.06	0.8	1.0	1.32	1.71	Spotty film on all surfaces	Thin film on all surfaces; light etched appearance; some machine marks visible
T 15	19	4.63	18.9	0.5348	0.5354	0.5344	−0.4	1.40	0.02	0.3	0.3	2.1	0.01	0.2	0.2	1.14	1.48	Spotty scale on all surfaces	Thin rust-colored film on all surfaces
T 16	22	5.38	12.6	0.5300	0.5307	0.5296	−0.4	1.40	0.02	0.3	0.3	2.1	0.01	0.2	0.2	0.90	1.17	Heavy flaky scale, some white deposits on all surfaces	No apparent film; machine marks clearly visible
18 Coupled Specimens (Type 347 Stainless Steel Rod and Spacers)																			
Type 347 Stainless Steel Specimens																			
792 A	1	1.13		0.6936	0.6884	0.6872	−6.4	1.07	0.29	4.05	4.76	1.89	0.17	2.3	2.7	3.28	4.24	Dark-brown scale on all surfaces; disturbed in contact area	Slight etching of all free surfaces except contact areas
793 A	2	1.19		0.6794	0.6742	0.6740	−5.4	1.07	0.25	3.44	4.04	1.89	0.14	2.0	2.3	3.20	4.14	Dark-brown scale on all surfaces; disturbed in contact area	Slight etching of all free surfaces except contact areas
794 A	3	1.50		0.6852	0.6847	0.6797	−5.5	1.07	0.25	3.36	3.95	1.89	0.14	1.9	2.2	2.93	3.79	Dark-brown scale on all surfaces; disturbed in contact area	Slight etching of all free surfaces except contact areas
795 A	5	1.87		0.6807	0.6782	0.6766	−4.1	1.07	0.19	2.61	3.06	1.89	0.11	1.5	1.7	2.62	3.39	Dark-brown scale on all surfaces; disturbed in contact area	Slight etching of all surfaces; machine marks visible
808 A	13	3.35		0.6800	0.6800	0.6785	−1.5	1.07	0.07	0.96	1.13	1.89	0.04	0.5	0.6	1.66	2.15	Dark-brown scale on all surfaces; disturbed in contact area	Thin tan film on all surfaces; machine marks visible
809 A	15	3.72		0.6783	0.6775	0.6773	−1.0	1.07	0.05	0.65	0.76	1.89	0.03	0.4	0.4	1.49	1.93	Dark-brown scale on all surfaces	Thin tan film on all surfaces; machine marks visible
810 A	17	4.09		0.6826	0.6817	0.6828	+0.2	1.07				1.89				1.34	1.73	Dark-brown scale on all surfaces	Thin tan film on all surfaces; machine marks visible
811 A	18	4.15		0.6737	0.6728	0.6735	−0.2	1.07	0.01	0.13	0.15	1.89	0.006	0.1	0.1	1.31	1.69	Dark-brown scale on all surfaces	Thin tan film on all surfaces; machine marks visible
Zircaloy-2 Specimens																			
Z 48	4	1.56		0.5663	0.5626	0.5620	−4.3	1.07	0.24	3.37	3.96	1.89	0.14	1.9	2.2	2.89	3.74	Dark-gray scale on contact surfaces; dark-brown scale on free surfaces	Slight etching of contact area; machine marks on other areas
Z 49	7	2.24		0.5651	0.5625	0.5618	−3.3	1.07	0.19	2.59	3.04	1.89	0.11	1.5	1.7	2.33	3.01	Dark-gray scale on contact surfaces; dark-brown scale on free surfaces	Machine marks visible on all surfaces; some scale in contact areas
Z 50	11	2.98		0.5645	0.5620	0.5619	−2.6	1.07	0.15	2.04	2.40	1.89	0.08	1.2	1.4	1.86	2.40	Dark scale on all surfaces; cracked in contact zone	Thin dark scale on some areas; machine marks visible
Z 51	16	3.78		0.5698	0.5683	0.5680	−1.8	1.07	0.10	1.42	1.67	1.89	0.06	0.8	1.0	1.47	1.90	Dark-brown scale on all surfaces	Thin dark scale on some areas; machine marks visible

*Corrosion rates have been calculated both for the nominally exposed and the total specimen areas.

**Two corrosion rates are presented: one based on the total operation time of 630.3 hr and one based on the total radiation time of 536.8 hr (3 Mwhr of reactor time equivalent to 1 hr of total radiation time).

TABLE 12.7 (continued)

Sample No.	Position	Distance from Front of Core Holder to Center of Specimen (in.)	Flow Velocity at Leading Edge (fps)	Initial Weight (g)	As-Removed Weight (g)	Defilmed Weight (g)	Weight Change (mg)	Exposed Specimen Area (cm^2)	Corrosion Penetration (mils)	Corrosion Rate* (mpy) 630.3** (hr)	Corrosion Rate* (mpy) 536.8** (hr)	Total Specimen Area (cm^2)	Corrosion Penetration (mils)	Corrosion Rate* (mpy) 630.3** (hr)	Corrosion Rate* (mpy) 536.8** (hr)	Neutron Flux at 3 Mw (neutrons/cm^2/sec $\times 10^{-12}$)	Power Density at 3 Mw (w/ml)	Surface Appearance: As Removed	Surface Appearance: After Defilming
Titanium Specimens (55AX)																			
T 44	6	1.93		0.3938	0.3935	0.3939	+0.1	1.07				1.89				2.58	3.34	Dark-brown scale on all surfaces; disturbed in contact area	Thin dark film on all surfaces; machine marks visible
T 46	8	2.30		0.3773	0.3760	0.3773	0.0	1.07	0.00	0.00	0.00	1.89	0.00	0.00	0.00	2.29	2.96	Dark-brown scale on all surfaces; disturbed in contact area	Machine marks visible on all surfaces; some scale in contact zone
T 47	9	2.61		0.3823	0.3818	0.3817	−0.5	1.07	0.04	0.57	0.67	1.89	0.02	0.3	0.4	2.10	2.71	Dark-brown scale on all surfaces; disturbed in contact area	Thin dark film on all surfaces; machine marks visible
T 50	10	2.67		0.3869	0.3850	0.3865	−0.4	1.07	0.03	0.45	0.53	1.89	0.02	0.3	0.3	2.07	2.68	Dark-brown scale on all surfaces; disturbed in contact area	Thin dark film on all surfaces; machine marks visible
T 52	12	3.04		0.3864	0.3856	0.3862	−0.2	1.07	0.02	0.23	0.27	1.89	0.01	0.1	0.2	1.84	2.38	Dark scale on all surfaces; cracked in contact zone	Thin dark film on all surfaces; machine marks visible
T 53	14	3.41		0.3979	0.3971	0.3973	−0.6	1.07	0.05	0.67	0.79	1.89	0.03	0.4	0.5	1.64	2.12	Dark-brown scale on all surfaces; disturbed in contact area	Thin dark scale on some areas; machine marks visible
Type 347 Stainless Steel Spacers																			
S 1	1	0.97		0.5966	0.5853	0.5843	−12.3	2.23	0.27	3.73	4.38	2.42	0.25	3.4	4.0	3.32	4.29		
S 2	2	1.34		0.6123	0.6044	0.6032	−9.1	2.23	0.20	2.76	3.24	2.42	0.18	2.5	3.0	2.95	3.81		
S 3	3	1.71		0.6140	0.6083	0.6070	−7.0	2.23	0.15	2.12	2.49	2.42	0.14	2.0	2.3	2.65	3.42		
S 4	4	2.08		0.5545	0.5499	0.5486	−5.9	2.23	0.13	1.79	2.10	2.42	0.12	1.7	1.9	2.49	3.22		
S 5	5	2.45		0.5958	0.5932	0.5917	−4.1	2.23	0.09	1.24	1.46	2.42	0.08	1.1	1.4	2.27	2.93		
S 6	6	2.82		0.5524	0.5519	0.5490	−3.4	2.23	0.08	1.03	1.21	2.42	0.07	1.0	1.1	2.05	2.65		
S 7	7	3.19		0.5726	0.5715	0.5700	−2.6	2.23	0.06	0.79	0.93	2.42	0.05	0.7	0.9	1.69	2.18		
S 8	8	3.56		0.5543	0.5542	0.5525	−1.8	2.23	0.04	0.55	0.65	2.42	0.04	0.5	0.6	1.37	1.77		
S 9	9	3.93		0.5782	0.5775	0.5772	−1.0	2.23	0.02	0.30	0.35	2.42	0.02	0.3	0.3	1.21	1.57		
S 10	10	4.30		0.5483	0.5462	0.5475	−0.8	2.23	0.02	0.25	0.29	2.42	0.02	0.2	0.3	1.14	1.47		
18 Coupled Specimens (Zircaloy-2 Rod and Spacers)																			
Type 347 Stainless Steel Specimens																			
788 A	4	1.56		0.6927	0.6867	0.6853	−7.4	1.07	0.34	4.7	5.5	1.89	0.19	2.7	3.1	2.89	3.74	Dark scale on all surfaces; disturbed in contact area	Dark speckled scale on free surfaces; brown in contact zone
789 A	5	1.87		0.6896	0.6836	0.6827	−6.9	1.07	0.32	4.4	5.1	1.89	0.18	2.5	2.9	2.61	3.37	Dark scale on all surfaces; disturbed in contact area	Dark, salted scale on all surfaces
790 A	13	3.35		0.6908	0.6882	0.6867	−4.1	1.07	0.19	2.6	3.0	1.89	0.11	1.5	1.7	1.67	2.16	Dark scale on all surfaces; disturbed in contact area	Dark, salted scale on all surfaces
791 A	15	3.72		0.6905	0.6899	0.6876	−2.9	1.07	0.13	1.8	2.2	1.89	0.08	1.0	1.2	1.50	1.94	Dark scale on all surfaces; disturbed in contact area	Dark, salted scale on all surfaces

*Corrosion rates have been calculated both for the nominally exposed and the total specimen areas.

**Two corrosion rates are presented: one based on the total operation time of 630.3 hr and one based on the total radiation time of 536.8 hr (3 Mwhr of reactor time equivalent to 1 hr of total radiation time).

TABLE 12.7 (continued)

Sample No.	Position	Distance from Front of Core Holder to Center of Specimen (in.)	Flow Velocity at Leading Edge (fps)	Initial Weight (g)	As-Removed Weight (g)	Defilmed Weight (g)	Weight Change (mg)	Exposed Specimen Area (cm^2)	Corrosion Penetrotion (mils)	Corrosion Rate* (mpy) 630.3** (hr)	Corrosion Rate* (mpy) 536.8** (hr)	Total Specimen Area (cm^2)	Corrosion Penetration (mils)	Corrosion Rate* (mpy) 630.3** (hr)	Corrosion Rate* (mpy) 536.8** (hr)	Neutron Flux at 3 Mw (neutrons/ cm^2/sec $\times 10^{-12}$)	Power Density at 3 Mw (w/ml)	Surface Appearance: As Removed	Surface Appearance: After Defilming
Zircaloy-2 Specimens																			
Z 40	1	1.13		0.5556	0.5513	0.5503	−5.3	1.07	0.30	4.1	4.9	1.89	0.17	2.3	2.8	3.29	4.25	Dark scale on all surfaces; disturbed in contact area	Dark, salted scale on all surfaces
Z 41	2	1.19		0.5772	0.5731	0.5726	−4.6	1.07	0.26	3.6	4.2	1.89	0.15	2.0	2.4	3.21	4.15	Dark scale on all surfaces; disturbed in contact area	Dark, salted scale on all surfaces
Z 42	3	1.50		0.5686	0.5648	0.5644	−4.2	1.07	0.24	3.3	3.8	1.89	0.13	1.9	2.2	2.92	3.77	Dark scale on all surfaces; disturbed in contact area	Dark, salted scale on all surfaces
Z 43	7	2.24		0.5701	0.5675	0.5658	−4.3	1.07	0.24	3.4	4.0	1.89	0.14	1.9	2.2	2.32	3.00	Dark scale on all surfaces; disturbed in contact area	Dark, salted scale on all surfaces
Z 44	11	2.98		0.5539	0.5511	0.5502	−3.7	1.07	0.21	2.9	3.4	1.89	0.12	1.6	1.9	1.87	2.42	Dark scale on all surfaces; disturbed in contact area	Dark, salted scale on all surfaces
Z 45	16	3.78		0.5605	0.5581	0.5574	−3.1	1.07	0.18	2.4	2.8	1.89	0.10	1.4	1.6	1.47	1.90	Dark scale on all surfaces; disturbed in contact area	Dark, salted scale on all surfaces
Z 46	17	4.09		0.5628	0.5608	0.5594	−3.4	1.07	0.19	2.6	3.1	1.89	0.11	1.5	1.8	1.34	1.73	Dark scale on all surfaces; disturbed in contact area	Dark, salted scale on all surfaces
Z 47	18	4.15		0.5732	0.5712	0.5699	−3.3	1.07	0.19	2.6	3.0	1.89	0.11	1.5	1.7	1.31	1.69	Dark scale on all surfaces; disturbed in contact area	Dark, salted scale on all surfaces
Titanium Specimens (55AX)																			
T 25	6	1.93		0.3825	0.3826	0.3824	−0.1	1.07	0.01	0.1	0.1	1.89	0.01	0.1	0.1	2.54	3.28	Dark scale on all surfaces; disturbed in contact area	Dark, salted scale on all surfaces
T 26	8	2.30		0.3857	0.3866	0.3858	+0.1	1.07				1.89				2.30	2.97	Dark scale on all surfaces; disturbed in contact area	Dark brown scale on all surfaces
T 27	9	2.61		0.3864	0.3871	0.3864	0.0	1.07	0.00	0.0	0.0	1.89	0.00	0.0	0.0	2.09	2.70	Dark scale on all surfaces; disturbed in contact area	Dark brown film on free surfaces; scale on contact areas
T 29	10	2.67		0.3911	0.3913	0.3914	+0.3	1.07				1.89				2.07	2.67	Dark scale on all surfaces; disturbed in contact area	Dark brown film on free surfaces; scale on contact areas
T 38	12	3.04		0.3912	0.3916	0.3915	+0.3	1.07				1.89				1.83	2.36	Dark scale on all surfaces; disturbed in contact area	Dark brown film on free surfaces; scale on contact areas
T 42	14	3.41		0.3780	0.3782	0.3771	−0.9	1.07	0.08	1.1	1.2	1.89	0.04	0.6	0.7	1.64	2.12	Dark scale on all surfaces; disturbed in contact area	Dark brown film on free surfaces; scale on contact areas
Zircaloy-2 Spacers																			
Z 1	1	0.97		0.5210	0.5179	0.5179	−3.1	2.23	0.07	0.9	1.1	2.42	0.06	0.9	1.0	3.45	4.46		
Z 2	2	1.34		0.5207	0.5188	0.5122	−8.5	2.23	0.19	2.6	3.0	2.42	0.17	2.4	2.8	3.14	4.06		
Z 3	3	1.71		0.5190	0.5113	0.5112	−7.8	2.23	0.17	2.4	2.8	2.42	0.16	2.2	2.6	3.04	3.93		
Z 4	4	2.08		0.5245	0.5224	0.5160	−8.5	2.23	0.19	2.6	3.0	2.42	0.17	2.4	2.8	2.77	3.58		
Z 5	5	2.45		0.5183	0.5168	0.5105	−7.8	2.23	0.17	2.4	2.8	2.42	0.16	2.2	2.6	2.32	2.99		
Z 6	6	2.82		0.5317	0.5308	0.5251	−6.6	2.23	0.15	2.0	2.4	2.42	0.13	1.8	2.2	2.07	2.68		
Z 7	7	3.19		0.5199	0.5150	0.5131	−6.8	2.23	0.15	2.1	2.4	2.42	0.14	1.9	2.2	1.78	2.31		
Z 8	8	3.56		0.5244	0.5200	0.5192	−5.2	2.23	0.12	1.6	1.9	2.42	0.11	1.5	1.7	1.72	2.22		
Z 9	9	3.93		0.5228	0.5183	0.5159	−6.9	2.23	0.15	2.1	2.5	2.42	0.14	1.9	2.3	1.71	2.21		
Z 10	10	4.30		0.5163	0.5135	0.5113	−5.0	2.23	0.11	1.5	1.8	2.42	0.10	1.4	1.6	1.34	1.74		

*Corrosion rates have been calculated both for the nominally exposed and the total specimen areas.

**Two corrosion rates are presented: one based on the total operation time of 630.3 hr and one based on the total radiation time of 536.8 hr (3 Mwhr of reactor time equivalent to 1 hr of total radiation time).

TABLE 12.7 (continued)

Sample No.	Position	Distance from Front of Core Holder to Center of Specimen (in.)	Flow Velocity at Leading Edge (fps)	Initial Weight (g)	As-Removed Weight (g)	Defilmed Weight (g)	Weight Change (mg)	Exposed Specimen Area (cm^2)	Corrosion Penetration (mils)	Corrosion Rate* (mpy) 630.3** (hr)	Corrosion Rate* (mpy) 536.8** (hr)	Total Specimen Area (cm^2)	Corrosion Penetration (mils)	Corrosion Rate* (mpy) 630.3** (hr)	Corrosion Rate* (mpy) 536.8** (hr)	Neutron Flux at 3 Mw (neutrons/cm^2/sec $\times 10^{-12}$)	Power Density at 3 Mw (w/ml)	Surface Appearance: As Removed	Surface Appearance: After Defilming
In-Line Corrosion Sample Coupons																			
Type 347 Stainless Steel Coupons																			
736 A	4		11.8	0.9547	0.9608	0.9524	−2.3	1.40	0.08	1.1	1.3	2.1	0.05	0.8	0.9			Heavy rust-colored scale on all surfaces	Clean; machine marks visible
737 A	5		13.1	0.9547	0.9606	0.9540	−0.7	1.40	0.03	0.4	0.4	2.1	0.02	0.2	0.3			Heavy rust-colored scale on all surfaces	Clean; machine marks visible
738 A	7		16.3	0.9526	0.9585	0.9506	−2.0	1.40	0.07	1.0	1.1	2.1	0.05	0.7	0.8			Heavy rust-colored scale on all surfaces	Slight staining of all surfaces; machine marks visible
739 A	10		26.0	0.9396	0.9453	0.9392	−0.4	1.40	0.01	0.2	0.2	2.1	0.01	0.1	0.2			Heavy rust-colored scale on all surfaces	Clean; machine marks visible
740 A	13		39.2	0.9509	0.9557			1.40				2.1						Heavy rust-colored scale on all surfaces	
741 A	18		22.3	0.9532	0.9570	0.9528	−0.4	1.40	0.01	0.2	0.2	2.1	0.01	0.1	0.2			Heavy rust-colored scale on all surfaces	Clean; machine marks visible
742 A	21		14.4	0.9504	0.9538	0.9499	−0.5	1.40	0.02	0.3	0.3	2.1	0.01	0.2	0.2			Heavy rust-colored scale on all surfaces	Clean; machine marks visible
786 A	24		10.4	0.9653	0.9691	0.9651	−0.2	1.57	0.01	0.1	0.1	2.1	0.004	0.1	0.1			Heavy rust-colored scale on all surfaces	Clean; machine marks visible
Zircaloy-2 Coupons																			
Z 1	2		9.9	0.7701	0.7750	0.7704	+0.3	1.40				2.1						Heavy rust-colored scale on all surfaces	Thin film on all surfaces; no machine marks visible
Z 3	3		10.7	0.7727	0.7785	0.7729	+0.2	1.40				2.1						Heavy rust-colored scale on all surfaces	Thin film on all surfaces; no machine marks visible
Z 5	8		18.6	0.7575	0.7636	0.7576	+0.1	1.40				2.1						Heavy rust-colored scale on all surfaces	Thin film on all surfaces
Z 12	11		34.0	0.7593	0.7653			1.40				2.1						Heavy rust-colored scale on all surfaces	
Z 13	14		42.5	0.7676	0.7727	0.7678	+0.2	1.40				2.1						Heavy rust-colored scale on all surfaces	Thin film on all surfaces
Z 15	15		47.8	0.7749	0.7795	0.7751	+0.2	1.40				2.1						Heavy rust-colored scale on all surfaces	Thin film on all surfaces
Z 16	20		16.1	0.7690	0.7734	0.7692	+0.2	1.40				2.1						Heavy rust-colored scale on all surfaces	Clean; machine marks visible
Z 17	23		11.5	0.7651	0.7701	0.7654	+0.3	1.40				2.1						Heavy rust-colored scale on all surfaces	

*Corrosion rates have been calculated both for the nominally exposed and the total specimen areas.

**Two corrosion rates are presented: one based on the total operation time of 630.3 hr and one based on the total radiation time of 536.8 hr (3 Mwhr of reactor time equivalent to 1 hr of total radiation time).

TABLE 12.7 (continued)

Sample No.	Position	Distance from Front of Core Holder to Center of Specimen (in.)	Flow Velocity at Leading Edge (fps)	Initial Weight (g)	As-Removed Weight (g)	Defilmed Weight (g)	Weight Change (mg)	Exposed Specimen Area (cm^2)	Corrosion Penetration (mils)	Corrosion Rate* (mpy) 630.3** (hr)	Corrosion Rate* (mpy) 536.8** (hr)	Total Specimen Area (cm^2)	Corrosion Penetration (mils)	Corrosion Rate* (mpy) 630.3** (hr)	Corrosion Rate* (mpy) 536.8** (hr)	Neutron Flux at 3 Mw (neutrons/ cm^2/sec $\times 10^{-12}$)	Power Density at 3 Mw (w/ml)	Surface Appearance: As Removed	Surface Appearance: After Defilming
Titanium (55AX) Coupons																			
T 0	1		9.2	0.5340	0.5379	0.5321	−1.9	1.57	0.11	1.5	1.7	2.1	0.08	1.1	1.3			Heavy rust-colored scale on all surfaces	Clean; slight stain on one side; no machine marks visible
T 1	6		14.4	0.5354	0.5412	0.5353	−0.1	1.40	0.006	0.1	0.1	2.1	0.004	0.1	0.1			Heavy rust-colored scale on all surfaces	Clean; machine marks visible
T 2	9		21.7	0.5384	0.5445	0.5383	−0.1	1.40	0.006	0.1	0.1	2.1	0.004	0.1	0.1			Heavy rust-colored scale on all surfaces	Slight stain on one side; machine marks visible
T 3	12		36.2	0.5379	0.5428			1.40				2.1						Heavy rust-colored scale on all surfaces	
T 4	16		34.1	0.5430	0.5472	0.5430	0.0	1.40	0.00	0.0	0.0	2.1	0.00	0.0	0.0			Heavy rust-colored scale on all surfaces	Clean
T 5	17		26.9	0.5364	0.5401	0.5363	−0.1	1.40	0.006	0.1	0.1	2.1	0.004	0.1	0.1			Heavy rust-colored scale on all surfaces	Clean
T 6	19		18.9	0.5422	0.5460	0.5422	0.0	1.40	0.00	0.0	0.0	2.1	0.00	0.0	0.0			Heavy rust-colored scale on all surfaces	Thin film on all surfaces
T 7	22		12.6	0.5348	0.5381	0.5346	−0.2	1.40	0.01	0.2	0.2	2.1	0.01	0.1	0.1			Heavy rust-colored scale on all surfaces	Thin film on all surfaces
Corrosion Sample Coupon Holders (Zircaloy-2)																			
Core Holder																			
Part A			3.00	76.0506	75.9368		−113.8	162.0	0.09	1.28	1.51	162.0	0.09	1.28	1.51	2.00	2.62		
Part B			3.00	77.0787	76.9449		−133.8									2.00	2.62		
In-Line Holder																			
Part A				96.9145	97.0823		+167.8	162.0				162.0							
Part B				94.6905	94.8652		+174.7												

*Corrosion rates have been calculated both for the nominally exposed and the total specimen areas.

**Two corrosion rates are presented: one based on the total operation time of 630.3 hr and one based on the total radiation time of 536.8 hr (3 Mwhr of reactor time equivalent to 1 hr of total radiation time).

TABLE 12.7 (continued)

Sample No.	Distance from Front of Core Holder to Center of Specimen (in.)	Initial Weight (g)	As-Removed Weight (g)	Defilmed Weight (g)	Weight Change (mg)	Exposed Specimen Area (cm^2)	Corrosion Penetration (mils)	Corrosion Rate* (mpy) 630.3** (hr)	Corrosion Rate* (mpy) 536.8** (hr)	Total Specimen Area (cm^2)	Corrosion Penetration (mils)	Corrosion Rate* (mpy) 630.3** (hr)	Corrosion Rate* (mpy) 536.8** (hr)	Strain (μin./in.)	Stress (psi)	Neutron Flux at 3 Mw (neutrons/cm^2/sec $\times 10^{-12}$)	Power Density at 3 Mw (w/ml)	Surface Appearance: As Removed	Surface Appearance: After Defilming
12 Stress-Corrosion Specimens																			
Type 347 Stainless Steel Specimens																			
SS 11	2.81	10.0773	10.0574	10.0436	−33.7	19.50	0.09	1.2	1.4	20.00	0.08	1.1	1.3	925	26,800	2.05	2.65	Thin brown scale on all surfaces; machine marks visible	Thin dark film on all surfaces
SS 12	2.81	10.1441	10.1159	10.1086	−35.5	19.50	0.09	1.2	1.4	20.00	0.09	1.2	1.4	915	26,500	2.05	2.65	Thin brown scale on all surfaces; machine marks visible	Thin dark film on all surfaces
SS 13	2.81	10.3518	10.3275	10.3257	−26.1	19.50	0.07	0.9	1.1	20.00	0.06	0.9	1.0	890	25,800	2.05	2.65	Thin brown scale on all surfaces; machine marks visible	Thin dark film on all surfaces
SS 14	2.81	10.0643	10.0416	10.0337	−30.6	19.50	0.08	1.1	1.3	20.00	0.08	1.0	1.2	945	27,400	2.05	2.65	Thin brown scale on all surfaces; machine marks visible	Thin dark film on all surfaces
Zircaloy-2 Specimens																			
Zr 2	2.81	8.6034	8.5156	8.5103	−93.1	19.50	0.29	4.0	4.7	20.00	0.28	3.9	4.5	1600	22,400	2.05	2.65	Apparently film free; scale on low flux holder and bolt only	Very thin film on all surfaces
Zr 3	2.81	8.0402	7.9518	7.9462	−94.0	19.50	0.29	4.0	4.7	20.00	0.28	3.9	4.6	1740	24,400	2.05	2.65	Apparently film free; scale on low flux holder and bolt only	Very thin film on all surfaces
Zr 4	2.81	8.4533	8.3805	8.3769	−76.4	19.50	0.24	3.3	3.8	20.00	0.23	3.2	3.7	1440	20,200	2.05	2.65	Apparently film free; scale on low flux holder and bolt only	Very thin film on all surfaces
Zr 5	2.81	7.9449	7.8722	7.8725	−72.4	19.50	0.23	3.1	3.6	20.00	0.22	3.0	3.5	1570	22,000	2.05	2.65	Apparently film free; scale on low flux holder and bolt only	Very thin film on all surfaces
Titanium Specimens (55AX)																			
Ti 1	2.81	5.8880	5.8920	5.8848	−3.2	19.50	0.01	0.2	0.2	20.00	0.01	0.2	0.2	1530	23,600	2.05	2.65	Some thin film on all surfaces; heavier at low flux end	Dark film on all surfaces; machine marks visible
Ti 2	2.81	5.8358	5.8374	5.8327	−3.1	19.50	0.01	0.2	0.2	20.00	0.01	0.2	0.2	1800	27,000	2.05	2.65	Some thin film on all surfaces; heavier at low flux end	Dark film on all surfaces; machine marks visible
Ti 11	2.81	5.8012	5.8029	5.7967	−4.5	19.50	0.02	0.3	0.3	20.00	0.02	0.3	0.3	1600	26,000	2.05	2.65	Some thin film on all surfaces; heavier at low flux end; dumbbell-shaped discoloration at fulcrum	Ski-shaped curve at low flux end; thin dark scale on all surfaces
Ti 12	2.81	5.9638	5.9647	5.9600	−3.8	19.50	0.02	0.2	0.3	20.00	0.02	0.2	0.3	1600	26,000	2.05	2.65	Some thin film on all surfaces; heavier at low flux end; dumbbell-shaped discoloration at fulcrum	Spotty thin dark scale; machine marks visible
Type 347 Stainless Steel Stress-Corrosion Specimen Holders																			
SS 1	0.75	11.2366	11.1740	11.1804	−56.2	10.00	0.28	3.8	4.5	10.00	0.28	3.8	4.5			3.50	4.52	Thin brown scale on all surfaces; machine marks visible	Some scale around bolt hole; machine marks visible
SS 2	4.75	11.1590	11.1629	11.1652	+6.2	10.00				10.00						1.10	1.42	Thin brown scale on all surfaces; machine marks visible	Some scale around bolt hole; machine marks visible
SS 3	0.75	11.1584	11.0987	11.0967	−61.7	10.00	0.30	4.2	4.9	10.00	0.30	4.2	4.9			3.50	4.52	Thin brown scale on all surfaces; machine marks visible	Some scale around bolt hole; machine marks visible
SS 4	4.75	11.2191	11.2245	11.2194	+0.3	10.00				10.00						1.10	1.42	Thin brown scale on all surfaces; machine marks visible	Some scale around bolt hole; machine marks visible

*Corrosion rates have been calculated both for the nominally exposed and the total specimen areas.

**Two corrosion rates are presented: one based on the total operation time of 630.3 hr and one based on the total radiation time of 536.8 hr (3 Mwhr of reactor time equivalent to 1 hr of total radiation time).

TABLE 12.7 (continued)

Sample No.	Distance from Front of Core Holder to Center of Specimen (in.)	Initial Weight (g)	As-Removed Weight (g)	Defilmed Weight (g)	Weight Change (mg)	Exposed Specimen Area (cm^2)	Corrosion Penetration (mils)	Corrosion Rate* (mpy) 630.3** (hr)	Corrosion Rate* (mpy) 536.8** (hr)	Total Specimen Area (cm^2)	Corrosion Penetration (mils)	Corrosion Rate* (mpy) 630.3** (hr)	Corrosion Rate* (mpy) 536.8** (hr)	Strain (μin./in.)	Stress (psi)	Neutron Flux at 3 Mw (neutrons/cm^2/sec $\times 10^{-12}$)	Power Density at 3 Mw (w/ml)	Surface Appearance: As Removed	Surface Appearance: After Defilming
Zircaloy-2 Stress-Corrosion Specimen Holders																			
Zr 1	0.75	9.4307				10.00				10.00						3.50	4.52	Apparently film free; scale on low flux holder and bolt only	Not defilmed
Zr 2	4.75	8.9833				10.00				10.00						1.10	1.42	Apparently film free; scale on low flux holder and bolt only	Not defilmed
Zr 3	0.75	9.0925	9.0716	9.0608	−31.7	10.00	0.19	2.6	3.1	10.00	0.19	2.6	3.1			3.50	4.52	Apparently film free; scale on low flux holder and bolt only	Thin film on all surfaces; machine marks visible
Zr 4	4.75	8.8223	8.8186	8.8109	−11.4	10.00	0.07	1.0	1.1	10.00	0.07	1.0	1.1			1.10	1.42	Apparently film free; scale on low flux holder and bolt only	Thin film on all surfaces; machine marks visible
Titanium Stress-Corrosion Specimen Holders (55AX)																			
Ti 1	0.75	6.5626	6.5621	6.5591	−3.5	10.00	0.03	0.4	0.5	10.00	0.03	0.4	0.5			3.50	4.52	Some thin film on all surfaces; heavier at low flux end	Beveled edges rough; flat surfaces clean
Ti 2	4.75	6.6108	6.6145	6.6103	−0.5	10.00	0.01	0.1	0.1	10.00	0.004	0.1	0.1			1.10	1.42	Some thin film on all surfaces; heavier at low flux end	Beveled edges rough; flat surfaces clean; some film around hole
Ti 3	0.75	6.4948	6.4919	6.4907	−4.1	10.00	0.04	0.5	0.6	10.00	0.04	0.5	0.6			3.50	4.52	Some thin film on all surfaces; heavier at low flux end; dumbbell-shaped discoloration at fulcrum	Beveled edges rough; flat surfaces clean; some film around hole
Ti 8	4.75	6.4321	6.4362	6.4320	−0.1	10.00	0.001	0.01	0.02	10.00	0.001	0.01	0.02			1.10	1.42	Some thin film on all surfaces; heavier at low flux end; dumbbell-shaped discoloration at fulcrum	Beveled edges rough; flat surfaces clean; some film around hole

*Corrosion rates have been calculated both for the nominally exposed and the total specimen areas.

**Two corrosion rates are presented: one based on the total operation time of 630.3 hr and one based on the total radiation time of 536.8 hr (3 Mwhr of reactor time equivalent to 1 hr of total radiation time).

UNCLASSIFIED
PHOTO 14689

Fig. 12.10. HRP In-Pile Loop EE Core Coupon Assembly.

areas such as the essentially stagnant area between the spacers and rods of the couple assemblies. This was particularly true of the Zircaloy assembly where corrosion product sealed the spacers to the rod. Disassembly of this rod required a screw-jack arrangement. Microscopic examination of the couple coupons indicated, at least qualitatively, that the actual contacting spots were attacked less than were the adjacent areas in which surface roughness prevented perfect matching. This could be an indication either of protection of the contact zone or increased corrosion in the crevice. The total corrosion was too small for any difference in appearance between the crevice surfaces and the free surface of the same coupon to be determined.

As mentioned in Sec. 12.1.2*b*, the core-reducer section of this loop contained a repaired pin hole similar to the one reported for loop FF.[4] Unlike the results of loop FF, there was no sign of a cavity or of localized attack in or around the region of the repair weld. A photograph of the weld region after exposure is shown in Fig. 12.11. No metallographic examination of this area is planned.

(c) Quantitative Results of Inspection and Evaluation. – The various coupons and specimens in the core assembly were all defilmed cathodically in an inhibited 5% sulfuric acid solution in the normal manner. All attempts to defilm the in-line coupons in the Solid State Division facilities failed. After the samples were returned to Building 4501, a further attempt was made to defilm the in-line coupons in a temporary arrangement. Better electrical contact with the specimen was obtained and most of the coupons were defilmed with the standard cathodic treatment at this time.

Coupons Z-12, T-3, and 740-A from the in-line group were not defilmed, because they had been transferred to the Solid State Division for x-ray and metallographic analysis. Coupons Z-20, 743-A, T-9, T-16, Z-37, and 787-A from the core array are to be analyzed by the X-Ray Diffraction and Metallographic groups. Portions of the stainless steel system from the core, pressurizer, and pressurizer heater will be examined metallographically, as will the various stress specimens.

All the remaining stainless steel and Zircaloy-2 coupons from the core array, together with the

Fig. 12.11. HRP In-Pile Loop EE Type 347 Stainless Steel Core Section, as Removed from the Loop.

spacers from the couple assemblies and three portions of the stainless steel core, were decontaminated chemically and transferred to the Analytical Chemistry Division for activation analyses. These data are presented in Table 12.6.

Sample weight data, together with other pertinent information, are presented in Table 12.7. Two different values for corrosive penetration were calculated for each specimen from the weight data. One value is based on only the exposed area of the specimen, and the other is based on the total area. Calculated values for corrosion rates which correspond to the two different penetration values are also shown. The value for the neutron flux, to which a given core specimen was exposed during operation, is also listed in the table. For those specimens which were subjected to activation analyses, the value shown is the measured one. Values for other specimens are those which correspond to the specimen position in the core and were obtained by reference to the flux-position plot in Fig. 12.8. The values for the stress specimens and for the core holders were obtained by averaging logarithmically the flux values at the ends of the specimen.

12.1.4 Discussion of Results of Experiment EE

(a) Zircaloy-2. – Corrosion rate values from Table 12.7 for Zircaloy-2 core specimens are plotted in Fig. 12.12 as a function of the fission power density to which the specimens were exposed. The rate values chosen for this plot are those calculated by using total specimen areas and radiation time. As can be seen in Fig. 12.12, values at different power densities for the core coupons and for those coupled specimens which were included in the stainless steel rod and spacer assembly are in near agreement. The solid, straight line appears to represent these data satisfactorily. The points for those coupled specimens which were on the Zircaloy-2 rod and spacer assembly are consistently above the solid line, and a second, broken line has been drawn through these points. The values for the stress specimens are appreciably higher than those for any of the coupons. Points for the stress-specimen holders, which were located at the extremities of the specimens, are in reasonable agreement with the coupon data.

From the results for coupons from a given couple assembly and from the core holder, there is no indication that, under irradiation, coupling has any effect on corrosion. It may be speculated that the difference between coupons from the two assemblies is connected with coupling in some way, but this is only speculation.

The results obtained with the stress specimens are not regarded as indicative of an accelerating effect of stress on the corrosion under irradiation. These specimens were prepared prior to exposure by sandblasting after heat treatment. In contrast, the coupons were sanded only enough to remove

[redacted] [redacted]

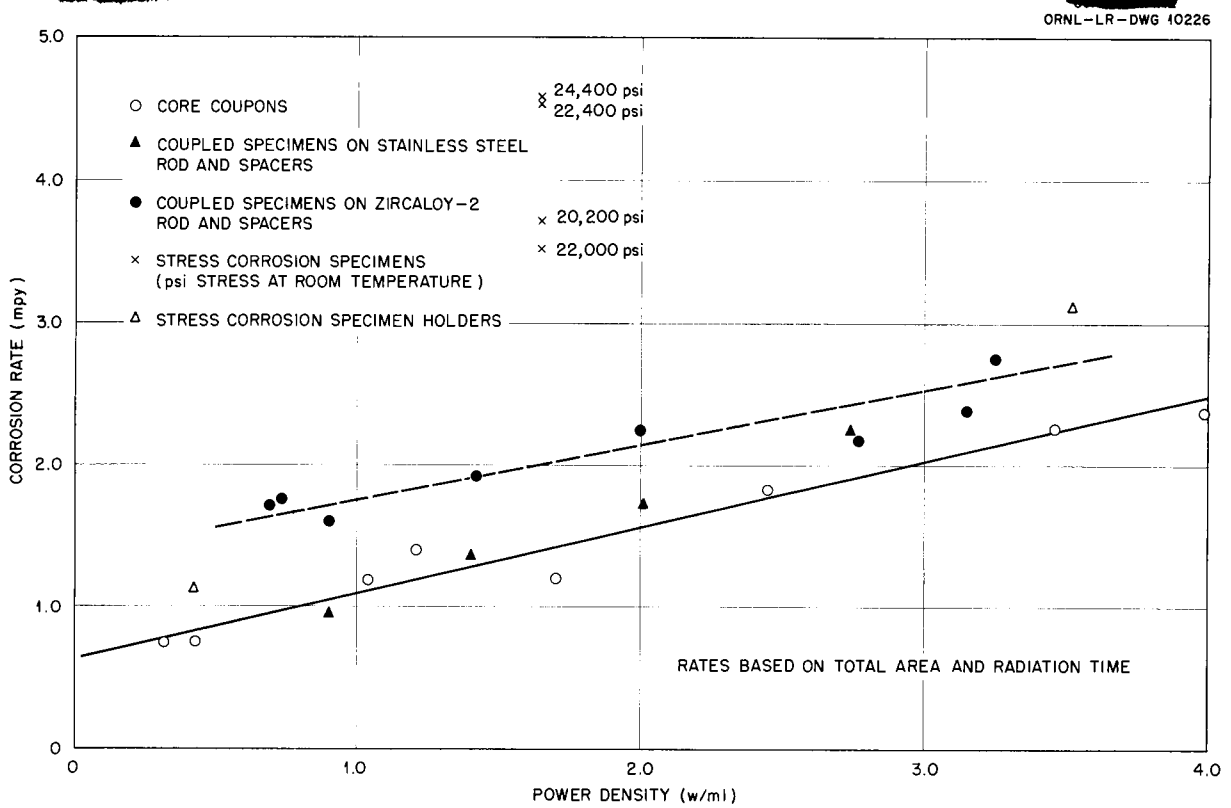

Fig. 12.12. Corrosion Rate of Zircaloy-2 Specimens vs Power Density for Loop EE.

the film developed during heat treatment. Consequently, the surface characteristics, for example, roughness, of the stress specimens and coupons were different, and this difference probably accounted for the observed difference in corrosion rates.

It should be pointed out that the calculation of the corrosion rates based on total specimen area of loop specimens is an innovation with this report. Prior to this time, the exposed area only was employed. As mentioned in Sec. 12.1.3*b*, no difference was apparent between the degree of attack on the exposed and covered areas for any of the specimens, except for those stainless steel specimens which were severely corroded. For these latter specimens the corrosion product probably sealed the crevice in the clamped portion and protected the clamped portion against further severe attack. For all Zircaloy-2 specimens exposed to date, the attack has been moderate, and, in general, crevices have probably not been sealed. The use of the total area thus appears to be justified. For comparison between the two methods of treatment of the data for Zircaloy-2, the corrosion rate values calculated on the basis of exposed area are plotted in Fig. 12.13, as were the total area values in Fig. 12.12. A difference is apparent in the indicated relationships between the attack of the different types of specimens. However, the conclusions which would be drawn from the plot of the data in Fig. 12.13 are about the same as those drawn from Fig. 12.12.

Results for the corrosive attack of Zircaloy-2 at different fission power densities, as indicated by the holder coupon data, are in near agreement with the results of the previous experiments, FF[4] and GG.[2] The data from the three experiments are compared in Fig. 12.14, where corrosion rate values calculated from exposed specimen area and radiation time are plotted against the power density at the specimen surface.

(b) Titanium 55AX. – Corrosion rate values for the various titanium specimens are plotted in

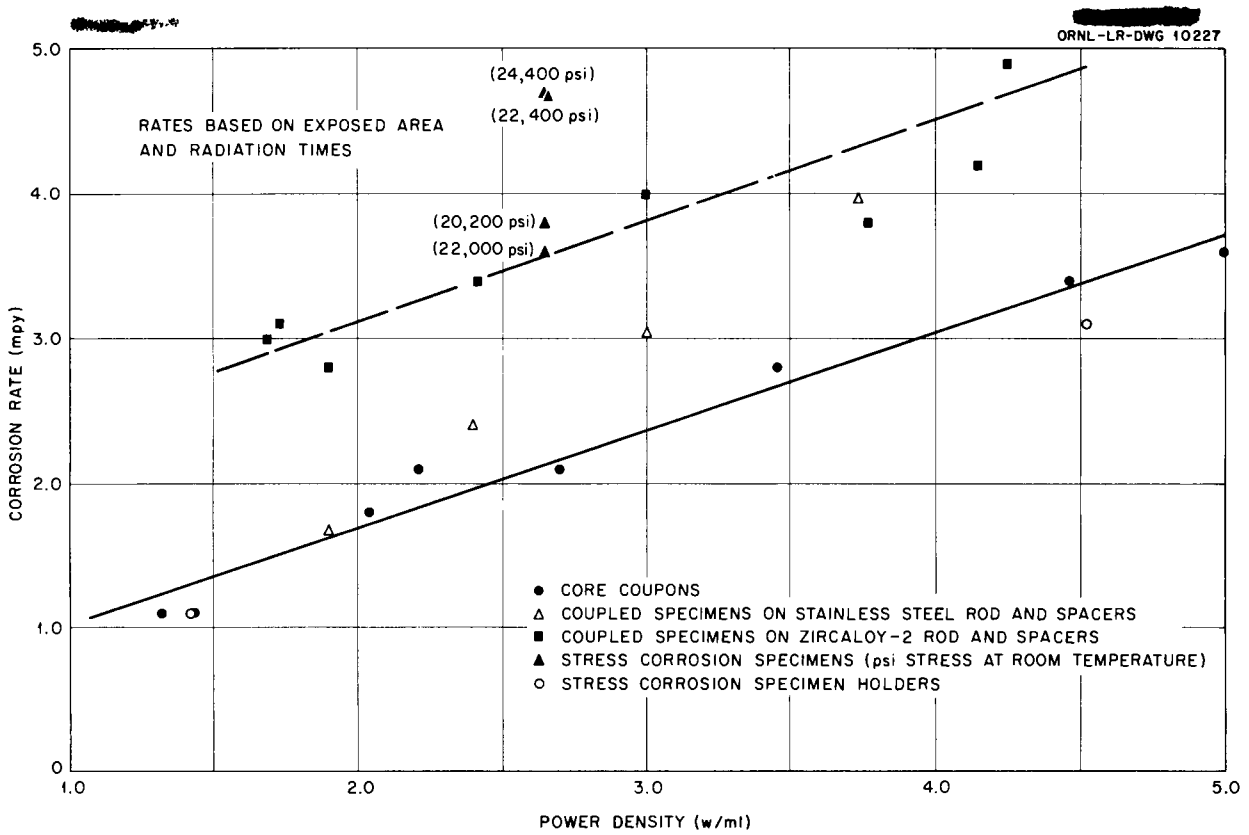

Fig. 12.13. Corrosion Rate of Zircaloy-2 Specimens vs Power Density for Loop EE.

Fig. 12.15 in the same manner as the Zircaloy-2 results were plotted in Fig. 12.12. Again, the rate values employed are those calculated from total area and radiation time.

The results for the core coupons shown in the plot are of especial interest. In contrast to the behavior of Zircaloy-2, no significant dependence is apparent between corrosion rate and power density at the specimen surface. However, a velocity dependence is indicated. The number adjacent to each point is the value for the solution velocity (in fps) past the lead edge of the specimen. The three coupons which exhibited significantly higher rates than the others were in the highest velocity region of the holder.

The results for the specimens from the coupled assemblies are in fair agreement with those for the low-velocity coupons in the holder. No evidence is apparent of an acceleration of corrosion due to coupling.

No increase of the average corrosion rate of titanium due to stress is indicated by the results of the stress specimens. These specimens were not sandblasted.

(c) Stainless Steel. – Corrosion rate values for the various stainless steel specimens are plotted in Fig. 12.16. Except as noted, these rate values were calculated from total areas and radiation time. It should be noted that the corrosion rate scale is broken and changed for the three coupons which were in forward position in the core holder. The corrosion rate for these specimens was in the range 50 to 60 mpy. None of the other holder coupons exhibited a rate of more than 2 mpy. The number adjacent to each holder-coupon point is the value for the solution velocity (in fps) past the lead edge of the specimen. No simple effect of velocity on the corrosion rate is apparent. The holder coupon results from Loop EE are compared in Fig. 12.17 with those from experiment DD. Here the penetration, which is calculated from weight data, is plotted along the ordinate, and specimen position in the holder is plotted on the abscissa. The front edge of the leading

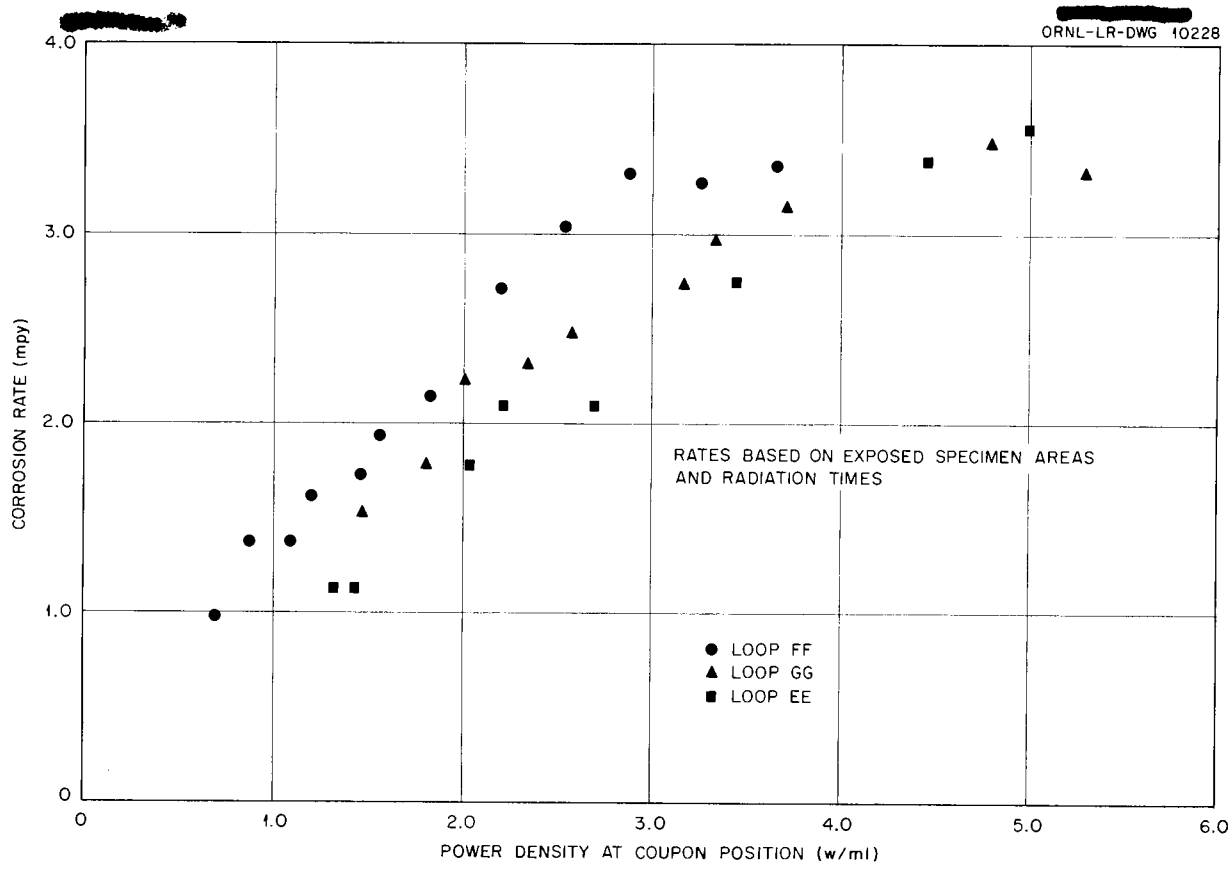

Fig. 12.14. Zircaloy-2 Core Coupon Corrosion Rates vs Power Density at Coupon Position.

specimen is the zero position. The LITR energy accumulated during the EE operation was about twice that for DD. Furthermore, the power density at a given position in EE was greater than twice that at the similar position in DD. However, the total penetration for a majority of the EE coupons was below that for the similarly located DD coupon. The initial solution for this experiment was the same as for DD, and no explanation is apparent for the lack of correlation.

No evidence of increased corrosion due to coupling or to stress is apparent from the results shown in Fig. 12.16.

Values for type 347 stainless steel corrosive penetration, which correspond to the amount of nickel and manganese found in the loop solution and to measured oxygen consumption, are plotted in Fig. 12.18. The method of calculation and of plotting is the same as that employed previously.[1-3] The curves are of the same general type as those obtained for experiment DD for which the initial solution charge was the same as for this experiment. The average corrosion rate, which is calculated from the oxygen data as plotted and from the total circulation time, is 1.7 mpy. The average rate for the exposure after the first 150 hr is only slightly lower at 1.6 mpy.

An attempt to correlate the nickel corrosion results with the weight-loss data for steel specimens suggests that some portion of the loop corroded at a rate that was much more rapid than average, or, alternatively, that the attack of the specimens is not representative of the attack of other surfaces which were presumably in similar environments. The total amount of steel oxidized during in-pile operation, according to the nickel data, is roughly 6.7 g. From the specimen weight data, it may be estimated, with certain assumptions as a basis, that the total amount of steel oxidized during this same period

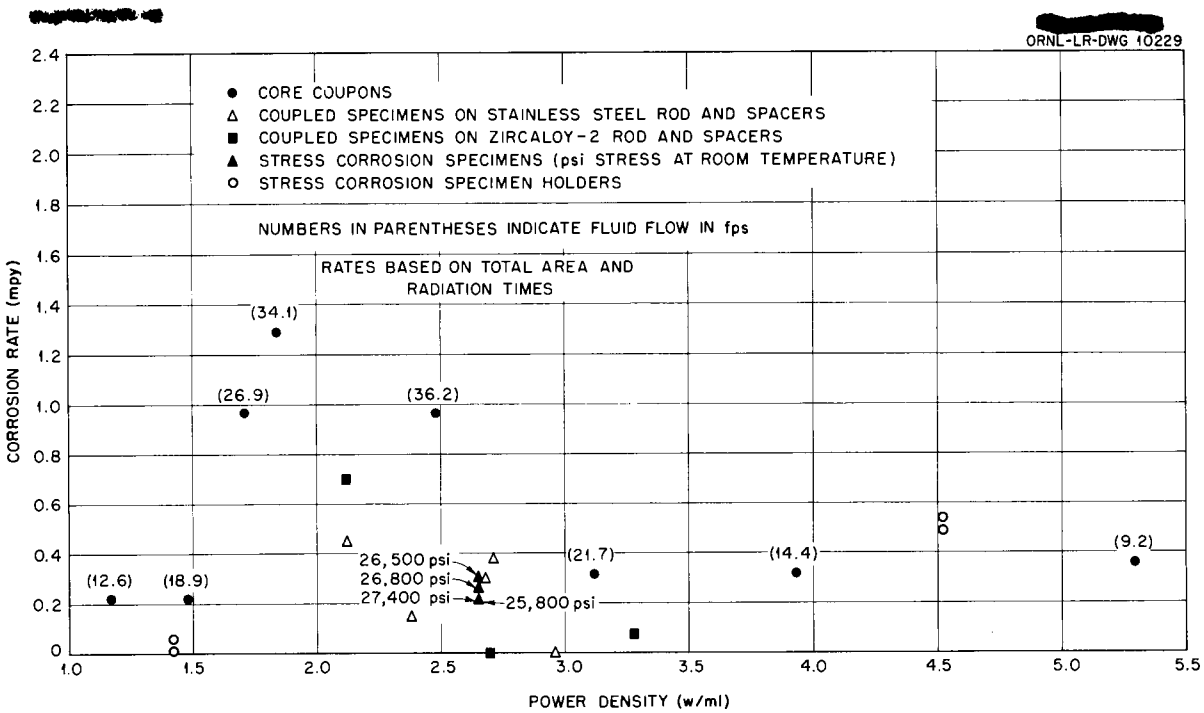

Fig. 12.15. Corrosion Rates of Titanium Specimens vs Power Density for Loop EE.

was 3.1 g. The basic assumptions are as follows: (1) all steel surfaces in contact with high-temperature solution, excluding the core, corroded uniformly and at an average rate equal to that for the in-line specimens and (2) the attack of a steel surface which was at a given flux in the core was the same as that measured for those specimens which were located outside the core holder and in the same given flux. The line shown in Fig. 12.16 was extrapolated to obtain values for the rates at the higher power densities in the core cap.

The most likely explanation of the discrepancy between the nickel and specimen data is that of localized attack in some area of the loop. Possible areas in which such localized attack may have taken place are the heater section of the main stream, which, as mentioned in Sec. 12.1.2*b*, was not subjected to the customary pretreatment, and the pressurizer.

[5]G. H. Jenks *et al.*, *HRP Quar. Prog. Rep. July 31, 1955*, ORNL-1943, p 126–130.

12.2 LITR BOMB TESTS

G. H. Jenks

A. L. Bacarella
W. E. Clark
H. O. Day
H. A. Fisch
D. T. Jones
K. S. Warren
L. F. Woo
W. C. Yee

12.2.1 Introduction

Further studies of the effect of reactor radiation on the corrosion of Zircaloy-2 by uranyl sulfate solutions have been conducted in the LITR during the past quarter. The bomb-dismantling equipment has also been put into operation, so that additional information, such as pin data and solution analyses, is available for some of the experiments reported previously. Experiments in type 347 stainless steel bombs are also being continued, especially with a view toward determining the effect of high oxygen pressure and excess acidity.

The intensities of reactor radiations at the bomb-exposure position in beam holes HB-5 and HB-6 have been determined previously[5] by means of cobalt monitor measurements; values of 1×10^{13} and 4.8×10^{12} neutrons/cm^2/sec, respectively, were reported for the fluxes in these positions.

[redacted] [redacted]

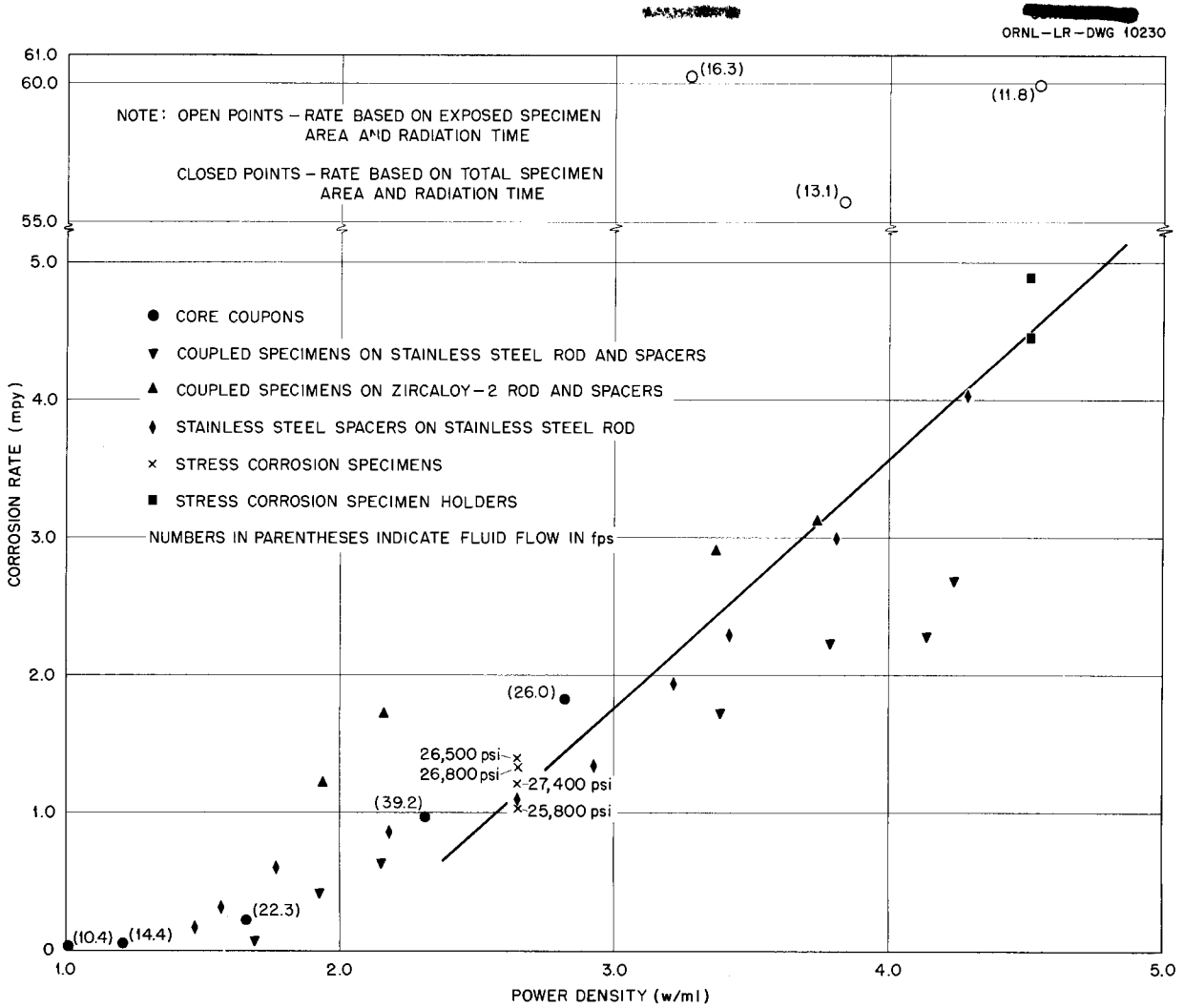

Fig. 12.16. Corrosion Rate of Stainless Steel Specimens vs Power Density for Loop EE.

Recently, data have been obtained from activation analyses of pins contained in the LITR bombs under irradiation. These data indicate that the values for the flux given previously must be revised upward, to 1.23×10^{13} for HB-5 and 6.8×10^{12} for HB-6. In Table 12.8, only the values for power density given for experiments Z-10 and Z-12 are based on actual experimental activation analyses. The figures given in column ten for the subsequent experiments have been estimated from Z-10 and Z-12 data by making appropriate adjustments for solution concentration, density, enrichment, and temperature.

12.2.2 Experimental Conditions and Results

Experimental conditions and data for recent in-pile experiments are given in Table 12.8. Column two lists the LITR beam hole in which the numbered bomb was irradiated. Some bombs were irradiated at more than one temperature and are so listed in column eight. Values given in column ten for fission-power density were calculated from the solution composition and from the neutron flux obtained from pin activation analyses when the LITR was operating at 3 Mw. In column eleven, irradiation time was calculated on the basis of

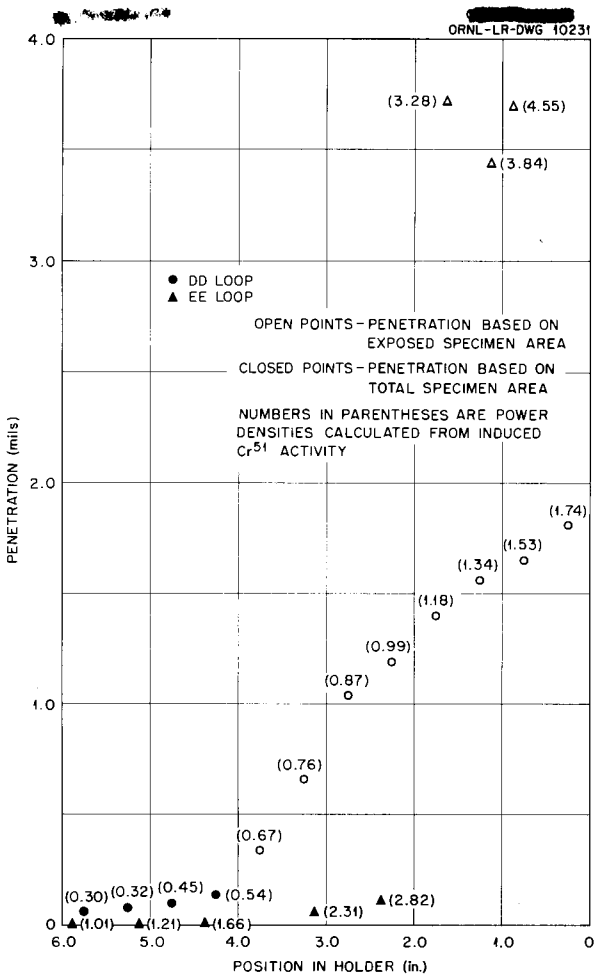

Fig. 12.17. Comparison of Corrosive Penetration of Specimens from the Core Holder from Loops DD and EE.

3 Mwhr of LITR energy equivalent to 1 hr of exposure.

Experiments Z-10, Z-12, Z-13, and H-85 were described previously.[5] The data are repeated because of the changes in the power densities and to show the correspondence between corrosion based on oxygen consumption and pin-weight loss where both are available. The results presented for experiments Z-15, H-93, and H-94 are preliminary and will be discussed in detail when all the data have been obtained.

12.3 MTR BOMB TESTS

G. H. Jenks

R. J. Davis R. A. Lorenz
D. T. Jones J. R. McWherter
H. H. Stone

12.3.1 Experiment ORNL-15-1

The bomb assembly from the first rocking-bomb experiment at the MTR was dismantled in the MTR hot cell and returned to ORNL for examination. The hot cell work at the MTR was carried out by personnel of the Phillips Petroleum Company.

12.3.2 Experiment ORNL-15-2

In-pile operation of a second MTR experiment, ORNL-15-2, has been completed. The conditions employed for this experiment were as follows:

Solution	
UO_2SO_4	0.04 *m* (93.2% enrichment)
$CuSO_4$	0.05 *m*
H_2SO_4	0.02 *m*
Bomb material	Zircaloy-2
Test temperature	~295°C

Two pin corrosion specimens of Zircaloy-2 were mounted in a rack within the bomb. The experiment was inserted during the month of August and removed about two weeks later during the scheduled reactor shutdown. During the inserted time the bomb was exposed to the high neutron flux for three different periods, which varied in length from 6 to 8 hr. For the remainder of the time the bomb was retracted into a cadmium sleeve. An estimated solution temperature of 295°C was maintained during the high-flux exposures. It should be pointed out, however, that the estimated temperature of the bomb walls which were in contact with the solution was 275 to 280°C during the high-flux operation. The solution temperature during the majority of the retracted operation was 240°C. The estimated maximum value for the average fission power for the high-flux operation was 35 w/ml; that for the retracted operation is uncertain, but it was probably less than 2 w/ml.

The results of oxygen pressure measurements of corrosion during the in-pile operation are shown

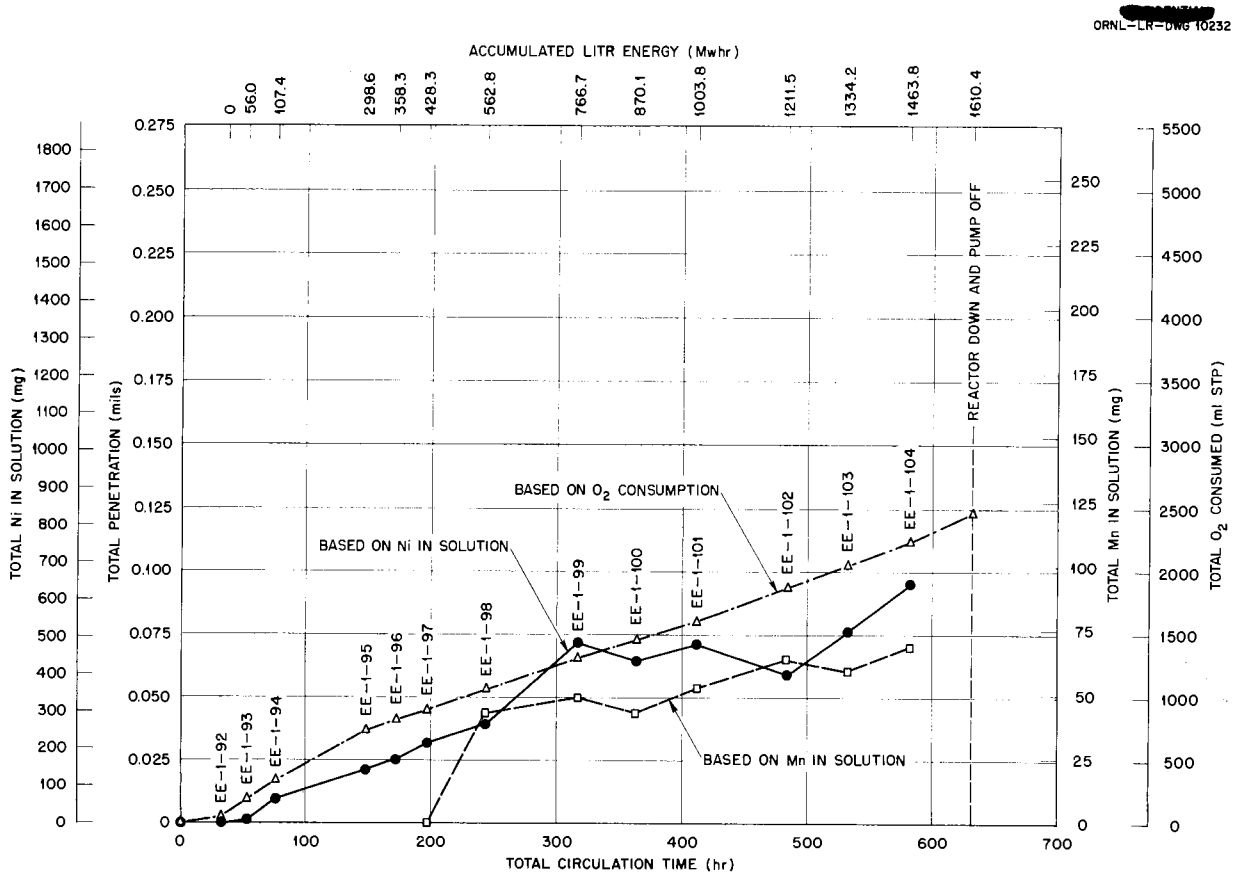

Fig. 12.18. Over-all Corrosion Penetration for Type 347 Stainless Steel.

in Fig. 12.19. The bomb position and the solution temperature during given periods of operation are also shown. The temperature of the solution during the time a given pressure measurement was made is indicated for each point by a symbol. The bomb was placed in the retracted position for each measurement.

The corrosion rate which is indicated by these results is about 49 mpy for the first exposure in the high-flux region. The indicated rates for the second and third exposures are somewhat lower; however, for these exposures the bomb was not fully inserted but was withdrawn ¼ and ½ in., respectively. This procedure was followed because the cooling capacity of the unit was insufficient to prevent overheating of the bomb when it was in the fully exposed position. This stemmed from accidental dislocation of a water-cooling line in a repair operation just prior to insertion.

For comparison with results at lower power densities, the comparable LITR experiment, Z-12, which was at an estimated power density of 3.5 to 4 w/ml, exhibited a corrosion rate of 10 mpy; that is, for a power density lower than the one for this experiment by a factor of 10, the corrosion rate was a factor of 5 lower.

The total pressure which is measured in an experiment of this type is a combination of the steam, radiolytic, and excess oxygen pressures. Due to uncertainties in the temperature of the solution, a result of intense radiation heating, the vapor pressure is difficult to determine accurately and, hence, the radiolytic-gas pressure cannot be determined accurately. However, as based on the estimated values of the solution temperatures which are considered most accurate, the radiolytic-gas pressures during the high-flux exposure were well below 100 psi. A pressure of 110 psi was predicted by extrapolation of LITR data to the higher power densities and higher temperatures of this experiment.

TABLE 12.8. LITR BOMB CORROSION STUDIES

Bomb No.	LITR Beam Hole	Bomb Material	Solution Composition (m)			Enrichment (% U^{235})	Exposure Temperature (°C)	Starting Oxygen Pressure at 100°C (psi)	Fission Power Density (w/ml)	Exposure (days)[a]	Corrosion Rate (mpy)	
			UO_2SO_4	$CuSO_4$	H_2SO_4						O_2 Data	Pin Data
Z-10	HB-6	Zircaloy-2	0.17	0.02		44	225	480	4.8	7.9	3.1	5.8
							250		4.6	4.5	5.7	5.8
							280		4.4	6.6	10.0	5.8
							290		4.3	1.7	12.2	5.8
Z-12	HB-5	Zircaloy-2	0.043	0.05	0.02	93.2	280	540	4.1	9.8	10.3	9.0
							300			5.4	10.3	9.0
Z-13	HB-5	Zircaloy-2	0.17	0.02		0.03	250	540	0.005[b]	23.4	1.2	c
							280			11.7		
							300			12.5		
							250			19.5		
Z-15	HB-5	Zircaloy-2	0.17	0.04	0.04	93.2	280	315	16.7[b]	4.2	14.6	c
H-85	HB-6	Type 347 stainless steel	0.17	0.01	0.015	93.2	250	750	~9.6[b]	12.8	<1	c
H-93	HB-6	Type 347 stainless steel	0.16	0.01	0.03	93.2	250	830	~9.4[b]	38.4	~1	c
H-94	HB-6	Type 347 stainless steel	0.16	0.01	0.03	93.2	250	300	~9.4[b]	Continuing		c

[a]3 Mwhr of LITR energy = 1 hr of exposure.

[b]Estimated from induced activity measurements obtained in Z-10 and Z-12.

[c]To be determined.

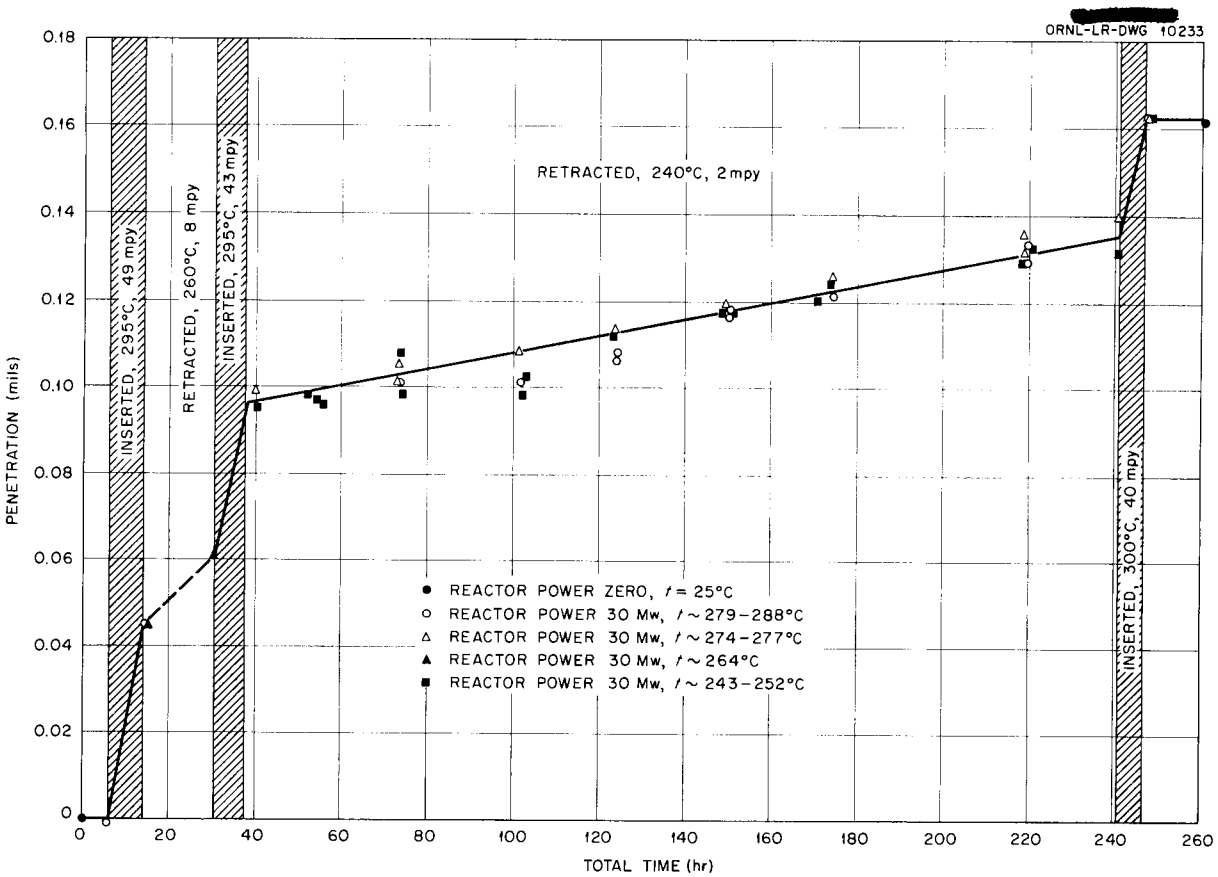

Fig. 12.19. Corrosion Data for MTR Bomb Experiment ORNL-15-2.

13. METALLURGY

G. M. Adamson
R. G. Berggren
G. E. Elder
J. I. Federer
W. J. Fretague
J. R. Johnson
J. L. Gregg
W. J. Leonard
M. L. Picklesimer
G. B. Wadsworth
J. C. Wilson
O. Zmeskal

13.1 PHYSICAL METALLURGY OF ZIRCONIUM AND ITS ALLOYS

M. L. Picklesimer

13.1.1 Properties of Zircaloy-2 Core-Tank Material

An investigation of the metallography, heat treatment, and mechanical properties of the Zircaloy-2 HRT core-tank material (plates 7 and 8) has been initiated to establish the changes in properties that may be expected in service.

Specimens of Zircaloy-2 plate 8 have been heat-treated to establish the beta-to-(alpha-plus-beta) and alpha-to-(alpha-plus-beta) temperatures and to provide metallographic standards for the interpretation of structures. The beta-to-(alpha-plus-beta) temperature has been found to be 985 ± 2°C and the alpha-to-(alpha-plus-beta) temperature to be at or above 825°C and probably not higher than 830°C. All specimens were held at temperature for 30 min and then water quenched. The beta grains in specimens containing 75%, or more, beta were very large, indicating that beta grain growth is very rapid. Full annealing of the hot-rolled alpha structure was shown metallographically to have occurred at 800°C without excessive grain growth. Stringers in the metal began to break up in the high alpha range and were almost completely dissolved after 1 hr at 1000°C.

The linear coefficient of expansion of the Zircaloy-2 (plate 8) material was determined as a function of rolling direction in the plate. Cylindrical specimens ¼ in. in diameter by 2 in. in length were run in air in a dilatometer. Duplicate heating and cooling curves from room temperature were determined. As shown by the data presented in Table 13.1, there was considerable preferred orientation in the plate.

13.2 WELDING DEVELOPMENT

W. J. Leonard

13.2.1 Substitution of Nitrogen for Argon as a Backup Gas in Inert Gas Arc Welding of Type 347 Stainless Steel

A series of welds was made to determine the feasibility of substituting nitrogen for the more expensive argon as a backup gas in the inert-gas-shielded tungsten arc welding of type 347 stainless steel. In HRP-2, and similar welding specifications, high-purity argon was used inside the pipe or vessel to prevent oxidation of either the molten or heated metal. In the reported tests

TABLE 13.1. MEAN LINEAR COEFFICIENT OF THERMAL EXPANSION (μin./in./°C) OF ZIRCALOY-2 PLATE AS A FUNCTION OF ROLLING DIRECTION

Temperature Range (°C)	Longitudinal		45 deg		Transverse	
	Run 1	Run 2	Run 1	Run 2	Run 1	Run 2
0–500	5.0	5.1	5.5	5.5	5.9	5.8
100–200	5.1	5.2	5.4	5.3	5.6	5.6
200–300	5.1	5.1	5.6	5.5	5.9	5.9
300–400	5.1	5.0	5.5	5.5	5.8	5.8
400–500	4.7	4.9	5.5	5.4	6.3	6.1

welds were made according to HRP-2 specifications, except that commercial nitrogen (water-pumped) was used as the backup gas in half of them. The pipe welded was 2½-in. IPS sched 40, type 347 stainless steel with a type 347 welding wire which deposited 7 to 10% ferrite.

All welds satisfactorily passed liquid penetrant tests upon completion of the root pass and radiographic inspection after the final filler passes. Mechanical testing revealed no differences in the physical properties of the two types of welds. If nitrogen is deliberately added to weld metal, a refined grain structure with a reduction in both massive and total ferrite is usually found; such was not the case in the welds made with the nitrogen backup. Metallographically, no hardened surfaces were noted on the root faces to indicate the formation of a nitride, nor were there any discernible microscopic structural differences in the constituents of the two types of welds (Fig. 13.1). Microhardness surveys of the welds did indicate one detectable difference. The hardness of the surface weld metal adjacent to the nitrogen and of the metal to a depth of approximately 0.030 in. was 210 VHN, while the balance of the weld metal averaged 185 VHN. The average hardness in the argon welds was 175 VHN with no hardness gradient present from the surface to the interior in these welds. This surface effect is ascribed to a solid-solution hardening by nitrogen and is not considered to be of any particular significance.

To evaluate their dynamic-corrosion resistance, coupon-type specimens, with the root reinforcement left intact, were machined from the two types of welds. The specimens were placed in a holder in such a position that the root and adjacent area would be exposed to the corrosive environment. The run, E-50, was made at 300°C for 404 hr in 0.004 *m* uranyl sulfate, containing 0.004 *m* sulfuric acid and 0.005 *m* copper sulfate, with 150 psi oxygen pressure. The velocity was computed to average 15 fps at the crown of the root face. The corrosion rates on all the specimens were essentially the same. The nitrogen gas-backed specimens averaged a loss of 18 mpy during the run, while the argon-backed specimens averaged a loss of 20 mpy. The results of radiographic, physical, and mechanical inspection and corrosion tests of welds made with the use of these two gases as an inert backup indicated no difference in the quality of the resultant welds.

13.2.2 Development of a Procedure for the Welding of Titanium–Carbon Steel Composites

Two basic designs, submitted by The Babcock & Wilcox Co. for possible welding of titanium-lined, carbon-steel pipe, were evaluated for feasibility and quality. Both these designs required accessibility from both sides and were intended only for very large pipe or plate. The aim in both cases was to produce a complete bond across the joint.

The first design consisted in a lap weld with the weld in the titanium liner being offset, longitudinally, about ½ in. from the root of the carbon

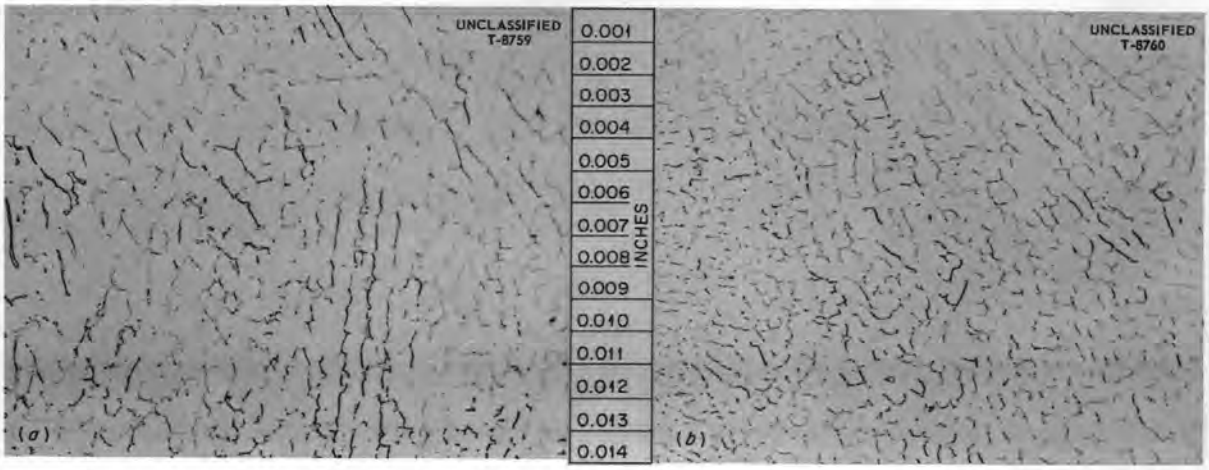

Fig. 13.1. Comparison of the Structure of Welds Made with Argon and Nitrogen as Backup Gases. (*a*) With nitrogen. (*b*) With argon.

steel weld. The procedure called for first welding the titanium from the back side and then completing the weld in the carbon steel, using standard ASME Boiler Code designs for the carbon steel weldments.

For evaluation of this joint design, a $\frac{1}{8}$-in. titanium plate was clamped to the root side of a $\frac{3}{4}$-in. carbon steel plate. The weld was made only in the steel, using a $\frac{1}{16}$-in. land, a $\frac{3}{16}$-in. root gap, and a 75-deg included angle; an E6010 electrode was used to make the weld. This condition simulated the weld design where the carbon steel root pass could penetrate the titanium liner. With this design a brittle joint with complete penetration of the titanium resulted. When the clamps were removed, the two plates fell apart. Figure 13.2 shows the underside of the steel and the top of the titanium. The carbon steel weld was of good quality in the portion above the root.

In the second design a $\frac{1}{8} \times \frac{3}{4}$ in. Armco ingot iron insert was placed on the titanium at the root of the steel weld. The insert was fitted into a groove machined in the face of the steel. A double butt type of weld was recommended. Penetration of the titanium weld metal into the ingot iron insert again resulted in a very brittle joint.

A composite insert was then made by tack-welding together the edges of $\frac{1}{16}$-in.-thick sheets of titanium and ingot iron. This composite insert, which was $\frac{1}{8} \times \frac{3}{4} \times 12$ in., was then used similarly to the one discussed above. Two plates were made with such an insert. In the first, the titanium welding was carried out in a dry box and in the second, in air. All steel welding was done in air.

In both cases, when the clamps were removed, the welds separated through the joint in the insert. The welding stresses had been sufficient to rupture the tack welds. As was intended, neither weld bead had completely penetrated its half of the insert, and no brittle phases were formed. Little difference was observed between the titanium weldments made in the dry box and those made in air. Both the steel and the titanium welds were satisfactory when considered individually.

Neither of these proposed designs appears feasible as a satisfactory method for welding titanium-lined, carbon steel pipe. The second method could probably be developed into a satisfactory procedure if the requirement of a bond between the steel and titanium were waived or if a ductile transition material were found.

UNCLASSIFIED
T-8523

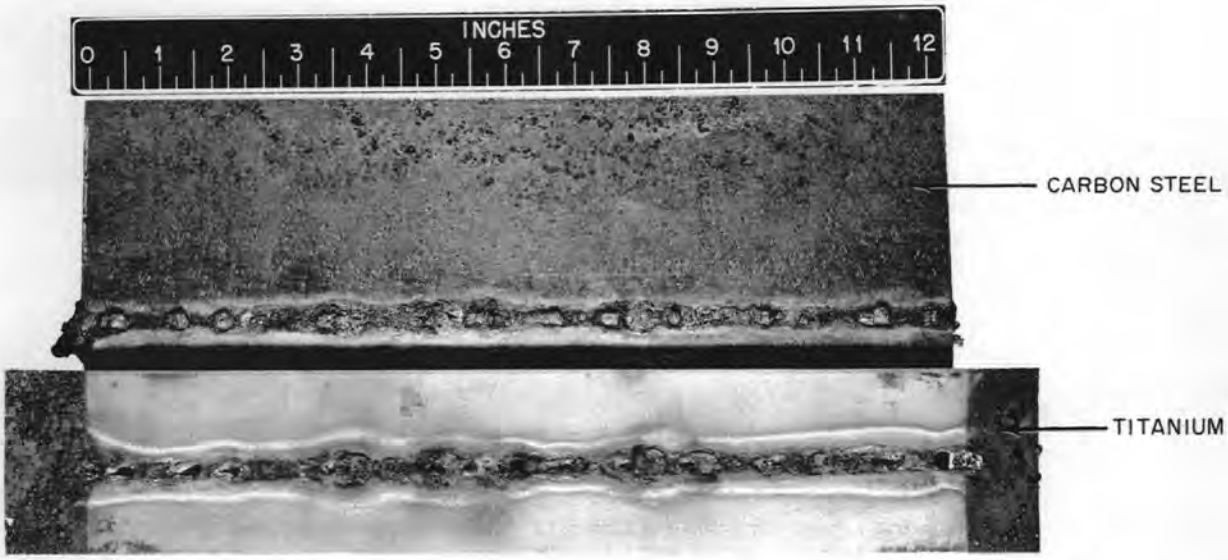

Fig. 13.2. Fracture Line in Butt-Welded Titanium–Carbon Steel Composite Plate. (*a*) Carbon steel. (*b*) Titanium.

13.3 METALLURGY OF CORROSION

J. I. Federer G. B. Wadsworth
J. R. Johnson O. Zmeskal

13.3.1 Stress Corrosion Cracking of Austenitic Stainless Steels

Operation of the stress corrosion apparatus described in previous reports[1,2] has been continued during this period. Several type 304L stainless steel specimens have been tested at stresses from 10,000 to 19,000 psi, with no indication as yet of a safe threshold stress above 10,000 psi. A specimen at 7,500 psi broke in the salt plug, and one at 5,000 psi broke in the vapor phase region. Duplicate specimens at the low stresses have not yet been run but are scheduled. No further work has been done on type 347 stainless steel.

Half-cell measurements against a calomel electrode have been made, in an etching solution of HCl, picric acid, and alcohol, on annealed and cold-worked type 304L stainless steel specimens. The cold-worked (partly martensitic) specimen was more negative than were the annealed specimens. The measurements were reasonably reproducible on freshly prepared surfaces but not on specimens that had been in the etching solution for an extended period of time. Full-cell measurements were made on cold-worked vs annealed specimens in the solution but were not reproducible, probably because the surfaces of the specimens were not freshly prepared. However, the emf was of the proper magnitude and direction.

13.3.2 Stress Corrosion Cracking of Inconel-X

Inconel-X is being investigated for possible use as a spring material for valves where it will only infrequently be in contact with uranyl sulfate solutions and for only short periods of time.

Duplicate Inconel-X stress corrosion specimens are under test in the magnesium chloride at 70,000 psi. The specimens were solution-treated at 2150°F and aged at 1500°F, according to the recommended practice for springs to be used below 1100°F. While the test times are still short, the results look encouraging.

[1]W. O. Harms, J. I. Federer, and G. B. Wadsworth, *HRP Quar. Prog. Rep. Jan. 31, 1955*, ORNL-1853, p 155–157.

[2]W. O. Harms, J. I. Federer, and G. B. Wadsworth, *HRP Quar. Prog. Rep. April 30, 1955*, ORNL-1895, p 161–166.

13.3.3 Effect of Hydrogen Content on the Corrosion Resistance of Zirconium Alloys

The apparatus which has been constructed for adding known quantities of gas to metal specimens has been described in a previous report.[3]

Zircaloy-2 specimens to be subjected to in-pile corrosion tests were hydrogenated in four groups of eight specimens to 500, 1000, 2000, and 3000 ppm hydrogen. The specimens were inserted into a molybdenum wire basket to prevent contact of the specimens with the quartz tube during the hydrogenation and homogeneization. A test blank run on the molybdenum wire basket for 18 hr at 400°C was made, and the hydrogen absorption by the basket was found to be negligible.

Difficulty in the proper preparation of the specimens was experienced during the first runs because of a hydride layer that was formed on the surfaces of the specimens when hydrogen was added at 400°C. Due to the rather large volume increase associated with the formation of the hydride, the surfaces of the specimens were cracked and broken. These conditions were remedied by homogeneizing the specimens at 900°C for 24 hr. The surfaces of the specimens so treated were not ideal, but the press of time prevented preparation of new specimens. Microexamination of the hydrogenated Zircaloy-2 material revealed that the hydride had precipitated in the grain boundaries instead of precipitating randomly throughout the specimen in the needlelike structure commonly observed in high-purity zirconium.

Specimens containing from 5 to 1000 ppm hydrogen have been prepared from arc-melted crystal-bar plate zirconium for metallographic standards and to provide experimental specimens for an attempt to develop a positive identification technique for zirconium hydride. A completely satisfactory etching procedure has not yet been established.

13.3.4 Nature of Zirconium Oxide Films

It was suggested that a study of the oxidation of zirconium and its alloys might reveal why corrosion under radiation is more severe than normal corrosion. An observation of the results of neutron damage to zirconium oxides, both monoclinic and cubic, indicated that the cubic phase may be more stable under irradiation. For a dose of 2×10^{20}

[3]W. O. Harms, J. I. Federer, and G. B. Wadsworth, *HRP Quar. Prog. Rep. Jan. 31, 1955*, ORNL-1853, p 158.

nvt (Hanford) it was found that, in a sample which originally was a mixture of the monoclinic and cubic phases, only the cubic phase remained. A dose of 1×10^{20} nvt showed a definite decrease in the amount of monoclinic phase present. It is well known that on heating monoclinic ZrO_2 a transformation, monoclinic to tetragonal (very similar to the cubic), occurs at about 1050°C. The transformation involves sufficient atomic rearrangement that pieces of ZrO_2 normally crack and crumble. It is suggested that the effect of neutrons on monoclinic ZrO_2 may be similar and that a protective monoclinic oxide film on the metal might be destroyed soon after its formation.

The protective film on zirconium alloys has been observed to be essentially monoclinic. Careful observations at Battelle indicate that a very thin tetragonal layer may lie next to the metal. Observations at ORNL, on much thicker layers, showed only monoclinic oxide.

The "stabilization" of cubic ZrO_2 by minor additions of other oxides to monoclinic ZrO_2 has been practiced for some time. The oxide mixtures are sintered to obtain solid solutions and the cubic phase. It was believed that if those metals, the oxides of which "stabilize" ZrO_2, were alloyed with zirconium, the cubic oxide rather than the monoclinic might form.

The investigation which followed included a study of numerous oxide additions to ZrO_2 in order to determine their relative "stabilizing" effects, the formation of several alloys of zirconium with the elements which appeared promising, a study of the oxides formed on these alloys when oxidized in air, and an investigation of the oxidation of those alloys in an autoclave.

The tendency of various metal oxides to stabilize the cubic modification of zirconium oxide was investigated by grinding zirconium oxide with relatively small amounts of these oxides and then heating (firing) the mixtures. Estimates of the relative amounts of monoclinic and cubic phases were made from x-ray diffraction studies of the fired oxides. The approximate percentages of cubic phase in the various oxide mixtures are shown in the following tabulations:

Oxide or Oxides Added to ZrO_2	Mole %	Maximum Stabilization (% Cubic Phase)
BaO	3	0
BeO	3	0
CaO	3	60
CaO	5	90
Cb_2O_5	3	30
Cb_2O_5	5	70
CeO_2	3	5
CeO_2	5	10
Cr_2O_3	3	0
Fe_2O_3	3	0
MgO	3	20
MgO	5	35
NiO	3	0
PbO	3	0
SnO_2	3	0
TiO_2	3	0
V_2O_5	3	5
Y_2O_3	3	50
Y_2O_3	5	70
ZnO	3	0
CeO_2 plus	2	10
Cb_2O_5	2	
SnO_2 plus	2	5
Cb_2O_5	2	
Y_2O_3 plus	2	0
Cb_2O_5	2	
CeO_2 plus	2	Questionable
Cb_2O_5	8	
SnO_2 plus	2	85
Cb_2O_5	8	
Y_2O_3 plus	2	75
Cb_2O_5	8	
V_2O_5 plus	2	90
Cb_2O_5	8	
SnO_2 plus	2	95
Cb_2O_5	15	

Zirconium-base alloys of the compositions shown below were made by melting on a crater-eroded copper hearth. All surfaces of specimens of these alloys were oxidized by heating in air until relatively thick oxide coatings were formed. The approximate percentages of cubic zirconium oxide in these coatings are also indicated below. It is

noted that in no case was there complete stabilization of the cubic oxide.

Addition to Zirconium (wt %)	Maximum Per Cent Cubic Oxide
Ag (6.7)	5
Ce (3)	5
Cb (2)	10
Cb (5)	50
Cb (7.5)	50
Cb (15)	80
Cs (2.25)	0
Sn (2)	0
Y (5)	20 + Y_2O_3

The metal samples used were in the as-cast condition and were coarse grained. In general, the oxide film was shiny, having a glassy appearance. Some grains were quite dark and others were very light; oxidation had an "etching" effect, revealing the grains. There appeared to be a definite orientation of the oxide with the metal, according to interpretations of x-ray diffraction line intensities; however, x-ray diffraction patterns of light and dark grains taken separately showed no differences. Some oxide stood in relief above or below oxide on adjacent grains. There was some cracking of the oxide film along metal grain boundaries, as well. A thick, white oxide occurred on rapid oxidation or at points where the surface may have been dirty (fingerprints, etc.).

The most promising addition to zirconium, with respect to formation of the cubic oxide when the metal is oxidized, seems to be columbium. The alloys containing 2 and 15% columbium were cold-rolled without difficulty. Alloys containing 5 and 7.5% columbium cracked when an attempt was made to cold-roll them. The alloy containing 15% columbium could be cold-rolled because the metastable beta phase had been retained on cooling of the ingot. A zirconium-base alloy consisting of the body-centered cubic beta phase might have much more desirable mechanical properties than Zircaloy-2 has, and attempts will be made to develop such an alloy. Wrought alloys containing 2 and 15% columbium will be exposed in an in-pile loop by the HRP Corrosion Group. Out-of-pile static corrosion test results are reported in Sec. 10.2.2.

13.4 MECHANICAL METALLURGY OF ZIRCONIUM ALLOYS

W. J. Fretague

Impact specimens of Zircaloy-2 were irradiated at the MTR (facility HB-3; temperature, <200°F) by the Solid State Division. After irradiation they were tested by the Metallurgy Division. The data obtained for the irradiated specimens are presented in Table 13.2, and those for the control specimens in Table 13.3.

The specimens irradiated in the MTR in air were not damaged so much as were those previously reported,[4] which had been exposed to fissioning uranyl sulfate solutions in in-pile corrosion loop GG. The impact data for the MTR specimens showed a transition temperature in the same temperature range as has been previously reported for Zircaloy-2 and gave similar impact values for temperatures below the transition region. The data from the specimens from loop GG were comparable at the lower temperatures but did not show a transition region.

Tensile and impact specimens of Zircaloy-2 have been aged at 250°C for 1000 hr. These specimens will be employed as controls for Zircaloy-2 specimens to be irradiated at 250°C in the MTR.

13.5 EFFECTS OF RADIATION ON STRUCTURAL METALS AND ALLOYS

R. G. Berggren J. C. Wilson

Few test results were obtained during the quarter; the main effort was directed toward equipment development and the design and construction of irradiation facilities for use in the MTR and LITR. Two irradiations were completed in the LITR. These irradiations contained impact and tensile specimens of a number of carbon steels and alloy steels and tensile specimens of some weld metals. An apparatus is being assembled for use in the HB-3 facility of the MTR, and design of an elevated temperature apparatus for use in the MTR is nearing completion.

A program for investigation of irradiation effects upon titanium and several Zircaloys has been drawn up and is being put in operation.

---

[4] W. J. Fretague, *HRP Quar. Prog. Rep. July 31, 1955*, ORNL-1943, p 167–168.

TABLE 13.2. VARIATION IN IMPACT ENERGY WITH TESTING TEMPERATURE FOR IRRADIATED ZIRCALOY-2 SPECIMENS

Specimen No.	Testing Temperature (°C)	Impact Energy (in.-lb)	Per Cent Fractured	nvt of Fast (>1 Mev) Neutrons, Calculated ($\times 10^{20}$)
547-2	−25	10	99	2.2
545-1	24	12	Complete	0.9
545-2	70	12	Complete	1.1
546-3	70	14	Complete	3
545-3	120	16	Complete	1.5
546-2	120	28	Complete	2.2
546-1	160	22	Complete	1.7
547-1	160	30	99	1.7
545-4	200	~50	90	2
546-4	200	~50	90	3.8
547-3	250	~50	80	3
547-4	273	~50	80	3.8

TABLE 13.3. VARIATION IN IMPACT ENERGY WITH TESTING TEMPERATURE FOR ZIRCALOY-2 CONTROL SPECIMENS

Specimen No.	Temperature (°C)	Impact Energy (in.-lb)	Per Cent Fractured
34-1	23	10	Complete
30-1	23	18	Complete
30-2	60	20	Complete
30-3	120	41	Complete
30-4	200	39	Complete

13.6 METALLURGICAL ENGINEERING SERVICES

G. E. Elder

13.6.1 Closure Joint in the HRT Pressure Vessel

The closure joint in the HRT pressure vessel as shown in Fig. 13.3 has been completed. The pressure vessel was formed from two hemispheres of 4-in. A212B carbon steel, lined with a ½-in. layer of type 347 stainless steel. The clad material and the hemispheres were produced by the Lukens Steel Company.

After the core vessel was assembled within the pressure vessel halves, the two hemispheres were fitted together and a type 347 stainless steel Electric Boat type of consumable insert was tack-welded in place. Some preheating (not exceeding 100°F) was applied to the weld area with strip heaters prior to the fusion of the Electric Boat insert. The vessel was sealed and then flushed with one cylinder of argon prior to welding, and a flow of 10 cfh of argon was maintained during the deposition of the first three layers of weld metal. The Electric Boat insert was fused with a Heliarc torch in increments of approximately 16 in. Each increment was then covered with two layers of type 347 stainless steel, deposited manually by the metallic arc process. The increments were welded in pairs which were 180 deg apart. The first three layers of the weld were gamma radiographed, and the radiographs showed the weld to be free of defects. An additional layer of type 347 stainless steel, followed by six passes of type 308L stainless steel, was then deposited. Due to the non-uniformity of the thickness of the stainless steel cladding and the eccentricity of the hemispheres, there was some misalignment of the stainless steel–carbon steel junction. The type 308L was deposited where required to establish a uniform level of weld metal. Two layers of type 308L were

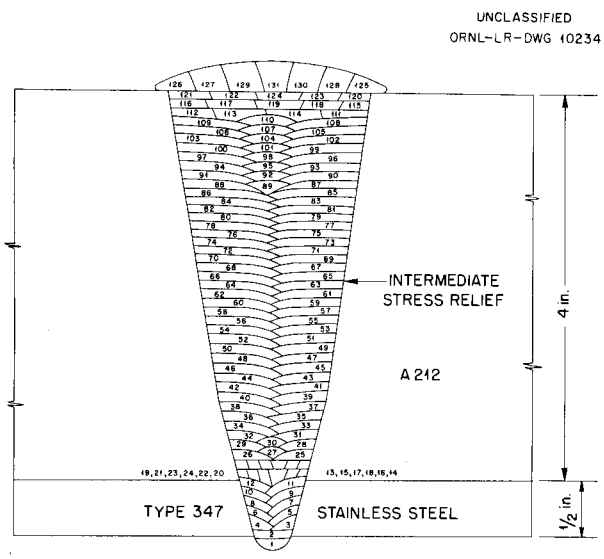

Layer	Passes Numbered	Amps	Arc Volts	Electrode	
				Size	Type
1	1	95	14		EB Weld Insert 347
2–4	2–6	82	24–25	1/8	Arcos Chromend 19–9CB
5–7	7–12	100	24–25	1/8	Arcos Chromend KLC
8–9	13–24	85	21–22	1/8	B&W Armco Iron
10–11	25–30	137	22–23	5/32	E7016 Airco 327
12–44	31–124	195	24–25	3/16	E7016 Airco 327
45	125–131	195	24–25	3/16	E7016 Airco 327

Fig. 13.3. Closure Joint Weld in the Stainless-Steel-Clad Carbon Steel Pressure Vessel for HRT.

deposited above the stainless steel–carbon steel junction.

Armco iron electrodes were used to make the metallurgical transition from the austenitic to the ferritic deposit in the joint. Considerable difficulty in minimizing the dilution of the Armco ingot iron by the type 308L stainless steel was encountered. Three procedure qualification welds were made in scrap pieces of the pressure vessel material. Radiographic examination of the first test weld revealed no defects, but ultrasonic inspection indicated cracks in the transition region of the weld and suspicious areas along the side walls. Macroetched specimens from the joint showed extensive cracking in the first layer of the Armco iron deposit and very little cracking in the second layer. The suspected areas along the walls were stringer inclusions in the carbon steel of the clad plate which the weld had opened. A number of small-scale test welds were made, and an improved welding technique for the Armco iron was developed. Some improvement was shown on the second full-scale test weld, but both layers of the Armco ingot iron showed cracks. A chemical analysis of a deposited weld pad indicated that the new lot of electrodes used for the second test weld did not meet the specifications. A third lot of electrodes was produced by the manufacturer, with special attention given to ensure a deposited weld metal which would duplicate as nearly as possible the chemical analysis of ingot iron. A third full-scale test weld using these electrodes was satisfactory.

Two layers (consisting of six passes each) of Armco ingot iron were deposited. One crack, approximately 1½ in. in length, was found, by use of the Magniflux technique, in the first layer, was ground out, and then repaired. After two layers of E7016 (see Fig. 13.3) were deposited around the entire circumference, the weld was radiographed again and no indications of defects were found. The remainder of the welding was performed concurrently by two welders on individual increments which were separated by one increment. After ⅜ in. of weld metal was deposited, the vessel was rotated and another section was welded.

The joint was given both an intermediate and final stress-relieving heat treatment. The heating was done locally by the electrical induction method at a rate not exceeding 125°F per hour. The joint was held at 975 ± 25°F for 10 hr for the intermediate treatment and for 16 hr for the final heat treatment and was cooled to room temperature at a rate not exceeding 125°F per hour. The core tank was filled with water, and a flow of 3 gpm was maintained throughout the heat treatment. An argon atmosphere was maintained in the blanket space to prevent oxidation of the stainless cladding.

The completed joint was examined with radiographic, Magniflux, and ultrasonic methods, and the weld was found to be sound without surface defects. The weld was re-examined by ultrasonic methods after the 4000-psi hydrostatic test, and the weld was found to be acceptable.

Part V

CHEMICAL ENGINEERING DEVELOPMENT

F. R. Bruce

14. THORIUM OXIDE SLURRY DEVELOPMENT

D. E. Ferguson
V. D. Allred
J. M. DallaValle
A. R. Jones
E. V. Jones
J. P. McBride
N. A. Krohn
L. E. Morse
C. E. Schilling
W. M. Woods

Development of a thorium oxide slurry for use in the blanket of the HRT continued.[1] Thorium oxide slurries containing 1000 g of thorium per kilogram of H_2O were readily agitated at 300°C in stainless steel bombs in the LITR and were apparently unaffected by the irradiation. Both silver and palladium oxides were shown to be good catalysts for the recombination of radiolytic hydrogen and oxygen. Oxide prepared by the pyrohydrolysis of thorium oxalate appeared to be unique and was very different from the oxide prepared by thermal decomposition. Pumping was found to degrade oxide particles and to increase the bulking characteristics. Settling characteristics were sensitive to slurry concentration, oxide calcination temperature, chemical additives, and additive concentration. Development of apparatus for the study of slurry properties at elevated temperatures and pressure continued.

14.1 THORIUM OXIDE SLURRY IRRADIATION STUDIES

A. R. Jones
N. A. Krohn
J. P. McBride
W. M. Woods

Studies to determine the effect of radiation on the properties of thorium oxide slurries have continued. Three pure thorium oxide slurries previously irradiated at 300°C in the LITR[1] and one irradiated in the ORNL Graphite Reactor were recovered. Five more in-pile experiments were carried out, three in the LITR and two in the Graphite Reactor. Additional irradiations were also carried out with the Co^{60} source. Slurries containing 1000 g of thorium per kilogram of H_2O were stirred without difficulty at 300°C in an improved model of the dash-pot irradiation bomb, both in- and out-of-pile.

14.1.1 Slurry Irradiations in the LITR

Three slurries containing 500 g of thorium per kilogram of H_2O, one of D-16 oxide[1] and two of D-16 oxide recalcined at 900 and 1100°C, respectively, irradiated at 300°C and in a thermal neutron flux of 3×10^{13} neutrons/cm^2/sec in the LITR (LITR-4, -5, and -6) were recovered for examination. The irradiation times were 66, 175, and 213 hr, respectively. The slurry solids from LITR-4 and -5 were easily removed, readily redispersed, and apparently unaffected by the irradiation (see Table 14.1). Only about 10% of the solids in LITR-6 were removed from the bomb by simple flushing. The recovered solids showed no gross change. The difficulty in solids recovery in the latter case should not necessarily be attributed to an effect of irradiation. The bomb had stood for seven weeks before being opened, and compaction of settled solids on standing has been observed with unirradiated slurries.

Three additional slurries were irradiated at 300°C in the LITR. The slurries were prepared from D-16 oxide, D-16 oxide recalcined at 900°C, and D-30 oxide, an oxide made up of a miscellany of oxide preparations refired at 950°C, which contained 3000 ppm SO_4 and had been pumped 200 hr at 300°C before being used in the irradiation experiment. The irradiation times were 165 hr, 2 min, and 200 hr, respectively. All slurries were mixed before being placed in the bombs, and the experimental setups were tested at temperature before being placed in the reactor. The irradiations were carried out in an improved model of the dash-pot bomb, employing dual solenoids to give a power stroke in both the up and down directions.

The slurry of D-16 oxide (500 g of thorium per kilogram of H_2O) showed an apparent maximum viscosity at about 260°C both in- and out-of-pile, but at 300°C its stirring behavior resembled that of water. No difficulties in stirring the slurry were experienced while the slurry was being irradiated. The slurry of D-16 oxide recalcined at 900°C (1000 g of thorium per kilogram of H_2O) was stirred easily at 300°C out-of-pile for a week, but the irradiation bomb began to leak almost immediately after its insertion in the reactor. The D-30 oxide

[1] D. E. Ferguson *et al.*, *HRP Quar. Prog. Rep. July 31, 1955*, ORNL-1943, p 175–198.

TABLE 14.1. SUMMARY OF DATA ON IRRADIATED SLURRIES

Experiment	Material	Slurry Concentration (g of Th per kg of H_2O)	Settled Density (g of Th per liter)			X-Ray Crystallite Size (Å)		
			Original	Irradiated	Control	Original	Irradiated	Control
LITR-3	D-16	500	1295	1480	985	123	195 ± 20	200 ± 20
LITR-4	D-16	500	1295	1610				
LITR-5	D-16 recalcined at 900°C	500	1548	1360	1110	474		650 ± 60
GR-3	Pyrohydrolyzed + 8% UO_3	500		457*	915*		220 ± 20	250 ± 30
GR-4	Lindsay + 8% UO_3 + CuO	500		400*	1270		180 ± 20	200 ± 20
GR-6	D-16	Settled	1295	1220				

*Material lumpy; values probably low.

slurry was stirred out-of-pile for 20 hr and then transferred to the reactor. It was stirred satisfactorily in-pile. Three timers, actuating the stirrer solenoids, failed during the irradiation and were replaced without causing a deterioration in the stirring behavior.

14.1.2 Slurry Irradiations in the Graphite Reactor

A settled slurry of D-16 oxide, which had been irradiated for 30 days at 300°C in a flux of 7×10^{11} neutrons/cm^2/sec in the Graphite Reactor (GR-6),[1] was readily removed from the radiation bomb and appeared to be unaffected by the irradiation (see Table 14.1).

Slurries of the D-30 oxide and a D-16 oxide, containing 0.32 wt % silver oxide, were each irradiated in a settled condition for 30 days at 300°C in the ORNL Graphite Reactor but have not yet been recovered.

14.1.3 Slurry Irradiations in the Co^{60} Source

The following settled slurries were irradiated simultaneously at room temperature for one month (830 hr) in the Co^{60} source at 12,000 r/min:

D-16, recalcined at 900°C, + silver oxide (0.32 wt %)
D-16, recalcined at 900°C, + $Th(SO_4)_2$ (3000 ppm SO_4^{--})
D-16, recalcined at 900°C, + $Th(SO_4)_2$ (3000 ppm SO_4^{--}) and $Na_4P_2O_7$ (0.005 *M*)
D-16, recalcined at 900°C, + $Na_4P_2O_7$ (0.005 *M*)
D-16, recalcined at 900°C, + $MgSO_4$ (0.005 *M*)
D-16, recalcined at 900°C, + Calgon (0.5% solution)

The recovered slurries appeared to be visually unchanged and showed no deterioration in slurry behavior. Further irradiations under a variety of chemical conditions are under way.

14.1.4 Postirradiation Examination of Slurries

Irradiated slurries which have been recovered are being characterized by their appearance, relative dispersibility, settled density, average sedimentation particle size,[2] and x-ray crystallite size. Delineation of the significance of these variables on slurry behavior has been under way for some time (see ref 1, p 181–196 and Secs. 14.3.1, 14.3.2, and 14.3.3 of this report). Any change in them in an irradiated slurry, inconsistent with common laboratory experience, would certainly indicate a radiation effect.

The pure thorium oxide slurries which have been irradiated (three in the Graphite Reactor; five in the LITR) have shown no significant changes in appearance, dispersibility, or bulk density. Slurries irradiated in the Co^{60} source under a variety of chemical conditions were equally unaffected. Sedimentation particle-size and x-ray

[2] G. W. Leddicotte and H. H. Miller, *Anal. Chem. Semiann. Prog. Rep. Oct. 20, 1954*, ORNL-1788, p 21.

crystallite size data, although incomplete, indicate no significant radiation-induced change (see Table 14.1; also ref 1, p 176–177).

Table 14.2 lists the sedimentation particle-size information which was obtained on pertinent oxide preparations that had been irradiated at room temperature in the Co^{60} source and agitated at 300°C in the dash-pot irradiation bomb. Comparative values for the original material and results of laboratory treatment are also included. The particulate degradation in the dash-pot irradiation bombs illustrates the difficulties in distinguishing particulate effects, associated with mechanical handling, from possible radiation effects.

Table 14.3 summarizes the x-ray crystallite size information obtained from a variety of oxide preparations and two irradiated samples. The relative insensitivity of the x-ray crystallite size to preparation method and pretreatment and its dependence on calcination temperature point up its usefulness not only as a variable for laboratory characterization but also as an indicator of radiation damage. Radiation-induced crystal growth or lattice deformation should be readily discerned by x-ray diffraction techniques.

14.1.5 Development of Facilities for Irradiation Studies

An effort is under way to develop small-scale devices suitable for in-pile use, to study, at least qualitatively, the changes occurring in properties of slurries, primarily viscosity, while they are under irradiation. Extensive out-of-pile testing of the simple dash-pot-stirred irradiation bomb has led to the design of a stirrer, which, in conjunction with a particular arrangement of the solenoid windings allows a slurry containing 1000 g of thorium per kilogram of H_2O to be readily agitated at temperatures up to 300°C, permitting the use of the bomb in the routine irradiation of slurries. More complicated devices for the in-pile study of slurries are being developed in cooperation with the Engineering and Maintenance Division. Under construction is a magnetic-impulse reciprocating-plunger viscometer employing concentric cylinders and a viscosity-sensitive plunger. Also in the shop is a bench model mockup of a bellows-type flow-tube viscometer.

To support the intensified irradiation effort on slurries, the Graphite Reactor irradiation facility is being modified to permit the simultaneous irradiation of three slurry bombs at elevated temperatures. A new vertical irradiation facility is being planned for the LITR; it will have an inside diameter of 3 in. and can be used independently of the operating schedule of the LITR.

14.2 GAS RECOMBINATION

L. E. Morse J. P. McBride

Development of an internal catalyst, to effect the recombination of the radiolytic hydrogen and oxygen to be produced in a thorium oxide slurry

TABLE 14.2. SEDIMENTATION PARTICLE-SIZE DATA* ON IRRADIATED THORIUM OXIDE

Treatment	650°C Calcined D-16 Oxide		900°C Recalcined D-16 Oxide	
	dg (μ)	σg	dg (μ)	σg
Original material	3	3	3	3
Wet-autoclaved at 300°C	2	4		
Co^{60} irradiated at room temperature	2	3	3	3
Blended in Waring Blendor	1	4	1	2
Pumped in dash-pot irradiation bomb (300°C)	1.5	4		
Pumped in dash-pot irradiation bomb (300°C)			1.7	4
Pumped in dash-pot irradiation bomb (300°C)			1.1	4

*dg = geometric mean diameter; σg = geometric standard deviation [T. Hatch and S. P. Choate, *J. Franklin Inst.* **207**, 369–387 (1929)].

TABLE 14.3. AVERAGE X-RAY CRYSTALLITE SIZE OF THORIUM OXIDE PREPARATIONS

Material	X-Ray Crystallite Size (Å) at Final Firing Temperature of					
	500°C	650°C	750°C	900°C	1000°C	1300°C
D-16[a]		103	191	412		2163; 1783
D-16; wet-autoclaved at 300°C		123	253	474	627	2470
Laboratory preparation[b]	78	143	250	550		
Laboratory preparation[a]	74	127	231	616		
Laboratory preparation[a]		131	236	441	858	
Laboratory preparation[c]	89	166	325	696		
Laboratory preparation[d]	92	185	250	775		
FMPC oxide		115	202			
Co^{60} irradiated D-16		103		430		
LITR irradiated D-16		195				
	83	139	255	549	743	2139

[a]Oxalate precipitated at 40°C.
[b]Oxalate precipitated at 10°C.
[c]Oxalate precipitated at 70°C.
[d]Oxalate precipitated at 100°C.

blanket, has continued, with studies being made of silver, nickel, copper, and palladium as catalysts. All four show sufficient activity to be considered for use in the HRT; but only silver and palladium are active enough for TBR use at concentrations compatible with the neutron economy required. For the latter use, a catalyst capable of recombining with oxygen 10 moles of hydrogen per hour per liter of slurry at 280°C and at a hydrogen partial pressure of 500 psi is considered satisfactory.

The studies were carried out with slurries containing 660 and 1000 g of thorium per kilogram of H_2O, prepared from 900°C refired D-16 oxide. Experimental details and methods of analyses have been described previously.[3,4] The addition of 0.02 *m* silver as Ag_2CO_3 to the slurry resulted in a combination rate, at 280°C and a hydrogen partial pressure of 500 psi, of 13 moles of hydrogen per hour per liter of slurry (see Table 14.4); this was about six-tenths the rate obtained when the higher-surface-area 650°C fired oxide was used. Nickel and copper, as metal or oxide powders, were less effective at concentrations as high as 0.1 *m*, recombining 2 or less moles of hydrogen per hour per liter of slurry under the same conditions. Palladium was extremely active at moderate temperatures (see Table 14.5). In a slurry containing 0.5 wt % uranium, with respect to the weight of thorium, with 1030 parts of palladium per million parts of thorium, the combination rate at 115°C and at a hydrogen partial pressure of 500 psi was 19 moles of hydrogen per hour per liter of slurry.

The reaction rate constant, k_{π}, and the rate of hydrogen combination with oxygen, in moles per hour per liter of slurry, listed in Tables 14.4 and 14.5 were obtained from the observed decrease in gas pressure with time, perfect gas behavior being assumed. First-order dependence of the rate on total gas pressure has been demonstrated. The amount of gas initially dissolved in the slurry and subsequently combined has been neglected, and hence the calculated combination rates are lower than the actual rates.

The nickel and copper, as oxide or metal powders, for use in the catalytic studies were prepared by

[3]D. E. Ferguson *et al.*, *HRP Quar. Prog. Rep. Oct. 31, 1954*, ORNL-1813, p 143–144.

[4]H. F. McDuffie *et al.*, *Reactor Sci. Technol.* 4(2), 23 (1954) (TID-2013).

TABLE 14.4. COMBINATION RATES AT 280°C OF STOICHIOMETRIC HYDROGEN AND OXYGEN MIXTURES IN THORIUM OXIDE SLURRIES WITH VARIOUS CATALYSTS

Slurry: 900°C refired D-16 ThO_2, 660 g of thorium per kilogram of H_2O

Catalyst Concentration (m)	Rate Constant, k_π (hr^{-1})	H_2 Combination Rate, P_{H_2} = 500 psi (moles/hr/liter)
0.01 m Ag	11	3
0.02 m Ag	42	13
0.1 m NiO (400°C in air*)	1	0.3
0.1 m Ni (390°C in H_2*)	0.4	0.1
0.1 m Ni (250°C in N_2*)	5	2
0.1 m CuO-Cu_2O (400°C in air*)	6	2
0.1 m Cu (390°C in H_2*)	3	1

*Catalyst prepared by calcining metal formates as indicated.

TABLE 14.5. COMBINATION RATES OF STOICHIOMETRIC HYDROGEN AND OXYGEN MIXTURES IN THORIUM OXIDE–URANIUM OXIDE SLURRIES CONTAINING PALLADIUM

Slurry: 900°C refired D-16 ThO_2, 1000 g of thorium per kilogram of H_2O, plus 0.5% uranium (as UO_3), 1030 parts of palladium per million parts of thorium

Temperature (°C)	Rate Constant, k_π (hr^{-1})	H_2 Combination Rate, P_{H_2} = 500 psi (moles/hr/liter)
32	3	3
76	14	12
91	17	14
115	26	19

heating the respective formates in air to produce the oxides and in hydrogen or nitrogen to produce the metals. The powders were added to the slurries and heated for 3 hr at 280°C in the presence of oxygen prior to the gas combination experiments. The nickel catalyst showing the highest activity was prepared by heating the formate at 250°C in N_2. The metal powder was pyrophoric and glowed on exposure to air. The other nickel powders prepared by heating the formate at 390 to 400°C in hydrogen and air showed little catalytic activity. The copper powders prepared by heating copper formate at 390 to 400°C in air and hydrogen were more active than the corresponding nickel preparations (see Table 14.4) but no more active than a catalyst prepared by simply adding the basic copper carbonate to a slurry and bringing it to 250°C.[3] Heating the ThO_2-CuO slurry at 200°C in the presence of a hydrogen partial pressure increased its catalytic activity somewhat, but a similar treatment did not affect the activity of the slurry containing the NiO catalyst.

The palladium catalyst was prepared by tumbling the dry ThO_2, $UO_3 \cdot H_2O$, and PdO powders for about 1 hr before dispersing the solids in water. The slurry of the mixed oxides was heated at 280°C for 3 hr in the presence of a partial pressure of oxygen (300 psi at room temperature). The catalyst showed a slight decline in catalytic activity in successive experiments at temperatures

below 115°C but regained full activity on being reheated at 120°C.

14.3 LABORATORY STUDIES

V. D. Allred J. P. McBride

Laboratory studies in support of the in-pile irradiation studies and the slurry development program have continued. The preparation of oxide by the pyrohydrolysis of thorium oxalate has been investigated. Further studies on the effect of additives on the hindered settling characteristics and bulking properties of thorium oxide have been carried out. The effect of pumping on particle size has been investigated. A high-temperature slurry viscometer is currently under test with slurries, and an apparatus for the study of hindered settling at temperature in stainless steel equipment has been designed and is under construction.

14.3.1 The Preparation of Thorium Oxide by the Pyrohydrolysis of Thorium Oxalate

V. D. Allred

Previous investigations[5] indicated that thorium oxide prepared by the pyrohydrolysis of an aqueous suspension of thorium oxalate at temperatures of 250 to 300°C was extremely uniform and finely divided. Furthermore, oxides so prepared and subsequently fired to temperatures up to 900°C had characteristically high surface areas (e.g., 20 m^2/g). The oxides were also relatively non-abrasive when tested in the jet impingement abrasion tester. Further work on the preparation method has been carried out which confirms previous experience on the uniformity and fineness of the oxide product and shows that the pyrohydrolysis product was uniquely different from the oxide prepared by the thermal decomposition of the oxalate and did not reflect the precipitation history, as is the case with the latter preparation method.

Thorium oxalate was prepared by precipitation at temperatures of 10 and 100°C by the same procedure used in the previous investigation of the thermal decomposition of oxalate (ref 1, p 181). Aqueous suspensions of the oxalate precipitates were then autoclaved for 24 hr at approximately 300°C. The resulting oxides were used as stock materials and were subsequently fired at 400, 500, 650, 750, and 900°C.

Electron micrographs typical of 400°C fired pyrohydrolysis products prepared from oxalate precipitated at 10 and 100°C are shown in Figs. 14.1*a* and 14.2*a*. Corresponding oxides prepared from similar oxalate preparations by thermal decomposition at 400°C are shown in Figs. 14.1*b* and 14.2*b*. It is seen that the oxalate precipitation temperature has little or no effect on the final particle size or shape of the pyrohydrolyzed oxide. The particles of the oxides from pyrohydrolysis are many times smaller than the corresponding thermally prepared oxide and appear to be agglomerates rather than crystals having a relic structure of the original oxalate.

Data on the surface area, x-ray crystallite size, and sedimentation particle size obtained with the pyrohydrolyzed material are summarized in Table 14.6. These data also show marked differences between the pyrohydrolyzed and thermally prepared oxides. For example, the product of the crystallite size, D, and the surface area, S, is not constant, as was the case with the thermally prepared oxide. It is also apparent that the pyrohydrolyzed oxide crystallites do not grow until a temperature in excess of 900°C is attained (see Fig. 14.3). Previous experience with thermally prepared oxide had indicated that the crystallites will grow within the primary particle which has the relic oxalate structure but that no growth or sintering takes place between particles below 900°C. This would indicate that in the case of pyrohydrolyzed oxide the crystallites are identical with the primary particles and that the particles seen in the electron micrographs and which are measured by sedimentation are agglomerates of fine particles. Furthermore, the surface area of the pyrohydrolyzed oxide decreases less with increasing firing temperature than does the surface area of the oxide from thermal decomposition and is much larger for the higher firing temperatures (see Fig. 14.4).

14.3.2 Hindered Settling Properties of Thorium Oxide Slurries

E. V. Jones

A study has been carried out on the effect of oxide calcination temperature and additive concentration on the settling characteristics of thorium oxide slurries. The objective of the study was to obtain room temperature settling data, with the

[5] D. E. Ferguson *et al.*, *HRP Quar. Prog. Rep. Jan. 31, 1954*, ORNL-1678, p 87.

view of eventually determining hindered settling characteristics at 300°C, and to determine the effect of various chemical environments on the dispersion characteristics of thorium oxide slurries.

An initially homogeneous and concentrated suspension of thorium oxide particles settles at a constant rate with a well-defined interface between the supernatant liquid and suspended particles.

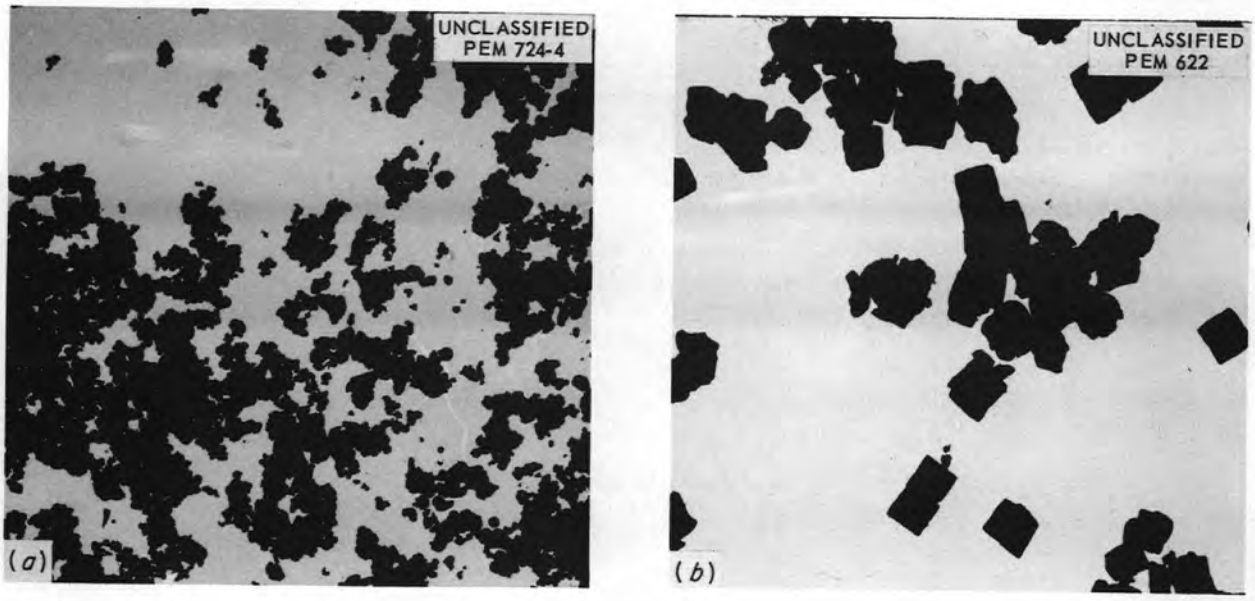

Fig. 14.1 (*a*) ThO_2 Prepared by Pyrohydrolysis of Oxalate (10°C Precipitation); Fired at 400°C for 24 hr. 9000X. (*b*) ThO_2 Prepared by Thermal Decomposition of Oxalate (10°C Precipitation); Fired at 400°C for 24 hr. 9000X.

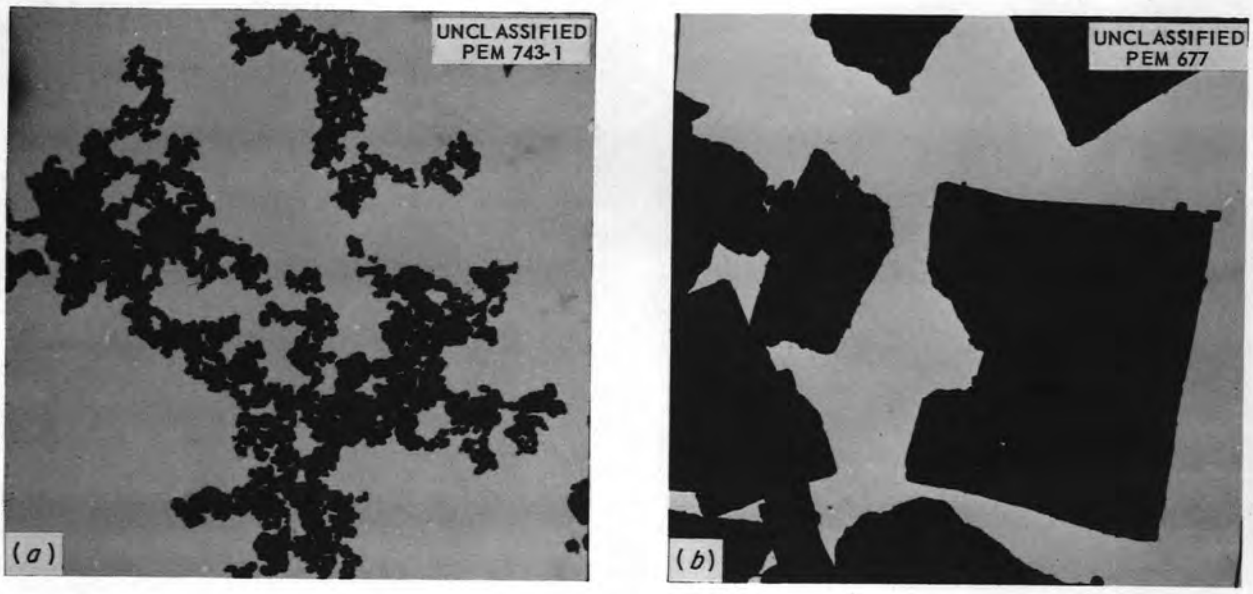

Fig. 14.2 (*a*) ThO_2 Prepared by Pyrohydrolysis of Oxalate (100°C Precipitation); Fired at 400°C for 24 hr. 9000X. (*b*) ThO_2 Prepared by Thermal Decomposition of Oxalate (100°C Precipitation); Fired at 400°C for 24 hr. 9000X.

TABLE 14.6. SUMMARY OF CHARACTERISTICS OF PYROHYDROLYZED ThO_2

Oxalate Precipitation Temperature* (°C)	Average Crystallite Diameter, D (Å)	Specific Surface Area, S (m^2/g)	SD ($\times 10^{-3}$)	Sedimentation Particle Size (μ) Amount Less Than Stated Size (wt %)				
				95	90	80	70	50
As Received from Autoclave								
10A	194	41.7	8.09					
10B	193			3.0	2.5	1.4	0.8	0.5
100C		28.8		27	20	14.2	11.0	7.3
100D								
Final Firing Temperature 400°C								
10A	164	40.0	6.56	3.0	1.9	1.0	0.8	0.5
10B	191			5.4	2.5	1.4	1.0	0.5
100C	204	33.2	6.77	15	10	6.0	4.2	1.6
100D	192			5.0	3.0	1.9	1.5	1.1
Final Firing Temperature 500°C								
10A	185	37.7	6.97	5.1	2.5	1.3	0.8	0.5
10B	187			5.0	3.0	1.9	1.2	0.5
100C	192	31.2	5.99	13	8.0	5.0	3.7	1.6
100D	217			7.1	5.0	1.9	1.5	1.1
Final Firing Temperature 650°C								
10A	163	35.6	5.80	4.0	2.2	1.3	0.8	0.5
10B	183			4.0	1.0	0.5		
100C	191	29.5	5.03	16	11	7.0	4.2	1.8
100D	206			3.7	2.6	1.6	1.4	1.1
Final Firing Temperature 750°C								
10A	182	32.0	5.8	2.5	1.8	1.3	0.7	0.5
10B	270			4.5	1.8	1.4	0.7	0.5
100C	188	29.5		15	9.0	5.1	3.7	1.9
100D	192			5.1	3.0	1.9	1.5	1.1
Final Firing Temperature 900°C								
10A	215	17.7	3.81	4.0	2.3	1.6	1.1	0.5
10B	262			15.0	7.1	2.2	1.4	0.4
100C	198	20.0	3.96	25	16	11	8.0	3.5
100D	211			8.0	4.2	2.4	1.7	1.1
Final Firing Temperature 1300°C								
10A								
10B	761							
100C								
100D	404	11.8	4.70					

*A, autoclaved at 280°C for 24 hr; B, autoclaved at 340°C for 24 hr; C, autoclaved at 300°C for 24 hr (x-ray analysis of this sample showed a strong oxalate pattern, indicating incomplete decomposition); D, autoclaved at 300°C for 24 hr.

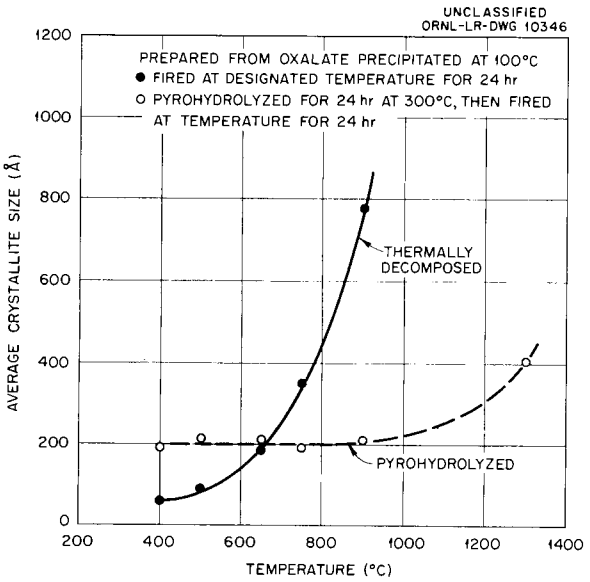

Fig. 14.3. Effect of Oxide Preparation Method on Crystallite Size.

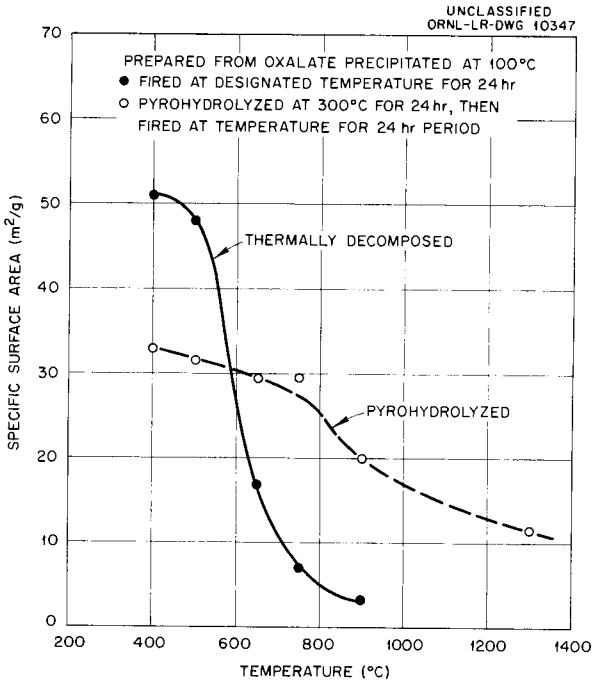

Fig. 14.4. Effect of Oxide Preparation Method on Surface Area.

This form of settling is called "hindered settling" in that there is mutual interference of the particles in their motion and Stokes' law does not apply to the settling of each individual particle. All particles move at the same rate, regardless of size.

Usually three zones of settling are observed: the initial zone, in which the motion of the interface from its initial level is uniform (hindered settling); a compressive zone, where the motion of the interface is also uniform but much slower; and a final stationary state. The first settling zone terminates when the interface reaches the settled mass of particles, and the slurry concentration in grams of thorium per liter, at this point of transition between the initial settling zone and the compressive zone, is termed the critical concentration. The slurry concentration in the final stationary state is called the settled concentration.

With thorium oxide slurries the hindered settling rates, critical densities, and settled densities all increased with increasing oxide calcination temperature. The hindered settling rate also increased with decreasing slurry concentration (see Tables 14.7 and 14.8). In the absence of a dispersing agent the settling rates were higher and the bulk density was lower at the pH's above 7. Slow settling rates, pronounced dispersion effects, and high bulk densities were obtained at lower pH's with sulfuric acid, phosphoric acid, and thorium phosphate additives (Tables 14.9–14.12).

The experiments were carried out with slurries of D-16 oxide (650°C calcination) and D-16 oxide refired at higher temperatures. Sulfuric acid, phosphoric acid, thorium phosphate, and $Na_4P_2O_7$ were the additives studied. In most experiments the slurries were placed in standard 50-ml graduates, with or without an additive, and tumbled overnight at room temperature before settling data were taken. Where the slurries were autoclaved prior to the settling-rate studies, the autoclaving was carried out in small stainless steel bombs, and the slurries were subsequently transferred to 10-ml centrifuge cones, where they were allowed to settle. With cylinders of smaller internal diameter than that of the 50-ml graduate (2.5 cm), the wall effects on the settling characteristics were appreciable. Slurry settling properties in 100-ml cylinders and those observed for the same slurries in 50-ml cylinders were virtually identical. Tumbling time beyond 2 hr had no appreciable effect on the settling rate, but the critical density decreased with time for about 48 hr, then leveled

TABLE 14.7. HINDERED SETTLING RATES FOR ThO_2 IN WATER AS A FUNCTION OF CONCENTRATION AND OXIDE CALCINATION TEMPERATURE

Slurry: D-16 oxide, tumbled for 2 hr at room temperature

Thorium Concentration (g per kg of H_2O)	Hindered Settling Rate (cm/sec)				
	Calcined at 650°C	Recalcined			
		At 800°C	At 900°C	At 1000°C	At 1300°C
250	0.05	0.06	0.075	0.10	0.123
500	0.022	0.029	0.038	0.085	0.032
650	0.00103	0.0037	0.014	0.024	0.024
800	0.00067	0.001	0.0013	0.0035	0.015
1000				0.0019	

TABLE 14.8. SETTLING CHARACTERISTICS OF SLURRIES OF D-16 OXIDE RECALCINED AT VARIOUS TEMPERATURES

Slurry: 500 g of thorium per kg of H_2O; tumbled for one day at room temperature

Calcination Temperature (°C)	Hindered Settling Rate (cm/sec)	Supernatant	Critical Concentration (g of Th per liter)	Settled Concentration (g of Th per liter)
650	0.0136	9.6	860	1230
750	0.0212	9.5	1010	1460
900	0.0460	9.5	1170	1520
1000		9.5	1200	1645

TABLE 14.9. EFFECT OF H_2SO_4 ON SETTLING PROPERTIES OF ThO_2 SLURRIES

Slurry: D-16 oxide recalcined at 900°C; 500 g of thorium per kg of H_2O; tumbled overnight at room temperature

Sulfate (ppm)	Hindered Settling Rate (cm/sec)	pH of Supernatant	pH of Settled Slurry	Critical Concentration (g of Th per liter)	Settled Concentration (g of Th per liter)
0	0.0565	8.7	9.7	930	1670
200	0.0514	8.7	9.7	935	1660
500	0.0694	8.7	9.7	930	1655
1,000	0.0644	8.15	9.0	935	1630
2,500	0.0489	5.7	7.4	955	1700
5,000	0.00667	3.1	3.3		1865
10,000	*	2.2	2.0		1875
20,000	0.00079	1.5	1.6		1450

*Settled too slowly to be read.

TABLE 14.10. EFFECT OF H_2SO_4 PLUS 0.005 *m* $Na_4P_2O_7$ ON SETTLING PROPERTIES OF ThO_2 SLURRIES

Slurry: D-16 oxide recalcined at 900°C; 500 g of thorium per kg of H_2O; tumbled overnight at room temperature

Sulfate (ppm)	Hindered Settling Rate (cm/sec)	pH of Supernatant	pH of Settled Slurry	Settled Concentration (g of Th per liter)
0	*	11.5	11.3	2255
200	*	11.4	11.4	2305
500	*	11.4	11.4	2230
1,000	*	10.9	11.1	2280
2,500	*	8.4	9.4	1825
5,000	*	5.1	3.8	2090
10,000	0.00687	2.2	2.1	2065
20,000	0.00667	1.7	1.6	2005

*Settled too slowly to be read.

TABLE 14.11. EFFECT OF H_3PO_4 SETTLING PROPERTIES OF ThO_2 SLURRIES

Slurry: D-16 oxide recalcined at 900°C; 500 g of thorium per kg of H_2O; tumbled overnight at room temperature

Phosphate (ppm)	pH of Supernatant	pH of Settled Slurry	Settled Concentration (g of Th per liter)
200	9.1	10.2	1590
500	8.9	8.9	1580
1,000	9.0	8.8	1530
2,500	7.0	6.9	2415
5,000	2.9	2.9	2390
10,000	2.3	2.5	2045
20,000	1.9	2.0	2045

off. The manner of mixing or agitating the slurries was important. Vigorous shaking occluded air in the slurries; this vitiated the settling results.

In slurries containing H_2SO_4, the pH's of the supernatant and of the settled slurry were constant at about 8.7 and 9.7, respectively, until 1000 ppm of sulfate had been added; then they dropped steadily to 1.5 at 20,000 ppm of sulfate. The initial settling rate and the settled density were practically constant until 2500 ppm of sulfate had been added. The settling rate then dropped sharply and passed through a minimum at 10,000 ppm of sulfate, while the settled density rose to a maximum of 1,875 g of thorium per liter at 10,000 ppm SO_4 and then dropped to the surprisingly low value of 1,450 at 20,000 ppm SO_4. With $Na_4P_2O_7$ added along with the H_2SO_4, the pH's of the supernatant and solid were initially the same (11.4), started to decrease at 2500 ppm of sulfate, and reached 1.6 at 20,000 ppm of sulfate. In most of the experiments settling rates were too slow to be read. In neither of the above systems was the settling rate related to the pH of the system. The settling rate passed through a minimum in the system to

TABLE 14.12. EFFECT OF H_3PO_4 AND $Th_3(PO_4)_4$ ON SETTLING PROPERTIES OF WET AUTOCLAVED ThO_2 SLURRIES

Slurry: 500 g of thorium per kilogram of H_2O (thorium as D-16 oxide recalcined at 900°C) with H_3PO_4 or $Th(PO_4)_4$ added. The slurries were autoclaved in stainless steel bombs at 300°C for 22 hr, and then were transferred to 10-ml centrifuge cones.

Phosphate (ppm)	pH of Supernatant	Critical Concentration (g of Th per liter)	Settled Concentration (g of Th per liter)
As H_3PO_4			
200	8.6	1075	1700
500	8.3	940	1570
1,000	8.0	1050	1645
2,500	6.3	1115	1825
5,000	5.2	*	2280
10,000	3.4	1170	1745
20,000	3.7	965	1515
As $Th_3(PO_4)_4$			
200	8.7	1025	1630
500	9.1	925	1540
1,720	6.5	1045	1670
2,500	7.5	1120	1895
5,000	4.5	*	2575
10,000	3.5	*	2055
20,000	3.7	825	1625

*Settled too slowly to be read.

which sulfate alone was added, but the pH did not. In the system with sulfate plus 0.005 *m* $Na_4P_2O_7$, the highest settling rates occurred in the two systems with the lowest pH. The settled densities were higher in this system and seemed to pass through a minimum at 2500 ppm of sulfate.

Phosphate additions, as H_3PO_4, gave supernatants and solids with pH values about the same as those obtained from similar additions of sulfate. The pH was about 2.0 for 20,000 ppm of phosphate, as H_3PO_4, after the slurry had been tumbled overnight at room temperature. Phosphoric acid affected the settling properties to a different degree than did the sulfuric acid. A stable, nonsettling system resulted from the use of 2500 and 5000 ppm of phosphate, as H_3PO_4. The settled densities showed a maximum of 2415 g of thorium per liter at 2500 ppm of phosphate.

When slurries of D-16 oxide recalcined at 900°C were autoclaved at 300°C for 22 hr, with phosphate added as phosphoric acid and as thorium phosphate, the results, in general, differed little from those obtained when the same slurries were tumbled overnight at room temperature with phosphoric acid. The change in the supernatant pH's for the tumbled systems was from 9.1 to 1.9 and for both autoclaved systems was from 8.7 to 3.7 as the phosphate increased. The spread of settled densities was greater for the tumbled systems. All three systems showed maximum stability (extremely slow settling) and maximum settled density at 5000 ppm of phosphate.

14.3.3 Characterization of Pumped Slurries

C. E. Schilling

Samples of thorium oxide slurries that had been pumped at 250 to 300°C in engineering loop studies carried out in the Reactor Experimental Engineering Division were studied to determine the effect of pumping on slurry properties. The average sedimentation particle size was considerably decreased by pumping, approaching an equilibrium value of approximately 0.5 μ in a relatively short time. The x-ray crystallite size seemed to be unaffected. The density of settled solids and the apparent Brookfield viscosities at high slurry concentrations were also obtained on the pumped slurries.

Tables 14.13, 14.14, and 14.15 summarize the information obtained. Table 14.13 also lists the conditions under which the loop test was carried out. Other than the obvious degradation of the oxide particles and, in some cases, decrease in bulk density, no clear-cut correlation can be seen between the properties determined and the pumping time or loop test conditions. The x-ray crystallites show no tendency to degrade on pumping or to grow under slight changes in chemical environment. The apparent Brookfield viscosities are uniformly high for slurries of the pumped oxides at concentrations of interest in the slurry blanket development program.

14.3.4 Slurry Viscosity Measurements at Elevated Temperature

J. M. DallaValle

Calibration with water of the high-temperature capillary viscometer developed to measure the viscosity of thorium oxide slurries at elevated temperatures has been completed, and viscosity measurements up to 160°C were carried out with a slurry of D-16 oxide containing 500 g of thorium per kilogram of H_2O. The viscosity of the slurry was found to be essentially that of water up to 100°C and to increase to approximately four times that of water at 160°C (see Fig. 14.5).

The viscometer, described in the previous quarterly report (ref 1, p 196–198), consists of two independent concentric stainless steel cylindrical reservoirs in a vertical position and connected by a capillary. Slurry is made to flow either from the inner reservoir to the outer or vice versa by a differential pressure applied through a DP cell. Pressure differentials from 10 to 100 in. of water

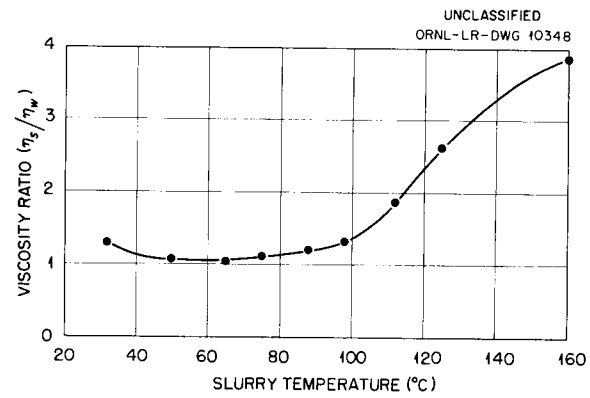

Fig. 14.5. Viscosity of ThO_2 Slurry (500 g of Thorium per kilogram of H_2O; D-16; 650°C) Relative to That of Water.

are obtainable. Direction of flow is controlled by means of air-operated valves through a solenoid mechanism. The unit is mounted in an aluminum block provided with heating units and controls to maintain, reasonably accurately, temperatures from room to over 300°C. Pressures up to 300 psi can be contained. The slurry in the inner reservoir is stirred by a solenoid-activated dash-pot stirrer and in the outer by a magnetically coupled, rotating stirring bar.

To operate the viscometer, the slurry (80 to 100 ml) is placed in the outer reservoir, the assembly is placed in the block furnace, and connections to the DP cell are made. The selected "overpressure" is applied and the unit is heated to temperature. When temperature is reached, a bleed valve is opened in the system to obtain the desired pressure differential across the capillary. The time to obtain passage of the slurry from one cylinder to the other is measured. A switch may then be thrown which reverses the pressure differential, and flow in the reverse direction takes place in the assembly. The times of "filling" and "emptying" are approximately the same.

In its present form, there is no method of measuring directly the volume of water or slurry transferred from one cylinder to the other through the capillary. This can only be estimated at any temperature by using a liquid, such as water, whose viscosity is known. In this way, using the Poiseuille relation, the volume of flow per unit time is determined. Since the time of filling and emptying the two cylinders is easily observed

TABLE 14.13. SUMMARY OF DATA ON THORIUM OXIDE SLURRIES PUMPED AT 250–300°C

Run No.	Duration (hr)	Oxide[a]	Calcination Temperature (°C)	Slurry Concentration (g of Th per kg of H_2O)	Additive[b]	Additive Concentration	Final pH of Supernatant	Particle Size, dg (μ)	Standard Deviation, σg	X-Ray Crystallite Size (Å)	Settled Concentration (g of Th per kg of H_2O)
X-4[c]	23	D10	650	645	SiO_3	0.01 *M*	10.3	0.9	8	117	3546
X-6[c]	1	D10	650	645	SiO_3 $Th(SO_4)_2$	0.001 *M* 2600 ppm	6.3	0.6	3	123	898
X-7[c]	148	D10	650	569	SiO_3	0.01 *M*	7.4	0.5	3	129	1443
X-10-C	72	L9	900	569	None		3.7	0.8	3	871	1641
X-11-C	205	D10	650	645	None		7.6	0.3	3	129	713
X-12-C	304	D15	800	645	None		8.1	0.7	2	292	1153
X-13-C	0.8	D10	650	645	SiO_3 $Th(SO_4)_2$	0.35 *M* 3700 ppm		1	2	120	1430
S-59-C[d]	335	D12	650	458	$Th(SO_4)_2$	1500 ppm	6.1	0.2	5	191	755
S-60-C	7	NL1239	750	458	None			0.3	4	394	982
S-61-C	42	NL1239	750	458	None		4.4	0.4	4	991	1256
S-62-C	14	NL1239	750	458	$Th(SO_4)_2$	1300 ppm	6.0	0.4	10	600	1222
S-63-C	104	NL1239	750	458	$Th(SO_4)_2$	1500 ppm	3.4	0.4	4	965	1196
S-64-C	375	D15	650	458	None		5.9	0.2	3	196	772
T-51-C	136	D15	650	363	None			0.4	2		586
U-19[e]	79	L9	900	645	CO_2	10 psi	6.4	1.2	2	711	1763
S-70-C	310	D31	800	1000	None			0.3	9		1715
S-71-8	274	D31	800	1000	$Th(SO_4)_2$	2000 ppm	5.6	0.4	4	264	1127
200A-1C	234	D27	800	500	$Th(SO_4)_2$	600 ppm	6.5	0.5	3	238	1170
200A-2-3	123	D35	800	1000	None		7.6	0.7	2	274	1481

[a]D-10, D-15, etc. – oxides prepared at ORNL from Thorex product thorium nitrate (see ref 1, p 181); NL1239 – oxide from Feed Materials Processing Center, Fernald, Ohio; L9 – oxide from Lindsay Chemical Co.

[b]O_2 overpressure used in all cases.

[c]A. S. Kitzes and R. B. Gallaher, *HRP Quar. Prog. Rep. April 30, 1955*, ORNL-1895, p 145.

[d]*Ibid.*, p 137–139.

[e]*Ibid.*, p 141.

TABLE 14.14. EFFECT OF PUMPING TIME ON THE PROPERTIES OF THORIUM OXIDE SLURRIES

Run* and Sample Number	Pumping Time (hr)	Geometric Mean Particle Size, dg (μ)	Geometric Standard Deviation, σg	X-Ray Crystallite Size (Å)	Settled Concentration (g of Th per kg of H_2O)
X-11-0	5	1.2	7	125	1615
X-11-1	47	0.7	13	120	925
X-11-2	114	0.3	3	128	654
X-11-3	161	0.4	3	130	682
X-11-C	205	0.3	3	129	713
X-12-0	6.2	0.9	4		1262
X-12-1	74	0.9	2		1088
X-12-2	167	0.6	2		1097
X-12-3	210	0.7	2		939
X-12-C	304	0.7	2		1153
S-70-0	42	0.7	4		1530
S-70-1	47	0.4	10		1157
S-70-2	119	0.4	5		780
S-70-3	239	0.2	6		1076
S-70-4	287	0.2	4		1205
S-70-5	310	0.2	5		1319
S-70-C	310	0.3	9		1715
D-31	0	2.5	4		1193
S-71-0	4.5	0.8	4	245	1163
S-71-1	21	0.6	3	255	748
S-71-2	44	0.4	4	238	961
S-71-3	53	0.4	4	228	1998
S-71-4	119	0.4	4	256	
S-71-5	167	0.4	4	231	948
S-71-6	204	0.4	4	270	1326
S-71-7	274	0.4	4	256	1239
S-71-8	274	0.4	4	264	1127
200A-1-3	42	0.8	4	217	834
200A-1-4	63	0.5	5	194	991
200A-1-5	157	0.5	4	215	632
200A-1-6	161	0.5	4	217	939
200A-1-8	204	0.6	4	231	871
200A-1-9	228	0.5	3	219	862
200A-1-10	234	0.6	4	238	870
200A-1-C	234	0.5	3		1170
200A-2-0		1.3	3	253	1637
200A-2-1	11.4	1.2	3	269	1719
200A-2-2	28.2	1.2	2	257	1732
200A-2-3	123	0.7	2	274	1481

*See Table 14.13 for conditions.

TABLE 14.15. SUMMARY OF VISCOSITY DATA ON PUMPED THORIUM OXIDE SLURRIES

Run* and Sample Number	Slurry** Concentration (g of Th per kg of H_2O)	Duration (hr)	Apparent Viscosities (poises) Spindle Speed (rpm)			
			6	12	30	60
X-4	1000	23	10	5	2	
X-6	1000	1		20	18	17
	1350	1	60	42	32	28
X-7	1350	148	25	28	8	6
X-10-C	1000	72		10	4	4
	1350	72	10	10		
X-11-0	1000	5	40	38	30	18
X-11-1	1000	47	65	38	16	16
X-11-2	1000	114	65	40	25	18
X-11-3	1000	161	40	35	14	15
X-11-C	1000	205	60	45	26	26
	1350	205	1000	300	126	78
X-12-0	1000	6.2	50	35	26	18
X-12-1	1000	74	20	28	14	10
X-12-2	1000	167	15	15	15	12
X-12-C	1000	304		10	6	8
	1350	304	530	272	119	68
X-13-C	1350	0.8	15	5	4	6
S-59-C	1000	335	51	50	30	30
	1350	335	450	265	138	87
S-60-C	1000	7	21	20	22	17
	1350	7	260	180	95	68
S-61-C	1000	42		20	26	15
	1350	42	45	30	35	30
S-62-C	1000	14	50	50	36	21
	1350		60	40	40	48
S-63-C	1000	104	30	30	32	27
	1350	104	165	112	66	54
S-64-C	1000	375	41	36	24	22
	1350	375	1000	1000	1000	1000

TABLE 14.15. (continued)

Run* and Sample Number	Slurry** Concentration (g of Th per kg of H_2O)	Duration (hr)	Apparent Viscosities (poises) Spindle Speed (rpm) 6	12	30	60
U-19	1000	79		20	8.2	7.1
	1350	79	10	15	8	12
S-70-0	1530	4.2	50	28	17	22
S-70-1	1157	47	35	20	18	25
S-70-2	780	119	20	15	16	15
S-70-3	1076	239	25	24	23	28
S-70-4	1205	287	52	32	28	32
S-70-5	1319	310	34	28	27	28
S-70-C	1715	310	2400	1000	400	240
D-31	1193	0	50	22	15	11
S-71-0	1163	4.5	58	36	26	22
S-71-1	748	21	40	21	12	12
S-71-2	961	44	26	17	16	12
S-71-3	1998	53	30	18	15	16
S-71-4		119	75	30	28	23
S-71-5	948	167	65	28	23	30
S-71-7	1239	274	45	30	18	27
S-71-8	1127	274	50	31	17	24
200A-1-3	834	42	20	13	10	9
200A-1-4	991	63	15	12	11	5.6
200A-1-5	632	157	10	10	6.8	2.5
200A-1-6	939	161	13	10	9	3.4
200A-1-8	871	204	16	12	10	3.9
200A-1-9	862	228	19	20	7.8	3.0
200A-1-10	870	234	1.3	12	6.0	4.7
200A-1-C	1170	234	190	110	48	34
200A-2-0	1637		75	43	17	11
200A-2-1	1719	11.4	61	31	17	11
200A-2-2	1732	28.2	15	17	12	10
200A-2-3	1481	123	60	30	20	13

*See Table 14.13 for conditions.

**Settled bed concentrations for samples from runs S-70, S-71, 200A-1, and 200A-2.

because of a marked drop in differential pressure, the total volume transferred is readily determined.

If the volume of water transferred (or time of transfer) is known at a given temperature, it is easy to obtain a measure of the viscosity of slurry at the temperature, provided that all conditions – capillary diameter, initial volume, differential pressure, etc. – are the same. Thus, if t_w is the time taken for a volume V of water to flow through a capillary of diameter D at a temperature T_1, then for a similar volume of slurry, if the time of passage is t_s,

$$\frac{\eta_s}{\eta_w} = \frac{t_s}{t_w},$$

where the η's correspond to the viscosities, the temperatures in each case being the same. If the differential pressures vary, corrections in time may be applied, since in capillary flow the rates vary directly with the pressure drop.

For a given capillary the differential pressure must be such that the flow through it at any temperature is streamlined. The requirement in this case is that the Reynold's number be less than 2000. If this criterion holds for water at every temperature in a given arrangement, then it may be expected to hold for slurries.

14.3.5 Hindered Settling of ThO_2 Suspensions at Elevated Temperatures

V. D. Allred J. P. McBride

Thorium oxide suspensions settling in stainless steel bombs were examined by means of x-ray absorption techniques. Preliminary work on a slurry settling at room temperature and atmospheric pressure gave excellent results.

Figure 14.6 shows radiographs of a ThO_2 (500 g/liter) in the settled and in a settling condition. These pictures were made at exposures of 3 to 5 sec, with a 200-kv x-ray source and a low-speed film. There is ample contrast to indicate that, with faster film and more intense x rays, exposure times of a fraction of a second can be obtained.

Equipment has been designed and is now being constructed for study of the hindered settling properties of thorium oxide suspensions at elevated temperatures and pressures in stainless steel by continuously photographing the settling slurries by x-ray techniques. Standard x-ray film will be transported at a controlled speed past a vertical slot in a lead shield behind which the slurry bomb and x-ray source are placed.

UNCLASSIFIED
PHOTO 15959

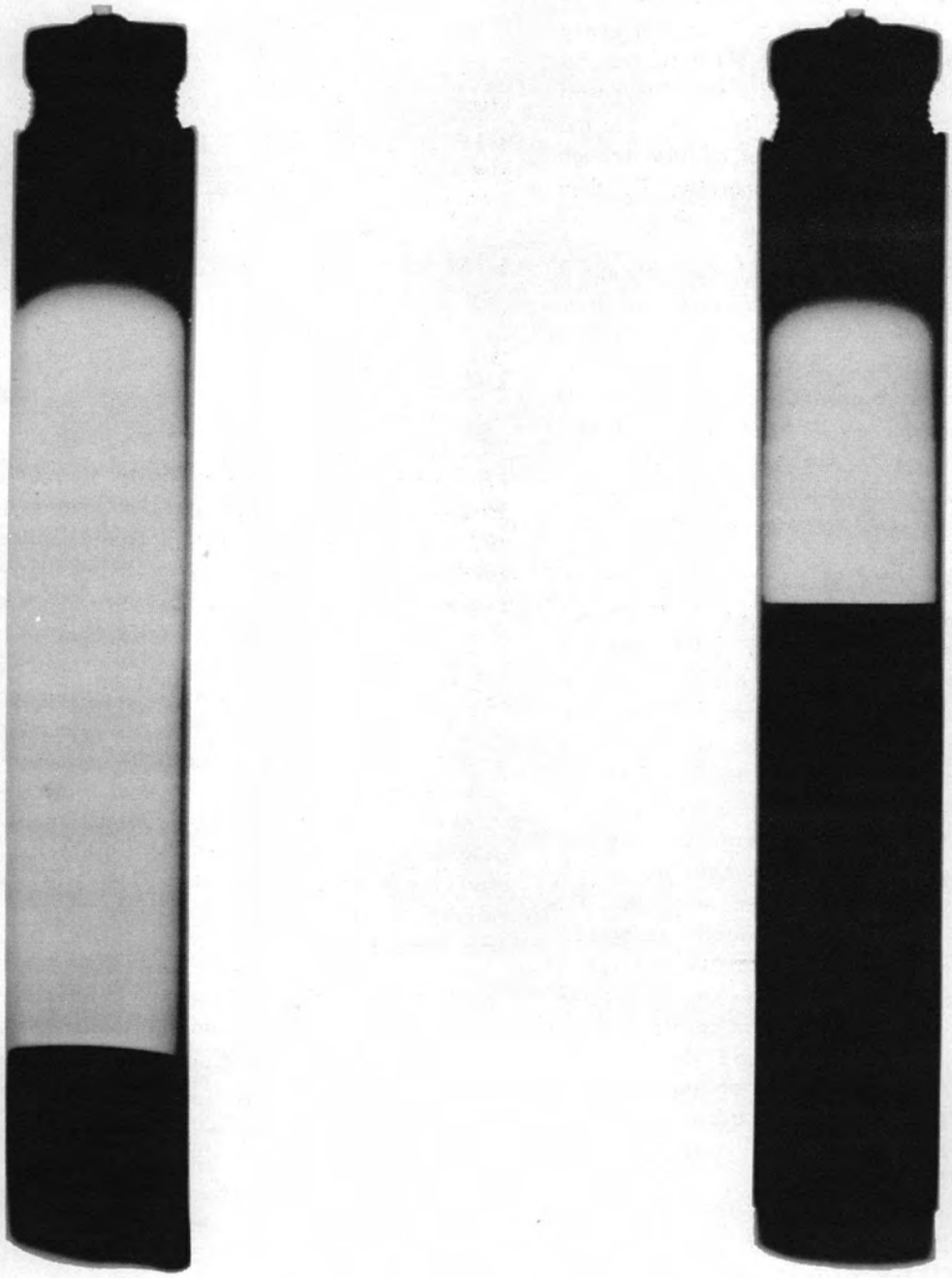

Fig. 14.6. X Radiographs of a Settled and a Settling ThO_2 Slurry in a Stainless Steel Bomb at Room Temperature.

15. FUEL PROCESSING

D. E. Ferguson
J. R. Engel
P. A. Haas
C. C. Haws, Jr.
R. W. Horton
E. O. Nurmi
S. S. Kirslis
J. K. Langsdon
R. A. McNees
S. Peterson

15.1 FISSION-PRODUCT CHEMISTRY

15.1.1 Rare-Earth Sulfate Precipitation from Fuel Solution

X-ray diffraction studies confirmed chemical indications[1] that the solid phase separating from simulated fuel solutions (0.02 *m* UO_2SO_4, 0.005 *m* H_2SO_4) containing less than 150 mg of $Nd_2(SO_4)_3$ per kilogram of H_2O differs from that obtained when larger amounts of $Nd_2(SO_4)_3$ are present. When 50 to 100 mole % excess H_2SO_4 was used in the fuel solution (0.01 to 0.02 *m* H_2SO_4), the yellow solid phase was obtained at a temperature about 10°C lower than that when the normal fuel was used. Comparison of these yellow crystals by x-ray diffraction techniques indicates that the major constituent is the same in both cases, but a second phase, as yet unidentified, is present in the solid obtained from the normal fuel solution.

Studies on $Ce_2(SO_4)_3$ were also carried out in the platinum-lined autoclave, with the use of a hot Zircaloy-2 finger.[2] From simulated fuel solutions containing $Ce_2(SO_4)_3$, colorless crystalline precipitates were sometimes obtained on the hot finger. These solids looked much like the $Nd_2(SO_4)_3 \cdot H_2O$ crystals previously reported.[1] X-ray diffraction data showed that the solids are not any known form of cerium oxide and do not correspond to any known hydrate of cerium sulfate. At other times a noncrystalline deposit was formed on all inner surfaces of the platinum liner. When Ce^{144} tracer was used, almost all the tracer activity was on the liner and almost none on the hot finger.

In circulating-loop studies with 0.04 *m* UO_2SO_4–0.01 *m* H_2SO_4, containing 5 g of Lindsay mixed rare earths per kilogram of H_2O, neodymium precipitated on hot metal surfaces in a form that readily redissolved when the metal was cooled, but cerium did not redissolve. The rare-earth mixture had the composition:

	Wt %
Cerium	48
Lanthanum	24
Neodymium	18
Praseodymium	6
Samarium	2
Others	2

The cerium precipitate partially redissolved in acidic hydrogen peroxide. Neodymium concentrations were the same at a given temperature whether the temperature was increasing or decreasing, but cerium concentrations differed (see Fig. 15.1).

The neodymium and cerium were traced, with Nd^{147} and Ce^{144}, and activity balances were 89 and 75%, respectively (see Table 15.1). In similar studies in which neodymium was the only rare earth present, 95% of the tracer was recovered. This indicates the formation of an insoluble species which will be difficult to remove from the heated surface. Only 60% of the total tracer activity was recovered in fuel removed from the loop.

15.1.2 Effects of Various Solutes on Neodymium Sulfate Solubility

It was previously reported[2] that the solubility of neodymium in uranyl sulfate solutions is increased by increasing the uranium concentration and decreased by the presence of other rare earths. In a continuation of this study it was found that neodymium sulfate is soluble in water to the extent of 1 mg per kilogram of H_2O at 290 to 300°C when only it or mixed rare-earth sulfates are present (no uranyl sulfate present).

In a solution 0.07 *m* in Na_2SO_4 (no UO_2SO_4 present) and 0.016 *m* H_2SO_4, neodymium sulfate was soluble at 275°C to the extent of only 6 to 8 mg per kilogram of H_2O. In a uranyl sulfate

[1] R. A. McNees and S. Peterson, *HRP Quar. Prog. Rep. July 31, 1955*, ORNL-1943, p 201.

[2] *Ibid.*, p 202.

TABLE 15.1. Nd^{147} AND Ce^{144} TRACER ACTIVITY BALANCES

Circulating fluid: 0.04 *m* UO_2SO_4–0.01 *m* H_2SO_4, containing 5 g of mixed fission products (traced with Nd^{147} and Ce^{144}) per kilogram of H_2O

Material	Volume (liters)		Nd^{147} Activity		Ce^{144} Activity	
	UO_2SO_4 Fuel	Wash Solution	Counts/min/ml $\times 10^3$	Counts/min $\times 10^6$	Counts/min/ml $\times 10^3$	Counts/min $\times 10^6$
Input						
Loop startup solution	9.5		None		None	
Rare-earth feed solution	2.10		110	231	242	509
Sample replacement fuel[a]	3.0		None		None	
Wash solutions		64.3	None		None	
Total	14.6	64.3		231		509
Output						
Loop drainings	9.4		16	151.0	18.0	169
Unrecycled samples (1st)[a]	0.07		260	18.2	730.0	51
Unrecycled samples (2nd)[a]	3.7		3.7	8.5	5.81	21.5
First water wash	1.0[b]	11.7	1.4	17.8	1.0	12.7
First acid wash[c]		13.0	None		0.13	2.7
First acid-H_2O_2 wash[d]		12.0	0.8	9.6	8.7	104.0
Second water wash		13.5	None		0.01	0.1
Second acid-H_2O_2 wash[d]		13.5	None		0.93	12.6
Total	14.17	63.7		205.1		373.6
Total recovery	97.1%	99%		89%		75%
Recovery in fuel	90.2%			80%		50%

[a]The presampling flushes were usually returned to the loop or were mixed with the loop drainings at the end of the run. The actual sample volumes were replaced by new fuel free of neodymium or other rare earths.

[b]The first water wash removed from the loop contained 12 g of uranium, probably as a result of incomplete drainage of the loop. This was equivalent to 1 liter of 0.05 *m* UO_2SO_4.

[c]An acid wash was 13 liters of H_2O plus 30 ml of concentrated sulfuric acid; this would be 0.04 *m*.

[d]An acid-peroxide wash was 13 liters of H_2O plus 30 ml of concentrated sulfuric acid and 1 lb of 30 to 35% H_2O_2.

solution of the same concentration at the same temperature, the solubility of neodymium sulfate was 450 to 500 mg per kilogram of H_2O.

In further tests it was shown that the amount of neodymium sulfate in solution in 0.02 *m* UO_2SO_4 was not affected by increasing the free sulfuric acid from 25 to 100 mole % excess (0.005 to 0.02 *m*).

15.1.3 Reactor Solids Dissolution

Since the homogeneous reactor processing scheme presently envisioned will concentrate the fission- and corrosion-product solids into a relatively small volume, some trouble may be anticipated in removing the resultant slurry from the processing equipment. Therefore some method for dissolving the major portion of these solids is desired. Solids for dissolution studies were prepared by heating to 285°C uranyl sulfate solutions containing sulfates of rare earths, nickel, chromium, iron, and manganese. Neodymium sulfate was easily leached from the solid residue by water or remained in the supernatant liquid from the solids-preparation step. The remaining solids were rather easily dissolved in 63% HNO_3 and in 37% HCl to give stable solutions. In 9 *m* H_2SO_4, dissolution was much slower, and the resultant solution was not stable. In 32% HNO_3 and 4.5 *m* H_2SO_4, dissolution was not complete, but the solids remaining were easily

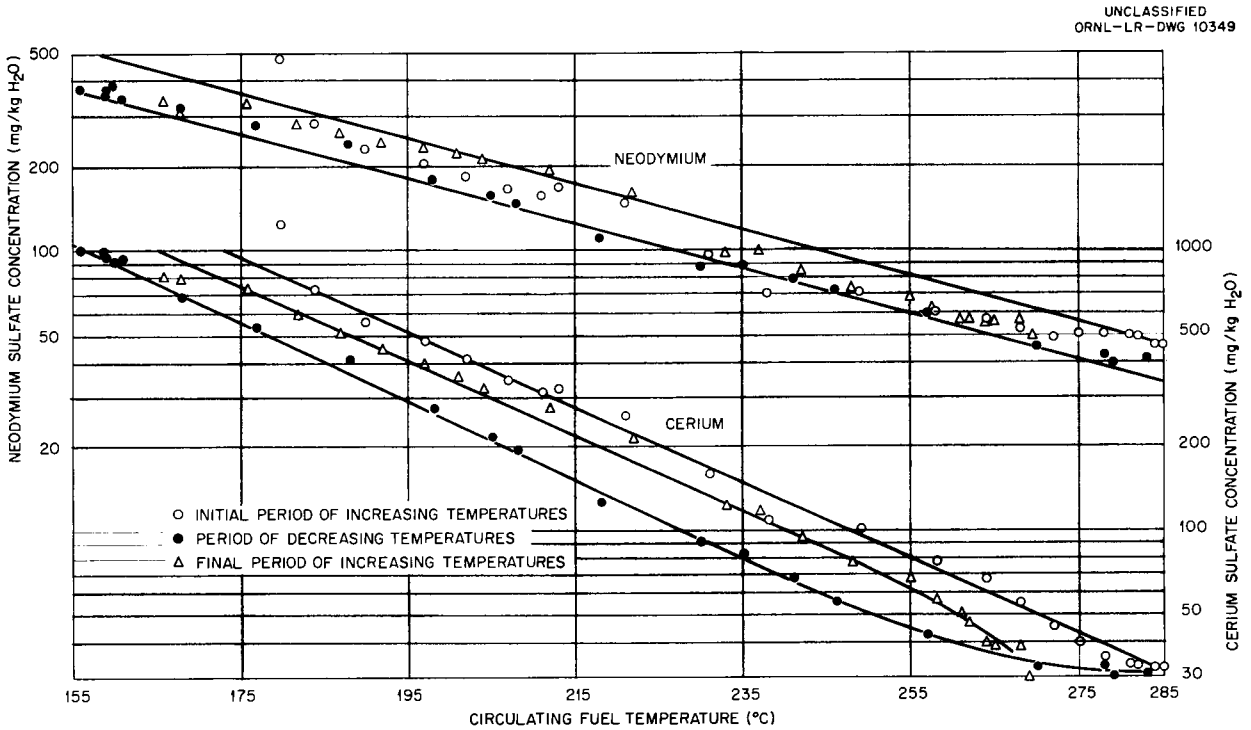

Fig. 15.1. Concentrations of Neodymium and Cerium Sulfates in Simulated Circulating Fuel at Various Temperatures.

dissolved in 63% HNO_3. In 57% HNO_3 the dissolution was markedly more rapid than it was when only 50% HNO_3 was used. These tests will be extended to solids containing zirconium, niobium, and tin as soon as suitable starting materials can be prepared.

15.1.4 In-Pile Solids Precipitation

A device was developed for comparing in-pile and out-of-pile solids deposition on hot Zircaloy-2 surfaces. It consists of a high-pressure bomb which contains a Zircaloy-2-clad hollow cylinder of soft iron. This cylinder is immersed in test liquid while being heated, and at the desired time it is withdrawn from the liquid by a solenoid coil and held out of the liquid by a catch. Hysteresis heating at 3000 kc was adequate to simulate in-pile heating.

15.1.5 Iodine

It was previously indicated[2] that the radiation-induced reduction of iodate ion to elemental iodine is strongly inhibited by uranium and favored by copper ions and acid, and this was confirmed. In further studies, under conditions such that about 25% of the iodate was reduced in the absence of uranium in 1 hr, reduction was scarcely detectable in the presence of 1 g of uranium (as uranyl sulfate) per kilogram of H_2O. Some typical results of iodate irradiation experiments are shown in Table 15.2.

TABLE 15.2. TYPICAL RESULTS OF IRRADIATION OF IODATE SOLUTION

HIO_3 in solution: 1×10^{-5} *m*
Uranium (as UO_2SO_4) in solution: 1.0 g per kilogram of H_2O
Irradiation: 11,000 r/min

$CuSO_4$ (*m*)	H_2SO_4 (*m*)	Exposure (hr)	Per Cent Reduced
0	0.003	2	<1
0	0.03	2	10
0.001	0.003	2	10
0.002–0.004	0.003	2	18
0.001–0.004	0.03	1–2	60
0.001–0.004	0.03	0.35	45

16. PLUTONIUM-PRODUCER BLANKET PROCESSING

D. E. Ferguson

R. E. Leuze R. H. Rainey

The proposed method for processing the uranyl sulfate blanket of the plutonium producer takes advantage of the low solubility of plutonium under reactor conditions. The PuO_2 is continuously concentrated in a small volume of blanket solution for removal and recovery. The study of plutonium chemistry has included adsorption of plutonium on metals, concentration of PuO_2 by a hydroclone, and in-pile studies.

16.1 ADSORPTION OF PLUTONIUM ON METALS

Results of continuous-flow laboratory experiments with metal disks indicated that the adsorption of plutonium on titanium and on Zircaloy-2 from 1.26 *m* UO_2SO_4 at 250°C is essentially nonreversible. It therefore appears that, in a reactor, plutonium will continue to be adsorbed on the walls until it is removed by abrasion or leaching solutions. The rate at which the plutonium is adsorbed is a function of the concentration of plutonium in solution. The plutonium is adsorbed as PuO_2 crystals.

In continuous-flow runs with feed containing 100 mg of plutonium per kilogram of H_2O, plutonium was adsorbed by titanium and Zircaloy-2 to the extent of about 0.5 mg/cm^2, with no indication that equilibrium had been reached (Fig. 16.1). These data are consistent with previous static data[1] in which equilibrium was not approached after 50 runs. The rate of adsorption was markedly dependent on the plutonium concentration of the solution. After six consecutive runs, in which the titanium disks continued to adsorb plutonium at the same rate, the feed was changed to one containing 3 mg of plutonium per kilogram of H_2O. Plutonium was neither adsorbed on nor desorbed from the disks during these runs. In one run, fresh Zircaloy-2 disks adsorbed 0.1 μg of plutonium per square centimeter from a feed containing 3 mg of plutonium per kilogram of H_2O, which is a factor of about 300 lower than that on the Zircaloy-2 disk in feed containing 100 mg of plutonium per kilogram of H_2O. There was little or no desorption of plutonium previously deposited when disks were exposed to uranyl sulfate solution containing no plutonium.

Since the plutonium concentration of the flowing stream decreased as a result of PuO_2 precipitation and adsorption as it passed through the vessel, disks near the inlet were exposed to much higher concentrations of plutonium. When the feed contained 100 mg of plutonium per kilogram of H_2O, the disks at the inlet adsorbed about five times as

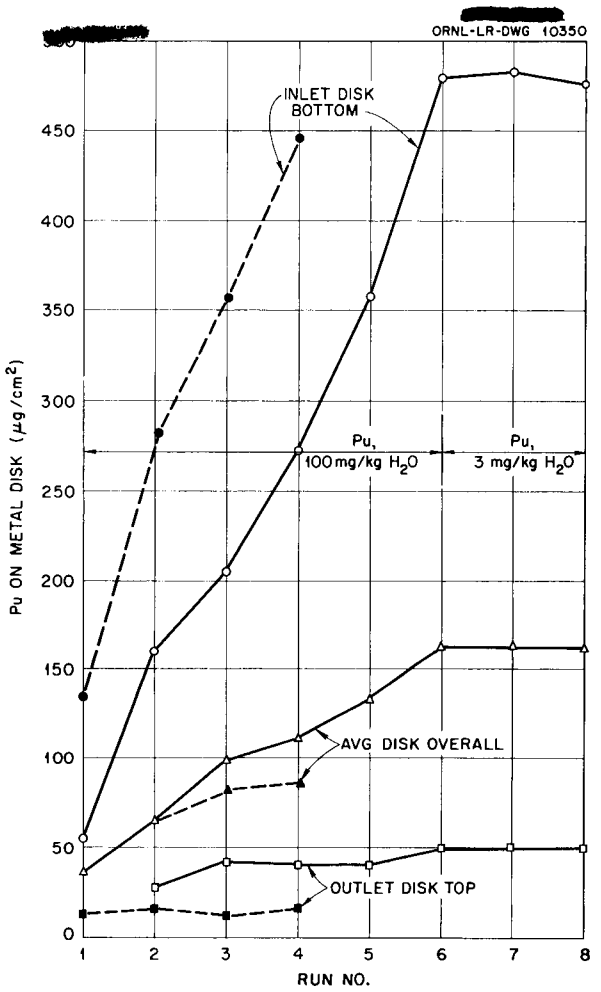

Fig. 16.1. Adsorption of Plutonium on Titanium and Zircaloy-2 from 1.26 *m* UO_2SO_4. Flowing stream, 1 liter/min.

[1] R. H. Rainey, *HRP Quar. Prog. Rep. Jan. 31, 1955*, ORNL-1853, p 193.

much plutonium in each run as did the disk at the outlet (Figs. 16.2 and 16.3). The bottoms of the disks adsorbed at least twice as much plutonium as did the tops. No explanation for this is offered. The distribution pattern of the plutonium was about the same on the two metals and did not change in repeated runs. No effect of position and no difference in the tops and bottoms were noted with the feed containing 3 mg of plutonium per kilogram of H_2O.

After the four Zircaloy-2 runs shown in Fig. 16.1 were made, the disks were rearranged, but in the next two runs deposition was characteristic of their new position in the reactor and not related to

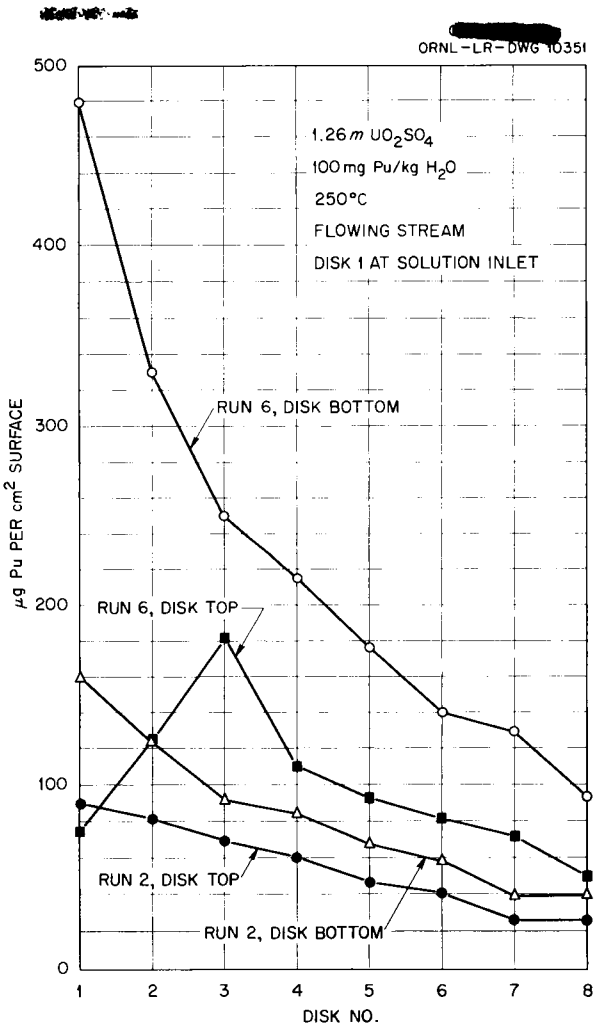

Fig. 16.2. Effect of Position of Sample in Holder on Rate of Plutonium Adsorption on Titanium.

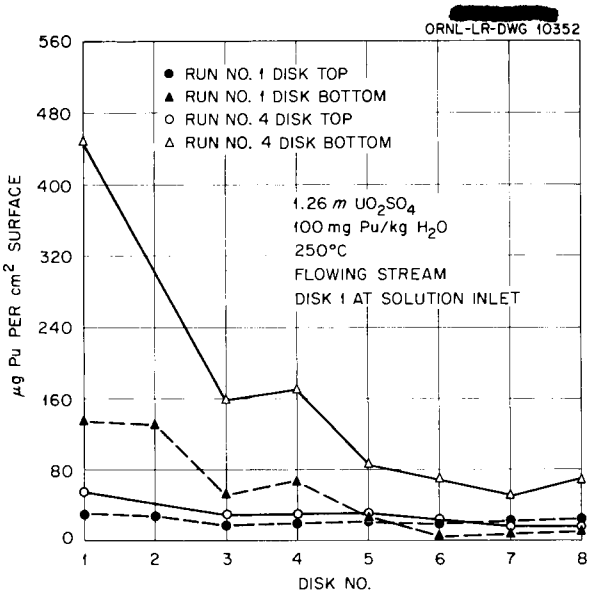

Fig. 16.3. Effect of Position of Sample in Holder on Rate of Plutonium Adsorption on Zircaloy-2.

their previous exposure. This indicates that the additional plutonium adsorption is not dependent on the amount of plutonium already adsorbed.

Adsorption of the plutonium appeared to start by the crystallizing of PuO_2 on the metal oxide or by the trapping of small PuO_2 crystals in this oxide. Plutonium then continued to be adsorbed by deposition on these crystals. Within the limit of an analysis, there was no adsorption of plutonium on gold surfaces, apparently because there are no sites on which crystallization may start.

Varying the amount of oxide film on the metal did not affect the rate of adsorption. In two runs the plutonium adsorption rate on disks with a normal oxidation coating, produced by conditioning at 250°C in 1.26 *m* UO_2SO_4 solution, was about the same, as shown by autoradiographs and visual inspection, as that on disks with a heavy oxidation coating produced by heating in a muffle furnace overnight at 800°C. In the first run, during the thermal cycling of the equipment, much of the heavy oxidation coating broke from the disk, carrying the plutonium.

Chemical analysis of a film from a Zircaloy-2 disk which by alpha count had adsorbed 1.16 mg of plutonium showed that it contained 1.34 mg of plutonium, 0.38 mg of uranium, and 6.81 mg of

zirconium. At least some of the zirconium came from the base metal as a result of corrosion during the defilming.

X-ray diffractive patterns of films scraped from titanium and Zircaloy-2 showed PuO_2 (and/or UO_2) and the base metal only. Some of the PuO_2 crystallites on the metal surfaces had diameters larger than 1000 Å as determined by x-ray diffraction line broadening, whereas the crystallites centrifuged from the solution had diameters less than 1000 Å.

Experiments were carried out in the equipment described previously.[1] A series of runs was made in which about 1 liter of 1.26 *m* UO_2SO_4 at 250°C containing plutonium was passed over eight metal disks (4.9 cm^2, 2.1 cm^2 on each side and 0.7 cm^2 on the edges). After each run the system was cooled to room temperature, and the disks were removed, washed with water, and dried. The amount of plutonium adsorbed was determined by direct counting in a low-geometry alpha counter. Several disks were chemically descaled, and the plutonium was determined by TTA analysis. The agreement between the two analyses was within 15%; the direct counting had the lower value, as would be expected from self-absorption.

16.2 SEPARATION OF PuO_2 BY A HYDROCLONE

Plutonium dioxide in water slurries was concentrated at room temperature with a ¼-in.-dia hydroclone by factors of 3.0 to 4.6. This amount of concentration is encouraging, since considerably higher factors can be expected at 250°C. Plutonium material balances through the hydroclone were low; however, some improvement was noted when PuO_2 was slurried in sodium nitrate solution or in water containing Ultrawet (a commercial wetting agent).

The hydroclone efficiency for PuO_2 concentration varied from 38 to 51% when the underflow volume was 9.4 to 12.6% (Table 16.1). This corresponds to concentration factors of 3.0 to 4.6, with an average value of 3.9. For ThO_2 [with a particle-size distribution of (by wt): 100% less than 2 μ, 50% less than 1 μ, and 10% less than 0.6 μ] the concentration was about twice as great and the hydroclone efficiency was 70%, with a 9.2% underflow volume. In a typical experiment with only water used to slurry the PuO_2, the material balance was 42%. When PuO_2 was slurried in 10% $NaNO_3$, the material balance was 64%. When PuO_2 was slurried in water containing Ultrawet, material balances varied from 52 to 80%.

The PuO_2 used in these experiments was recovered from the waste stream in the continuous-flow adsorption experiments. The PuO_2 was centrifuged, washed free of UO_2SO_4, and reslurried in water. The tests were made with a standard hydroclone, taking a small stream for the underflow.

A ¼-in.-dia hydroclone with a 35-ml underflow pot was constructed for future experiments. This new hydroclone is designed so that the underflow

TABLE 16.1. PuO_2 AND ThO_2 CONCENTRATION BY A HYDROCLONE

Conditions: ¼-in.-dia hydroclone, 400 ml of feed, room temperature

Experiment No.	Hydroclone Feed		Material Balance (%)	Underflow Volume (%)	Separation Efficiency* (%)	Concentration Factor*
	Solid	Liquid				
1	29.4 mg of ThO_2	Water	153	9.2	70	7.6
2	1.4–2.1 mg of PuO_2	Water	42	10.0	46	4.6
3	1.4–2.1 mg of PuO_2	10% $NaNO_3$	64	12.0	41	3.4
4	1.4–2.1 mg of PuO_2	Water and Ultrawet	76	9.4	41	4.4
5	1.4–2.1 mg of PuO_2	Water and Ultrawet	52	12.6	51	4.0
6	1.4–2.1 mg of PuO_2	Water and Ultrawet	80	12.6	38	3.0
7	1.4–2.1 mg of PuO_2	Water and Ultrawet	55	12.6	47	3.7

*Based on the relation Pu in overflow + Pu in underflow = Pu in feed.

pot can be opened and its contents completely removed for analysis. The system is being tested with ThO_2 prior to its installation in a glove box for use with PuO_2.

16.3 IN-PILE CHEMISTRY OF PLUTONIUM AND NEPTUNIUM

Measurements of plutonium solubility and adsorption determined by experiments in which 1.26 *m* UO_2SO_4 (0.03% U^{235}) was irradiated in the LITR at 250°C were not reproducible. This was probably a result of the handling procedure, since it was necessary to allow a radioactive decay period of several days before the bomb was opened and the solution, precipitate, and oxide film on the bomb were sampled. It was assumed that neither neptunium nor plutonium migrated to other locations during this period, and adjustments were made for neptunium decay and plutonium growth between the end of the irradiation and the time of analysis. With this limitation in mind, a brief summary of the results is presented.

Plutonium in solution at the end of the irradiation varied from 6 to 28 mg per kilogram of H_2O. Adsorption of plutonium on titanium bomb walls was only 1 to 3 $\mu g/cm^2$; however, this represented from 25 to 50% of the total plutonium present. At least 80% of the neptunium was in solution.

The plutonium in solution was much greater than the 3 mg per kilogram of H_2O measured in out-of-pile experiments. This may be a result of plutonium or neptunium migration during the decay period, or it may be a result of improper reduction-oxidation conditions, since no radiolytic hydrogen and oxygen were noted even with only 0.005 *m* $CuSO_4$ catalyst.

16.4 TEST LOOPS

The loop for testing plutonium producer blanket processing equipment has been designed and is being constructed. It will be made of titanium.

17. THERMAL-BREEDER BLANKET PROCESSING

D. E. Ferguson

R. E. Leuze W. E. Tomlin

17.1 LEACHING OF IRRADIATED THORIUM OXIDE

Refluxing of irradiated ThO_2 in 6 to 8 *M* H_2SO_4 for 2 hr converts essentially all the oxide to $Th(SO_4)_2$, which is only slightly soluble in the acid leach liquor. During this conversion protactinium is partially dissolved. In previously reported tests,[1] 95% of the protactinium was dissolved when 15 mg of ThO_2 was treated with a 620-fold excess of 7 *M* H_2SO_4 for 2 hr. Treatment of larger amounts of ThO_2 gave lower protactinium recovery; for example, only 50% of the protactinium was removed from 4.8 g of ThO_2. This was apparently a result of poor contacting, which resulted in slower leaching rates. Greater protactinium recovery from 3- to 11-g batches of ThO_2 was obtained by refluxing in 100 ml of 8 *M* H_2SO_4 for 3 hr, diluting to 1 liter to dissolve the resulting $Th(SO_4)_2$, and recrystallizing the $Th(SO_4)_2$ by evaporation at 80°C. The results in Table 17.1 show that 60 to 70% of the protactinium was leached with thorium losses of less than 0.5%. In order to remove 95% of the protactinium, it was necessary to dissolve 6 to 11% of the thorium. The data also show that additional recovery of protactinium by washing the $Th(SO_4)_2$ results in additional thorium dissolution. All these experiments were made with tracer quantities of protactinium (10^8 to 10^{10} gamma counts/min). Owing to the large volumes required, this procedure of dissolving and recrystallizing the $Th(SO_4)_2$ is not attractive for full-scale processing.

The study of leaching techniques has been temporarily discontinued, since they do not seem to offer much, if any, advantage over complete dissolution of ThO_2 and solvent extraction methods

[1] D. E. Ferguson, R. E. Leuze, and W. E. Tomlin, *HRP Quar. Prog. Rep. July 31, 1955*, ORNL-1943, p 221-222.

TABLE 17.1. LEACHING OF PROTACTINIUM FROM IRRADIATED ThO_2

ThO_2 (calcined at 650°C) leached in 100 ml of 8 *M* H_2SO_4 for 3 hr
Resulting $Th(SO_4)_2$ dissolved by diluting to 1 liter and recrystallized by evaporation at 80°C
Washing consisted in dissolving $Th(SO_4)_2$ in 1 liter of water and evaporating at 80°C
Total Pa in each run: 10^8 to 10^{10} gamma counts/min

ThO_2 (g)	Leach Filtrate (ml)	Wash Filtrate (ml)	Thorium Removal (%)			Protactinium Removal (%)		
			Leach	Wash	Total	Leach	Wash	Total
3.4	96	None	0.024		0.024	73		73
3.25[a]	120	None	0.048		0.048	75		75
9.0	180	None	2.8		2.8	82		82
10.0	100[b]	28[b]	0.5	0.1	0.6	57.7	19.5	77.2
10.0	150	50[b]	1.6	0.8	2.4	64.7	20.0	84.7
6.0	140	93	0.6	9.3	9.9	73	22	95
9.7	168	160	1.5	9.5	11.0	72.4	22.7	95.1
11.1	220	148[c]	5.1	0.8	5.9	91.5	5.4	96.9

[a] ThO_2 calcined at 900°C.

[b] Recrystallization carried out stepwise, that is, partial evaporation followed by filtration and further evaporation of the filtrate to the final volume.

[c] 100 ml of 8 *M* H_2SO_4 added to wash.

for processing the ThO_2 blanket of the thorium-breeder reactor.

17.2 CONVERSION OF $Th(SO_4)_2$ TO ThO_2

It was previously reported[1] that sulfate can be removed, from the residue resulting when ThO_2 is leached with sulfuric acid, by calcining in air at 900°C. Calcination at 900°C for 5 hr reduced the sulfate content to about 0.2%; further removal was extremely slow. Essentially complete removal of sulfate was achieved by calcining a 1-g sample of such a residue at 900°C for 24 hr, followed by washing in 25 ml of water for 2 hr. After calcination the sulfate content was 0.11%, and after the water wash only 100 ppm of sulfate remained.

18. EQUIPMENT DECONTAMINATION

D. E. Ferguson

R. E. Leuze R. D. Baybarz

A program was initiated to develop methods of decontaminating reactor equipment and chemical processing equipment used in connection with homogeneous reactors.

18.1 SCALE REMOVAL FROM STAINLESS STEEL

During decontamination of the HRE, fission products were found to be bound within the corrosion film deposited on the stainless steel. For effective decontamination it was necessary to remove this film. In scouting tests, solutions containing strong reducing agents effectively reduced the tenacious black oxide, formed on type 347 stainless steel by uranyl sulfate solution at 250 to 300°C, to a loosely held reddish-brown oxide. The oxide was easily removed from the metal by washing with a stream of water. The most effective reducing agents tested were titanous chloride, nascent hydrogen, chromous sulfate, and stannous chloride. Of these, titanous chloride gave the most rapid reduction and dissolved the scale. However, the use of titanous chloride may not be practical, since it oxidizes and hydrolyzes to produce a very fine TiO_2 precipitate and HCl, and removal of these materials from the reactor system would be difficult. At room temperature, solutions containing 20, 10, 2, and 1% $TiCl_3$ removed such a scale from type 347 stainless steel in 1, 4, 20, and 25 hr, respectively. Corrosion samples placed in solutions containing less than 5% $TiCl_3$ showed no weight loss in 90 hr. The samples corroded at a rate of 0.35, 0.11, and 0.025 mil/day in solutions at room temperature containing 20, 10, and 5% $TiCl_3$, respectively.

Mineral acids were tried in an attempt to remove the oxide film, but none was found that gave satisfactory descaling. A solution containing 1.8 *M* H_2SO_4 and 1.2 *M* HCl removed the oxide in large flakes, with no apparent dissolution of the oxide but considerable corrosion of the stainless steel. A solution containing 15% HNO_3, 42% CH_3COOH, and 43% H_3PO_4 did not remove the oxide film.

It is apparent that the nature of the oxide film deposited on type 347 stainless steel varies, since the effectiveness of oxalic acid in removing the film varied. A corrosion film deposited on type 347 stainless steel by uranyl sulfate at 250 to 300°C (detailed history unknown) in a corrosion loop at Y-12 was not removed by oxalic acid. However, oxalic acid was effective in removing the film from samples of stainless steel exposed to 0.04 *m* UO_2SO_4 at 250 to 300°C for 1500 hr in loop A. The time for complete removal at 87°C varied from 6 hr with 8% oxalic acid to 18 hr with 0.5% oxalic acid. The mechanism of scale removal is not known; however, it appeared that the oxalic acid attacked either the film or the metal at the interface and caused the scale to flake off.

The use of other reducing agents for removing scale from stainless steel will be investigated, and descaling of titanium and Zircaloy-2 will be studied. Special emphasis will be placed on the removal of plutonium from these films.

19. SUMMARY OF WORK OF VITRO LABORATORIES[1]

A series of experiments was concluded in which small quantities of iodine (as HI) were introduced into a stainless steel bomb containing simulated core solution at 280 and 330°C. The iodine concentration was varied from 0.001 to 0.10 g/liter. Liquid and vapor samples were removed from the apparatus after equilibrium had been obtained, and both samples were analyzed for I_2 by I^{131} counting. Preliminary runs were made in a small bomb covering a temperature range of 280 to 330°C and concentrations of 0.01 to 0.1 g per kilogram of H_2O. The vapor-liquid equilibrium of I_2 was also determined for the case of water at various pH values. These tests led to the following conclusions, where the equilibrium constant is the ratio of the mole fraction of iodine in the vapor phase to the mole fraction of elemental iodine in the liquid phase:

1. The vapor-liquid equilibrium constant for I_2 in fuel solution is approximately 7 and is not affected by temperature and iodine concentration to any great extent.
2. The vapor-liquid equilibrium constant for I_2 in water solution is 0.25 and is not affected by variations in temperature or pH to any great extent in the range 3.8 to 9.9.

Distillation, which had been considered as a possible means of removing iodine from fuel solution, has been eliminated because of the two-phase mixture which occurs at the temperatures required for boiling the fuel at reactor pressures. Present thoughts are directed toward inert-gas stripping, with O_2 used as a means of removing I_2 from fuel solutions.

The inert-gas stripping of fuel solution using O_2 in a countercurrent packed column was considered in a series of calculations.

From the dimensions and the power level of the proposed TBR, an iodine generation rate of about 30 mg/min was calculated; this corresponds to a concentration of about 0.12 mg/liter in the core, assuming a 40-min processing cycle. From an iodine material balance around the stripping process the following equation was found:

$$R = \frac{250}{E},$$

where R equals liters/minute to be processed and E equals efficiency of once-through removal process. Calculations were made for determining the number of stripping columns required to process 250 liters/minute, assuming that $E = 1$. Assuming a countercurrent process in a packed column, with oxygen contacting the liquid feed at 280°C and 2000 psia, calculations were made on the basis of total flow (under column loading conditions) and the number of stages required to effect a separation. Results of these calculations indicate that for ten parallel packed columns (6-in. ID to handle the material from the standpoint of flow) an infinite number of transfer units would be required to get a separation greater than 3.5 (concentration of I_2 inlet stream ÷ concentration of I_2 outlet stream).

Due to the number of stripping columns required, inert-gas stripping by means of a venturi was considered. Several tests were made on a small venturi to determine the air flow at various air inlet pressures. The results indicate a low air-to-water weight ratio through the venturi [1/208 at 28 in. (abs) Hg]. These weight ratio results are not good, but then a venturi is not the ideal piece of equipment for moving large volumes of gases. An ejector type of fume scrubber would be more acceptable from the gas-handling standpoint; one is presently being designed for incorporation in a high-pressure loop.

The conceptual flow sheet for an iodine-processing cycle for a full-scale reactor is shown in Fig. 19.1. The process may be summarized as follows:

1. stripping iodine from the fuel solution in an ejector, using O_2 as an inert gas;
2. chemical fixation of iodine in a scrubbing solution, with provisions for diverting the xenon daughter to an activated charcoal bed;
3. recycling O_2 gas to the ejector (with makeup O_2 being added).

In a flowsheet employing inert-gas stripping, consideration must be given to whether the inert gas can be discarded by venting to the atmosphere after passing through a fixation process or whether the gas must be recovered, recompressed, and reused. Due to the volume of O_2 required for inert gas stripping and from a safety standpoint, the

[1] Summary of KLX-10012.

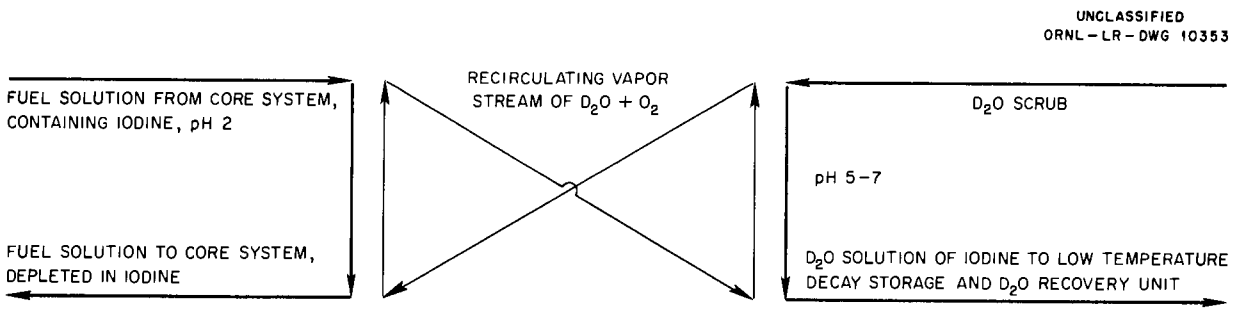

Fig. 19.1. Conceptual Flowsheet for Iodine Removal from the Core Solution of a Thermal Breeder Reactor.

gas must be recycled. As yet, canned-rotor gas compressors are not in an advanced state of development.

Preliminary work was started on the design of bench-scale equipment for countercurrent iodine stripping with oxygen. A high-pressure stripping column (1-in. ID and approximately 16 in. deep to allow a packed column of approximately 11 in.) and packing ($\frac{1}{8}$-in.-dia stainless steel balls) have been ordered. This experimental apparatus will later be modified for continuous countercurrent high-pressure scrubbing tests in which various scrubbing solutions to absorb iodine from an iodine-steam-O_2 stream are used.

Part VI

SUPPORTING CHEMICAL RESEARCH

E. H. Taylor

20. AQUEOUS SYSTEMS AT ELEVATED TEMPERATURES

C. H. Secoy

F. E. Clark
J. S. Gill
G. M. Hebert
F. J. Loprest
W. L. Marshall
J. E. Ricci[1]
D. W. Sherwood
R. Slusher

20.1 ALKALINE CARBONATE–URANIUM TRIOXIDE SYSTEMS AT 250°C

F. J. Loprest W. L. Marshall

The investigation[2] of alkaline carbonate–uranium trioxide systems at 250°C has been continued. Additional data for the system Li_2O-UO_3-CO_2-H_2O have been obtained and are listed in Table 20.1. Most of the experiments were designed in an effort to obtain a more accurate idea of the limits of the unsaturated liquid region and in an attempt to prepare and study a composition in the unsaturated region.

In Figs. 20.1 and 20.2 are plotted the data for experiments II-67 and II-82. The solid phase in these runs was Li_2CO_3 (analysis of the air-dried solid from II-67 gave Li_2O, 40.50%; CO_2, 59.20%; CO_2/Li_2O mole ratio, 0.993). The liquid-phase compositions at 1500 psi may be read from the figures; in the case of II-82, it was UO_3, 2.09%, and Li_2O, 0.82%. A 2% correction applied for residual CO_2 gives the following point on the Jänecke projection: UO_3, 2.13%, and Li_2O, 0.84%. Within experimental accuracy this composition is that of point B in a previously reported phase diagram.[3] This clearly shows that the solubility surfaces of lithium carbonate and the uranyl carbonates, postulated as the saturating phases of liquid B, practically touch each other. It is seen,

[1]New York University.

[2]F. J. Loprest and W. L. Marshall, *HRP Quar. Prog. Rep. July 31, 1955*, ORNL-1943, p 227–235.

[3]*Ibid.*, Fig. 19.7, p 228.

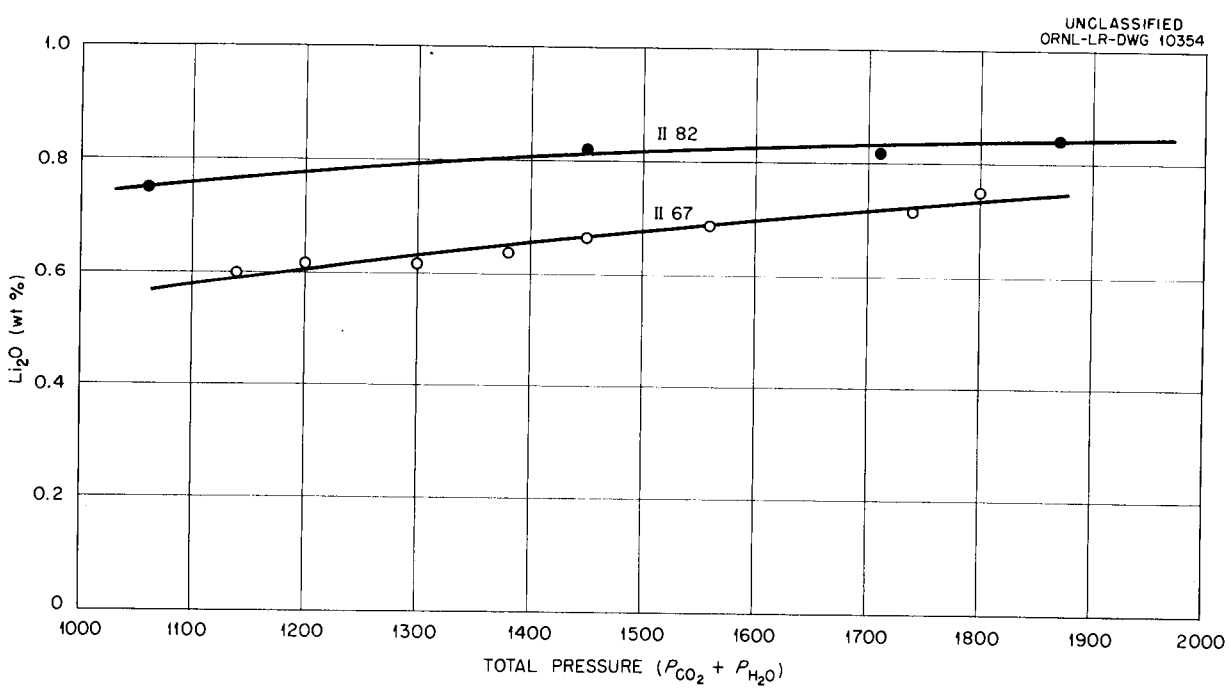

Fig. 20.1. Per Cent of Li_2O in Liquid Phase; System Li_2O-UO_3-CO_2-H_2O.

TABLE 20.1. THE SYSTEM Li_2O-UO_3-CO_2-H_2O AT 250°C

Run No.	Total Mixture[a] (%)		Liquid Phase[b] (%)		Density of Liquid[c]	Total Pressure[d] (psi)	Agitation Time[e] (hr)	Mole Ratio of Li/U in Liquid
	UO_3	Li_2O	UO_3	Li_2O				
II-67	0.980	5.033	1.110	0.750	1.017	1800	1	12.9
			1.131	0.719	1.035	1740	1	12.2
			1.094	0.693	1.021	1560	1	12.1
			1.093	0.681	1.006	1560	4	11.9
			1.066	0.668	1.019	1450	2	12.0
			1.082	0.641		1380	1	11.3
			1.071	0.636		1390	2	11.4
			1.071	0.621		1300	3	11.1
			0.982	0.622		1200	2	12.1
			1.074	0.602	1.017	1140	2	10.7
II-72	3.723	5.695	3.527	1.006	1.055	1740	4	5.45
			3.551	1.039	1.056	1520	1	5.60
			3.022	0.894	1.048	1280	1	5.67
			2.300	0.724		1120	5	6.03
II-76	3.273	2.944	3.462	1.039	1.053	1820	3	5.75
			3.292	1.070	1.052	1600	2	6.22
			2.059	0.933	1.034	1400	4	8.68
			1.782	0.785		1220	3	8.43
II-79	1.943	0.584	1.237	0.561	1.018	1670	2	8.68
			1.268	0.577	1.020	1400	2	8.71
			1.343	0.593	1.021	1780	2	8.45
			1.265	0.568	1.023	1760	2	8.60
II-82	2.038	4.888	2.006	0.842	1.032	1870	2	8.04
			2.087	0.820	1.041	1660	2	7.54
			2.093	0.824	1.036	1450	2	7.54
			2.081		1.035	1210	3	
			2.061	0.750	1.034	1060	2	6.97
II-85	1.002[f]	0.550	1.101	0.616	1.021	1730	2	10.7
			1.076	0.608	1.021	1250	1	10.8
			1.084	0.616	1.021	2000	2	10.9
			1.095[g]	0.609	1.021	1980	2	10.6
			1.104[g]	0.597	1.021	1560	2	10.4
			0.937[g]	0.518	1.017	1150	1	10.6
II-90	1.038	0.547	1.039	0.584	1.018	1750	2	10.8
			1.053	0.563	1.018	1150	3	10.2
			1.064	0.558	1.021	1820	2	10.0
			1.056[g]	0.563	1.021	1800	3	10.2
			1.086[g]	0.569		1560	3	10.0
			[g]	0.563		1260	3	

[a]Points on Jänecke projection on Li_2O-UO_3-H_2O face.
[b]Not corrected for residual CO_2 and are not points on the projection.
[c]Density measured at room temperature with 1- or 2-ml volumetric pipet.
[d]50 psi of O_2 introduced at 100°C.
[e]Not cumulative.
[f]In doubt because of loss of some water vapor through a leak.
[g]Equilibria at 260°C.

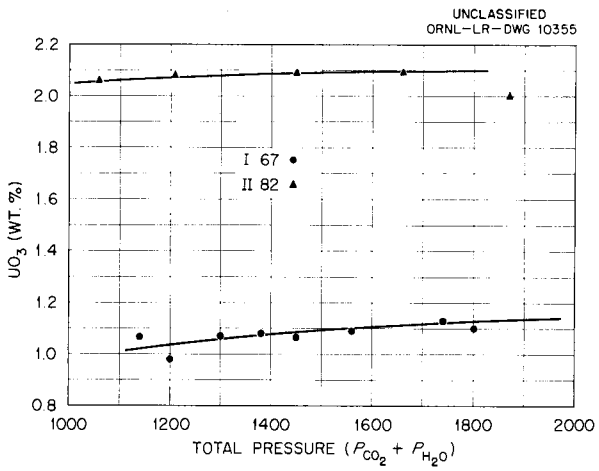

Fig. 20.2. Per Cent of UO_3 in Liquid Phase; System Li_2O-UO_3-CO_2-H_2O.

therefore, that it would be very difficult in actual practice to maintain, unsaturated, a solution containing a maximum amount of uranium (at 1500 psi, point A of the previously reported diagram[3]). Experiments II-79, II-85, and II-90 were attempts to prepare and study an unsaturated solution. The data indicate that an unsaturated solution was obtained at 250°C and probably at 260°C. At the completion of these runs the bomb was rapidly cooled and then opened, and in II-90 there was no solid phase, while in II-85 only a trace of yellow solid was evident. It is obvious that experiment II-79 did not result in an unsaturated solution. An appreciable amount of yellow solid was found after the run was completed. To obtain further information about the phase stability of unsaturated solutions, a bomb containing windows and capable of withstanding the pressures involved has been designed and is now being constructed.

The general argument has been advanced that carbonate solutions, being alkaline, would at least present a different and probably improved corrosion behavior from an acid solution such as uranyl sulfate; it should be pointed out that this argument may not be valid. Even though carbonate solutions of uranium can be prepared with a room-temperature pH higher than 7, these solutions at high temperature and under moderately high CO_2 pressure are almost certainly on the acid side of neutral.

The solutions which are proposed for further study are probably most easily prepared by mixing the appropriate amount of solid UO_3, or a hydrate of known water content, with a solution or mixture of the desired strength of Li_2CO_3 in H_2O. Mixtures prepared in this manner containing uranium in a concentration up to at least 8 g per 1000 g of water appear to be completely phase-stable up to 260°C, if maintained under a total pressure (H_2O + CO_2) between 1200 and 2000 psi measured at 250°C. In all cases the equivalent of about 50 psi of oxygen measured at 100°C is used to prevent reduction of the uranium. The amounts of materials to be used are expressed in terms of the desired grams of uranium per 1000 g of water.

For $0 < g \leqq 8.32$,

$$m = 0.0064g + 0.1352 \quad (1)$$

where m is the moles of Li_2CO_3 per 1000 g of H_2O and g is the grams of uranium per 1000 g of water. This equation is essentially that of a straight line drawn down the center of the unsaturated region. For example, if a solution containing 5 g of uranium per 1000 g of water were desired, m would be 0.1672; a 12.3544-g quantity of Li_2CO_3 would be added to one kilogram of water and a 6.0081-g quantity of UO_3 would then be added. In such mixtures all the solids may not go into solution readily at room temperature but probably always will if a little CO_2 gas is bubbled through the mixture while it is stirred.

Solutions containing as much as 29 g of uranium per 1000 g of water can also be specified, but these will probably always give small amounts of precipitate at high temperatures for the reasons stated above. In this case, where $8.32 < g \leqq 29.13$,

$$m = 0.0086g + 0.1168 \quad (2)$$

where m and g are defined as above.

A single run (II-94) has been made in the system NH_3-UO_3-H_2O. A mixture, containing 2.212% UO_3 and 0.890% $(NH_4)_2O$ (added as NH_4HCO_3) and water, was equilibrated at total pressures (CO_2 + H_2O) of 1200, 1620, and 1740 psi. The liquid phase was water-white, indicating a UO_3 concentration of less than 0.05%. The liquid phase did contain NH_3 – determined qualitatively with strong NaOH solution. The solid phase was bright orange. A slightly washed portion of the solid phase was treated with HNO_3, and there was no evolution of CO_2. It appears that the solid is not an ammonium uranyl carbonate but an ammonium uranate. To obtain a soluble ammonium uranyl carbonate as the solid phase may require a considerably higher pressure of CO_2.

Low-temperature solubility data indicate that systems involving UO_3-CO_2-H_2O and either rubidium oxide or thallous oxide may have liquid phases with high uranium contents at high temperatures. Thallous carbonate has been ordered, and an investigation of the Rb_2O system has been started. Thus far, solutions containing between 2 and 2.5% of UO_3 at a Rb/U ratio of about 15 have been obtained at total pressures between 1200 and 1900 psi.

20.2 OXIDATION OF CHROMIC(III) HYDROXIDE BY OXYGEN AT 250°C

J. E. Ricci[1] W. L. Marshall
C. H. Secoy

The observation of Cr(VI) in solutions from some corrosion tests and equilibrium studies in stainless steel containers but not from others gave rise to the question of whether or not an equilibrium can be established between solid phase Cr(III) and Cr(VI) in solution starting with an aqueous suspension of $Cr(OH)_3$ under oxygen pressure. Furthermore, if such an equilibrium exists, the effect of varying the pH and oxygen pressure was of interest. A series of 15 experiments has been performed in an attempt to answer these questions.

20.2.1 Experiment and Discussion

A washed suspension of precipitated $Cr(OH)_3$, with various initial values of room-temperature pH (fixed by LiOH, H_2SO_4, and CrO_3), was treated at 250°C with oxygen gas, rocked in a 100-cc-volume stainless steel pressure bomb, and sampled by a technique described previously.[2,4] The solution sample was then analyzed coulometrically for Cr(VI) by the Analytical Chemistry Division, and the pH was determined with a Beckman pH meter.

The results for most of the experiments show:

1. poor reproducibility,
2. failure to come to a really constant concentration of Cr(VI) in solution,
3. variability apparently depending on nature, history, age, etc., of the solid.

However, contrary to expectation, Cr(III) in the solid, $Cr(OH)_3$, is definitely oxidized to Cr(VI) in solution even at pH values as low as 2. At pH values over approximately 2.5 the Cr(III) in solid $Cr(OH)_3$ is oxidized rapidly (within 5 to 10 min), resulting in a pH approaching 2. The rate of oxidation, however, slows down markedly as pH 2 is approached. After several days there is still a slow but perceptible increase in Cr(VI) concentration in solution due to oxidation of Cr(III).

In several runs at 250 and 290°C the oxygen pressure was varied from 200 to 1500 psi. In all runs, with the exception of run X, starting at pH's above 2, Cr(III) was oxidized rapidly until a pH of 2 to 2.5 was approached. It appears, therefore, that the pH, rather than the oxygen pressure, is the predominating factor in determining the relative stability of Cr(VI) and Cr(III).

In order to determine whether there is a pH value (near 2) critical for the formation of Cr(VI) in solution from the solid $Cr(OH)_3$ phase, runs XI through XV (See Table 20.2) were made under very nearly uniform conditions:

Fixed initial CrO_3, 0.00167 *m*
Fixed initial $Cr(OH)_3$ solid, 4 mmoles
Varying initial pH (varied by means of H_2SO_4)
Fixed initial O_2 pressure (300 psi measured at room temperature)
Temperature, 250°C
Volume of solution, 60 cc
Volume of bomb, 100 cc

In three of these runs (XI, XII, and XV) the initial calculated pH values were 1.7, 1.8, and 1.9, respectively. In each run the Cr(VI) concentration in solution *decreased* during the treatment at 250°C and the pH *increased*, but not to a value over 2.

In the other two runs (XIII and XIV) the initial calculated pH values were 2.09 and 2.46, respectively, and more Cr(VI) was formed from the solid $Cr(III)(OH)_3$. The pH *decreased*, but not to a value below 2. Analytical results and pH values of samples indicate that in both cases, that is, approach from lower and higher pH's than 2, a "stable" value of Cr(VI) is attained in a relatively short time (10 to 15 min) but still changes slowly over a longer period of time (one to three days).

These five experiments suggest, at best, that for this pressure of oxygen at 250°C the equilibrium is in favor of Cr(VI) at a pH greater than 2 and is in favor of Cr(III) at a pH less than 2.

---

[4] W. L. Marshall, *The pH of UO_3-H_2SO_4-H_2O Mixtures at 25°C and Its Application to the Determination of the Solubility of UO_3 in Sulfuric Acid at Elevated Temperatures*, ORNL-1797 (Nov. 1, 1954).

TABLE 20.2. TYPICAL EXPERIMENTAL DATA ON THE OXIDATION OF CHROMIC(III) HYDROXIDE BY OXYGEN AT 250°C

(O_2 pressure = 300 psi at room temperature)

Run No.	Initial H_2SO_4 Concentration (*m*)	Initial CrO_3 Concentration (*m*)	Initial pH, Calculated	Rocking Time Between Samplings	Solution pH at 250°C	Cr(VI) in Solution (*m*)
XI	0.0146	0.00167	1.7	½ hr to temp		
				10 min	1.91	0.0011
				30 min	1.87	0.00064
				2 hr	1.83	0.00021
				2½ hr	1.85	0.00002
XII	0.0104	0.00167	1.8	½ hr to temp		
				10 min	1.99	0.00148
				1¾ hr	1.87	0.00151
				2 hr	1.87	0.00128
				2 hr	1.80	0.00106
XIII	0.00417	0.00167	2.1	½ hr to temp		
				10 min	2.09	0.00448
				1 hr	2.03	0.00477
				1¼ hr	2.07	0.00475
					2.02	0.00466
					2.02	0.00661
XIV	0.00104	0.00167	2.5	½ hr to temp		
				10 min	2.12	0.00683
				1 hr	2.11	0.00724
				1¼ hr	2.12	0.00727
				2 hr	2.12	0.00737
				2 hr	2.13	0.00727
				16 hr	2.13	0.00676
XV	0.00521	0.00533	1.9	½ hr to temp		
				10 min	1.99	0.00467
				1½ hr	1.96	0.00480
				2 hr	1.98	0.00471
				2½ hr	1.97	0.00466
				16 hr	1.97	0.00433

20.2.2 Preparation and Characteristics of the Solid Phases

The solid $Cr(OH)_3$ was precipitated by the dropwise addition of NH_4OH or LiOH solution to a hot (~70°C) solution of chromic nitrate. The precipitated solid was washed repeatedly with distilled water. The solid was separated each time from the wash water by centrifugation. This solid was green in color and would settle only very slowly at room temperature as a gelatinous precipitate.

When solid $Cr(OH)_3$ was placed in distilled water or in CrO_3-LiOH-H_2SO_4-H_2O solutions at 250 and 290°C under an atmosphere of nitrogen and at room-temperature pH's of 6 to 8, the solid still possessed most of the characteristics of the freshly precipitated material. It was not possible to obtain liquid samples free of solid $Cr(OH)_3$ from the sampling apparatus under these conditions during a two- to four-day period. The color and general appearance of the solid also remained the same as that of the fresh precipitate. However, within 4 to 5 min after the addition of oxygen pressure, clear liquid samples were obtained which already showed considerable oxidation of Cr(III) to Cr(VI), as indicated by the increased concentration of Cr(VI) in solution. The character of the solid phase changed, and compact, rapid settling (within several seconds) occurred. After 5 min the pH had decreased to the range 2 to 2.5. After the runs under oxygen pressure, the solid, upon examination, had a gray color (except in runs XI through XV), and, upon x-ray examination by the Metallurgy Division, appeared to have the structure, CrO(OH), reported by Shafer and Roy.[5]

The solid, in contact with solution before treatment with oxygen, dissolved in mineral acids; however, after oxygen treatment, it was difficult (or impossible) to dissolve the solid in the same acids, hot or cold.

20.2.3 Summary

Contrary to an original expectation that the pH (measured at 25°C) above which Cr(VI) predominates would lie in the range of 4 to 4.5, it is shown that the transition pH is approximately 2 at 250°C. Above this pH, under 300-psi oxygen pressure at 250°C, Cr(III) in $Cr(OH)_3$ is oxidized rapidly to hexavalent chromium (i.e., CrO_3), which dissolves in aqueous solution. Below this value, hexavalent chromium is reduced to Cr(III) and is hydrolytically precipitated as $Cr(OH)_3$ under the same conditions. From a series of runs at 250 and 290°C at oxygen pressures from 50 to 1000 psi, and at pH's of from 1.8 to 12 at 25°C, it appears that the pH is the critical factor determining the favored stability between Cr(III) and Cr(VI), rather than the partial pressure of oxygen on the system.

[5]M. W. Shafer and R. Roy, *Z. anorg. u. allgem. Chem.* **276**, 275 (1954).

20.3 THE QUATERNARY SYSTEMS NiO-UO_3-SO_3-H_2O AND CuO-UO_3-SO_3-H_2O

F. E. Clark R. Slusher
J. S. Gill C. H. Secoy

Equilibrations of various solid-liquid mixtures in the systems NiO-UO_3-SO_3-H_2O and CuO-UO_3-SO_3-H_2O in pyrex vessels at 100°C have indicated considerable reaction with the glass. The extent of the attack has not been determined, but it appears to be greater in the nickel system than in the copper system; the richer the system is in nickel, the greater the attack appears to be. Data obtained from these equilibrations are not regarded as satisfactory and are not presented.

In order to avoid this difficulty, the use of fluorothene tubes is being developed. Initial work indicates that fluorothene will be very satisfactory for use at 100°C. At higher temperatures titanium bombs or lined steel bombs will be used.

The identity of the compound $3CuO{\cdot}SO_3{\cdot}2H_2O$, previously reported[6] as a predominate solid phase in the CuO-UO_3-SO_3-H_2O system, has been proved by the identity of its x-ray diffraction pattern[7] with that reported by Posnjak and Tunell[8] and with that reported for the mineral antlerite.

A new solid phase has been encountered in this system, with compositions of higher solute concentrations than those reported previously. The identity of this solid has been established by chemical analysis, by optical and electron microscopy,[9] and by x-ray diffraction. It is in all respects identical with the mineral johannite, which has the composition $CuO{\cdot}2UO_3{\cdot}2SO_3{\cdot}7H_2O$.

The scope of liquid compositions with which johannite is the stable equilibrium solid phase has been partially established and will be reported when complete.

[6]F. E. Clark, R. Slusher, and C. H. Secoy, *HRP Quar. Prog. Rep. July 31, 1955*, ORNL-1943, p 236–240.

[7]R. Ellison, Chemistry Division.

[8]E. Posnjak and G. Tunell, *Am. J. Sci.* **218**, 1–34 (1929).

[9]T. E. Willmarth, Analytical Chemistry Division.

Further work on the solid phases appearing at 100°C in the UO_3-saturated portion of the system UO_3-SO_3-H_2O has established the fact that the previously reported K-salt[10] is identical with the rare mineral uranopilite, $6UO_3 \cdot SO_3 \cdot 17H_2O$. The composition, previously reported as $8UO_3 \cdot 3SO_3 \cdot 16$–$18H_2O$, was in error presumably because the solids studied were actually mixtures. The new assignment is based on careful preparation of pure solid samples, analytical data, and comparison of crystallographic and x-ray diffraction data with data supplied to us by the U.S. Geological Survey. However, the previously reported G-salt,[10] which has the composition $5UO_3 \cdot 2SO_3 \cdot xH_2O$, is not identical with any known mineral or reported compound.

[10] C. H. Secoy *et al.*, *HRP Quar. Prog. Rep. Oct. 31, 1953*, ORNL-1658, p 87–90.

21. ADSORPTION ON INORGANIC MATERIALS

K. A. Kraus

T. A. Carlson
D. J. Coombe
J. S. Johnson
H. O. Phillips

Study continued of the adsorptive properties of various inorganic materials for ions in aqueous solutions. Principal emphasis centered, as in the previous quarter,[1] on the cation-exchange properties of zirconium phosphate and zirconium tungstate and on the anion-exchange properties of zirconium hydroxide. In addition, some experiments were carried out on the adsorbability of protactinium on zirconium phosphate.

21.1 ZIRCONIUM HYDROXIDE

One of the principal variables investigated during the last quarter was the effect of drying temperature on both anion- and cation-exchange properties of zirconium hydroxide. Zirconium hydroxide was dried for about 24 hr at a number of temperatures (see Table 21.1) and the chromate uptake was determined in a series of column experiments. As shown in Table 21.1 (series A) the uptake of chromate ions by the hydroxide decreases slowly with increasing firing temperature but remains high even after a firing of 300°C for 24 hr. The samples of hydroxide were regenerated with NaOH, and the uptake was measured again after a week (Table 21.1, series B). The values agreed closely with the earlier measurements.

[1]K. A. Kraus *et al.*, *HRP Quar. Prog. Rep. July 31, 1955*, ORNL-1943, p 246–251.

TABLE 21.1. ADSORPTION OF CHROMATE BY ZIRCONIUM HYDROXIDE

Solution of 0.1 *M* K_2CrO_4–0.2 *M* HCl

Drying Temperature (°C)	Uptake of Chromate (moles/kg)	
	A	B*
32	1.31	1.44
105	1.25	1.25
202	0.91	0.91
320	0.45	0.45
500	0.15	0.14
800	0.05	0.05

*Measurements on series B made one week after series A measurements were made.

The cation-exchange properties of the same materials were investigated (Table 21.2) by measuring the distribution coefficient D (amount per kilogram of adsorbent/amount per liter of solution) of tracer cesium in 0.1 *M* NaOH as well as the Na^+ uptake. As in the case of the anion-exchange properties, both uptake and selectivities decrease with increasing firing temperature, the effect becoming large beyond 300°C.

TABLE 21.2. CATION-EXCHANGE PROPERTIES OF ZIRCONIUM HYDROXIDE

Solution of 0.1 *M* NaOH

Drying Temperature (°C)	D_{Cs}	Na^+ Uptake (moles/kg)
32	16.5	0.80
105	11.1	0.72
202	8.0	0.63
320	2.0	0.50
500	0.9	0.18
800	0.5	0.05

Further experiments were carried out on the adsorption of chloride complexes on zirconium hydroxide. Gold(III) and silver(I) were chosen, since they should be negatively charged complexes at any reasonable HCl concentrations. Definite separation of these two elements, presumably by an anion-exchange mechanism, can be achieved (see Fig. 21.1). However, the selectivities are low compared with those obtained with strong-base organic ion exchangers.

21.2 ZIRCONIUM TUNGSTATE

The adsorption of the alkali metals on zirconium tungstate was studied in some detail, both in

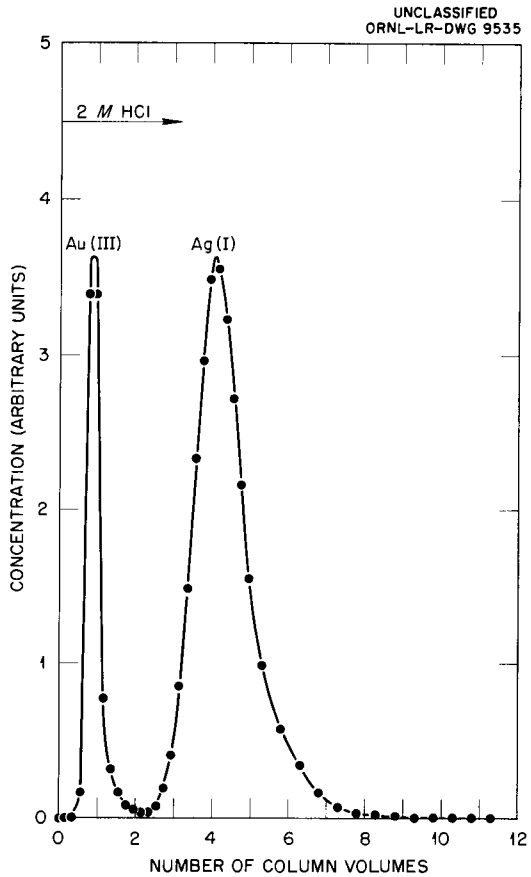

Fig. 21.1. Separation of Au(III) and Ag(I). "Zirconium hydroxide"; 200°C; 3.6 cm × 0.28 cm^2 column; flow rate, 0.5 cm/min.

HCl and in NH_4Cl solutions. The relative adsorbabilities are demonstrated in Table 21.3, where the observed distribution coefficients (D), multiplied by the molality (m_{A^+}) of H^+ or NH_4^+, are listed for cesium, rubidium, potassium, and sodium. Adsorbabilities of the alkali metals vary widely, implying that separation on small columns should be feasible. In addition, the differences in the relative adsorbabilities in HCl and in NH_4Cl solutions are striking, the higher alkali metals showing very much better adsorption from HCl than from NH_4Cl solutions.

This difference may be due, in part, to an unusual behavior of the activity coefficients of the higher alkali metals in the zirconium tungstate phase. This is demonstrated in Fig. 21.2, a plot of $D \cdot m_{A^+}$ vs moles of alkali metals adsorbed per kilogram of adsorbent. In HCl solutions the

TABLE 21.3. ADSORPTION OF ALKALI METALS ON ZIRCONIUM TUNGSTATE

Medium	$D \times m_{A^+}$			
	Cs	Rb	K	Na
HCl	55	6.7	1.4	0.2
NH_4Cl	6.5	2.1	1.1	0.2

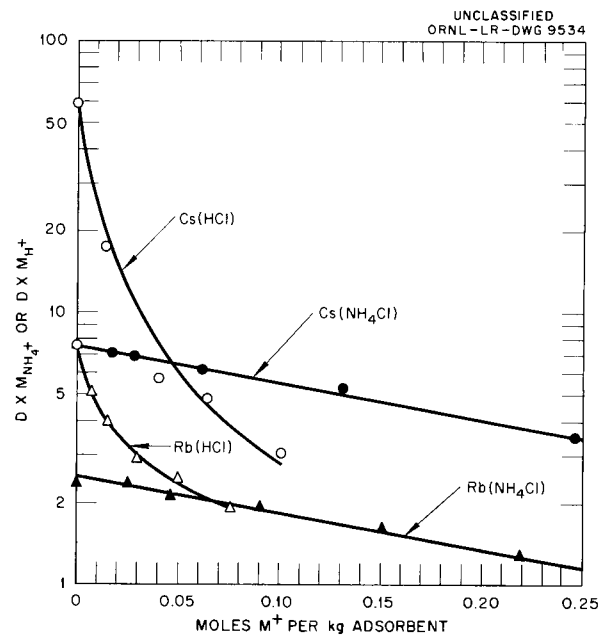

Fig. 21.2. Adsorption of Cs(I) and Rb(I) on "Zirconium Tungstate." Drying Temperature, 25°C.

distribution coefficients decrease rapidly with uptake, while only a moderate decrease occurs for NH_4Cl solutions.

Based on the distribution coefficients listed in Table 21.3, and less-quantitative data on Li^+, a separation scheme was devised for the alkali metals Li^+ to Cs^+. Results are summarized in Fig. 21.3. Conditions of the separation are also summarized in the figure.

21.3 ZIRCONIUM PHOSPHATE

The effect of drying temperature on the cation-exchange properties of zirconium phosphate was investigated. The materials were dried for about 24 hr at various temperatures (see Table 21.4)

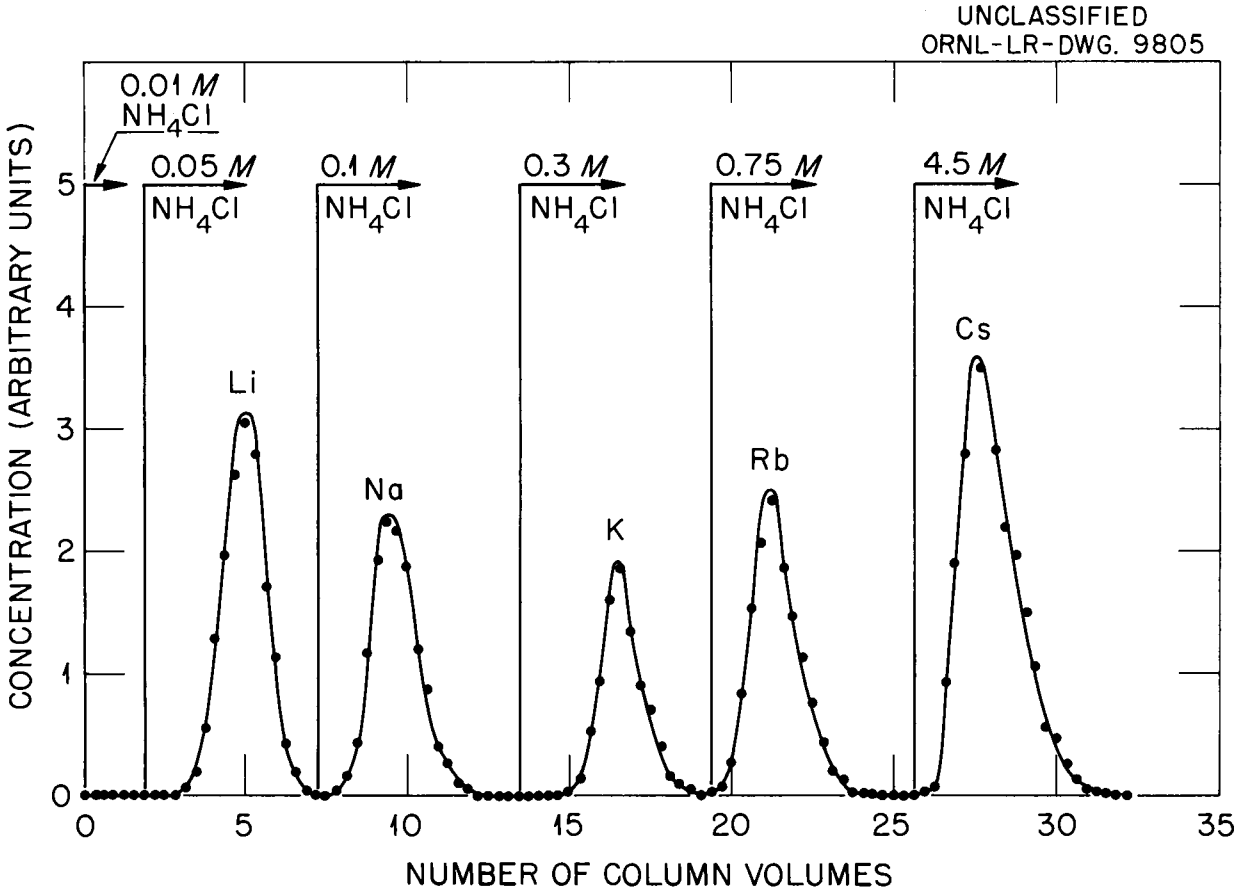

Fig. 21.3. Separation of the Alkali Metals. "Zirconium tungstate"; 12.3 cm × 0.13 cm^2 column; flow rate, about 0.75 cm/min.

TABLE 21.4. CATION-EXCHANGE PROPERTIES OF ZIRCONIUM PHOSPHATE

Adsorption of Cs(I) from 0.1 *M* CsCl

Drying Temperature (°C)	Cesium Uptake (moles/kg)
25	1.03
78	1.10
105	0.99
150	0.87
200	0.70
300	0.34
400	0.27
600	0.20
900	≦0.03

and uptake of cesium was measured from 0.1 *M* CsCl solutions. As shown in Table 21.4, uptake decreases with increasing firing temperature, although this decrease does not become serious up to 200°C.

The alkali metals exhibited large differences in adsorbability on zirconium phosphate, as they did on zirconium tungstate. The results are summarized in Table 21.5. As in the case of the tungstate, there are large differences in the adsorbabilities from HCl and from NH_4Cl solutions. Experiments are now under way to develop a separations procedure for the alkali metals, based on the observed differences in adsorbabilities. Some difficulties are encountered, however, which result mainly from the fact that the ratio of the adsorbabilities is so large that it is difficult to handle all elements with the same adsorbent. For example, lithium tends to elute in 10^{-3} *M* NH_4Cl solutions while cesium barely can be removed in concentrated

TABLE 21.5. ADSORPTION OF ALKALI METALS ON ZIRCONIUM PHOSPHATE

Medium	$D \times m_{A^+}$			
	Cs	Rb	K	Na
HCl	627	50	7.0	0.03
NH_4Cl	30	7.3	3.0	0.02

NH_4Cl. However, for the intermediate alkali metals, excellent separations can be achieved. For example, trace amounts of potassium can be removed readily from relatively concentrated NaCl solutions. Presumably, quantities, of the order of 100 column volumes, of a 0.1 *M* NaCl solution containing potassium of low concentration could be processed.

In view of the excellent adsorbability of cesium on zirconium phosphate, some exploratory experiments are under way to determine adsorbability of cesium from concentrated electrolyte solutions. In particular, it was found that the distribution coefficient of cesium is of the order of 200 in 2 *M* $Al(NO_3)_3$ solutions, which opens a definite possibility of removing fission-product cesium from concentrated raffinates.

21.4 ADSORPTION OF PROTACTINIUM ON ZIRCONIUM PHOSPHATE

It has been known for a long time that zirconium phosphate is an excellent carrier for protactinium. In these carrying experiments it is standard practice to precipitate zirconium phosphate from the solutions. It was hoped that the zirconium phosphates which had been used in the various cation-exchange studies might also act as an adsorbent for protactinium. In a series of equilibration experiments it was established that this was, in fact, the case and that protactinium could be adsorbed even from fairly concentrated electrolyte solutions. A number of typical distribution coefficients are listed in Table 21.6. Most of the experiments were carried out with Pa^{233} tracer, which was prepared by neutron bombardment of thorium oxide. A few were carried out with Pa^{233} tracer from Thorex dissolver solutions. On the basis of these data it should be feasible to adsorb protactinium from a number of waste solutions as

TABLE 21.6. ADSORPTION OF PROTACTINIUM TRACER ON ZIRCONIUM PHOSPHATE

Concentration of Components of Medium (*M*)				Distribution Coefficient
$Th(NO_3)_4$	$Al(NO_3)_3$	HNO_3	Other	
1.8		0.15		150
	1.7	0.15		$>10^4$
0.90	0.86	0.15		350
0.90	0.86	0.13	0.02 KF	350
	1.70	0.15	0.01 KF	$>10^4$
	1.70	0.15	0.05 KF	$>10^4$
	1.48	0.25	0.20 KF	$>10^4$
1.0	0.40	5.5	0.03 KF	350
	1.26	5.7	0.02 KF	1300
	1.00		0.03 KF*	$>10^3$
	1.00		0.5 $Fe(NO_3)_3$, 0.03 KF*	~50
		0.05	1 $ZrOCl_2$	~50
		0.05	1 $ZrOCl_2$, 0.04 KF	~30

*Protactinium from Chemical Technology raffinate diluted in synthetic raffinate.

well as from dissolver solutions in the Thorex process. In collaboration with the Chemical Technology Division, adsorption experiments were carried out on a dissolver solution from a current Thorex run as well as a solution from a raffinate. Good adsorption was obtained in the former case, while adsorption from the raffinate was very poor. The reason for the failure in the latter case is not clear.

At present no method is known which will effectively remove protactinium from the phosphate without dissolving the latter.

22. HRP ANALYTICAL CHEMISTRY

O. Menis

R. G. Ball
C. M. Boyd
R. E. Corcoran
N. M. Ferguson
H. P. House
M. L. Hubbard
U. Koskela
D. L. Manning
J. J. McCown
T. C. Rains
I. B. Rubin

22.1 ANALYSIS OF URANYL SULFATE SOLUTIONS

During the past quarter, methods for analyzing solutions of uranyl sulfate for mercury, tin, and chloride have been developed.

An amperometric method, based on the reaction of mercury with tetraphenylarsonium chloride, was developed for the determination of mercury in uranyl sulfate solutions. Mercury, in the range of 0.3 μg to 2.5 mg in dilute nitric acid, is titrated with a solution of tetraphenylarsonium chloride at 0.5 v vs the SCE. Uranium does not interfere in concentrations up to 10 mg per milliliter.

Methods were investigated for the separation and determination of tin in uranyl sulfate solutions that contain copper and the corrosion products of stainless steel. Distillation and carrier-precipitation procedures for this separation were tested. The distillation procedure for tin was unsatisfactory because the reagent blanks were too high. A satisfactory separation of tin was achieved when it was precipitated as the hydroxide, in the presence of aluminum as a carrier, from a basic carbonate medium. After the hydroxide precipitate was dissolved in hydrochloric acid, tin was determined polarographically in an ethyl alcohol–hydrochloric acid medium that contained a trace of tetraphenylarsonium chloride. The precision was better than 10% when the diffusion current of the second tin wave, which involves the reduction of $SnCl_4^{--}$ to Sn^0, was utilized for the estimation of tin in the range of 2 to 50 μg in 15 ml.

An indirect flame photometric method was developed for the determination of chloride, in the range of 0.5 to 10 ppm, in uranyl sulfate solutions. In this method, chloride is precipitated as AgCl in a dilute solution of silver nitrate, after which the chloride equivalent to the silver is ascertained from the decrease in luminescence of the solution at 328 mμ. The method is simple, rapid, and of particular value for the determination of chloride in concentration ranges for which ordinary methods of potentiometry are unsatisfactory or in colored solutions for which turbidimetric methods are unsatisfactory; the precision is of the order of 5%.

Microgram quantities of chloride may also be determined in solutions of high ionic strength with the use of a concentration cell composed of two Ag-AgCl electrodes. The potential difference in millivolts existing between a Ag-AgCl electrode immersed in a 0.001 *M* chloride solution and a Ag-AgCl electrode immersed in the unknown chloride solution is measured potentiometrically. This potential difference is used to find the unknown concentration from a nomogram constructed with the use of the Nernst equation. The concentration of other ions present must be identical in all solutions, and the liquid-liquid interface must be kept as small as possible to eliminate activity and junction effects.

The method has been used successfully to determine chloride in concentrations as low as 0.3 ppm in 0.4 *M* H_2SO_4 solutions. It is desired to determine 0.1 ppm of chloride in homogeneous-reactor-type solutions. Because of the necessity of removing the cations from the homogeneous-reactor-type solutions, so as to control the ion concentrations in the unknown within certain limits, and because of the limited amount of sample available for a determination, methods of concentrating the chloride are being studied.

This method is potentially useful in analyzing highly radioactive solutions where the flame photometric method would be of no use.

22.2 ANALYSIS OF THORIUM OXIDE

Methods have been developed for the determination of carbonate, silicon, and titanium in thorium oxide. The use of the Andreasen pipet method to determine the particle-size distribution of thorium oxide in different media has been investigated.

Microgram quantities of carbonate in thorium oxide were determined by means of a gas-evolution method. The sample is dissolved in nitric acid that contains a few drops of hydrofluoric acid. The carbon dioxide thus evolved is absorbed in a known amount of barium hydroxide, following which the excess base is titrated potentiometrically with

[redacted]

standard acid. Carbonate values for standard solutions of sodium carbonate, test portions of which contained carbonate equivalent to 250 to 750 μg of CO_2, and for a Bureau of Standards sample of fluorspar were 10 to 25% less than the known value.

A spectrophotometric method was investigated for the determination of silicon dioxide in thorium oxide as the silicomolybdate complex. The elimination of interferences due to thorium and the dissolution of thorium oxide without loss of silicon dioxide were studied particularly. The reaction whereby the silicomolybdate complex is developed was carried out under the conditions recommended in the literature. Under these conditions thorium molybdate is precipitated, but, after the silicomolybdate complex is reduced to the heteropoly acid, the thorium molybdate is dissolved by adding tartrate and raising the pH from 1.4 to 3.0.

Since it is essential that the insoluble silicon dioxide be converted to the soluble silicate without evolution of the volatile tetrafluoride, the dissolution procedure for thorium oxide was modified. The oxide is dissolved in 4 *N* nitric acid (to which 2 drops of hydrofluoric acid are added) at low heat and constant liquid volume. Silicon dioxide in thorium oxide was ascertained with a precision of about 10%. As little as 5 μg of silicon can be detected in a gram sample of thorium oxide.

A spectrophotometric method, based on the formation and the extraction of the titanium-8-quinolinol complex, was developed for the determination of titanium in thorium oxide. Although a number of interfering ions, Fe^{3+}, Cr^{6+}, and Ni^{2+}, are separated from titanium by electrolysis, other ions such as Al^{3+}, Zr^{4+}, and Si^{4+} are not removed. When the 8-quinolinol extract was treated with peroxide, however, the absorption spectrum of the titanium-8-quinolinol complex was shifted and enhanced without similarly affecting the absorption spectrum of the interfering ions. The difference in the absorbancy at 440 mμ, before and after peroxide treatment, was utilized in the estimation of titanium in samples of thorium oxide. Up to 0.5 g of thorium can be analyzed for titanium by this method without serious interference from thorium and other impurities, while as little as 20 ppm of titanium in the oxide can be detected. The precision and reliability of this method are being studied.

Sedimentation methods are being investigated for use in establishing the particle-size distribution of thorium oxide. In one method that was studied, the Andreasen pipet was used to determine the particle-size distribution after the thorium oxide had been dispersed in a suitable medium. Since it is essential that the solid aggregates be completely dispersed, several factors relative to the maximum dispersion of thorium oxide were investigated. The degrees of effectiveness of sodium pyrophosphate, sodium oxalate, and hydrochloric acid as dispersing or wetting agents were determined. Tests were also made in which the method of agitation, as well as the agitation time (5 min to 24 hr), was evaluated. It was noted that maximum dispersion was attained when the thorium oxide was mechanically shaken with 0.1 *M* hydrochloric acid for 15 hr or more.

Tests of thorium oxide (D-17) ignited at 600, 800, 1000, 1200, and 1400°C, which were carried out in 0.1 *M* HCl (shaking time, 18 hr), indicated that maximum dispersion was attained with materials that had been ignited at 800°C. As a consequence of ignition at higher temperatures, the degree of dispersion was found to be significantly less.

Since the Andreasen pipet method does not distinguish between particles with diameters of less than 0.4 μ, a fraction of a suspension that contained particles with diameters less than 0.4 μ was submitted to T. E. Willmarth[1] for electron microscopy. Willmarth reported that the diameters of the primary particles in the fraction were 0.01 μ or less, whereas those of the secondary particles ranged from 0.04 to 0.1 μ.

22.3 ANALYSIS OF OFF-GASES FROM DYNAMIC LOOP TESTS

A semiquantitative method was devised for the determination of carbon dioxide in the oxygen off-gases from dynamic test loops. The amount of carbon dioxide in the oxygen is used as a measure of the decomposition of carbon bearings in the loop. Carbon dioxide, 0.02 to 0.2 g per 5 ft^3 of oxygen, is absorbed, from a rapidly flowing stream of oxygen, in a solution of barium hydroxide that is contained in a gas-scrubbing tower of special design. Samples of the solution are removed periodically from the tower and titrated with standard acid. The change in hydroxyl concentration is a measure of the carbon dioxide absorbed in the solution.

[1] T. E. Willmarth, *Anal. Chem. Semiann. Prog. Rep. Oct. 20, 1955*, ORNL-1973 (in press).

[redacted]